The Free-Fall Three-Body Problem: Escape and Collision

Hiroaki Umehara

Doctor of Science

Department of Astronomical Science
School of Mathematical and Physical Science
The Graduate University for Advanced Studies
2-21-1, Osawa, Mitaka, Tokyo 181-8588, Japan

1997 (School Year)

The Free-Fall Three-Body Problem: Escape and Collision

Thesis Presented by

Hiroaki Umehara

H i r o a k i U m e h a r a

Department of Astronomical Science

School of Mathematical and Physical Science

The Graduate University for Advanced Studies

2-21-1, Osawa, Mitaka, Tokyo 181-8588, Japan

e-mail address: umehara@milano.mtk.nao.ac.jp

1997 (School Year)

Address from 1st April 1998 :

Space Systems Section, Kashima Space Research Center

Communications Research Laboratory

893-1, Hirai, Kashima, Ibaraki 314-0012, Japan

e-mail address: ume@crl.go.jp

Acknowledgments

I would like to express my thanks to Professor K. Tanikawa in National Astronomical Observatory Japan for introducing me the three-body problem and for leading the researches with continuous encouragement during the works over four years. Without his guide, the present thesis would not have been completed and I could not have reached the final stage. I have enjoyed fruitful collaborations with him through the entire course of my graduate study. I express my thanks to Professors H. Kinoshita and S. M. Miyama for many helps, comments, discussions and continuous encouragements during my graduate study.

I thank Professor J. P. Anosova who continues to study the free-fall problem for thirty years. The professor stayed in National Astronomical Observatory Japan for one year. After that, the professor provided valuable suggestions and discussions on the numerical investigations of the free-fall three-body problem for me. I express my thanks to Professor J. Yoshida for many comments and discussions on the analysis of escape phenomena. The professor showed me the numerical results obtained by Professor J. P. Anosova for the first time. I thank Professor S. Mikkola for valuable suggestions and discussions on methods of numerical integrations. The professor also stayed in National Astronomical Observatory Japan for three months. After that, the professor provided valuable comments for me. I thank Professor H. Yoshida for many comments and discussions on the analysis of triple-collision singularity. I thank to Professor Y. Aizawa for fruitful suggestions on the analysis of chaos in the Hamiltonian systems.

Finally, I express my acknowledgments to all the members of the Theoretical Astrophysics Division, the Celestial Mechanics Division, and Astronomical Data Analysis Center of the National Astronomical Observatory for their helps and many valuable discussions. Most of numerical computations were carried out on the workstations in the Theoretical Astrophysics Division and the Astronomical Data Analysis Center.

Abstract

The escape phenomena in the three-body problem with zero initial velocities and equal masses are studied both numerically and analytically. In particular, the effects of triple and binary collisions are considered in detail. Here, escape means that two particles form a binary and the third particle recedes from the binary to infinity. Collision is defined as the event when the distance between particles vanishes.

First, escape orbits are searched for by a numerical survey of the initial-value space and compared with collision orbits obtained by Tanikawa et al. (*Cele. Mech. Dyna. Astr.*, **62** (1995) 335-362). Most escape phenomena occur after triple encounter as a result of slingshot. A particle passes through between the other particles receding from each other. It is found that escape orbits due to slingshot distribute around a particular family of binary-collision orbits which maintain nearly isosceles configuration. The configuration and the velocity vectors are almost symmetric. Moreover, if orbits approach sufficiently close to triple collision, all escape orbits distribute around the binary-collision orbits. Furthermore, orbits without escape during the first triple encounter are also found sufficiently close to triple-collision orbits. Therefore, it becomes clear that explaining the distribution of escape orbits only by triple-collision orbits is impossible. The particular family of binary-collision orbits has a central role in escape phenomena as well as triple collision does.

Discovery of escape orbits due to exchange encounter is also one of the results. Two close approaches between different pairs successively occur. The dynamical features of slingshot and exchange are compared with each other. Escape probabilities and increments of binding energies are evaluated statistically for the respective encounter-types. It is shown that some of slingshot encounters result in more energetic evolution than all of exchange encounters. So the conditions of slingshot configurations restrictive and favorable for escape are searched for, respectively. Using the slingshot conditions, it is answered why slingshot-escape orbits distribute around the particular binary-collision orbits showing nearly symmetrical motion.

Finally, it is proved analytically that both escape and non-escape orbits after the first triple encounter exist arbitrarily close to the particular triple-collision orbit, the homothetic-equilateral triple-collision orbit. It is proved that in the initial-value space escape orbits distribute around three kinds of isosceles orbits where different particles escape and non-escape orbits are distributed in between. In order to show this, it is proved that the homothetic-equilateral orbit is isolated from other triple-collision orbits so far as

the collision during the first triple encounter concerns. Moreover, the escape criterion is formulated in the planar isosceles problem and translated into the words of regularizing variables. The results explain the orbital structure numerically obtained in the beginning of the present thesis. With the aid of numerical integrations, it is shown that the distribution of escape orbits around another triple-collision orbit are topologically similar to the one around the homothetic-equilateral orbit. Here, it is found that the binary collision has an important role in determining the dynamical evolution.

Contents

Chapter 1

Introduction

1.1 Three-body problems in astrophysics

In the present thesis, escape phenomena in the free-fall three-body problem with equal masses are studied both numerically and analytically. The free-fall three-body problem is the case with zero initial velocities. In particular, the effect of triple and binary collisions are studied in detail.

In the present section consisting of three subsections, we review various works which lead the author to the study of escape, triple collision and binary collision. In Section 1.2, the purpose and the outline of the present paper are described. In Section 1.3, we will introduce several numerical methods to analyze the three-body problem in the present thesis. They are the initial-value space, the escape criterion and the procedure searching binary-collision orbits.

1.1.1 Works on final motions

The gravitational three-body problem is a simple problem where three particles attract each other by the Newtonian law. However, the three-body problem is too complicated to be explored completely. Under various situations in the field of astrophysics, many types of the three-body problem are considered: binary-single star scattering (hereafter referred to as the *scattering system*), hierarchical triple stars (hereafter as the *hierarchical system*), sun and two planets (hereafter as the *planetary system*), wide galaxy triplets, and so on.

The scattering system means a system of a binary and a third star which approaches

the binary from a distance. This system has been investigated by Yabushita (1966), Heggie (1975), Saslaw et al. (1974), Lin and Saslaw (1977), Hut and Bahcall (1983), Hut (1983), Mikkola (1984a, 1984b), Hut (1993), Heggie and Hut (1993), McMillan and Heggie (1996), Hut and McMillan (1996). In the hierarchical system, a binary and a third star are also located at a distance; however, the third star revolves around the binary. See Harrington (1975), Szebehely and Zare (1977), Graziani and Black (1981), Black (1982), Kiseleva, Eggleton and Anosova (1994), Kiseleva, Eggleton and Orlov (1994), Anosova (1996), and Mikkola and Tanikawa (1998). The planetary system means that two planets revolve around a central star. See Nacozy (1976), Laskar and Robutel (1995), Robutel (1995). In the system of wide galaxy triplets, intergalactic distances and respective masses are comparable to each other, respectively. Moreover, the velocities are not so large. This system is investigated by Chernin et al. (1994) and Dolgachev and Chernin (1997).

The common purposes of the works in the above three-body systems can be categorized into two:

Common purposes

(1) determining the location of the partition of final states in the phase space,

(2) finding out factors which effect the distribution of the phase-space partition,

where a final state means a state of the system as time goes to infinity. In order to achieve the above goal, it is first necessary to classify possible final states in a given system.

In the beginning of 20th century, a French astronomer and mathematician Chazy (1922) described all possible types of final motions in the three-body problem. If the total energy of the system is negative, more varieties of final motions exist compared with the zero-energy and positive-energy systems. Final motions are classified into the following four categories for the negative-energy system. Here, r_j, $j = 1, 2, 3$ denotes the distance between particle k and l, where (j, k, l) is $(1, 2, 3)$ or its permutation. The time is denoted by t.

1. Hyperbolic-elliptic escape for m_j:
   As $t \to \infty$, $r_j < C$, $r_k \to \infty$ and $r_k/t \to C_k > 0$, $j \neq k$.

2. Parabolic-elliptic escape for m_j:
   As $t \to \infty$, $r_j < C$, $r_k \to \infty$ and $r_k/t^{2/3} \to C_k > 0$, $j \neq k$.

3. Bounded motion:

   for all $j = 1, 2, 3$, $r_j < C < \infty$ during $t \in [0, \infty)$.

4. Oscillatory motion:

   at least one of the r_j is unbounded, however it does not tend to infinity.

From purely logical considerations, Chazy (1922) asserted the existence of the oscillatory motion. This existence had been remained in doubt for a long time. After about 40 years, it was found in the restricted three-body problem where the symmetrical configuration is maintained (Sitnikov, 1959). Its existence for the general three-body problem has been proved by Alekseev (1968) for the three-dimensional case with $m_1 = m_2 \gg m_3$ and Xia (1994) for the planar case with $m_1 \gg m_2 \gg m_3$. Tanikawa and Umehara (1998) contributed to the problem for $m_1 = m_2 = m_3$.

Moreover, in the zero-angular-momentum case, there is triple-collision motion of which the final motion can not be defined. If triple collision occurs at a finite time, almost all solutions after triple collision can not be defined (Siegel, 1941; McGehee, 1974).

Sundman (1912) proved that triple collision is possible only in the system with zero angular momentum. From the equations of motion, Sundman derived an inequality which is now called *Sundman's inequality*. The inequality shows the relation between the behavior of the moment of inertia $I(t)$, the total energy h and the total angular momentum c. From the inequality, Sundman also proved that it is necessary for a triple collision to occur that the angular momentum c is equal to zero. Sundman's inequality shows that $I(t)$ vanishes only if $c = 0$. Zero moment of inertia means triple collision.

In contrast to the negative-energy system, there is not any drastic difference among final motions in zero-energy or positive-energy systems. The possible motion in both systems is only disruption. Here, disruption means that either one particle escapes or three particles recede from each other. There are neither bounded nor oscillatory motion. See Alekseev (1981) which contains a good review of final motions, and Siegel and Moser (1971) which contains the classical analysis of triple collision.

Therefore, many negative-energy systems are investigated intensively. After Chazy's classification, the distribution of phase-space partitions of final motions and the factor determining final motions are searched for by both analytic and numerical methods.

It has been considered that the close triple encounter is important to escape phe-

nomena in negative-energy systems. Many authors investigated the relation between close triple encounter and escape phenomena, and attempted to quantify the triple encounter leading to escape.

For a system where the total energy is negative and the total angular momentum is not zero, Birkhoff (1927) was the first to mention the importance of the close triple encounter as a necessary mechanism for escape. Analysis by Birkhoff is based on the time-dependent moment of inertia $I(t)$ of the three particles. Using Sundman's inequality, it was asserted that $I(t)$ increases indefinitely as $t \to \infty$ if it has the minimum less than a critical value I_c. The divergence $I(t) \to \infty$ means the hyperbolic-elliptic or parabolic-elliptic escape. Such a formulation is called the *escape criterion* since we can judge one of final states in a finite time.

From the critical value I_c, we can construct the boundaries in the phase space. These boundaries separate the phase space into two kinds of regions: a region in which I of a phase point is less than I_c and a region where $I > I_c$. If a phase trajectory enters the region satisfying $I \leq I_c$ once, $I(t)$ along the trajectory is controlled to increase monotonically as $t \to \infty$. However, the location of the boundaries does not agree with one of the phase-space partition perfectly. Since the escape criterion is only a sufficient condition, we can conjecture a rough distribution of the partition. Moreover, it is verified that the close triple encounter is a dominant factor for escape.

After that, a lower boundary of I where the system leads to escape in the non-zero-angular-momentum case has been improved by Merman (1955, 1958), Sibahara and Yoshida (1963), Szebehely (1973b), Zare (1981), Laskar and Marchal (1984) and Marchal et al. (1984a). The work of Birkhoff has been reviewed by Szebehely (1973a).

However, the lower boundary of I leading to escape is not available for the system with zero angular momentum. In zero-angular-momentum system, quantifying the close triple encounter leading to escape has been not successful. The zero-angular-momentum system is treated only in the final part of the paper by Zare (1981). However, escape criterion is not mentioned in this system.

Without moment of inertia $I(t)$, confinement of regions in the phase space where the system leads to escape is formulated by Khil'mi (1951), Merman (1952, 1953, 1954), Alekseev (1961), Tevzadze (1962), Standish (1971), Yoshida(1972, 1974) and Marchal et al. (1984b). These formulae describe necessary conditions of the hyperbolic-elliptic escape at a finite time, and so they are also called the *escape criteria*.

Although escape criteria by the above authors avoid the judgement of escape during the close triple encounter, the inequalities of the criteria define regions in the phase space, and so we may determine a rough distribution of the phase-space partition of escape even if the system is of zero-angular-momentum.

Szebehely (1973a) reviewed the proof of the escape criteria derived until 1971. Yoshida (1972, 1974) unified the criteria by Merman (1954), Tevzadze (1962) and Standish (1971) into the improved formulation. Marchal (1984b) refined the criterion in the phase-space region corresponding to the close triple encounter.

A new method analyzing the three-body problem began in 1960s. This method is the numerical integration. The first numerical investigation was done in Yabushita (1966) who analyzed the scattering three-body problem.

Szebehely and Peters (1967) observed the behavior of one orbit leading to escape after many times of the interplay motion among three particles. The three masses of the system are not equal (mass-ratio is $3:4:5$). The initial velocities of the three masses are zero. The system with zero initial velocities is a special case of the zero angular momentum. They showed that the exact solution can be evaluated by the integration with the suitable regularization between the closest two particles even if the motion is complicated enough. Moreover, from the result of the evaluated orbits, the close triple encounter is confirmed to be one of the effective factors for escape phenomenon.

The system with zero initial velocities is called the *free-fall* system.

Agekian and Anosova (1967) started the project to determine the partition in the phase space with the aid of numerical integration. Agekian and Anosova (1967, 1968) investigated the final states for 100 initial values in the system with small angular momentum. Anosova (1969) investigated the free-fall system with unequal-masses. The mass combinations were $9:3:1$, $3:3:1$ and $3:1:1$. Instead of the moment of inertia $I(t)$, they used the time-dependent perimeter $p(t)$ of the triangle, and observed that the escape practically always occurs if the minimum value of $p(t)$ is so small. Agekian et al. (1969) and Agekian and Anosova (1971) also showed the importance of triple encounter for escape phenomena by observing 1600 and 10000 systems, respectively. The initial configuration and initial velocities were sampled at random. They evaluated the potential energy U when the moment of inertia $I(t)$ becomes minimum for each system.

Until 1986, Agekian, Anosova and their collaborators continued to investigate various systems and to publish their results in the Russian journals. See the references in

Anosova (1986). The results obtained during about 20 years are summarized in Anosova (1986). The minimum value of $p(t)$ and the binding energy of the formed binary as a result of escape are found to be well correlated in the sense that close triple encounters produce tight binaries. The investigated systems are the following four: the free-fall system with equal masses, the planar non-zero-angular-momentum system with equal masses, the three-dimensional non-zero-angular-momentum system with equal masses and with unequal masses. Anosova (1989) reviewed the numerical results of three-body systems since 1960s.

After that, Anosova and Zavalov (1989) observed systematically the initial-value dependence of the escape orbits in the free-fall system with equal masses. They found a sequence of sets of orbits escaping just after the first triple encounter without interplay. According to them, moreover, most of these escape orbits seem to have the minimum values of $p(t)$ smaller than non-escape orbits.

Agekian and Anosova (1990) defined the time-dependent current size $\rho(t)$ as the maximum distance of the components from the gravity center of the three particles. They evaluated a minimum value of $\rho(t)$ in the same system as in Anosova and Zavalov (1989). The result of $\min \rho(t)$-distribution of the escape orbits were similar to that of $\min p(t)$-distribution by Anosova and Zavalov (1989).

Johnstone and Rucinski (1991) also observed the initial-value-dependence of final motions in the free-fall system with equal-mass case. They evaluated the life-time and $\min \rho(t)$, and confirmed the above conclusions. According to their results, in general, the initial value leading to a small value of $\rho(t)$ causes the system to escape at an early time. Anosova (1991), Anosova and Orlov (1992, 1994) increase the sample number of initial values, and confirmed the above conclusions.

In 1990s, there appeared numerical works showing the relation between escape and minimum value of the time-dependent moment of inertia $I(t)$. Aarseth et al. (1994a, 1994b) evaluated the minimum value of $I(t)$ in the free-fall systems with both cases of equal masses and unequal masses, and confirmed the above conclusions.

The importance of the close triple encounter for escape phenomenon is stressed by the above numerical works evaluating $\min p(t)$, U, $\min \rho(t)$ and $\min I(t)$. However, the confinement of the phase space leading to escape is not successful by numerical as well as by analytical methods. In this stage, it is expected naturally that there exists a non-escape orbit experiencing sufficiently close triple encounters.

1.1.2 Works analyzing chaotic behavior

In the field of mathematical theory of the three-body problem, a new method analyzing orbits close to triple collision is developed in 1970s. In almost all cases of the three-body problem, triple collisions show non-regularizable features, and so the continuity of the solutions does not hold at the configurational point representing triple collision. Therefore, the solution close to triple collision is complicated and difficult to analyze. However, the research of the motion close to triple collision has begun with the aid of a device due to Waldvogel (1973) and McGehee (1974) which blows up the singular point in the configurational space to a high-dimensional manifold. This manifold is referred to as the triple-collision manifold.

McGehee (1974) developed blow-up variables in the collinear three-body problem. Although the flow on the triple-collision manifold is entirely fictitious since orbits on it do not correspond to any orbit in the original phase space, the flow in the blow-up coordinates extends smoothly over the fictitious flow on the triple-collision manifold. We can describe the solutions close to the triple collision if the fictitious flow is described. By investigation of flows in the triple-collision manifold, we can understand behavior close to triple collision. The set of orbits ending in triple collision in the original phase space is interpreted so as to form the stable manifold of the equilibrium point on the triple-collision manifold. The orbit close to triple collision corresponds to the flow starting to recede in the direction of the unstable manifold of the equilibrium point after approaching the equilibrium point along the stable manifold.

Furthermore, McGehee (1974) found one possible mechanism for escape: one particle may get an arbitrarily large velocity as an orbit approaches triple-collision manifold. This implies that the motion closer to triple collision tends to escape in the collinear system.

In 1980s, the analysis of triple collision has been progressed in the planar isosceles problem by McGehee's blow-up method where the motion maintains symmetric configuration of an isosceles triangle shape forever on the two-dimensional plane. Devaney (1980) developed the blow-up variables and derived the triple-collision manifold in the planar isosceles problem. The fictitious flows on the triple-collision manifold, especially the unstable and stable manifolds, with any mass ratio are analyzed by Simó (1980). Simó and Martínez (1988) considered the near-collision flow and proved the existence of various features about the behavior close to triple collision. They also suggested the relation

between close triple encounter and escape in the planar isosceles problem as well as in the collinear problem. Now, Umehara and Tanikawa (1997) completed the proof of the relation between triple collision and escape in the case with equal masses. See Section 4.2 for a detail.

In the collinear and planar isosceles systems, the close triple encounter seems to be the only factor effective for escape phenomenon.

Investigations of the planar problem by the blow-up method also started in 1980s (Waldvogel, 1979, 1982; Moeckel, 1983; Simó and Susín, 1989; Susín and Simó, 1991). Waldvogel (1982) introduced the blow-up variables in the planar problem. Moeckel (1983) investigated the existence of the connection of the stable and unstable manifolds among various equilibrium points, and made a list of possible motions passing near triple collision. There are escape phenomena for each of the three particles after the close triple encounter in the list of possible motion.

In the above theoretical works, however, it is still unknown whether bounded orbits distribute close to a triple collision orbit or not in the planar problem. It is also not known how escape orbits distribute around a triple collision orbit in the planar problem. Therefore, it is naturally expected that there is another factor except close triple encounter effective for escape phenomenon.

1.1.3 Expected effects of binary collision

In the present thesis, we will verify that binary collision as well as triple collision are closely related to escape phenomenon. Tanikawa et al. (1995) was the first to suggest it. Some preliminary numerical results in this relation have already been reported in Umehara et al. (1995), and Umehara and Tanikawa (1996).

Expecting the importance of binary collision is novel. In the field of the numerical astronomy and the theoretical mathematics, binary collision seems to be considered as a worthless event hitherto.

In the numerical works, triple and binary collisions are ignored both consciously and unconsciously. Since the phase space of the three-body problem is high dimensional and broad, authors in statistical field may consider that collision orbits are detected accidentally if we sample orbits randomly. Moreover, they may want to avoid collisions since the numerical error increases rapidly if the orbit passes through close to collision singularity.

On the other hand, various authors in the mathematical field consider triple-collision

singularity as the origin of chaos. Since binary-collision singularity is regularizable, it seems to be considered that there is not any remarkable event around binary-collision singularity in the phase space. Several authors concentrated their attention on binary-collision orbits in the general three-body problem (Delibaltas, 1983; Hadjidemetriou, 1984). However, they used binary-collision orbits as a tool to search periodic orbits in the planetary system. So they did not consider any relation between binary collision and escape.

Binary collision in the two-body problem is not any effective factor for the evolution of the system. In the three-body problem, however, binary collision can become a candidate for an influential factor because of the existence of the third mass.

The following works on the two-body problem and on the restricted three-body problem suggest the relation between binary collision and chaotic phenomenon: Devaney (1982), Llibre (1982), Lacomba and Llibre (1988), Delgado-Fernández (1988), and Llibre and Piñol (1990).

In the two-body problem, Devaney (1982) described analytic formulae of binary-collision orbits by means of blowing up binary-collision singularity. It was shown that binary-collision singularity is transformed to a manifold, a binary-collision manifold. As a result, a set of binary-collision orbits in the original phase space is transformed to stable manifolds of fixed points on the binary-collision manifold.

In the circular restricted three-body problem, Llibre (1982) considered binary collisions between one component of a finite-mass binary and a mass-less particle and developed the blow-up variables. As a result, stable and unstable manifolds corresponding to an orbit ending at binary collision and starting at binary collision are found. Lacomba and Llibre (1988) and Delgado-Fernández (1988) showed that these stable and unstable manifolds intersect transversely with each other in some limiting cases. In other words, binary collision singularity in the restricted three-body problem has been shown to be the origin of chaos. Therefore, we expect that binary collision as well as triple collision have a central role for chaotic phenomena even in the general three-body problem.

The following works on the various Hamiltonian systems suggest the relation between chaotic phenomenon and escape: Ding et al. (1990), Meyer et al. (1995) and Toda (1995, 1997). Some chaotic phenomena result in disruption of the system in the Hamiltonian system where the phase space is not closed but open. The phase space in the general

three-body problem is also open even if the total energy is negative.

In some simple but non-integrable Hamiltonian systems, it is well-known that phase-space partitions of final states have fractal structures. Moreover, phase trajectories leading to disruption of the system distribute around unstable manifolds of a periodic orbit which extend to infinity. Ding et al. (1990) and Meyer et al. (1995) show such phenomena in the scattering problems with the fixed potential and with rotating rigid discs, respectively. The structure of stable and unstable manifolds of the invariant manifold in the three-body scattering system with lower-bounded potential is investigated by Toda (1995, 1997). However, due to the difference of purposes, Toda (1995, 1997) did not mention physical states in the unstable manifolds.

In the gravitational three-body problem, there are works by Boyd and McMillan (1992, 1993) and Mikkola and Hietarinta (1989, 1990, 1991) who studied the topological structure of phase-partitions of final motions. Boyd and McMillan (1992, 1993) investigated initial-value distribution of escape phenomena in the scattering system. Mikkola and Hietarinta (1989, 1990, 1991) investigated phase-space structures of final motions in the collinear problem. In both three-body systems, fractal structures of phase-space partitions of escape motions have been observed.

The above works imply the close relation between escape phenomena and unstable manifolds even in the general three-body problem. Thus escape orbits may distribute around unstable manifolds of fixed points corresponding to triple or binary collision. Many works considering triple encounter have shown that the close triple encounter is not only one factor effective for escape. Therefore, not only triple collision but also binary collision may be crucial to escape phenomena in the three-body problem.

Furthermore, behavior of escape orbits with respect to binary collision were expected by Tanikawa et al. (1995). Let us consider a near-binary-collision orbit which is perturbed from an orbit experiencing binary collision in the presence of a faraway third particle. Two components of the near-collision binary approach and begin to recede from each other. One of the components of the receding binary passes through the linear arc connecting the other component and the third particle. At this configuration, particles outside may be receding from each other. In general, when a particle passes through between two particles which are receding from each other, it is possible that the passing particle obtains enough kinetic energy to escape. See Fig.3 of Tanikawa et al.(1995) and Fig. 3.26 in Subsection 3.4.2 of the present thesis. This suggests that escape orbits are distributed

around binary collision orbits.

The mechanism obtaining kinetic energy suggested in the above scenario is called "slingshot" which is one type of triple encounters. The triple encounters have been classified in three categories by Anosova and Zavalov (1981) for the first time, and summarized by Valtonen (1988).

1. A single particle goes through between components of a temporary binary in a nearly straight line orbit, which is called as "slingshot" by Saslaw et al. (1974).

2. A single particle scatters strongly from one of the components of a temporary binary, which is called as "fly-by".

3. A single particle exchanges its place with one of the components of a temporary binary, which is called as "exchange".

Slingshot encounter is investigated by Saslaw (1974), Lin and Saslaw (1977), Anosova (1986), Anosova and Zavalov (1989), Mikkola and Valtonen (1990), Agekian and Anosova (1991), Xia (1992), Hut and Rees (1992), Basu et al. (1993), Valtonen et al. (1994), Anosova and Tanikawa (1995), Zare and Szebehely (1995), Umehara and Tanikawa (1996), Valtonen (1996), and Anosova (1997). Fly-by and exchange encounters are investigated by Heggie (1975), Mikkola (1983), Hut and Bahcall (1983), Hut (1983), Mikkola (1984a, 1984b), Heggie and Seatman (1991), Hut (1993), Heggie and Hut (1993), McMillan and Heggie (1996), and Hut and McMillan (1996).

The slingshot is an effective mechanism for the energy transfer between a binary and the third particle. This mechanism has been used to prove the existence of an oscillatory motion in the three-body problem (Sitnikov, 1960; Tanikawa and Umehara, 1998) and to verify the existence of a non-collision singularity in the five-body problem (Xia, 1992). Recently, the mechanism of energy increment for the escaping particle due to slingshot was analyzed by Zare and Szebehely (1995) in the planar isosceles three-body problem. The microscopic mechanism to obtain kinetic energy from a binary is clarified in the case of the idealized configurations.

Roughly speaking, a third particle is accelerated by the gravity of a binary if the third particle passes through the gravity center of the binary when the components are receding from each other. In this way, the third particle can escape obtaining enough kinetic energy from the binary. Conversely, the third particle is decelerated if it passes through the gravity center of the binary when the components are approaching each other.

Note that these mechanisms are considered in the isosceles problem. In the planar system, the slingshot configurations leading to escape are searched by Agekian and Anosova (1991). However, surveying grid size in the phase space is coarse, and so it is necessary to investigate more intensively the condition of slingshot configurations leading to escape in the planar or three-dimensional three-body problem.

1.2 Goal of the research and outline of the thesis

The main purpose of the present paper is to explain the features of escapes by way of not only triple collision orbits but also binary collision orbits. The main result of the present paper is that the dominant motion for escape is a particular type of binary collisions, i.e., the slingshot close to isosceles configurations after the binary collision. In order to derive this result, we will investigate the free-fall three-body system. Triple collisions may occur in the free-fall problem. So this system is adequate to study the relation between escape phenomena and collisions. In the free-fall three-body problem, we will follow the two purposes mentioned at the beginning of the present chapter.

In Chapter 2, we will investigate the initial-value distributions of escape, binary collision and triple collision in the free-fall problem. In Section 2.3, we survey the initial-value space numerically. The dominant encounter for escape is the slingshot which experiences binary collision maintaining isosceles configurations approximately. See Section 2.4. By the survey, we find another type of encounter, exchange, in the free-fall problem with equal masses. It will be described in Section 2.5.

Motions close to triple collision will be considered in Subsection 2.4.2. We will find initial values of orbits which are sufficiently close to the initial value ending in triple collision but do not escape just after the first triple encounter. From the result, we find that the close triple encounter is not the only cause of escape phenomena. We will also find that escape orbits experiencing close triple encounter distribute around binary collision orbit. So we can conclude that binary collision is also an important factor.

In Chapter 3, we will compare the difference of physical features between respective encounters, slingshot and exchange, by the statistical analysis of the samples evaluated numerically. In Section 3.2, probabilities of escape due to respective encounters are evaluated and compared with each other. In Section 3.3, energy transfers due to respective encounters are evaluated and compared with each other. We will conclude that the slingshot

encounter is more important to the evolution of the system than the exchange encounter. In Section 3.4, conditions of slingshot configurations leading to escape in the free-fall problem are determined numerically, and frequent configurations of slingshot leading to escape are shown. In particular, the escape behavior expected in the above around binary collision orbits is confirmed in Subsection 3.4.2.

In Chapter 4, we will concentrate our attention to motions close to triple collision. In Section 4.2, we will prove that initial values of orbits leading to escape just after the first triple encounter distribute around the planar-isosceles orbits arbitrarily close to initial value ending in *homothetic-equilateral* triple collision, i.e., triple collision maintaining the equilateral triangle configuration. Using the result, we will prove that initial values of orbits which do not escape just after the first triple encounter also distribute arbitrarily close to the initial value ending in homothetic-equilateral triple collision. The planar-isosceles motion is shown to be important to escape phenomena around the homothetic-equilateral-triple-collision orbit. In Section 4.3, we will assert that these features around the special collision, are also established around the other triple collisions with the aid of systematical analysis by numerical integrations. From the results, it will be clear that behavior of the binary collision orbit close to triple collision tends to maintain planar-isosceles configuration. Using such a feature, it will be confirmed that binary-collision orbits are important to escape phenomena experiencing the close triple encounter.

In Chapter 5, we will compare the dynamical features in the free-fall problem shown by us and the scattering problem. The respective fractal structures of phase-space partitions of escape are similar to the structure in the free-fall problem. Therefore, we will conjecture that binary collision as well as triple collision are also crucial to escape in the different types of three-body systems, although we analyzed the limiting case, the free-fall system.

Before starting the project, in the next section, we will introduce the initial-value space in the free-fall problem, review initial-value dependence of escape orbits in the free-fall problem, and also review initial-value dependence of collision orbits in the free-fall problem, respectively.

1.3 Tools for studying the free-fall three-body problem

1.3.1 Initial-value space in the free-fall three-body problem

In the present subsection, we explain why studying the free-fall problem is favorable for considering the common purposes mentioned at the beginning of Subsection 1.1.1. After that, we introduce the initial-value space of the free-fall problem.

The free-fall problem has advantageous features in investigating the relation between collisions and escape phenomena. Since the total angular momentum of the system is zero, it contains triple collision orbits. Moreover, there exist both orbits which experience and do not experience binary collision. Because of the existence of collisionless orbits, we expect to extract some effects of binary collision upon escape phenomena. This is in contrast to the collinear and the planar isosceles systems with total negative energies. In these cases binary collision occurs inevitably.

Furthermore, the initial-value space is a low-dimensional subspace in a high-dimensional phase space. The phase space in the planar system is a five-dimensional manifold with constant energy. So, in general, a systematical survey by numerical integrations is difficult in the planar system. In the free-fall problem, however, the initial-value space is reduced to a two-dimensional surface which we will explain below. The dimension is low, and so systematical survey is possible.

Let us introduce the exact definition of the free-fall three-body problem (Agekian and Anosova, 1967; Tanikawa et al., 1995; Broucke, 1995). We consider the three-body problem in $\mathbf{R}^2$ of particles with positive masses $m_j > 0$, $j = 1, 2, 3$ which interact according to the mutual gravitational attraction. Let $\boldsymbol{q}_j \in \mathbf{R}^2$, $j = 1, 2, 3$, be the position vectors of the particles of mass m_j. Their dynamical evolution is described by the Newtonian equations of motion as

$$\ddot{\boldsymbol{q}}_j = \sum_{k \neq j}^{3} \frac{m_k}{r_{jk}^3}(\boldsymbol{q}_k - \boldsymbol{q}_j) \qquad \text{where} \quad r_{jk} = |\boldsymbol{q}_k - \boldsymbol{q}_j|. \tag{1.1}$$

Following Broucke (1995), we consider the rectangular (x, y)-coordinates in the plane. The half-plane $\{(x, y)|y \geq 0\}$ is denoted by $\grave{D}$. Let three mass points m_1, m_2 and m_3 stand still at $P(x, y) \in \{(x, y)|y \geq 0\}$, $A(-0.5, 0)$ and $B(0.5, 0)$, respectively. If m_1 changes its position on $\grave{D}$, then triangles with given masses located at the respective vertices are exhausted. Conversely, any weighted triangle is similar to one of the triangles

formed by m_1, m_2 and m_3 under rotation in $\mathbf{R}^2$ and reflection. Motions starting from similar weighted triangles transform into one another with appropriate changes of scales of length and time, so we identify these motions. Then the positions of m_1 specify all possible initial conditions, i.e., $\grave{D}$ is the initial-value space of the free-fall three-body problem with given masses.

The present paper explores the case where all particles have equal masses, i.e., $m_i = 1$, $i = 1, 2, 3$. In this case, the initial-value space can be further specified owing to the additional symmetry (Agekian and Anosova, 1967; Tanikawa et al., 1995). Let us define region D by

$$D = \{(x, y) | x \geq 0, y \geq 0, (x + 0.5)^2 + y^2 \leq 1\}. \tag{1.2}$$

Let m_1 stand at $P(x, y) \in D$. If m_1 changes position in D, then triangles satisfying the relations $\overline{AB} \geq \overline{PA} \geq \overline{PB}$ among edges are exhausted. Conversely, any triangle is similar to one of the triangles formed by m_1, m_2 and m_3. Motions starting from similar triangles transform into one another under appropriate changes of coordinates and time, so we identify these motions. Then a position of m_1, $P \in D$, specifies any possible initial condition with the equal-mass case. The initial-value space of the free-fall three-body problem with equal masses is D. Hereafter $\grave{D}$ is called the extended initial-value space. We will use $\grave{D}$ as well as D for later convenience.

In the case of equal masses, the initial-value set of isosceles configurations with the base of the same pair forms one-dimensional curve. We will call this an *isosceles curve.* Orbits starting from this curve maintain isosceles configurations. Let I_j denote an isosceles curve corresponding to the isosceles configuration with base $m_k m_l$ where each j, k, l belongs to a cyclic permutation of $1, 2, 3$. The equations of I_j, $j = 1, 2, 3$ can be represented by x and y:

$$I_1 : x = 0, \quad I_2 : (x + 0.5)^2 + y^2 = 1, \quad I_3 : (x - 0.5)^2 + y^2 = 1. \tag{1.3}$$

If we provide the unit length and the unit mass as $1[\mathrm{pc}]$ and $1[\mathrm{M}_\odot]$, respectively, then the unit time is 1.5×10^7[year]. If we provide the unit length and the unit mass as $1[\mathrm{AU}]$ and $1[\mathrm{M}_\oplus]$, respectively, then the unit time is 92[year]. The free-fall time, which is defined as the time necessary for the system to collapse to the triple collision starting from the equilateral triangle with unit edges until the triple collision, is equal to $\frac{\pi}{\sqrt{24}} \simeq 0.641$.

1.3.2 Escape criteria for the general three-body problem

In the general three-body problem, the classification of the types of final motion, i.e., motion as $t \to \infty$, is well-known after investigation by Chazy (1922). After that, many authors investigated the initial-value dependence of final motion. However, it is difficult to determine the types of motion for any given initial condition.

If we investigate the final motion by computer simulations without any criterion, it takes an infinite time to follow the orbits. Fortunately, there are criteria for the hyperbolic-elliptic motion, where one particle recedes to infinity with non-zero velocity and the other two particles form a binary as $t \to \infty$. Let r be the distance between the closest two particles, and ρ denotes the distance between the third particle and the gravity center of the closest particles. In order to determine that the motion is of hyperbolic-elliptic type, it is sufficient to prove that $\rho(t)$ increases indefinitely with order t as $t \to +\infty$ and $r(t)$ is bounded for $t > t_1$.

Yoshida (1972) developed escape criteria. Corollary by Yoshida (1972) is convenient to numerical integration. After that, Yoshida (1974) revised the criterion as follows:

Corollary (Yoshida, 1972, 1974). *Suppose that $h = -H > 0$ and $m_i \leq m_j$. Let*

$$\lambda = \frac{m_j}{m_i + m_j}, \qquad \text{and} \qquad \mu = \frac{m_i}{m_i + m_j}. \tag{1.4}$$

If there exist positives d and $a > \lambda$ such that

$$d \geq \frac{m_i m_j}{h}, \tag{1.5}$$

$$\rho(t_1) \geq ad \geq ar(t_1), \tag{1.6}$$

and moreover

$$\dot{\rho}(t_1) > \sqrt{2M\left\{\frac{\lambda}{\rho(t_1) + \nu d} + \frac{\nu}{\rho(t_1) - \lambda d}\right\}}, \tag{1.7}$$

then the motion of the system is of hyperbolic-elliptic type as $t \to +\infty$, and

$$r < \frac{m_i m_j}{h} \quad \text{for} \quad t \geq t_1. \tag{1.8}$$

Also, if $m_i \geq m_j$, then the above conditions are replaced by

$$a > \nu, \quad \text{and} \quad \dot{\rho}(t_1) > \sqrt{2M\left\{\frac{\lambda}{\rho(t_1) - \nu d} + \frac{\nu}{\rho(t_1) + \lambda d}\right\}}, \tag{1.9}$$

In the present thesis, the constant values d and a are fixed as

$$d = \frac{m_i m_j}{h} \qquad \text{and} \qquad a = 1, \tag{1.10}$$

and all masses are assumed to be equal to each other. Therefore, we will use the following formulae.

The escape criterion applied to the present work. *Let $h = -H > 0$. If at some arbitrary time $t = t_1$ the following conditions are satisfied:*

$$\rho(t_1) \geq \frac{m_i m_j}{h}, \tag{1.11}$$

$$\rho(t_1) \geq r(t_1), \tag{1.12}$$

and

$$\dot{\rho}(t_1) > \sqrt{2M\left\{\frac{1}{2\rho(t_1)+1} + \frac{1}{2\rho(t_1)-\lambda}\right\}}, \tag{1.13}$$

then the motion of the system is of hyperbolic-elliptic type as $t \to +\infty$, and

$$r < \frac{m_i m_j}{h} \quad \textit{for} \quad t \geq t_1. \tag{1.14}$$

The dynamical meaning of the escape criterion is the following. When the above inequalities are satisfied at some t_1, they remain so forever for $t > t_1$. These conditions separate the phase space into two regions: the region where the conditions are not satisfied (hereafter referred to as region I), and the region where they are satisfied (hereafter as region II). The passages of orbits are possible only in one direction: from the region I to the region II.

The procedure deriving the escape criterion is summarized as follows: first, a lower bound of the acceleration at a given time is derived; second, using the energy integral and the inequality representing the bounded acceleration, it is proved that the minimum distance is finite; finally, the escape velocity is shown to be positive forever using the above inequality.

1.3.3 Numerical search for collision orbits

Tanikawa et al. (1995) developed a systematical procedure searching for binary collision orbits and found the initial values which experience binary collisions in the free-fall problem.

The procedure is summarized as follows. The *close approach* is defined as a state of the system when the time-dependent distance between the closest two particles experiences a minimal value. Let us find a binary-collision orbit such that the collision occurs when the i-th close approach. Hereafter, we call such a collision orbit the *orbit* $B^{(i)}$. For a sufficiently small $R > 0$, there is a region on the initial-value space which includes the initial point of the binary orbit such that all orbits starting on the region experiences the approach of two particles within a distance R after the $(i-1)$-th close approach.

For each orbit, we sample the direction angle of the relative velocity between the two particles approaching at a distance R. These angle are denoted by $\phi \in [-\pi/2, \pi/2]$. Motions of the colliding particles are almost rectilinear at a binary collision when seen from their center of mass. So binary-collision orbits are characterized by $\phi \simeq 0$.

We consider two orbits under the opposite perturbations to the collision. Suppose that a direction angle of one orbit is $\phi > 0$ when a distance between the approaching particles becomes R. Then the angle of the other orbit is $\phi < 0$. Therefore, there is a sub-region where the direction angle is positive and the other sub-region where the angle is negative. Then initial values experiencing binary collision at the i-th close approach lies in between.

Tanikawa et al. (1995) examined the isosceles curves located on the boundary of D which corresponds to the known initial values of binary collision in order to justify the procedure. It was shown that the signs of the direction angles on the both sides of the isosceles curve are opposite.

The initial values satisfying $\phi = 0$ are detected for several integer numbers i. It was found that the initial values experiencing binary collision form one-dimensional curves on the two-dimensional initial-value space. A curve which consists of initial values experiencing binary collision is called a *binary-collision curve*.

This phenomenon can be suggested by the dimension analysis if a set of solution flows corresponding to binary-collision orbits intersect the initial-value space. However, the transversality can not be proved. The transversality is one of our numerical results.

Moreover, Tanikawa et al. (1995) found a lot of initial values leading to triple collision. It is obtained as a cross point of three binary collision curves where the respective

colliding pairs are different and the respective step numbers of minimal mutual distance until the collision are the same as each other. An initial point leading to triple collision is called a *triple-collision point.*

Chapter 2

Qualitative results

2.1 Introduction

In the present chapter, we will clarify the qualitative relation between escape phenomena and collisions. Most escape orbits are found to distribute around a particular type of binary-collision orbits. It becomes clear that among orbits which are close to triple-collision orbits, the escape orbits distribute around the binary-collision orbits.

In Section 2.2, we prepare for the numerical and analytical investigations in subsequent sections. Here, we define the state of triple encounter in order to investigate initial-value distribution of escape orbits, taking account of the frequency of triple encounters. There already exist several definitions of triple encounter based on the virial-equilibrium theorem. We simulate many free-fall systems under several definitions and clarify that these definitions fail in counting the number of triple encounters. Wide triple encounters have been frequently missed. Thus we should seek for a scale larger than the one which characterizes the virial equilibrium, and so we will find a suitable scale for the definition.

In Section 2.3, we study regions leading to escape on the extended initial-value space $\grave{D}$ by detailed numerical computations, and we find a fractal distribution of escape orbits. In most escape orbits, escape phenomena occur after the triple encounter of slingshot type, where an escaper passes through between a binary whose components are receding from each other.

In Section 2.4, we compare the initial-value dependences of escape and collision in order to investigate what is the dominant factor for the fractal structure. As a result, we see that on the initial-value space, regions where the systems lead to escape after surviving the first triple encounter spread around triple collision points. Moreover, we show that the respective regions corresponding to the different particle's escape converge

to triple-collision points, and regions where no particle escapes after surviving the first triple encounter also converge to triple-collision points. This shows that phase trajectories without escape exist in any small neighborhood of a triple collision trajectory, and so we can comprehend that the occurrence of close triple encounter is not sufficient for escape.

We clarify that not only triple collision but also binary collision plays the dominant role on escape. The escape regions converge to triple-collision points. In a neighborhood of a triple-collision point, each of the escape regions spreads along a binary collision curve. The escape regions extend around particular binary collision curves, where the configuration after the triple encounter maintains approximately isosceles. Anosova (1991) emphasized the importance of slingshot behavior. We find that among various slingshot motions, the above special slingshot lies at the center of each escape regions. This isosceles-like slingshot will be called the *near-isosceles slingshot.*

We discover a different type of triple encounter in the free-fall system with equal masses in Section 2.5. It is the exchange type: successive binary close approaches occur. Escape regions due to slingshot and due to exchange are connected each other. Thus we have defined the dynamically reasonable boundaries between them. From the location of the boundaries, we have concluded that exchange-escape orbits do not distribute around any triple-collision orbit. It suggests that the escape due to slingshot is more important to the evolution of the system than the escape due to exchange.

A classification of the triple encounters leading to escape has been summarized by Anosova (1986, 1991) for both equal-mass and unequal-mass cases. In the system with zero angular momentum, there are two types of triple encounters, slingshot and exchange.

In the slingshot encounter, a temporary binary is first formed, while the third particle passes through between components of the binary when the components are receding from each other. This phenomenon leads to acceleration of the passing particle. Passage through a line segment connecting the binary components is called the *syzygy crossing.*

In contrast to acceleration due to slingshot, the syzygy crossing when binary components are approaching affects decelerating phenomenon of third particle. We will call it the *inverse slingshot.*

Another type of triple encounter is *exchange*. Successive approaches between two particles occur. We should distinguish between the exchange type of triple encounters and the exchange type of final evolutions. Chazy (1922) classified types of final states and conjectured possible evolutions from original states to final ones. Here, the final state is defined by asymptotic motion as time $t \to +\infty$, whereas the original state is defined by

motion as $t \to -\infty$. Recently Marchal (1990, p.424,425,494,495) summarized the main combinations between original and final states. According to them, the definition of exchange is that the original state is escape for one particle (say m_i, $i = 1, 2$, or 3) and the final state is escape for another particle, i.e., m_j, $j \neq i$.

We must notice that exchange type of final evolution is impossible in the free-fall problem. Both time evolution as $t \to +\infty$ and one as $t \to -\infty$ are identical by the symmetry of time inversion in this problem. Thus in the present thesis, exchange type of triple encounter is called *exchange* simply.

Anosova (1986, 1991) mentioned that exchange can occasionally result in escape of the particles of intermediate or maximum mass in the unequal-mass case. Anosova also asserted that escape phenomena after exchange type of triple encounter seldom take place in the equal-mass system. However, we will show that probability of exchange-type escape is not small in the free-fall problem with the equal-mass case in Section 3.2 of the next chapter.

Aarseth et al. (1994b) suggested the existence of orbits showing a strange triple encounter which is different from slingshot by their statistics. So they conjectured that their strange encounters are due to exchange. However, we have found that the procedure to sample the behavior during triple encounter is not reasonable. More detailed explanation will appear in Subsection 3.4.1.

2.2 Triple-encounter criteria

2.2.1 Previous and new definitions of triple encounter

We will classify escape orbits by the frequency of triple encounters until leading to escape. Any three-body system with negative-total energy which begins to shrinking once expands if the system does not end in triple collision. After that, the size of the three-body configuration will oscillate as long as one particle does not escape to infinity or the system does not end in triple collision. Let us define the triple encounter as the following way.

Let $t_{\min}$ be a time t when the time-dependent moment of inertia $I(t)$ becomes minimal or zero. Let $\boldsymbol{\rho}$ be a vector from the gravity center of the nearest two particles to the third particle. The absolute value of $\boldsymbol{\rho}$ is denoted by ρ (i.e., $\rho = |\boldsymbol{\rho}|$). The total energy of the system is h. We assume $h < 0$.

If $\rho(t_{\min}) > \rho_0$, the system is defined as out of triple encounter, where

$$\rho_0 = \frac{M_*}{|h|}, \qquad M_* = m_1m_2 + m_2m_3 + m_3m_1 \tag{2.1}$$

Otherwise, we define a time interval during a triple encounter as follows.

Before defining the time interval, we introduce t_ρ^-, t_ρ^+, $t_{\rm mom}^-$, $t_{\rm mom}^+$, $t_{\rm inf}^-$, and $t_{\rm inf}^+$. Let t_ρ^- and t_ρ^+ $(t_\rho^- < t_\rho^+)$ denote endpoints of a connected maximal interval containing $t_{\min}$ on which the system satisfies $\rho \le \rho_0$ if $I(t_{\min}) \neq 0$ and such endpoints exist. If such an initial time or a terminal time does not exist, t_ρ^- or t_ρ^+ is considered as $-\infty$ or $+\infty$, respectively. For example, it is possible that no particle recedes from the other particles and $\rho(t)$ continues to be less than ρ_0. In this case, we define $t_\rho^+ = +\infty$.

Let $t_{\rm mom}^-$ and $t_{\rm mom}^+$ $(t_{\rm mom}^- < t_{\rm mom}^+)$ denote endpoints of a connected maximal interval containing $t_{\min}$ on which the system satisfies $I \le I_0$ if $I(t_{\min}) \neq 0$ and such endpoints exist, where

$$I_0 = \frac{M_*^3}{4Mh^2}. \tag{2.2}$$

If $I(t_{\min}) = 0$ which corresponds to the triple collision, we define $t_{\rm mom}^+ = t_{\min}$. If such an initial time or a terminal time does not exist, $t_{\rm mom}^-$ or $t_{\rm mom}^+$ is considered as $-\infty$ or $+\infty$, respectively.

Let $t_{\rm inf}^-$ and $t_{\rm inf}^+$ $(t_{\rm inf}^- < t_{\rm inf}^+)$ denote endpoints of a connected maximal interval containing $t_{\min}$ on which the system satisfies $\ddot{I}(t) \ge 0$ if such points exist. If $I(t_{\min}) = 0$, we define $t_{\rm inf}^+ = t_{\min}$. If such an initial time or a terminal time does not exist, $t_{\rm inf}^-$ or $t_{\rm inf}^+$ is considered as $-\infty$ or $+\infty$, respectively.

Triple-encounter criterion (Our definition of triple encounter). *The system with negative energy is called to be in triple encounter during the time interval* $t \in [t_{\rm enc}^-, t_{\rm enc}^+]$, *where an initial time* $t_{\rm enc}^-$ *and a terminal time* $t_{\rm enc}^+$ *of the triple encounter are defined as*

$$t_{\rm enc}^- = \max\{t_\rho^-, t_{\rm mom}^-, t_{\rm inf}^-\}, \qquad t_{\rm enc}^+ = \min\{t_\rho^+, t_{\rm mom}^+, t_{\rm inf}^+\}. \tag{2.3}$$

At the time $t_{\rm enc}^+$, *the system is called to survive the triple encounter.*

Until we revise the definition of the triple encounter as above, the following three definitions are formulated. The first definition is presented by Agekian and Martynova (1973). They paid attention to the time-evolution of the moment of inertia.

Definition 2.1 (Agekian and Martynova, 1973). *The system with negative energy is called to be in triple encounter during the time interval* $t \in [t_{\rm inf}^-, t_{\rm inf}^+]$.

Anosova and Zavalov (1989) formulated another definition in terms of the perimeter of the triangle formed by the three particles.

Definition 2.2 (Anosova and Zavalov, 1989). *The system with negative energy is called to be in triple encounter if* $\sigma < \sigma_0$, *where* σ *is a perimeter of the configuration triangle and*

$$\sigma_0 = 3d_{\rm unit}, \qquad d_{\rm unit} = \frac{\rho_0}{2}. \tag{2.4}$$

Recall that ρ_0 is expressed in eq.(2.1). Physically, $d_{\rm unit}$ is the mean harmonic separation between the particles in virial equilibrium. Thus, in this definition, the size of the system during the triple encounter is considered as smaller than the proper size of the length-scale in virial equilibrium.

Here, we review the derivation of the length-scale $d_{\rm unit}$ in virial equilibrium. When the system is in steady state, it is considered that $\ddot{I}(t) = 0$. It is known that any gravitational n-body system satisfies the so-called Lagrange-Jacobi equation:

$$\frac{d^2}{dt^2} I(t) = 2(U(t) + 2h), \tag{2.5}$$

where h and U denote the total energy and the absolute value of the potential energy, respectively. The mean harmonic distance $d_{\rm unit}$ is defined as

$$\frac{1}{d_{\rm unit}} \sum_{j \neq k} m_j m_k = \sum_{j \neq k} \frac{m_j m_k}{r_{jk}} = U. \tag{2.6}$$

where m_j and r_{jk} denote the mass of the j-th particle and the distance between particles j and k, respectively. The equality $U = -2h$ is considered to hold in virial equilibrium, and so

$$d_{\rm unit} = \frac{\sum_{j \neq k} m_j m_k}{U} = \frac{\sum_{j \neq k} m_j m_k}{2|h|}. \tag{2.7}$$

Therefore, $d_{\rm unit}$ is described as in eq.(2.4).

The following definition is developed by Junzo Yoshida (1997) from Definition 2.1. The moment of inertia is considered again.

Definition 2.3 (J.Yoshida, 1997). *The system with negative energy is called to be in triple encounter during the time interval* $t \in [t^-_{\rm mom}, t^+_{\rm mom}]$.

In Triple-encounter criterion, we unify Definition 2.1, Definition 2.3, and the condition $\rho(t) \leq \rho_0$. Definition 2.1 and Definition 2.3 consider the moment of inertia $I(t)$ while the perimeter of the configuration triangle $\sigma(t)$ is used in Definition 2.2.

In Section 4, we will follow the time-evolution of the square root of the moment of inertia $\sqrt{I(t)}$ in order to investigate behavior near triple collision by the blow-up analysis which is explained later. Thus, if we use the moment of inertia $I(t)$ in the criterion of triple encounter, it is easy to check results by the blow-up analysis with the criterion. Therefore, we choose Definition 2.1 and Definition 2.3 while we eliminate Definition 2.2 which does not mention any relation with $I(t)$ directly.

However, if we adopt only Definition 2.1 in the criterion of triple encounter, it is useless since Definition 2.1 is too week to define the triple encounter. We will explain it in the next subsection with the numerical results. On the other hand, Definition 2.3 is too strong to define the triple encounter. Thus, some triple encounters are not detected under Definition 2.3 although three particles approach each other widely. We will also confirm it in the next subsection with the numerical results. In order to define the so-called wide triple encounter, it is necessary to add some condition to the criterion of triple encounter. The condition $\rho(t) \leq \rho_0$ is considered to be suitable. The reason is described in the next subsection.

2.2.2 Numerical experiments

Global results under the respective definitions

Let us investigate the initial-value dependence of escape orbits by surveying the initial-value space numerically. We search for system leading to escape until the n-th triple encounter by the respective definitions (where $n \in \mathbf{N}$). and make four diagrams showing the initial-value distributions of the n-th escape orbits under the respective definitions of triple encounter. After that, we compare four diagrams with each other.

We continue to integrate orbits according to the following flow-chart under each of the criteria of triple encounter, Definition 2.x ($x \in \{1, 2, 3\}$) and Triple-encounter criterion. Let $\dot{\rho}$ be the radial component of the time derivative of $\boldsymbol{\rho}$, i.e.,

$$\dot{\rho} = \frac{\boldsymbol{\rho} \cdot \dot{\boldsymbol{\rho}}}{\rho^2}. \tag{2.8}$$

The initial-value space is divided into a large amount of small rectangle grids. We investigate the time-evolution of the system starting at the vertices of the grids.

The flow-chart of the integration until the n-th triple encounter by Definition 2.x or by Triple-encounter criterion.

If $\dot{\rho} > 0$, *then*
  if the system satisfies the escape criterion by Yoshida (1972, 1974), then
    the final state is determined as escape
    and the integration is terminated,
  else if $\rho > 20 d_{\rm unit}$, *then*
    the system is considered as the conditional escape
    and the integration is terminated,
  endif.
Else if $\dot{\rho} \leq 0$, *then*
  if the system is in the n-th triple encounter due to Definition 2.x
  or Triple-encounter criterion, then
    the system begins to shrink after surviving the n-th triple encounter
    and the integration is terminated,
  endif,
endif.

There are two kinds of the conditional-escape orbits: one is an oribt leading to escape which does not satisfy the escape criterion for $\rho \leq 20 d_{\rm unit}$; the other is an orbit in which a particle is ejected from a binary by more than $20 d_{\rm unit}$.

Figure 2.1 shows the numerical result of the initial-value distribution of escape orbits where the system leads to escape until the third triple encounter ($n \leq 3$) under Definition 2.1. We integrated 2×10^4 initial points. For convenience, the structure beyond the circular boundary is also shown. The size δx of the grid elements in the x direction on the initial-value space (x, y) is the same as the one in the y direction, and equal to 5×10^{-3}.

Similarly, Figures 2.2, 2.3, and 2.4 show the initial-value distributions of escape orbits until the third triple encounter under Definition 2.2, Definition 2.3, and Triple-encounter criterion, respectively.

In four figures, initial values of systems leading to escape until the third triple encounter are shown as three kinds of marks on the initial-value space. A dark-gray element of grids stands for the initial value where the system escapes after the first triple encounter. A light-gray element and a cross (+) represent the initial values leading to escape after the second and the third triple encounters, respectively. The isosceles curves are shown in the figures.

Later in the present subsection, we will give detailed descriptions of the reason why Triple-encounter criterion is more suitable for the definition of triple encounter than the other previous definitions. Here, we summarize the scenario.

Anosova and Zavalov (1989) surveyed the initial-value space in the free-fall three-body problem systematically for the first time, and they found a sequence of at least five band-like regions leading to escape after the first triple encounter by Definition 2.2. Here, these regions are called $S_i \subset D$ for $i = 1, 2, \cdots, 5$. Moreover, they expected that S_i continues to infinity.

We can confirm in Section 2.4 that there is an infinite sequence of the first escape regions S_i, $= 1, 2, \ldots$ in the shape of bands which accumulates to the lower-right corner $(0.5, 0)$ on the initial-value space D. Each of the band-like regions extends to the x-axis and the isosceles curve $(x+0.5)^2+y^2 = 1$. Therefore, we consider the following conjecture as true.

Conjecture 2.1. *There exist escape points after the first triple encounter around the lower-right corner* $(0.5, 0)$ *on the initial-value space.*

Despite the coarseness of the grid, we can see that band-like escape regions other than S_i cross the x-axis. Some regions fold back and do not contact with the isosceles curve. The band containing $\{(x, y)|x = 0.11, y < 0.1\}$ continues upwards and bends around $y = 0.32$. This band will be denoted by A in the present subsection. The folding band does not accord with any S_i since S_i includes a part of the isosceles curve. In fact, A is located in between S_1 and S_2. Note that S_1 distributes around y-axis. See

also Fig.2.10. The x-positions of S_i, $i = 2, 3, 4$ on the x-axis are 0.180, 0.255, 0.295, respectively. Therefore, we consider the following conjecture as true.

Conjecture 2.2. *Systems in the bended band-like region lead to escape after at least the second triple encounter.*

We will confirm this conjecture later in the present section by observing the time-evolution of the moment of inertia.

See Table 2.1 and notice that only the result in Figure 2.4 which is the simulated result under Triple-encounter criterion satisfies two conjectures. Definition 2.1, Definition 2.2, and Definition 2.3 are not suitable for the behavior of whole orbits.

We used the TRIPLE code of Aarseth for integration leading to escape. It is composed by the numerical method with Aarseth-Zare (1974) regularization and Bulirsch-Stoer (1966) integrator. We adopt the escape criterion of Yoshida (1972, 1974) which is reviewed in Subsection 1.3.2.

Table 2.1: Definitions satisfying two conjectures.

	Conjecture 2.1	Conjecture 2.2
Figure 2.1 (Definition 2.1)	false	true
Figure 2.2 (Definition 2.2)	true	false
Figure 2.3 (Definition 2.3)	true	false
Figure 2.4 (Triple-encounter criterion)	true	true

Problems in Definition 2.2

There have already been numerical results simulated systematically under Definition 2.2. Thus, before investigating problems of Definition 2.1, we show the problems of Definition 2.2.

Anosova and Zavalov (1989) showed orbits starting in the escape regions S_i. According to them, the systems in S_i experience the i-th close approach of the two particles m_1 and m_3 during triple encounter.

Tanikawa et al. (1995) found that there are triple-collision points on the isosceles

curve such that the triple collision occurs at the time of the i-th binary collision between m_1 and m_3 for any $i \in \mathbf{N}$. Therefore, it is expected that also for $i \geq 6$, there are systems such that the first triple encounter occurs at the i-th close approach of m_1 and m_3. We will make clear in Section 2.4 that each of triple-collision points on the isosceles curve is included in the first escape region S_i for a sufficiently large i. Thus, we conjecture that the regions S_i form an infinite sequence and accumulate to the lower-right corner of D, i.e., $B(0.5, 0)$.

Anosova and Zavalov (1989) simulated only 5000 initial points. Thus we survey the initial-value space with a finer grid. The number of the integrated systems is quadruple. As a result, we show many initial points in the lower-right part of the initial-value space in Fig.2.2. There are many regions S_i, $i \geq 6$ leading to escape after the first triple encounter in the lower-right corner, and so Conjecture 2.1 is true.

However, except for S_i, $i = 1, 2, \cdots$, there is an additional band A on $\{(x, y) | x = 0.11, y < 0.1\}$ where the system leads to escape after the first triple encounter under Definition 2.2.

The behavior of the system starting on the additional band is shown in Fig.2.5(a). The upper frame shows the time-dependence of the distances between the respective particles and the perimeter of the configuration triangle. In the lower frame, the time-dependence of the moment of inertia is shown. The initial value is $(0.11, 0.07)$. The three curves in the upper frame stand for the distances between the respective two particles. The bold curve represents the distance between m_2 and m_3. The lightest and the middle-gray curves show the distances between m_3 and m_1, and m_1 and m_2, respectively. The fine curve stands for the time-dpendence of the perimeter. The horizontal line in the upper frame represents the critical value of the perimeter σ_0. Recall that σ_0 is expressed in eq.(2.4). In the lower frame, the curve shows the time-evolution of the moment of inertia $I(t)$. The horizontal line represents the critical value I_0. Recall that I_0 is described in eq.(2.2). The time interval indicated by the bold curve between the vertical lines means the period with positive $\ddot{I}(t)$. We will consider the relation between $I(t)$ and the triple encounter later in the present subsection.

At the terminal point of the curve (at $t = 1.2606$), the system satisfies the escape criterion. In the time interval $t \in [0, 1.2606]$, it is apparent that the triple encounters occurs twice. There are two minimal values of $I(t)$ in the figure. At the times $t = 0.4834, 1.1823$ which are indicated by two arrows, $I(t)$ becomes minimal.

At the first minimal time, the perimeter also becomes small. However, at this time

the perimeter is slightly larger than the critical value σ_0. Thus, the system can not be called in triple encounter around this time according to Definition 2.2. On the other hand, the perimeter is less than σ_0 around the time $t = 1.1823$ denoted by the second arrow. Therefore, the system is said to experience triple encounter around $t = 1.1823$ for the first time, and the system is judged to escape after the first triple encounter although the fact is the escape after the second triple encounter.

Moreover, we found another evidence showing that the system in Fig.2.5(a) must be in triple encounter twice until it escapes. A similar motion as the one in Fig.2.5(a) is found in Fig.2.5(b) where the system starts at the initial point $(0.18, 0.30)$. This result implies that the initial point $(0.18, 0.30)$ is located in the band which is considered as the continuation of the additional band A. One can confirm it in Fig.2.2. In this case, however, the system escapes after the second triple encounter according to Definition 2.2. In fact, the perimeter becomes less than the critical value σ_0 around the time $t = 0.5605$ denoted by the first arrow. After that, the perimeter becomes minimum at $t = 1.3559$ and less than σ_0 again. As a result, the system (a) starting at $(0.11, 0.07)$ must also be in triple encounter twice until it escapes.

Problems in Definition 2.1

Agekian and Martynova (1973) paid attention to the time-evolution of the moment of inertia. (See Definition 2.1.) This definition means that the system with negative energy is called to be in triple encounter during $\ddot{I}(t) \geq 0$. According to this definition, however, the system may be said to be in triple encounter even if $I(t)$ is monotonically increasing or decreasing without any minimal value. In Fig.2.5(a), there are five time-intervals with negative $\ddot{I}$. In these intervals, if $I(t)$ becomes minimal or the system ends in triple collision during $\ddot{I} > 0$, it may be suitable that the system is called to be in triple encounter.

Figure 2.1 shows the initial-value distributions of escape orbits until the third triple encounter based on Definition 2.1. According to this definition, the system starting on the additional band A leads to escape after the second triple encounter. It agrees with the fact. See again the behavior of $I(t)$ in Fig.2.5.

However, $I(t)$ often becomes minimal even if three particles do not approach each other. We show two examples in Figs.2.6(a) and (b). Notations in the figures are the same as those in Figs.2.5(a) and (b). We do not draw the time-evolution of the triangle perimeter.

In Fig.2.6(a), the system starts at the initial value $(0.44, 0.12)$. At the terminal point of the curve (at $t = 0.6457$), the system satisfies the escape criterion. In this time interval, it is intuitively obvious that the triple encounter occurs only once although there are two minimal values of $I(t)$ shown by arrows in the figure. The size of the system is still large at the first minimal time ($t = 0.0391$).

In fact, m_2 is still distant from the other particles around the first minimal. See the three curves in the upper frame. The three curves stands for the distance of the respective two particles as the same way in Figs.2.5(a) and (b). After eight close approaches between m_3 and m_1, the configuration size of the system becomes small. The system begins to expand, and so m_3 leads to escape.

In Fig.2.6(b), another example is shown for the the initial value $(0.12, 0.44)$. The notation is the same as in the figure (a). There are three minimal values at times $t = 0.5690, 1.3447, 2.2053$. At the terminal point of the curve (at $t = 2.389$), the system satisfies the escape criterion. We see intuitively that the triple encounters occur only twice.

In fact, m_3 is receding from the other particles around the second minimal of $I(t)$. After three particles are released with zero velocities, the close approach between m_3 and m_1 occurs. The configuration size of the system becomes small around the time at the first minimal. The system begins to expand, and so m_3 recedes from the other particles. After three close approaches between m_1 and m_2, the system shrinks again. As a result of the triple encounter, the system satisfies the escape criterion where m_1 leads to escape.

Problems in Definition 2.3

We found in the above numerical experiment that the condition that the curve of $I(t)$ is concave from below is insufficient to determine triple encounter. Therefore, we need a suitable critical value of the moment of inertia. J.Yoshida (1997) found that I_0 is suitable for distinguishing the state of the triple encounter. Recall that I_0 is described in eq.(2.2). He proved that the inequality $I < I_0$ is a sufficient condition to satisfy $\ddot{I} > 0$, and so defined the triple encounter as in Definition 2.3. We will review the proof in the end of the present section.

Theorem by J.Yoshida (1997) *If* $I(t) \leq I_0$, *then* $\ddot{I}(t) > 0$.

Note that the equality $\ddot{I} = 0$ holds in virial equilibrium. Thus, by the definition of

triple encounter, the size of the system during triple encounter is smaller than the size in virial equilibrium.

Figure 2.3 shows the initial-value distributions of escape orbits until the third triple encounter defined by J.Yoshida (1997). According to Definition 2.3, the systems starting at $(0.44, 0.12)$ and $(0.12, 0.44)$ lead to escape after the first and the second triple encounters, respectively. Both cases agree with the fact. See Figs.2.6(a) and (b).

However, the problem about the additional band A appears again. The behavior starting on A around $\{(x, y)|x = 0.11, y < 0.1\}$ is regarded as the escape after the first triple encounter although the fact is the escape after the second triple encounter. See Fig.2.5(a) again. In the upper frame of the figure, the curve $I(t)$ does not crosses the critical level I_0 around the time $t = 0.4834$ with the first minimal value of $I(t)$. Thus, the system is said to be out of triple encounter around this time by J.Yoshida's definition.

Results under the new definition

We confirmed that some systems do not satisfy Definition 2.3 when three particles approach each other widely. It is necessary to add some condition of the so-called wide triple encounter to Definition 2.3.

The definitions of the triple encounter are hitherto related with the virial equilibrium. In both Definition 2.1 and Definition 2.3, the state of the triple encounter begins and ends when $\ddot{I}(t) = 0$. Definition 2.2 regards the triple encounter as the state during the period when the mean distance between particles is less than the length-scale in virial equilibrium.

The mean harmonic distance between the particles in virial equilibrium is equal to $d_{\text{unit}} = \rho_0/2$. However, this length-scale $\rho_0/2$ is so small for defining the wide triple encounter, and another scale which is larger than the virial scale should be required. We consider ρ_0 as the second smallest scale.

This is suggested from the following fact: the distance between the nearest two particle is bounded from above. Let r_{min} be the distance between the nearest particles. It is clear that the inequality $r_{\text{min}} \leq \rho_0$ always holds for the negative total energy even if a pair of the closest particles may change successively. This is because

$$|h| \leq \frac{m_1 m_2}{r_{12}} + \frac{m_2 m_3}{r_{23}} + \frac{m_3 m_1}{r_{31}} \leq \frac{m_1 m_2 + m_2 m_3 + m_3 m_1}{r_{\text{min}}}. \tag{2.9}$$

The left inequality is derived from the fact $|h| \leq U$. Therefore, we consider that the system is in triple encounter when the distant particle approaches the nearest particle within ρ_0. See Triple-encounter criterion.

Moreover, the numerical investigation by Agekian and Anosova (1990) shows that the condition $\rho(t) \leq \rho_0$ is suitable for the definition of the triple encounter. They evaluated minimal values of the time-dependent $\rho(t)$ for 200 systems. The total energy is fixed at $h = -\sum_i^3 m_i/2$. It is found from their results that all cases satisfy $\min \rho(t) < 2.0$ in the simulated samples. Notice that h is normalized at $h = -3/2$ in the equal-mass case, and so $r_{\min} = 2$. We conjecture that any three-body system satisfies the inequality $\rho(t) \leq r_{\min}$, and so we consider this inequality as the condition of the triple encounter.

Figure 2.4 shows the initial-value distributions of escape orbits until the third triple encounter defined by us. It is clear that the system starting in the additional band A leads to escape after at least the second triple encounter. We confirmed that each of the systems in Figs.2.5(a) and (b) experiences triple encounters twice until it leads to escape although a number of triple encounters is counted as one in the systems starting at the initial values of the figures if Definition 2.2 and Definition 2.3 are adopted. See also Figs.2.2 and 2.3. Both initial values are located on A. Only in Fig.2.1, the band A is the region where the system leads to escape after the second triple encounter.

In Fig.2.1, however, systems leading to escapes after the first triple encounters are rare around the lower-right corner $(0.5, 0)$ on the initial-value space. Except this figure, Figures 2.2, 2.3, and 2.4 show that many initial points around the corner $(0.5, 0)$. Recall that the respective figures follow Definition 2.2, Definition 2.3, and Triple-encounter criterion. Agekian and Anosova (1989) and we conjecture that band-like regions form an infinite sequence converging to the corner $(0.5, 0)$. On these band-like regions, systems lead to escape after the first triple encounter. We will explain in the next section that this conjecture about convergence is adequate.

Let us emphasize here that only Figure 2.4 where the triple encounter is defined by us satisfies two conjectures which are the existence of an infinite-sequence bands and the non-existence of an additional band where systems lead to escape after the first triple encounter. See Table 2.1 again.

2.2.3 Similarity between Definition 2.2 and Definition 2.3

Finally, we discuss the relations among the previous definitions. Definition 2.1 and Definition 2.3 consider the moment of inertia. Definition 2.3 is more restrictive than Definition 2.1. On the other hand, Anosova and Zavalov (1989) used the configuration perimeter in Definition 2.2, and so this definition is not related to the moment of inertia $I(t)$ directly.

However, the numerical results surveyed on the initial-value space by Definition 2.2 and Definition 2.3 are similar to each other although both methods counting triple encounters are wrong in some systems. See Figs.2.2 and 2.3. Definition 2.2 and Definition 2.3 have some relations with the virial theorem. We expect that both definitions have some direct relation with each other. In other words, we expect some relations between Definition 2.2 and the moment of inertia. So we will confirm it.

J.Yoshida (1997) proved that the inequality $I \leq I_0$ is a sufficient condition of $\ddot{I} \geq 0$. We found that Definition 2.2 also satisfies $\ddot{I} \geq 0$ if three masses are equal. In other words, $I(t)$ has at most only one minimal value during the time interval with $\sigma \leq \sigma_0$. It is a similar statement as Theorem by J.Yoshida (1997). Therefore, both results in Figs.2.2 and 2.3 must be similar to each other.

According to the next lemma which is proved later, $\ddot{I} > 0$ while $\sigma < \sigma_0$ if three masses are equal.

Lemma 2.1. *If $\sigma < \bar{\sigma}_0$, then $\ddot{I} > 0$, where*

$$\bar{\sigma}_0 = \frac{9m'\bar{m}}{2|h|}, \tag{2.10}$$

and m', $\bar{m}$ and $\bar{m}'$ are the smallest, middle and the largest of the three masses, respectively (i.e., $m' \leq \bar{m} \leq \bar{m}'$).

Proof. Since $m' \leq \bar{m} \leq \bar{m}'$,

$$U = \frac{m_1 m_2}{r_{12}} + \frac{m_2 m_3}{r_{23}} + \frac{m_3 m_1}{r_{31}} \geq m'\bar{m}\left(\frac{1}{r_{12}} + \frac{1}{r_{23}} + \frac{1}{r_{31}}\right). \tag{2.11}$$

Therefore,

$$\sigma U \geq m'\bar{m}(r_{12} + r_{23} + r_{31})\left(\frac{1}{r_{12}} + \frac{1}{r_{23}} + \frac{1}{r_{31}}\right) \geq 9m'\bar{m}, \tag{2.12}$$

and so

$$U \geq \frac{9m'\bar{m}}{\sigma}. \tag{2.13}$$

From the assumption,

$$\frac{9m'\bar{m}}{\sigma} > 2|h|. \tag{2.14}$$

and so the above two inequalities yield $U > 2|h|$. Therefore, $\ddot{I}(t) > 0$. □

Notice that for any mass ratio, the following inequality holds:

$$\sigma_0 \leq \bar{\sigma}_0, \tag{2.15}$$

since

$$M_* = m'\bar{m} + (m' + \bar{m})\bar{m}' \geq 3m'\bar{m}. \tag{2.16}$$

With equal masses ($m_j = 1, j = 1, 2, 3$), the equality holds as

$$\sigma_0 = \bar{\sigma}_0 = \frac{9}{2|h|}. \tag{2.17}$$

In the final part of the present section, we referred to the proof of Theorem by J.Yoshida (1997): if $I(t) \leq I_0$, then $\ddot{I}(t) > 0$. Sibahara and Yoshida (1963) derived the following inequality.

$$U \geq \sqrt{\frac{M_*^3}{MI}}, \tag{2.18}$$

which we will also derive later. With the assumption $I(t) \leq I_0$, eq.(2.2) yields

$$\sqrt{\frac{M_*^3}{MI}} > 2|h|. \tag{2.19}$$

The above two inequalities result in $U > 2|h|$, i.e., $\ddot{I} > 0$.

We review the proof of eq.(2.18). Consider three points P_j, $j = 1, 2, 3$ which are located at

$$P_j = \left(r_{kl}^2, \frac{1}{r_{kl}}\right), \tag{2.20}$$

on the (x, y)-plane, where (j, k, l) is $(1, 2, 3)$ or its cyclic permutation. These points are located on a curve $x = 1/y^2$. At each point P_j, we give a mass $m_k m_l$. The gravity center of the weighted points standing at

$$(x_c, y_c) = \left(\sum_{k \neq l} \frac{m_k m_l r_{kl}^2}{M_*}, \sum_{k \neq l} \frac{m_k m_l / r_{kl}}{M_*}\right) = \left(\frac{MI}{M_*}, \frac{U}{M_*}\right). \tag{2.21}$$

lies in the triangle formed by the three points. Hence, $x_c \geq 1/y_c^2$, and so

$$\frac{MI}{M_*} \geq \left(\frac{M_*}{U}\right)^2. \tag{2.22}$$

Therefore,

$$IU^2 \geq \frac{M_*^3}{M}. \tag{2.23}$$

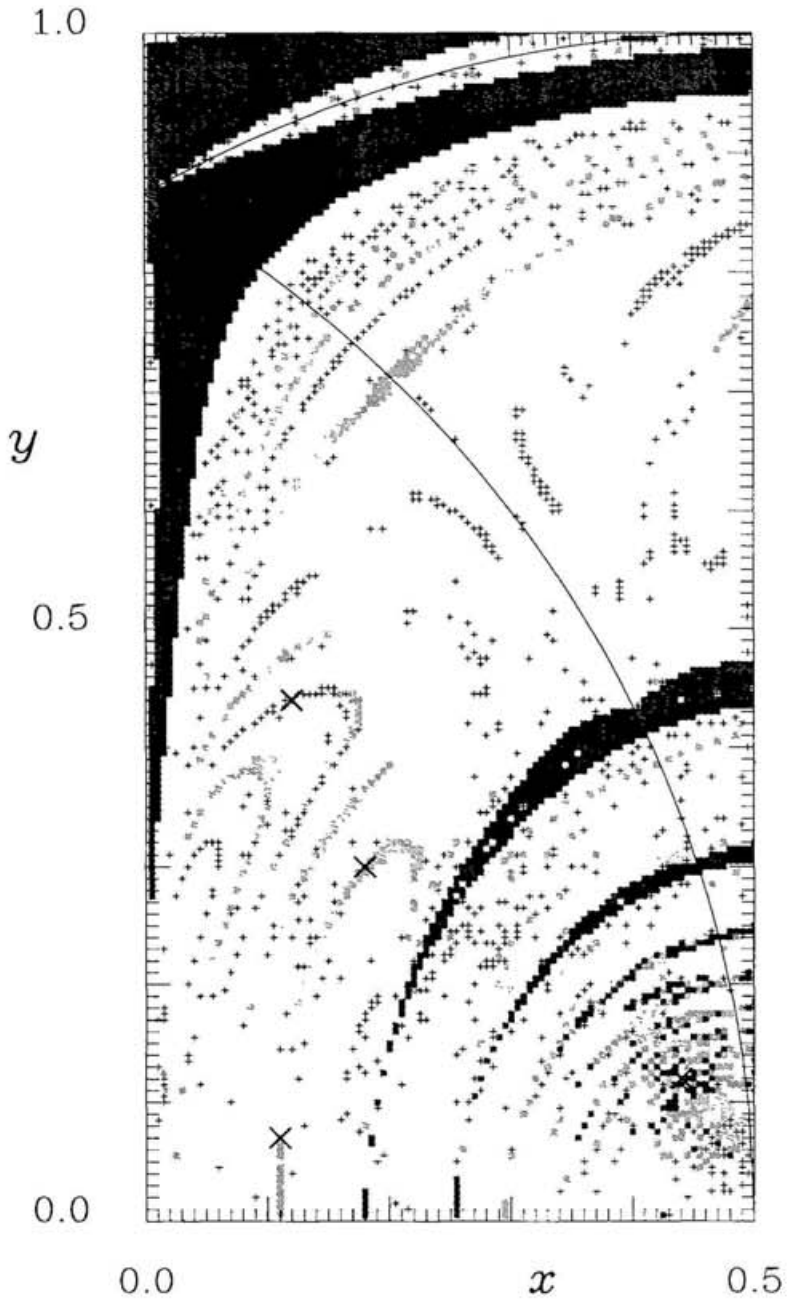

Figure 2.1: Initial-value distribution of escape orbits until the third triple encounter under Definition 2.1 (Agekian and Martynova, 1973). Four crosses represent initial values show that the respective time evolution of the distance between two particles and the moment of inertia in the succeeding figures.

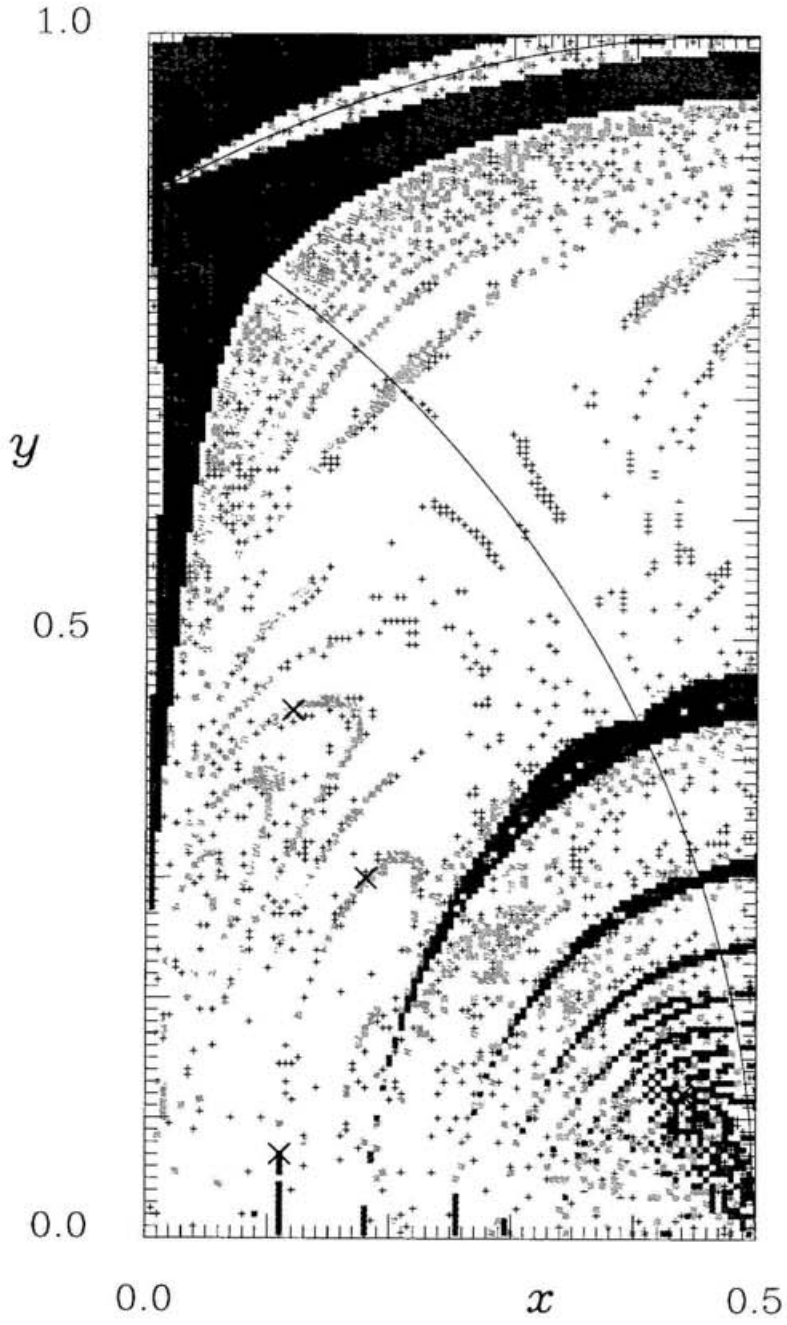

Figure 2.2: Initial-value distribution of escape orbits until the third triple encounter under Definition 2.2 (Anosova and Zavalov, 1989).

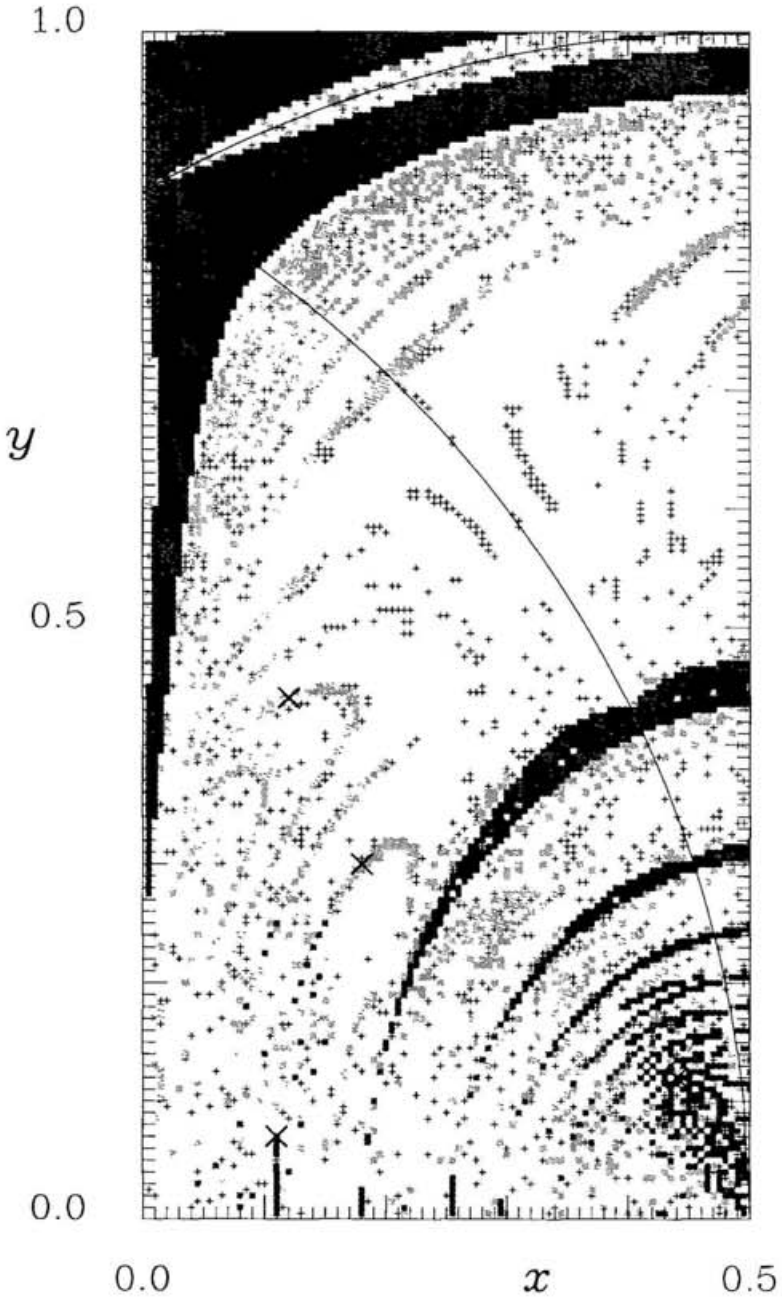

Figure 2.3: Initial-value distribution of escape orbits until the third triple encounter under Definition 2.3 (J.Yoshida, 1997).

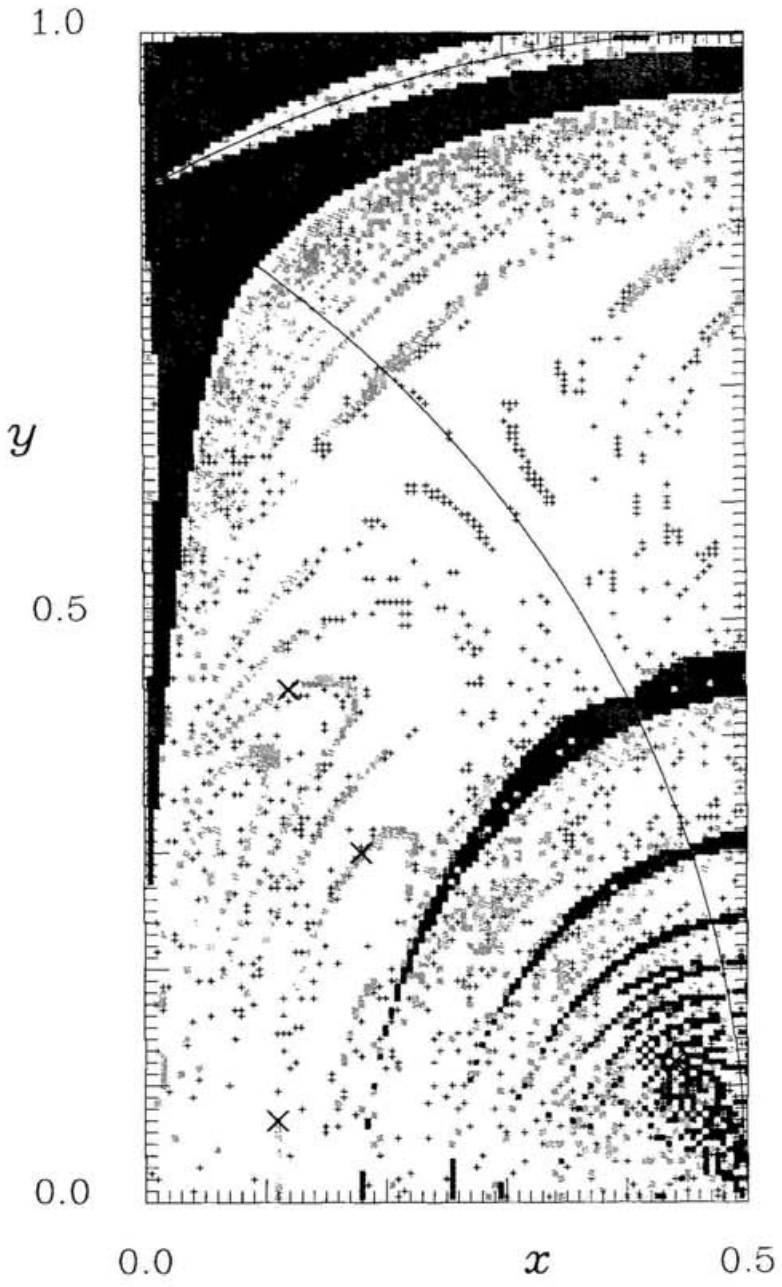

Figure 2.4: Initial-value distribution of escape orbits until the third triple encounter under Triple-encounter criterion (Our definition of triple encounter).

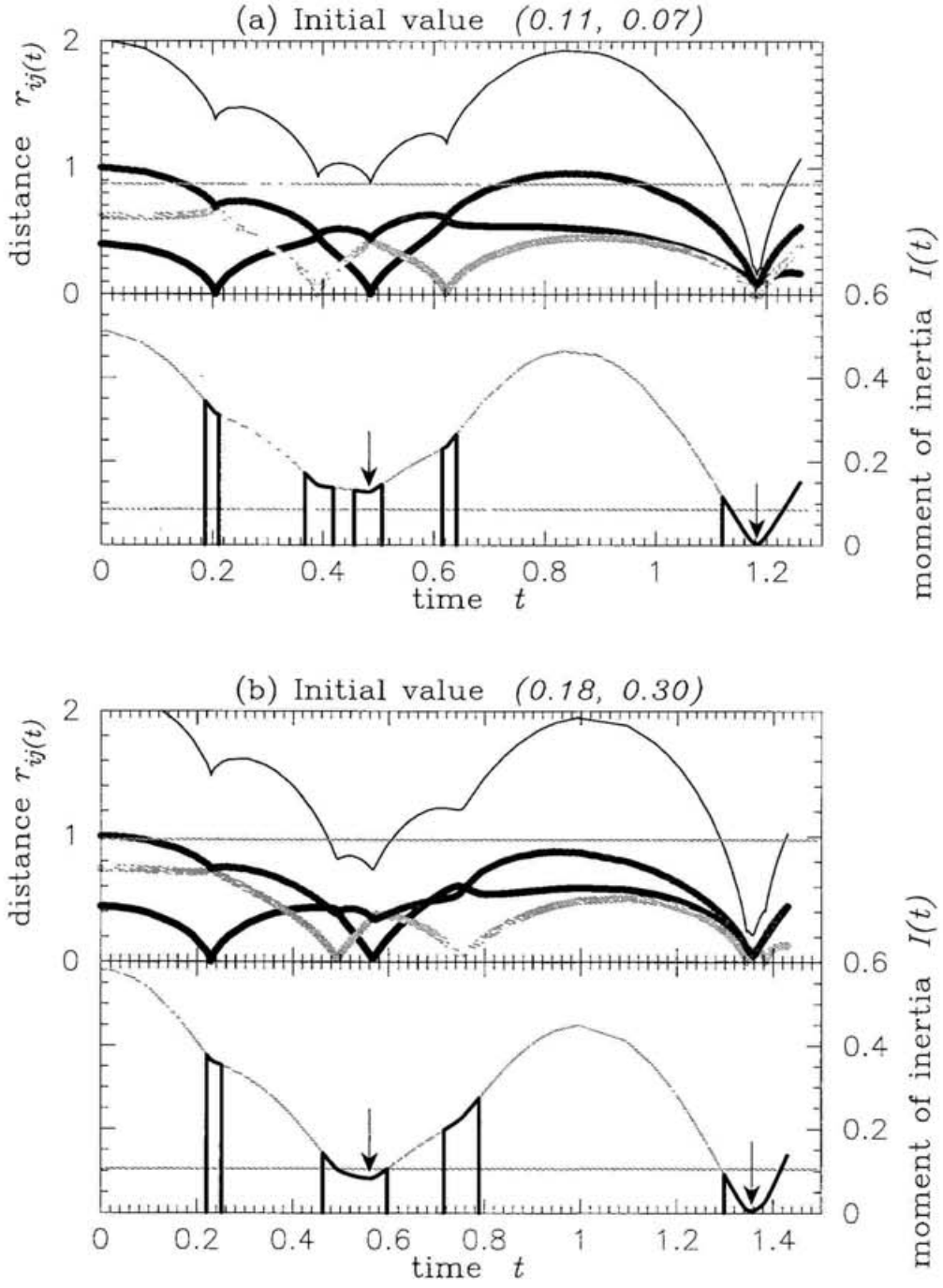

Figure 2.5: Time evolution of the distances between the respective particles and the moment of inertia. The initial values are located in the additional band A.

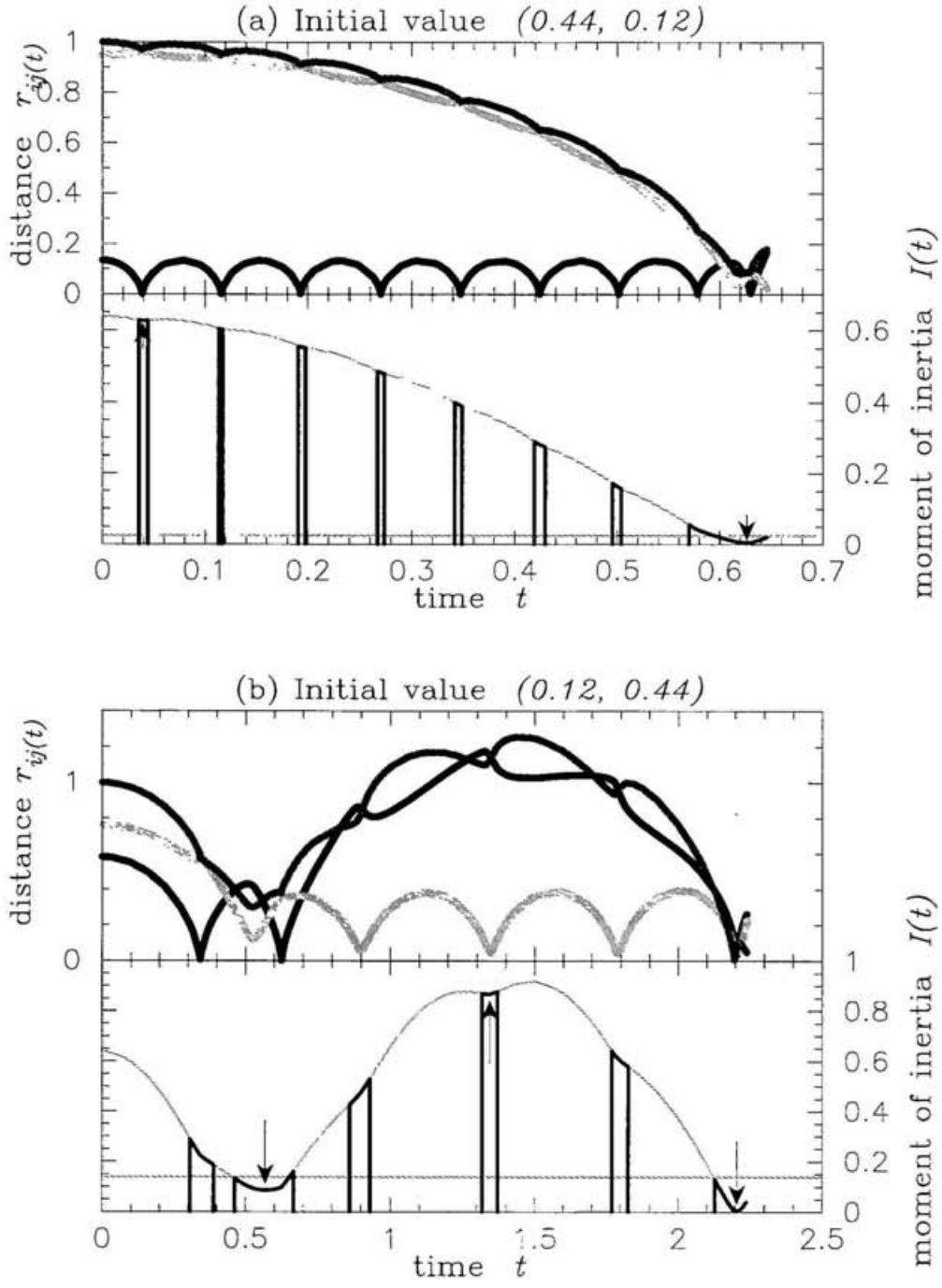

Figure 2.6: Time evolution of the distances between the respective particles and the moment of inertia.

2.3 Global features of escape orbits

2.3.1 Fractal distribution of escape regions

In the present subsection, a detailed survey of the initial-value distribution of escape orbits is executed, adopting Triple-encounter criterion in the preceding subsection. Finer structure of the distribution will be shown.

Before showing the numerical results, we will introduce several terms. An initial point leading to hyperbolic-elliptic escape or parabolic-elliptic escape after the i-th triple encounter will be called an *i-th hyperbolic point* or an *i-th parabolic point*, respectively, where i is a positive integer. Here, a hyperbolic-elliptic (or parabolic-elliptic) escape means that one particle escapes to infinity with positive (or zero) limiting velocity. From the continuous dependence of solutions on initial data, orbits in a neighborhood of the hyperbolic-elliptic escape orbit also result in escape with positive velocity. Hence hyperbolic points form an open set in the two-dimensional initial-value space. An open region formed with the i-th hyperbolic points will be called an *i-th hyperbolic region* or an *i-th escape region* simply. Similarly, an initial point where the system survives an escape until the i-th triple encounter will be called an *i-th non-escape point* or an *i-th ejection point*, and a region of the i-th non-escape points will be called an *i-th non-escape region* or an *i-th ejection region*.

We follow the flow-chart of the numerical integration until the i-th triple encounter. It is described in the preceding subsection. We terminate each integration at $i = 3$.

Figure 2.7 shows a more detailed result of the initial-value distribution of escape orbits where the system leads to escape until the third triple encounter ($i \leq 3$) defined by us. See Triple-encounter criterion in Subsection 2.2.1. We survey 5×10^5 initial points on the extended initial-value space $\grave{D}$. The size δx of the grid elements in the x direction is the same as the one in the y direction, and equal to 1×10^{-3}. In the present simulation, we use the same conditions of terminating calculation as the conditions in Fig.2.4. In other words, the same criteria not only for escape but also for triple encounter are implemented.

The number of simulated samples in this figure is 25 times larger than the one inFig.2.4.

Yellow, orange and green regions represent the first, second and third hyperbolic regions, respectively. These regions are obtained as the sets of initial points where the systems satisfy the escape criterion until the integrations are terminated by the other conditions in the flow-chart in the preceding subsection. The escape criterion is a sufficient condition, and so the true sizes of hyperbolic-elliptic regions are larger by a small amount than those shown in the figure. Therefore, a blank region represents a third non-escape region or a zone of the conditional escape.

In the present thesis, only initial values of orbits satisfying the escape criterion by Yoshida (1972, 1974) are called hyperbolic points.

Solid curves stand for the isosceles curves, I_1, I_2 and I_3 which are defined in eq.(1.3) in Subsection 1.3.1.

The most remarkable feature in the figure is a self-similar accumulation of band-like hyperbolic regions. The previous result by Anosova and Zavalov (1989) showed only five band-like regions S_i, $i = 1, 2, \ldots, 5$ where the system escapes after the first triple encounter. Our result shows a larger number of the first escape regions S_i, $i > 5$ in Fig.2.7. Moreover, we find that many second hyperbolic regions painted orange form a sequence and accumulate towards a boundary of each first hyperbolic region colored in yellow. This phenomenon is apparent in the lower part of each boundary of the hyperbolic region. Furthermore, we can see a sequence of the third hyperbolic regions accumulating towards a boundary of each second hyperbolic region.

In Fig.2.7, we have terminated the numerical integration before the fourth triple encounter. Nevertheless, we conjecture that for every positive integer number i, an infinite number of band-like escape regions after the $(i+1)$-th triple encounter accumulate towards the boundary of each band-like escape region after the i-th triple encounter. The accumulated distribution was not shown in the three-body scattering system of Boyd and McMillan (1992).

From this observation, Tanikawa and Umehara (1998) deduced the existence and the distribution of the oscillatory solutions in the free-fall three-body problem with equal masses. One kind of the oscillatory solutions is expressed as the behavior where the particle repeats return and ejection forever, expanding the ejecting distance to infinity. According to previous works, the existence of the oscillatory solution proved in the cases where masses of particles differ large. There is no proof in the equal-mass system.

Tanikawa and Umehara (1998) found that the oscillatory behavior occurs at an uncountable number of initial points.

In Fig.2.7, a limit curve seems not to coincide with the boundary; however, we are sure that the band-like escape regions forming the infinite sequence go into the zone of the conditional escape. If we do not terminate the integrations, the true boundary of the regions is shown slightly outside. The accumulation curves may coincide with the true boundary of the escape region.

Let us continue to integrate beyond the third triple encounter. We investigate the distribution of the value representing final motions on the initial-value space of the free-fall three-body problem. This value is related to the escape angle of the final motion. Here, the *escape angle* is defined as the following: if a particle m_i escapes, we draw a vector from the initial position of the partile m_i to the origin (i.e., the gravity center of the system); this vector is denoted by $\boldsymbol{q}_{\rm init}$; similarly, $\boldsymbol{q}_{\rm final}$ denotes the vector from the origin to the final position of the escaping particle m_i, when the escape criterion is satisfied; we define the absolute value of the angle between $\boldsymbol{q}_{\rm init}$ and $\boldsymbol{q}_{\rm final}$ as the *escape angle*.

It is confirmed that the structure of the distribution is similar to the one in the three-body scattering problem shown by Boyd and McMillan (1992) and the one in the scattering problem with the fixed potential shown by Ding et al. (1990). In other words, we find that in the free-fall three-body problem the distribution of escape angles shows cantor-sets on the initial-value space.

There is the numerical results of escape angles in Fig.2.8. A gray-scale value is assigned to each point of the extended initial value space $\grave{D}$. The escape angle is a value in the interval between 0 to π. In each figure, escape angle 0 is colored white, while escape angle π is colored black. The gray scale varies linearly with the angle. For convenience of understanding, we also show the initial-value-dependence beyond D.

In Fig.2.8, several regions of very smooth behavior exist in the initial-value space D. These regions correspond to the escape regions after the first triple encounter. Systems starting in these regions have only one opportunity of changing angles.

On the other hand, there are large regions where the escape-angle function is wildly fluctuated on the initial value space. These regions are composed of initial values where escape does not take place after the first triple encounter. An ejected particle from the temporary binary oscillates a large number of times before eventual escape.

If we observe the fluctuated-function region at a finer resolution, an intricately nested

pattern of smooth-function and fluctuated-function bands is revealed. This pattern may possess the fractal characteristic of self-similar structure on all scales. In each smooth-behavior region corresponding a first escape region, the escape angle is less than $\pi/4$ or more than $\pi/2$. In almost all orbits in first escape regions, an escape particle goes in a nearly straight line trajectory, whereas an escape particle is strongly distorted in a narrow region. This region passes through the first escape region.

From the next subsection, we will concentrate our attention to the motions just after the first triple encounter, and terminate our integrations if the three particles begin to approach each other again. That is because one of our main purposes is to know the factor effecting initial-value distribution of escape orbits. Recall the two common purposes in the various three-body problems described at "Common purposes" in Subsection 1.1.1. If the integration extends to the time until final motions of all orbits are determined, the effecting factor might not be found out.

Johnstone and Rucinski (1991) explored the initial-value-dependence of the escape behavior. They represent initial-value-distribution of the life-time and the final minimal value of the running size ρ. Here, a life-time is defined as the time until the system satisfies an escape criterion, and ρ is defined as the distance of the fastest receding particle from the gravity center of the three particles. According to them, roughly speaking, the initial-value with small ρ leads to escape at an early time. However, the ρ as a function of initial values is not continuous on almost all regions of the initial-value space. Johnstone and Rucinski (1991) continued the integration until all systems starting at surveyed initial values lead to escape. By their surveying, the fine structures in the initial-value space were not clarified. Therefore, we will study the escape orbits and non-escape ones after surviving the first triple encounter.

2.3.2 Slingshot in escape regions

Anosova and Zavalov (1989) described a rough structure of band-like regions S_i, $i = 1, 2, \cdots, 5$. According to them, each region S_i consists of three sub-bands lying side by side. Two of them are relatively wide in which m_2 and m_3 escape, and m_1 escapes in the narrow sub-band between them. Furthermore, they claimed that the center of each region S_i is along a certain circle.

We observe similar features in S_i, $i \in \{1, 2, \cdots, 19, 26, \cdots, 30, 36, \cdots, 40, 50\}$. The

procedure to determine the number i of S_i is shown in the following diagram. Here, r_j denotes the distance between m_k and m_l for $(j,k,l) = (1,2,3), (2,3,1)$, or $(3,1,2)$.

The procedure to determine i of S_i.

The following routine is executed as far as $r_2(t)$ is less than any other mutual distance.
if $r_2(t)$ attains a maximal value for t, then $r_{max} = r_2(t)$.
if $r_{max} < r_3(t)$ and $r_{max} < r_1(t)$, then
if $r_2(t)$ attains a minimal value, then $i = i + 1$.
Else if $r_2(t)$ becomes greater than one of the other mutual distances, then
the subsequent routine is not executed afterward,
and the number i at this stage is defined as i of S_i.
endif.

It is well-known that three particles approaching close to each other tend to result in escape for one particle. The moment of inertia can be used to characterize triple encounter. We define the *minimal moment of inertia* $I_{\min}$ as the minimal value of the moment of inertia with respect to time, when the distance ρ from the gravity center of two nearest particles to the other particle is less than ρ_0, where

$$\rho_0 = \frac{m_1m_2 + m_2m_3 + m_3m_1}{|h|}. \tag{2.24}$$

Recall that ρ_0 has been defined in eq.(2.1) in Subsection 2.2.

After a suitable scaling of variables and time, we can restrict to the energy level $H = \hat{h}$. Recall that $\boldsymbol{q}_j \in \mathbf{R}^2$, j=1,2,3, is the position vectors of particles m_j from the gravity center of the system. The equations of motion in the gravitational three-body problem are invariant under the following transformations: $\hat{\boldsymbol{q}}_j = \alpha \boldsymbol{q}_j$ and $\hat{t} = \beta t$ for $\alpha^3/\beta^2 = 1$. Here, a hat ($\hat{}$) represents the normalized value, and α and β are units of length and time, respectively. Thus the same orbit up to the scale change exists for any energy restricted to the same sign (negative or positive). Then we will scale the initial values so that the energy of the system becomes $\hat{h}$. The normalized minimal moment of inertia $\hat{I}_{\min}$ is defined as

$$\hat{I}_{\min} = \frac{1}{m_1 + m_2 + m_3} \sum m_j m_k \hat{x}_i^2 = \alpha^2 I_{\min}, \tag{2.25}$$

The normalizing factor α is calculated only from the initial value. In fact, the system

starts from zero velocities with equal masses, and so the total energy of the system is

$$h = -\sum \frac{1}{r_j(t=0)}. \tag{2.26}$$

The scaled energy is transformed as

$$\hat{h} = -\sum \frac{m_k m_l}{\hat{r}_j(t=0)} = \frac{1}{\alpha} h. \tag{2.27}$$

Thus the normalizing factor α is evaluated as

$$\alpha = \frac{h}{\hat{h}} = \frac{1}{\hat{h}} \sum \frac{m_k m_l}{r_j(t=0)}. \tag{2.28}$$

Figure 2.9 shows the initial-value dependence of the normalized minimal moment of inertia $\hat{I}_{\min}$ with $\hat{h} = -1$ during the first triple encounter. The number of initial values in the figure is 5×10^5, and the grid size of the numerical survey is 0.001. The lightness is proportional to the logscale of the value $\hat{I}_{\min}$. The darkest element shows $\log_{10} \hat{I}_{\min} = -5$, and the lightest one represents $\log_{10} \hat{I}_{\min} = -1$.

The topographical map of $\hat{I}_{\min}$ shows a sequence of valleys, i.e., dark zones where the minimal moment of inertia is small. Each first escape region distributes around the valley. This result shows that the small values of the minimal moment of inertia distributes in the escape regions.

We comment that the statement by Anosova and Zavalov (1989) is incorrect. According to them, the center of each escape region is along a cirtain circle. Our result shows that there is not any circle in the valleys corresponding to relatively small values of $\hat{I}_{\min}$.

A triple-collision point corresponds to an infinitely deep hole in the topography of $\hat{I}_{\min}$. It is natural that the triple-collision point lies in the regions where the minimal moment of inertia is relatively small. The bottom of the valley forms a curve which connects infinity deep holes. We found that this bottom is along a binary-collision curve. This implies the relation between binary collision and escape phenomena.

2.4 Dominant roles of collisions in escape

2.4.1 Near-isosceles slingshot dominating escape phenomena

Let us start to investigate the relation between collisions and escape phenomena from the present subsection. We will consider both binary and triple collisions. First, we superpose the map of the hyperbolic regions with the map showing binary-collision

curves and triple-collision points in Fig.2.10. The adopted grids spread over the extended initial-value space $\grave{D}$. Binary collision-curves and triple-collision points are taken from Tanikawa et al. (1995) and Tanikawa and Umehara (1998).

We have found the direct relation between escape and triple collision, as follows: at least one triple-collision point sits in each band-like escape region S_i. Therefore, each set of escape orbits includes a triple-collision orbit in the phase space.

Tanikawa et al. (1995) positioned triple-collision points (See table IV of them). Let T_i be the triple-collision points on the isosceles curve I_2, where i is the number of minima of the smallest distance. We have found that each triple-collision point T_i is included in the escape region S_i for $i = 1, 2, \cdots, 20$. Note that Umehara et al. (1995) found it only for $i = 1, 2$.

We have found that each center of band-like regions S_i for $i = 1, 2, \cdots, 6$ is along a particular type of the binary-collision curve. It is the type 1 called by Tanikawa et al. (1995). Recall that the number of type corresponds to the number of the particle which does not participate in binary collision, i.e., the binary collision between m_2 and m_3 occurs on the binary-collision curve of type 1. The initial values where minimal moments of inertia are smaller is along the binary-collision curve of type 1. The binary-collision curves of type 1 do not accord with the circles which Anosova and Zavalov (1989) mentioned. These circles are formulated as

$$\left\{x - \frac{c_i^2 + 1}{2(c_i^2 - 1)}\right\}^2 + y^2 = \left\{\frac{c_i}{c_i^2 - 1}\right\}^2, \tag{2.29}$$

where

$$c_i^2 = c_{i-1}^2 + i + 2, \quad c_1 = 1, \qquad \text{for} \quad i = 2, 3, \cdots. \tag{2.30}$$

See also Anosova (1991).

A binary-collision orbit of type 1 is shown in Fig.2.11. The particle m_1 passes through between m_2 and m_3 which are approaching each other. While m_2 and m_3 collide with each other and recede from each other, m_1 is decelerated suddenly and returns, and so m_1 passes through again. At this moment, the crossing point on the straight line connecting m_2 and m_3 is nearly the gravity center of the binary, and the velocity vector of the escaper is nearly orthogonal to the line. Furthermore, m_2 and m_3 are receding from each other. Getting enough energy from the binary, m_1 escapes maintaining an isosceles configuration of three particles approximately. All binary collisions of type 1 exhibit similar configurations as the above. We call these collision orbits of type 1 the *near-isosceles slingshot.*

The state that one particle passes through a straight line segment connecting the other particles is called *syzygy crossing*. Zare and Szebehely (1995) used this term.

On binary-collision curves sufficiently close to a triple-collision point, the orbits lead to escape without returning. On the other hand, the escape after the first triple encounter occurs neither at the binary-collision points of type 2 or 3 nor at points far from the triple collision points. On the binary-collision curves of type 1 in S_1, there also exist binary-collision points where three particles return.

All orbits except triple-collision orbits seem to escape on the binary-collision curve of type 1 in S_i for each $i \geq 2$. However, it is not sure whether there are not really any non-escape point on these curves or not. It will be verified in Subsection 3.4.3. The behavior starting on the binary-collision curve of type 1 is nearly isosceles motion, and so the syzygy crossing may be approximated to the isosceles motion. As a first step, we will evaluate the conditions of syzygy crossing leading to escape without returning in the planar isosceles problem by the numerical integrations. After that, it will be shown that all of one-parameter families which start on the respective binary-collision curves of type 1 in S_i, $i = 2, 3, \cdots$ satisfy the evaluated escape condition at the isosceles syzygy crossings.

2.4.2 Motion close to triple collision

In order to clarify that triple collision is not the only mechanism of escape, more detailed survey is conducted on the initial-value space in the neighborhood of the triple-collision points.

Figures 2.12(a) and (b) show the numerical result of the survey on the initial-value space around T_1 and T_2 for 10000 initial points, respectively. It is obvious that the homothetic equilateral point T_1 is located at $(0, \sqrt{3}/2)$ as the cross point of the three isosceles curves on the extended initial-value space $\grave{D}$. The other triple-collision point T_2 is at $(0.4035896, 0.4284000)$ which is found by Tanikawa et al. (1995). In Fig.2.12(a), the size of the grid elements in the x direction is $\delta x = 2 \times 10^{-5}$, and the one in the y direction is $\delta y = 2 \times 10^{-4}$. In Fig.2.12(b), $\delta x = \delta y = 2 \times 10^{-5}$. The distributions of binary-collision curves, the triple-collision points, and the first hyperbolic regions are shown. The isosceles curves are included in Figs.2.12(a) and (b) as the special type of binary-collision curves. Solid curves stand for the binary-collision curves. In the Figs.2.12(a) and (b), four curves denoted by I_1, I_2, and I_3 are isosceles curves and two curves denoted by type 1 and type 3 are binary-collision curves on which two particles collide with each other asymmetri-

cally. A dark gray region, a light gray region, and a meshed region represent the first hyperbolic regions where m_1, m_2, and m_3 escape, respectively. A blank region is a first non-escape region. The first hyperbolic points are obtained as the initial values of orbits satisfying the escape criterion which is a sufficient condition, and so the true sizes of the hyperbolic-elliptic regions are larger as pointed out earlier.

We find four remarkable features in Fig.2.12. The first result of the numerical survey shows topology of initial values leading to triple collision.

Observation 2.1. *There are no first triple-collision points sufficiently close to the triple-collision points T_1 and T_2.*

It is not apparent that the triple-collision point is isolated from other triple-collision points on the initial-value space. According to Waldvogel (1982), a set of triple-collision orbits approaching equilateral configurations asymptotically forms a smooth three-dimensional submanifold of the constant energy surface. (This submanifold will be derived in Section 4.2.2.) The initial-value space is a two-dimensional section in the five-dimensional phase space with the constant energy. Without analytical consideration or detailed surveys of numerical integrations, we can not remove the possibility that the intersection of triple-collision orbits and the initial-value space forms a curve or a region. Moreover, we suspect that this intersection forms a cantor-like set. If the distribution of the triple-collision points shows a cantor-like set, some triple-collision points may exist in a sufficiently close to T_1 or T_2.

In Section 4.2.2, we will consider the distribution of the triple-collision points around T_1. We will restrict ourselves to the triple-collision points on which the systems end in collision during the first triple encounter. We will prove that T_1 is isolated from the other triple-collision points during the first triple encounter. Such points do not form a cantor-like set around T_1.

The second result concerns with the structure of the hyperbolic regions and the triple-collision points.

Observation 2.2. *The first-hyperbolic regions seem to converge to T_1 and T_2, respectively. Six parts of the first-hyperbolic regions exist around each triple-collision point.*

These parts consist of three large and three narrow regions where the particles m_1, m_2 and m_3 escape in the respective regions.

The respective large regions and narrow regions are located around each triple-collision point alternately. Some notations are introduced in order to explain the escape-region distribution more precisely. Let L_j and N_j denote large and narrow regions of m_j escaping, respectively. The first-escape regions are arranged as L_1, N_2, L_3, N_1, L_2, and N_3 in a counterclockwise sequence around each triple-collision point. In Fig 2.12 (a), it is difficult to identify all narrow regions except one which forms a lobe-like region where m_1 escapes; however, their existence is assured by the symmetry of initial configurations with the equal-mass case. In Fig 2.12 (b), we observe one lobe-like hyperbolic region where m_2 escapes. It exists between the large regions where m_1 and m_3 escapes, respectively. According to a more detailed survey on the initial-value space between the large regions where m_3 and m_2 escapes, respectively, we observe one narrow region where m_1 escapes. Then the existence of the narrow region where m_3 escapes is assured by the symmetry of initial configurations with the equal-mass case.

The third of numerical results is the relation between the first non-escape orbits and the triple-collision orbits.

Observation 2.3. *The first non-escape regions exist between any two hyperbolic regions. The first non-escape regions also converge to each triple-collision point.*

Although convergence of the non-escape regions is difficult to verify both analytically and numerically, their existence is easy to prove if the second result is correct in an arbitrarily small neighborhood of the triple-collision point. We will prove it in Section 4.2.1. The outline is the following: Observation 2.2 shows that there is any kind of the first-hyperbolic regions where each of three particles escapes in an arbitrarily small neighborhood of each triple collision, and two hyperbolic regions where escape particles are different do not contact with each other except at the triple-collision point since an escape particle is at most one in the negative-energy case.

The fourth result concerns with the structure of the hyperbolic regions and the binary-collision curves.

Observation 2.4. *Each binary-collision curve of type j, $j = 1, 2, 3$ passes through the first-hyperbolic region where m_j escapes.*

Any narrow region distributes along the binary collision of type j up to T_1, and the large region where the same particle escapes spreads to the other direction with respect to T_1. In other words, if the system starts on any binary-collision curve in a sufficiently small neighborhood of a triple-collision point, a particle which does not experience binary collision leads to escape.

Observation 2.2 means that the escape orbits are distributed around the triple-collision orbit. Such a distribution seems obvious since it is expected that orbits passing near triple-collision singularity tend to escape. According to Observation 2.3, however, a mechanism other than the close triple encounter is necessary to explain escape phenomena. For, orbits failing to escape also seem to exist arbitrarily close to triple-collision singularity.

The existence of factors other than triple collision is clearly seen in Figs.2.13(a) and (b). These figures show the initial-value dependence of the normalized minimal moment of inertia as the total energy is -1 around T_1 and T_2, respectively. The survey region, the number of initial values, and the grid size in each figure are the same as those in Fig.2.12 (a) and (b). The darkness is proportional to the logscale of the value $\hat{I}_{\min}$. The darker element of the grid represents the initial values experiencing the closer triple encounter. The interval of this gray scale is $-6 \leq \log_{10} \hat{I}_{\min} \leq -3$. Both minimum and maximum values of this scale are smaller than the ones in Fig.2.9. The range in Fig.2.9 is $5 \leq \log_{10} \hat{I}_{\min} \leq -1$.

From topographical maps, we observe that valleys of the minimal moment of inertia are along the binary-collision curves of the near-isosceles-slingshot type. The holes are observed around the triple-collision points T_1 and T_2. The remarkable feature is that $\hat{I}_{\min}$ on any first non-escape region around each triple-collision point is also small. There is no difference of the values between escape and non-escape regions.

From Observation 2.4, we expect that escape phenomena are characterized not only by triple collision but also by binary collision. Later we will verify the importance of binary collision for escape (see Chapter 4). Around T_1 which is the initial value of the homothetic-equilateral-triple-collision orbit, we could accomplish the proof of Observation 2.4. See Umehara and Tanikawa (1997) and Section 4.2 in the present paper. Note

that Umehara and Tanikawa (1997) also proved that Observations 2.1 and 2.2 are correct around T_1. Observation 2.3 is partially proved. The existence of both escape and non-escape regions after the first triple encounter is proved around T_1.

Around T_i, there are three large regions and three narrow ones. We find that the behavior of slingshot starting in the large regions is different from the behavior in the narrow ones.

Behavior of orbits during triple encounters in the respective first escape regions can be understood from Fig.2.14(a) and (b). These figures show the initial-value dependence of the *escape angle* around T_1 and T_2, respectively. Here, the *escape angle* ϕ is defined as in Subsection 2.3.1. The darkness is proportional to the value ϕ. An escape particle is deflected strongly during the triple encounter as the grid element of the initial value is dark. The survey region, the number of initial values, and the grid size in each figure are the same as in Fig.2.12(a) and (b).

Anosova and Orlov (1992) classified the close triple encounters of slingshot type in the following two categories:

forward slingshot - an escape particle goes through a temporary binary in a nearly straight line trajectory;

backward slingshot - an escape particle is strongly deflected during passing through a temporary binary.

In each category, a temporary binary becomes harder after an escape particle flies away. Anosova and Orlov (1992) showed that the forward slingshot constitute 62% of all slingshots resulting in escape if a "nearly straight line" is defined as $\phi \leq 45$.

The three narrow regions is darker than the three large escape regions. We find that the backward slingshot occurs on the narrow regions while the forward slingshot does on the large regions. Moreover, the near-isosceles slingshot orbit belongs to the category of the backward slingshot.

2.5 Discovery of exchange escape in the free-fall problem

We find in Fig.2.10 new escape regions where m_3 escapes. Anosova and Zavalov (1989) did not mention their existence. Figure 2.15 is the magnification of the lower-right

part of Fig.2.10. The number of initial values in the figure is 10000. The grid size of the numerical survey is 0.001 which is the same as in Fig.2.9. These regions have tongue-like shapes. We will call each of them a *tongue-like region.* Each tongue-like region lies between S_{i-1} and S_i for $i = 5, 6, \cdots$, so we will denote it E_i.

We found that the binary-collision curve of type 2 penetrates each tongue-like region E_i. Notice that the pair of colliding particles is different from the binary formed by triple encounter. This is in contrast with the binary-collision orbits of type 1 and type 3. The motion of type 2 is different from the ones of type 1 and type 3 where slingshot encounters occur. From Fig.2.16, we have found that the exchange type of triple encounter occurs in this case. Figure 2.16 shows the trajectories of three particles starting on the binary-collision curve of type 2 in E_5. The orbit of type 2 experiences the binary collision after the particle m_2 is decelerated by the syzygy crossing of an approaching binary. Such a deceleration phenomenon is called the *inverse slingshot.* It is natural to conjecture that in this case escape does not occur. However, there exist escape orbits on the binary-collision curve of type 2.

Just before the i-th approach of the binary m_1 and m_3, the third particle m_2 approaches m_1. The particle m_2 is decelerated by the inverse-slingshot effect. The trajectory of m_1 is deflected by the existence of m_2 and collides with m_3. Then m_3 is reflected to the opposite side of m_2 with respect to m_1, and so m_3 escapes to infinity. The particles m_1 and m_2 approach each other again and become a binary at last.

There are no triple-collision point in any tongue-like region E_n. We will assert it from the following consideration. We can not find any triple-collision point T_n searched by Tanikawa et al. (1995) in E_i although the regions S_i and E_i contact with each other for $i = 6, 7, \cdots$. We will draw a boundary between S_i and E_i later. In other words, we will distinguish between slingshot motion and exchange one. As a result, it will be clear that E_i does not converge to a point T_i.

Does other triple collision point exist in E_n? Let us consider the initial-value distribution of the normalized minimum moment of inertia $\hat{I}_{\min}$ (see the definition in Subsection 2.3.2). A gray scale in Fig.2.17 shows that $I_{\min}$ in E_n is larger than the one in S_i. The lightness is proportional to the logscale of the value $\hat{I}_{\min}$. In Fig.2.17, we see a sequence of valleys, i.e., dark zones where the minimal moment of inertia is small. Each S_i distributes around a valley. On the other hand, $\hat{I}_{\min}$ on E_i is larger than one on S_i. Moreover, this

numerical result suggests that the topography of $\hat{I}_{\min}$ on and around E_i is not steep and does not have any singular hole representing a triple-collision point. Hence, there is no triple-collision point in any tongue-like region E_i.

All escape orbits in tongue-like regions are of exchange type even if they do not experience binary collision. The continuous dependence of all solutions starting in E_n is established since they avoid triple collision. As a result of the perturbation from the binary-collision orbit after close approach between m_1 and m_2, a close approach between m_1 and m_3 takes place. Under a small perturbation, m_3 does not form any slingshot configuration.

For $i \geq 6$, the regions S_i and E_i connect with each other near the triple-collision point T_i. We will define a boundary of the connected part between S_i and E_i in order to investigate the effects of triple-encounter types upon the evolution of the systems in the next chapter.

Here, we summarize the procedure to determine their boundary by noting the difference of motion between the slingshot and the exchange. The particle m_3 escapes in E_i. The particle m_3 also escapes in the sub-band of S_i neighboring E_i. In E_i, the distance between m_2 and m_3 never become the minimum of the mutual distances. On the other hand, it becomes the minimum in the part of S_i neighboring E_i.

Connection between S_i and E_i suggests that continuous deformation between a slingshot-escape orbit and an exchange-escape one is possible. However, there are first non-escape points like a gap between S_i and E_i which are far from T_i, and so most escape orbits due to slingshot are separated from those due to exchange. For example, in a segment $\{(x,y)|0.420 \leq x \leq 0.435, y = 0.19\}$, there is an interval where the systems fail in escape after the first triple encounter. We will refer to the behavior on both sides of the interval and extract a suitable definition of the boundary from the difference between slingshot and exchange.

Let us observe four orbits starting on the segment $\{(x,y)|0.420 \leq x \leq 0.435, y = 0.19\}$ bridging over the gap region between S_5 and E_5. The initial values of Fig.2.18(a), (b), (c) and (d) are $(0.420, 0.19)$, $(0.425, 0.19)$, $(0.430, 0.19)$, and $(0.435, 0.19)$, respectively. Orbit (a) is an escape orbit where m_3 escapes. The type of escape is exchange. Orbit (d) is an escape orbit where m_3 escapes due to slingshot. For each orbit (b) and (c), m_3 is ejected without escape. In the case of exchange motion (a), m_2 approaches m_1 and the trajectory of m_2 is deflected in the opposite direction to the position of m_3. Also

the trajectory of m_3 is deflected in the opposite direction to the position of m_2 by the existence of m_1 when the i-th close approach between m_3 and m_1 happens.

From this observation, we obtain the following feature on the time evolution of mutual distances between particles:

Observation 2.5. *If the system leads to escape after the first triple encounter due to exchange in the free-fall problem, the distance between m_2 and m_3 is not closest among the distances between the respective particles for all time.*

Figure 2.19 shows the time evolution of distances $r_{jk}(t)$, $j = 1, 2, 3$, $k \neq j$, where r_{jk} is the distance between particle m_j and m_k. The upper figure (a) shows the evolution of the exchange type whereas the lower one (d) shows one of the slingshot type. The respective initial values are the same as in Fig.2.18(a) and (d). A bold curve represents r_{23} and the other curves are for r_{12} and r_{31}. In the exchange case (a), $r_{23}(t) > \min\{r_{12}(t), r_{31}(t)\}$ for all time. On the other hand, r_{23} becomes less than r_{12} and r_{31} around $t \simeq 0.63$ in the slingshot case (d).

The inverse of Observation 2.5 is not always true, i.e., the closest approach between m_2 and m_3 is a necessary condition of exchange escape. If m_3 escapes due to slingshot, m_3 is possible to approach m_2 when m_3 passes through between m_1 and m_2. At the syzygy crossing of m_3, $r_{31} = r_{23} + r_{31}$, and so there exist two cases $\min\{r_{21}, r_{23}, r_{31}\} = r_{23}$ and $\min\{r_{21}, r_{23}, r_{31}\} = r_{31}$. We can not assert that the exchange occurs since r_{23} does not experience the minimum value among the mutual distances for all time.

In the regions where m_3 escapes, we investigate behavior whether m_2 and m_3 approaches each other or not. Figure 2.20 shows escape regions where m_3 leads to escape after the first triple encounter. A cross (+) stands for the grid element of the initial value where the system experiences $\min\{r_{21}, r_{23}, r_{31}\} = r_{23}$; on the other hand, a filled box (■) represents the initial-value grid where $\min\{r_{21}, r_{23}, r_{31}\} \neq r_{23}$ for all time. Observation 2.5 shows that the type of triple encounter is slingshot if the orbit starts at the cross point (+). The band-like region S_i contains both elements, i.e., cross and filled box. It is true that the two cases exist in slingshot escape. However, in the vicinity of the triple-collision point T_i, cross elements (+) occupy the neighboring side of S_i with respect to E_i. In contrast with S_i, all grid elements in tongue-like regions E_i are occupied by filled boxes, i.e., m_2 and m_3 do not approach each other. Two types of elements are divided around the connected part between S_i and E_i, $i \geq 6$. Here, the boundary between S_i and E_i

appears clearly. A curve which divides crosses and filled boxes are the boundary. We define E_i as a connected region where the system satisfies $\min\{r_{21}, r_{23}, r_{31}\} \neq r_{23}$ for all time starting in a tongue-like region.

From the location of the boundary, it becomes clear that each E_i does not include triple-collision point T_i. In this stage, the nonexistence of triple-collision points in E_i is completely verified.

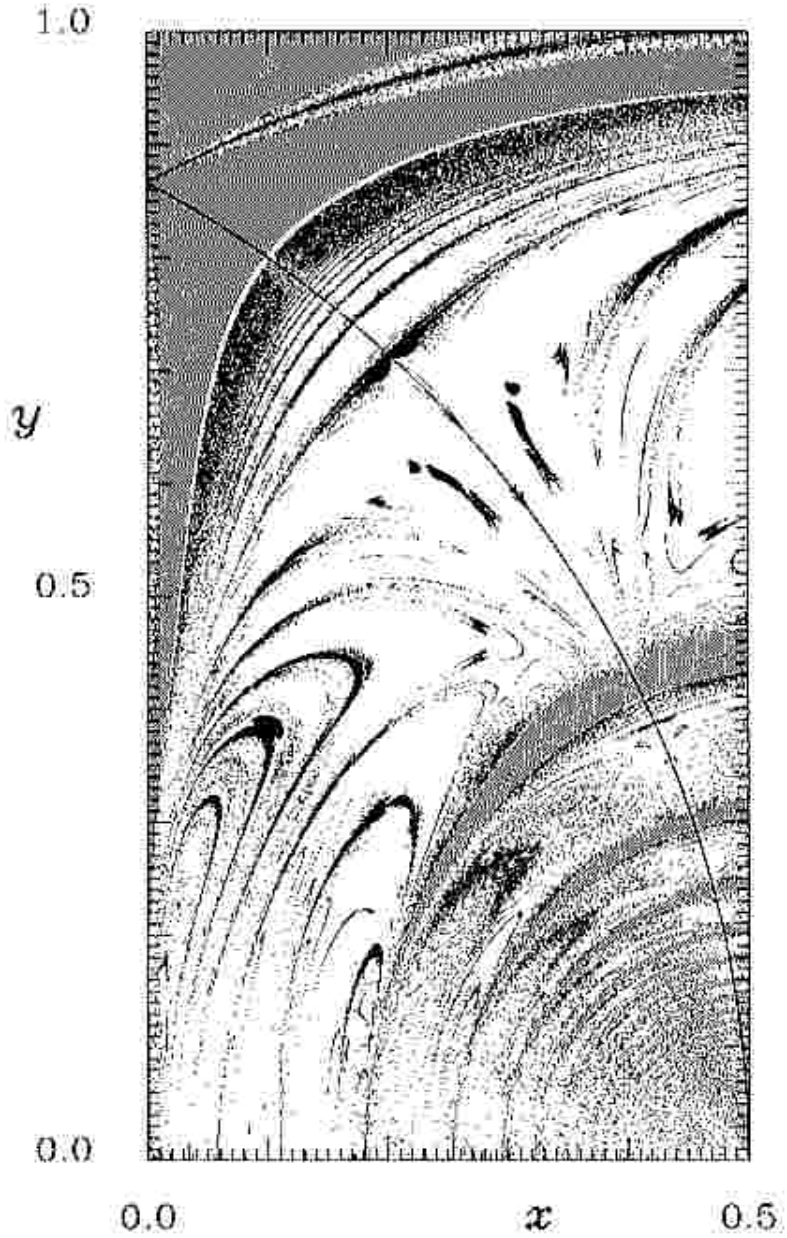

Figure 2.7: Escape regions until the fourth triple encounter, in the extended initial-value space $\hat{D}$.

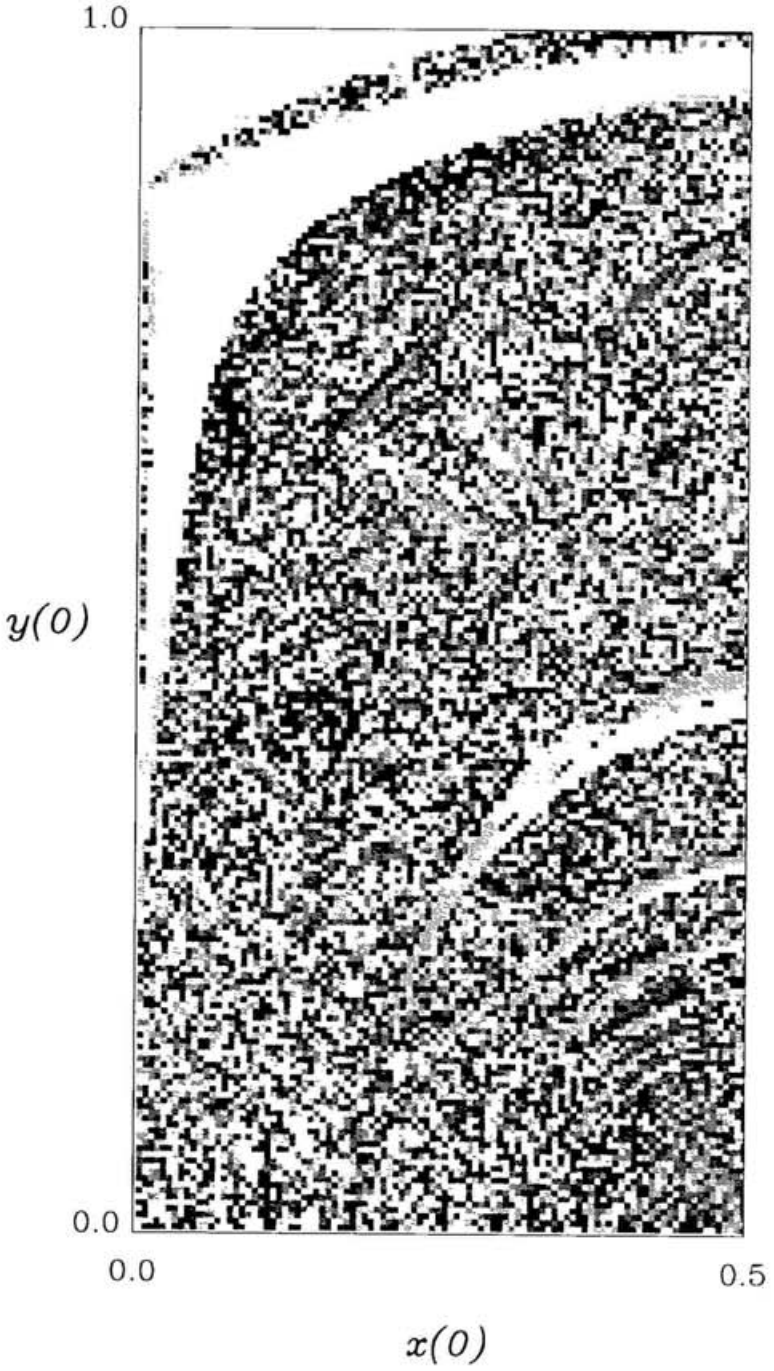

Figure 2.8: Initial-value dependence of the escape angle which is definded as an absolute value of angle between a vector from the origin to the position of escapeing particle at the time of satisfying escape criterion and a vector from the origin to the initial position of the same particle at the escape. A gray scale varies linearly as the angle from 0 (the lightest element) to π (the darkest element).

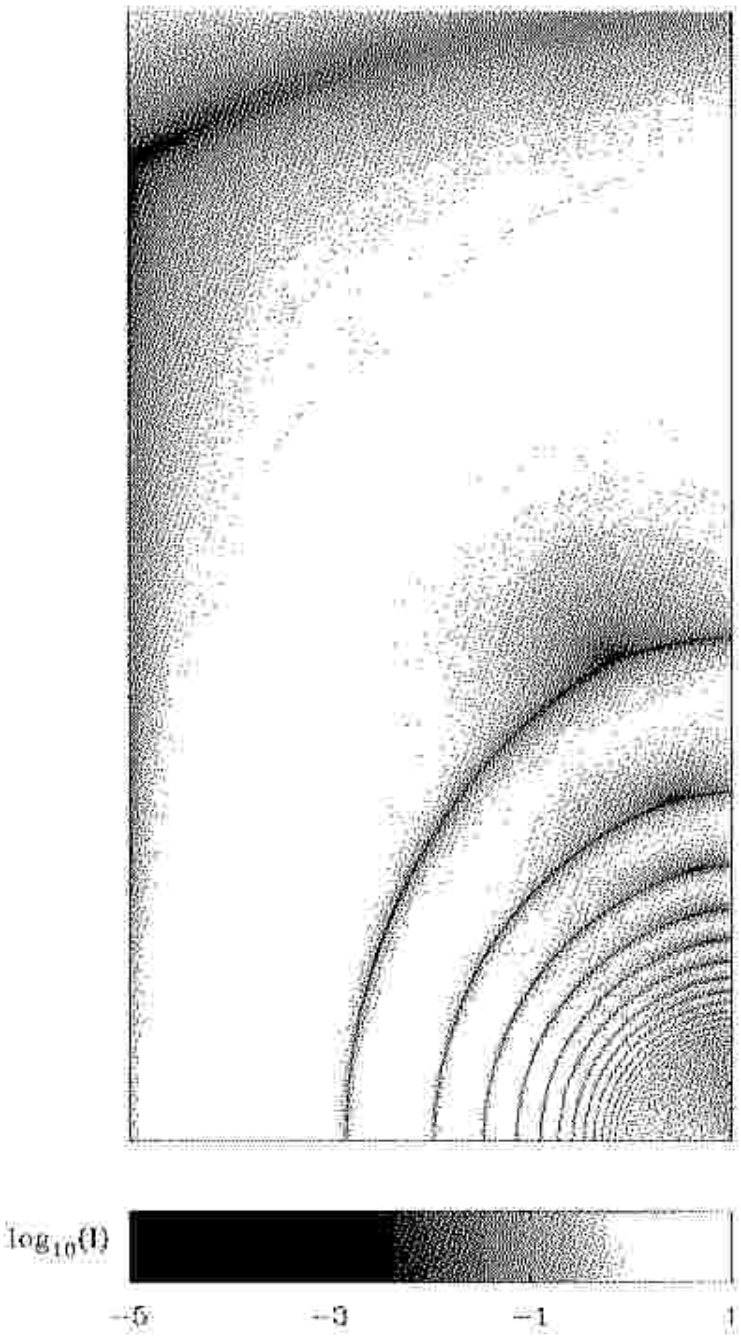

Figure 2.9: Initial-value dependence of the normalized minimum moment of inertia during the first triple encounter $\hat{I}_{\min}$ defined as the minimal value of the moment of inertia with respect to time in the scaled system such that the total energy is -1. A gray scale varies linearly as the logscale of the normalized values: the darker color represents the smaller value.

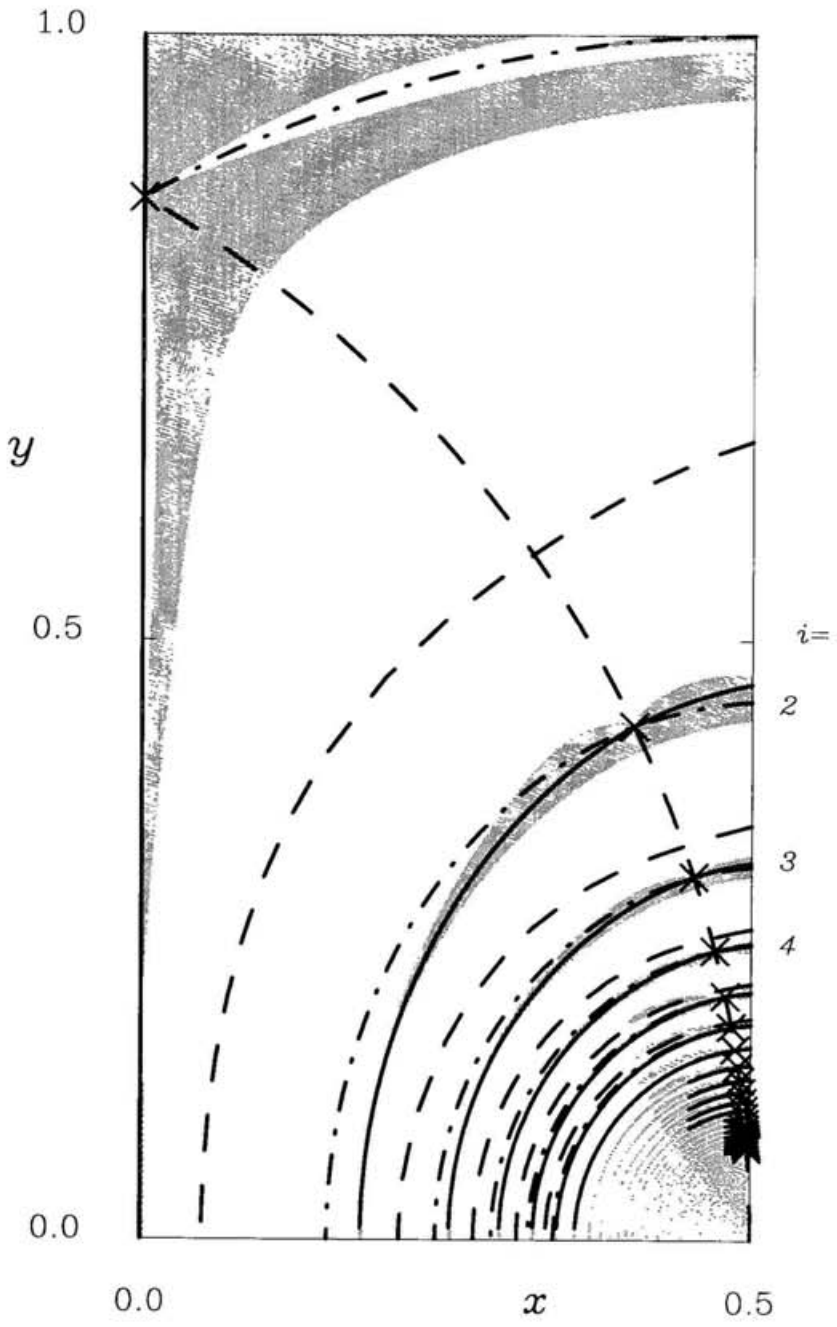

Figure 2.10: Triple-collision points, binary-collision curves, and first escape regions in a part of the initial-value space and its extension. Curves represent binary collisions. A solid bold curve shows collision between m_2 and m_3 (near-isosceles-slingshot type). A dashed bold and a solid fine curves are collisions between m_3 and m_1, m_1 and m_2, respectively. A cross $\times$ shows the triple-collision point. A gray region represents the first escape region.

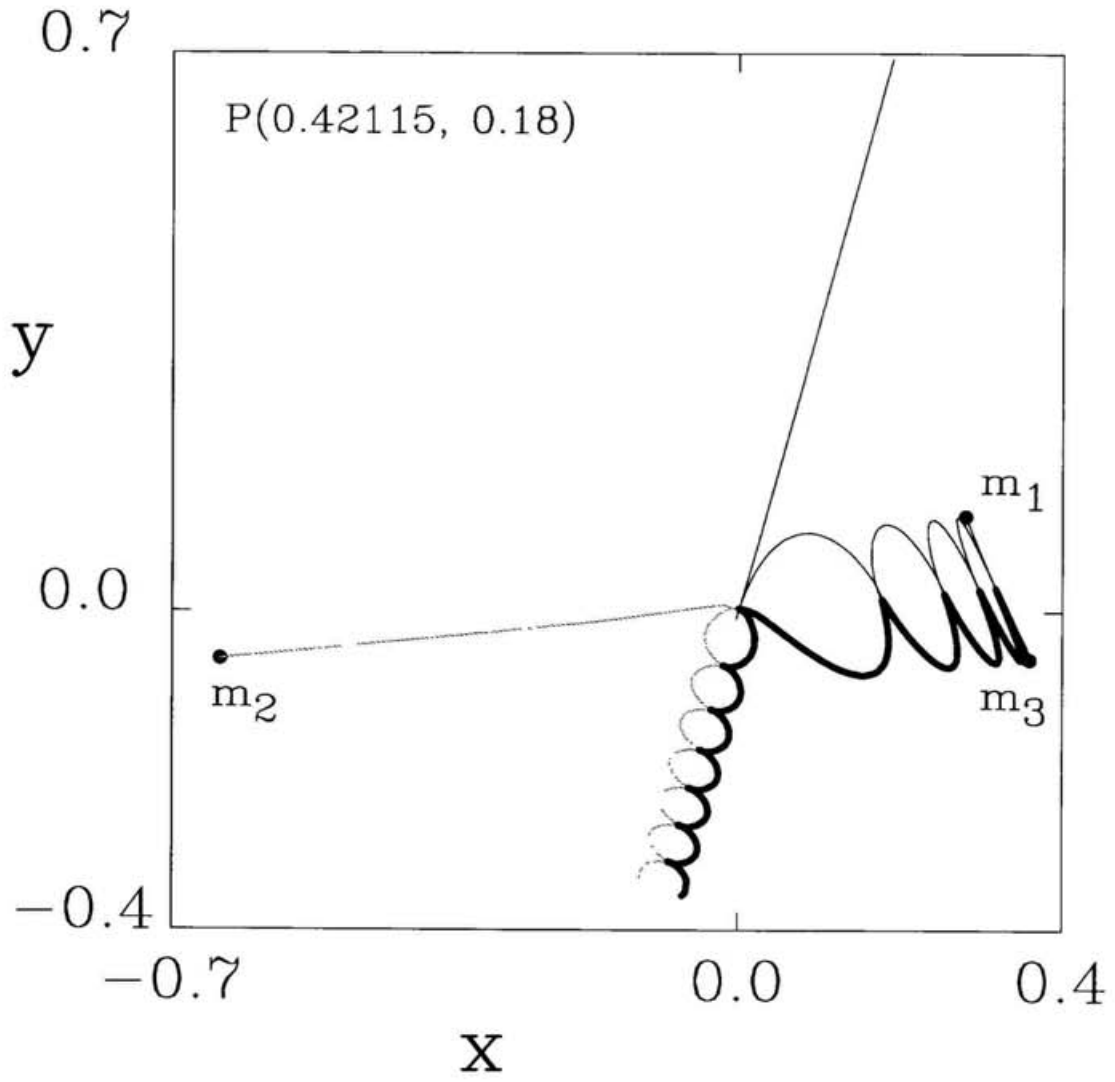

Figure 2.11: A near-isosceles-slingshot orbit. It is defined as the binary-collision orbit which results escape maintaining isosceles configuration approximately, where a collision occurs just before the last syzygy crossing of the escape particle.

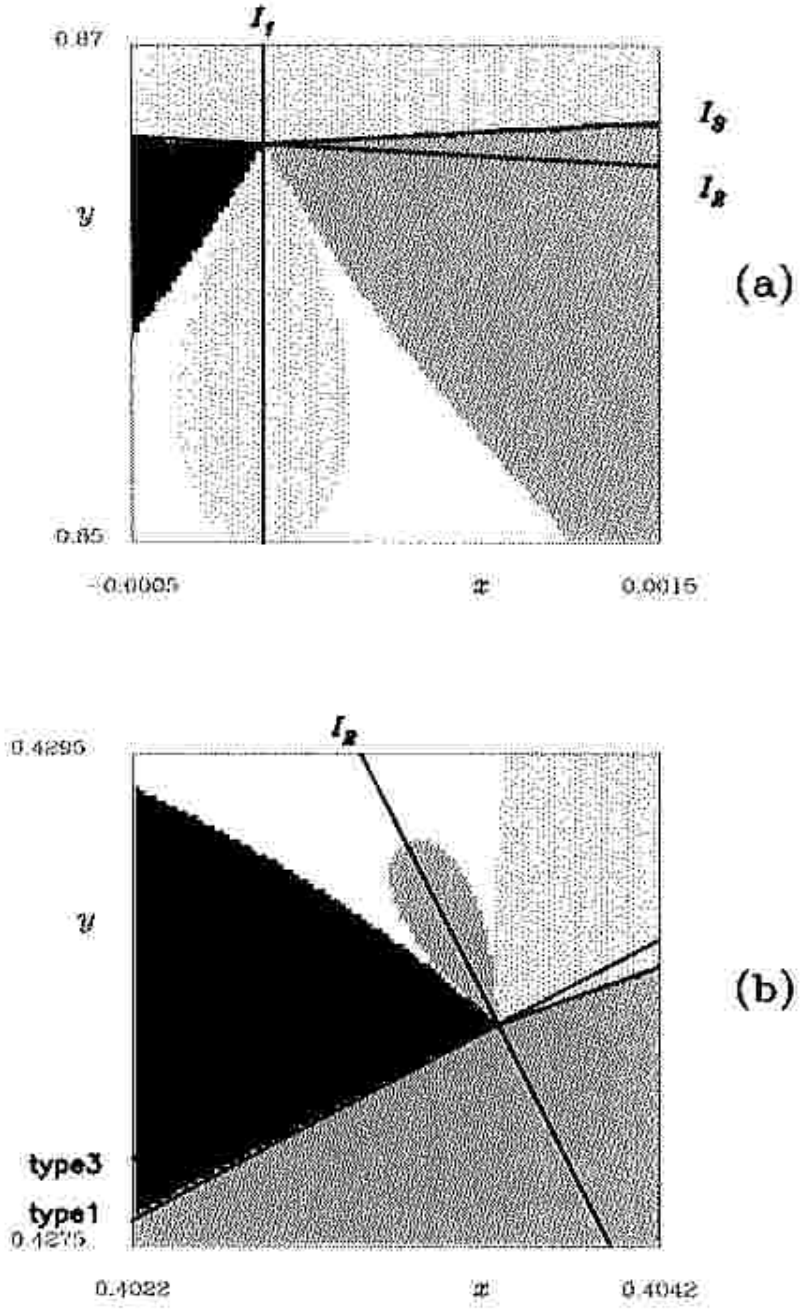

Figure 2.12: Escape regions after the first triple encounter and the binary-collision curves and triple-collision points in the vicinity of the triple-collision points. The upper figure (a) shows such a feature around T_1, and the lower one (b) T_2. A dark gray, a light gray, and a meshed regions represent escape regions where where m_1, m_2, and m_3 escape, represently. Bold curves stand for isosceles curves and binary-collision curves. The isosceles curve is denoted by I_j, $j = 1, 2, 3$, outside the frame. The type of binary collision is denoted beside the curves, where the number of type means the particle identity which does not attend a binary collision. The triple-collision points are obtained as the cross points of respective three binary-collision curves.

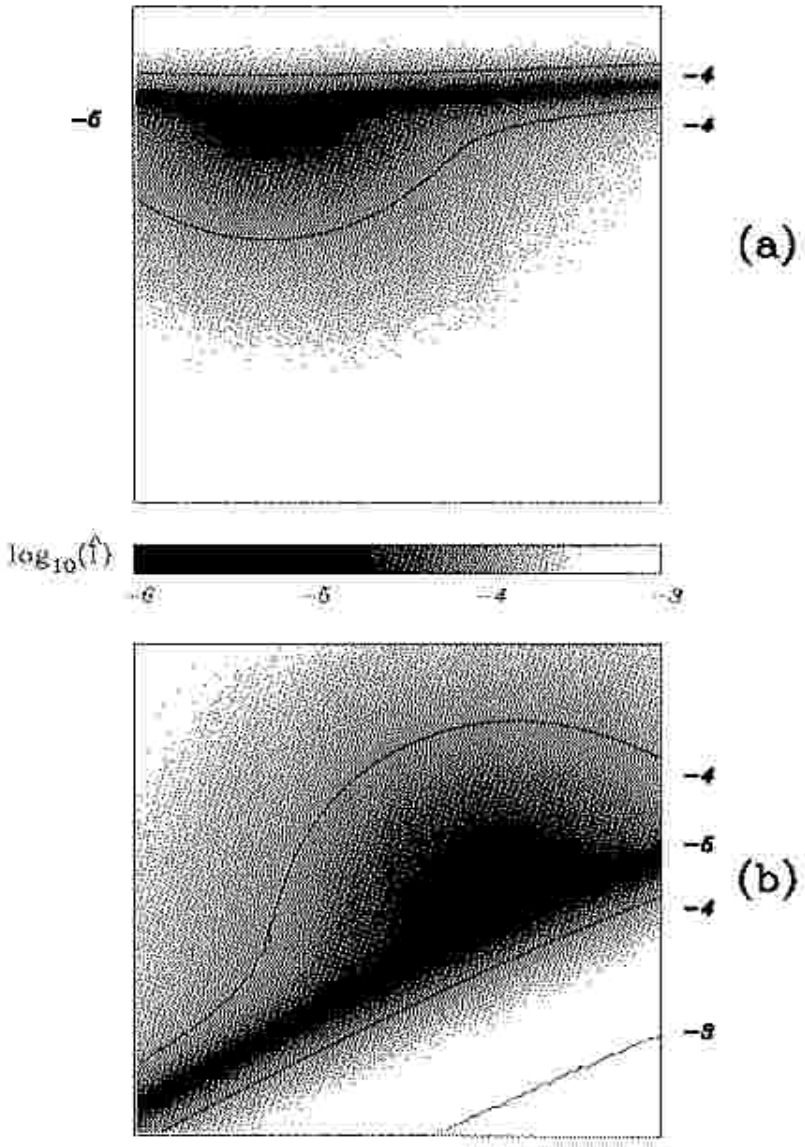

Figure 2.13: Initial-value dependence of the normalized minimum moment of inertia $\hat{I}_{\min}$ until second shrink of the system, where $\hat{I}_{\min}$ is definded as the minimal value of the moment of inertia with respect to time in the scaled system such that the total energy is -1. A gray scale varies linearly as the logscale of the normalized values: the darker color represents the smaller value.

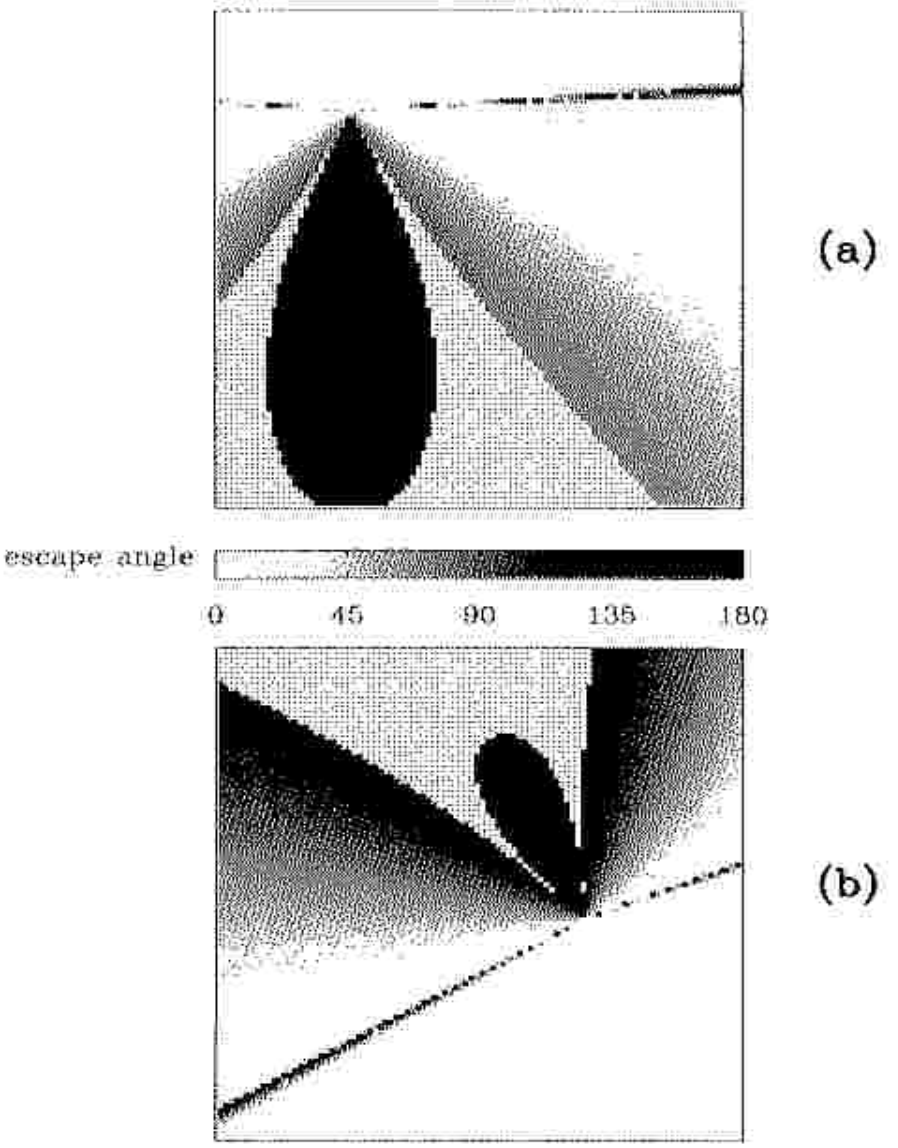

Figure 2.14: Initial-value dependence of the escape angle which is defined as an absolute value of angle between a vector from the origin to the position of escapeing particle at the time of satisfying escape criterion and a vector from the origin to the initial position of the same particle at the escape. A gray scale varies linearly as the angle from 0 (the lightest element) to π (the darkest element).

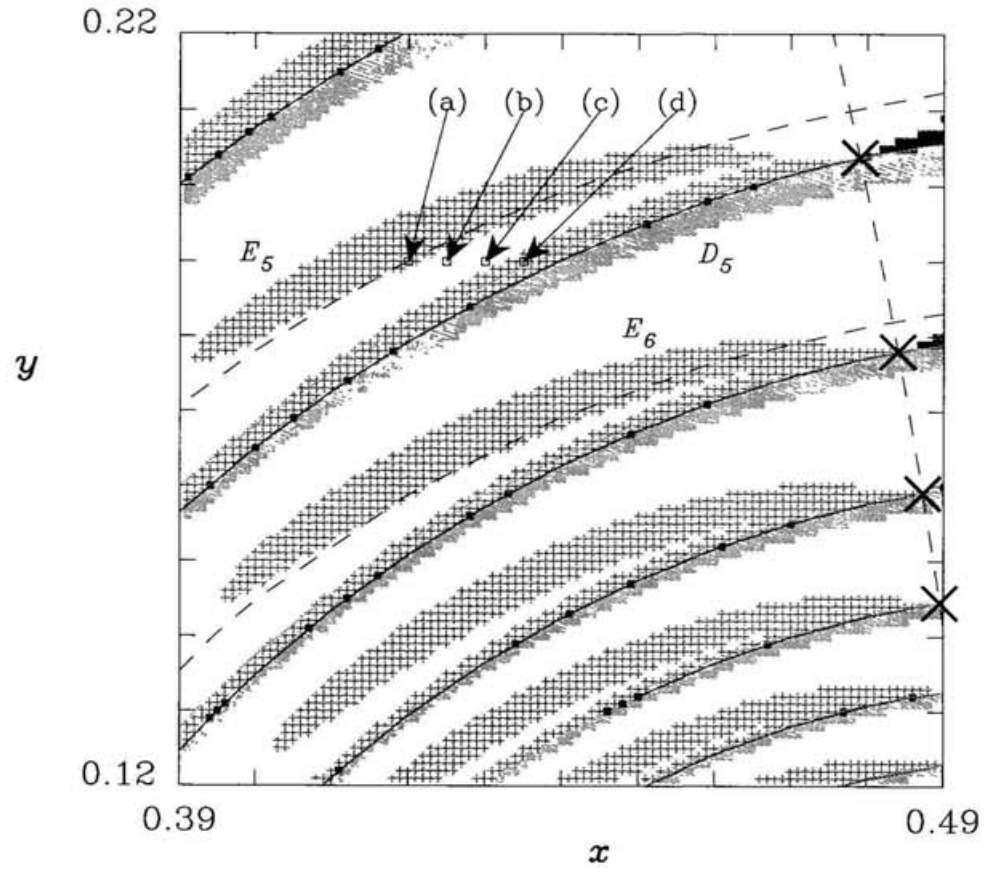

Figure 2.15: Escape regions after the first triple encounter, the binary-collision curves, and triple-collision points in the lower right part of the initial-value space D. A dark gray, a light gray, and a meshed regions represent escape regions where where m_1, m_2 and m_3 escape, represently. Bold curves stand for binary-collision curves. The triple-collision points are obtained as the cross points of respective three binary-collision curves.

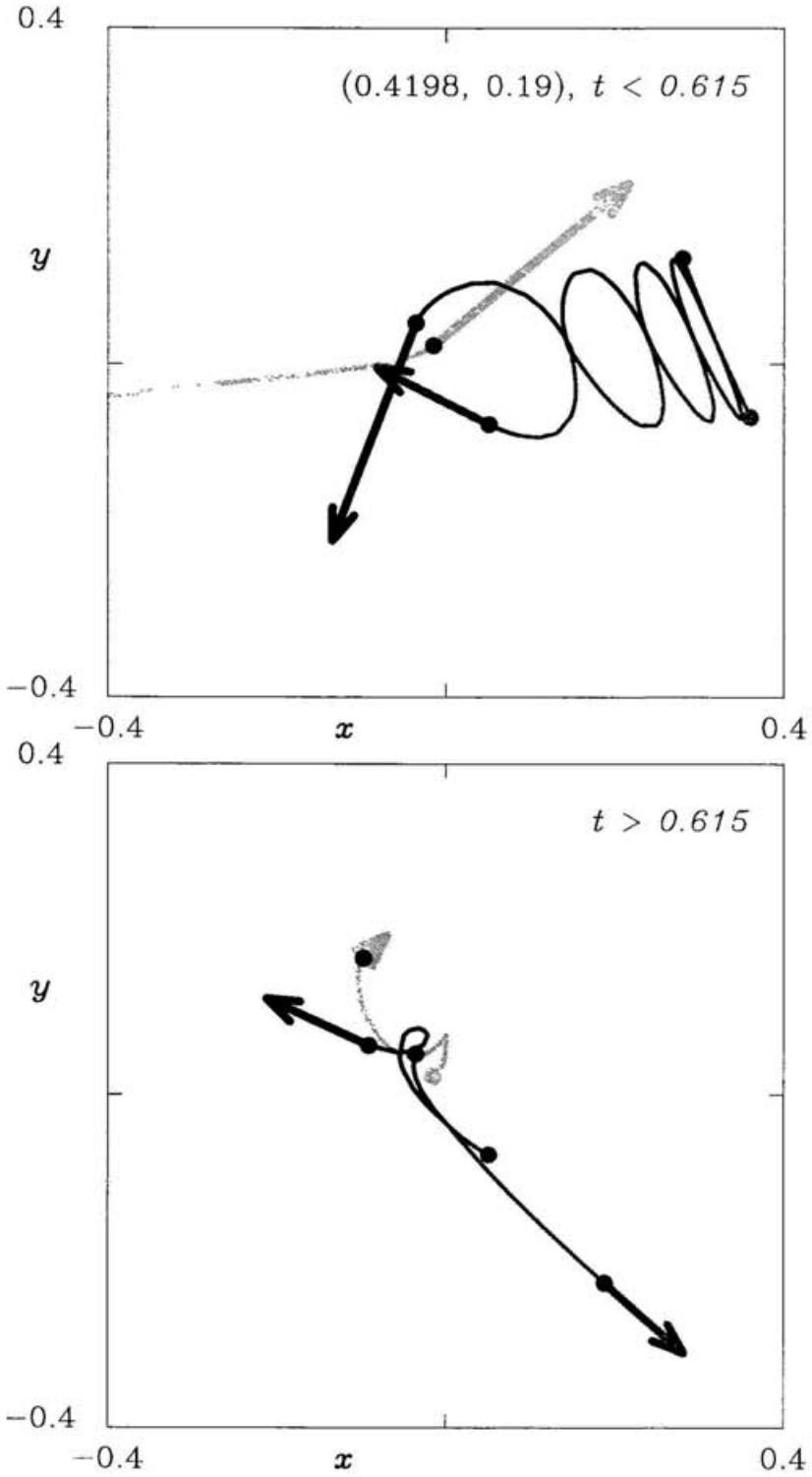

Figure 2.16: A binary-collision orbit which is of type 2. The particle m_3 leads to escape after the binary collision between m_3 and m_1. A type of triple encounter is exchange. First, m_1 approach m_2, and m_1 collides with m_3.

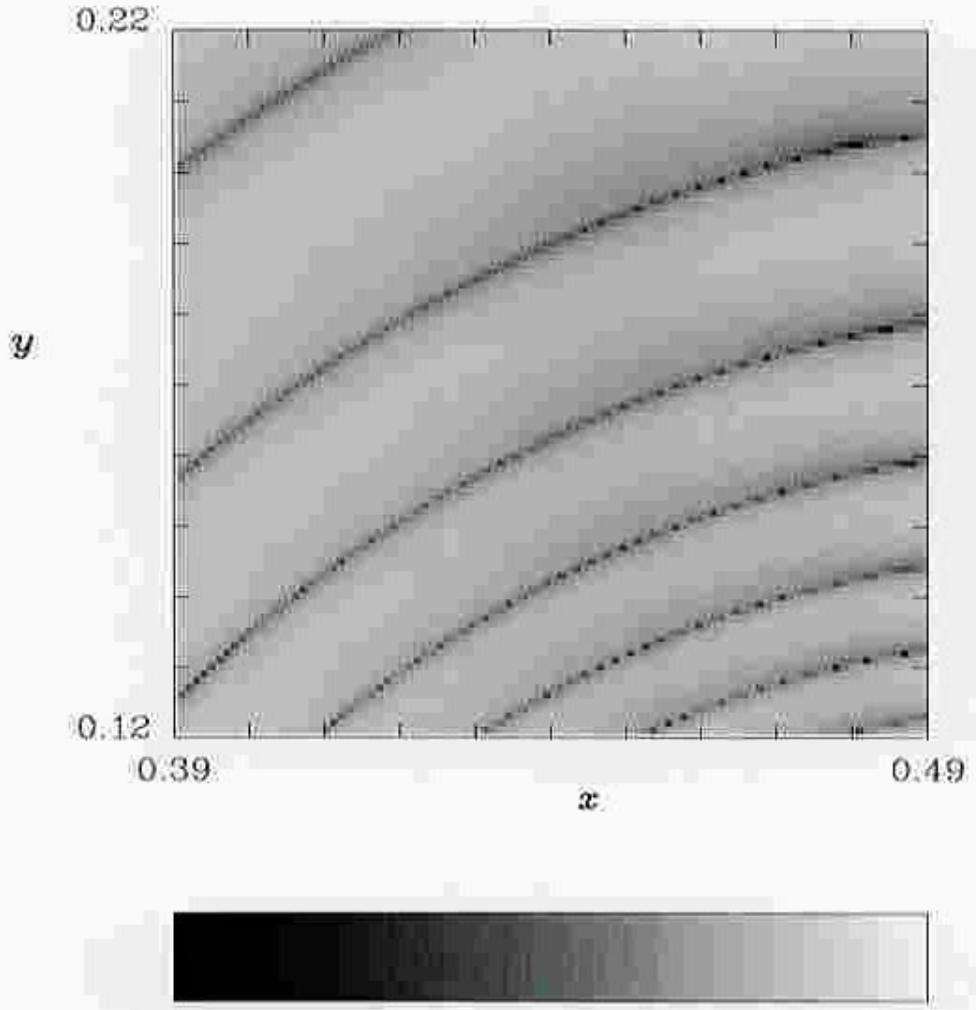

Figure 2.17: Initial-value dependence of the normalized minimum moment of inertia until second shrink of the system, which is definded as the minimal value of the moment of inertia with respect to time in the scaled system such that the total energy is -1. A gray scale varies linearly as the logscale of the normalized values. The darkest element shows $\log_{10} \hat{I}_{\min} = -5$, and the lightest one represents $\log_{10} \hat{I}_{\min} = -1$.

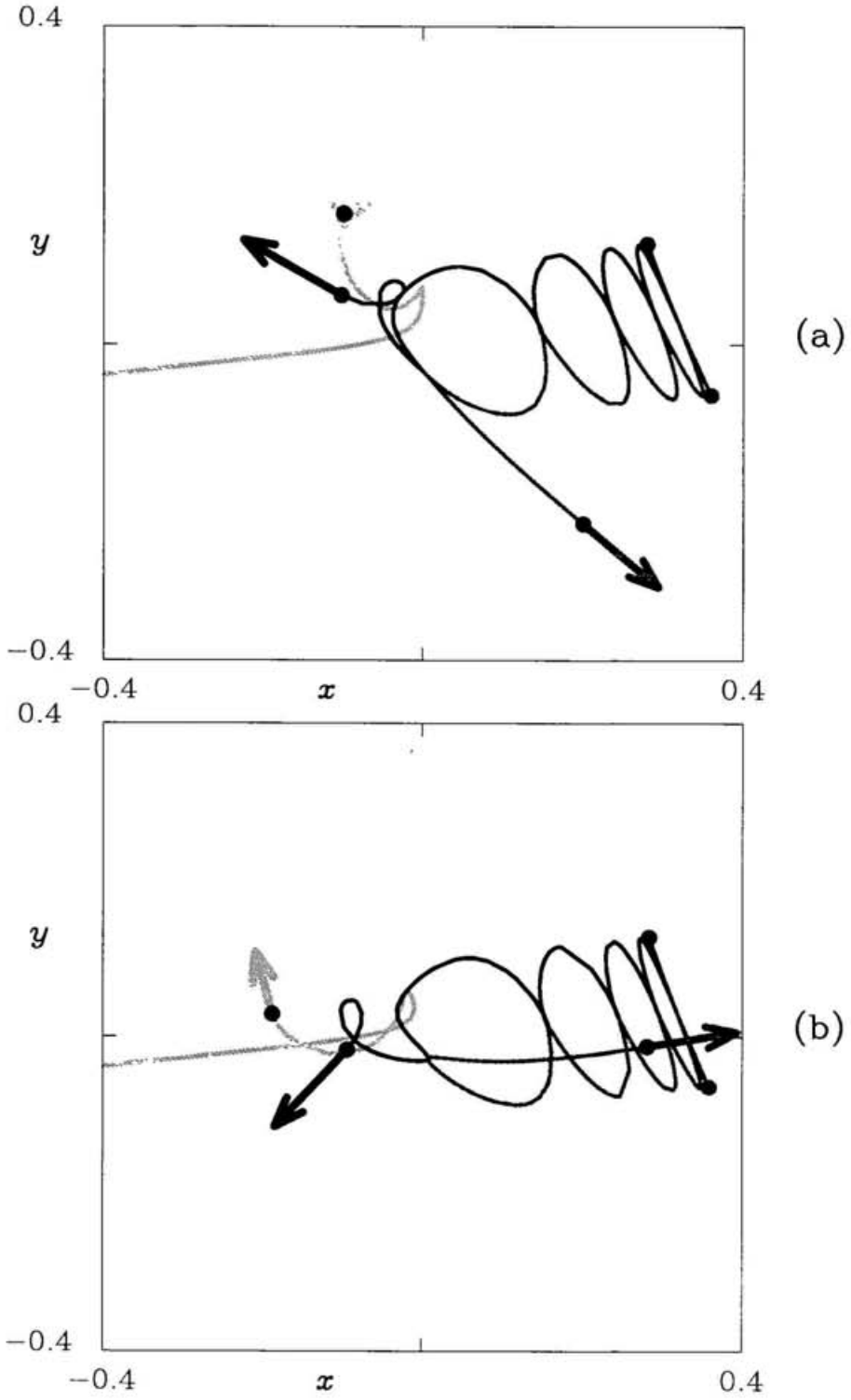

Figure 2.18: (a) An exchange orbit leading to escape for m_3. The initial value is $(0.420, 0.19)$ located in the tongue-like region E_5. (b) An exchange orbit failing in escape after the first triple encounter, although m_3 is ejected at once. The initial value is $(0.425, 0.19)$ located in a blank region between E_5 and S_5.

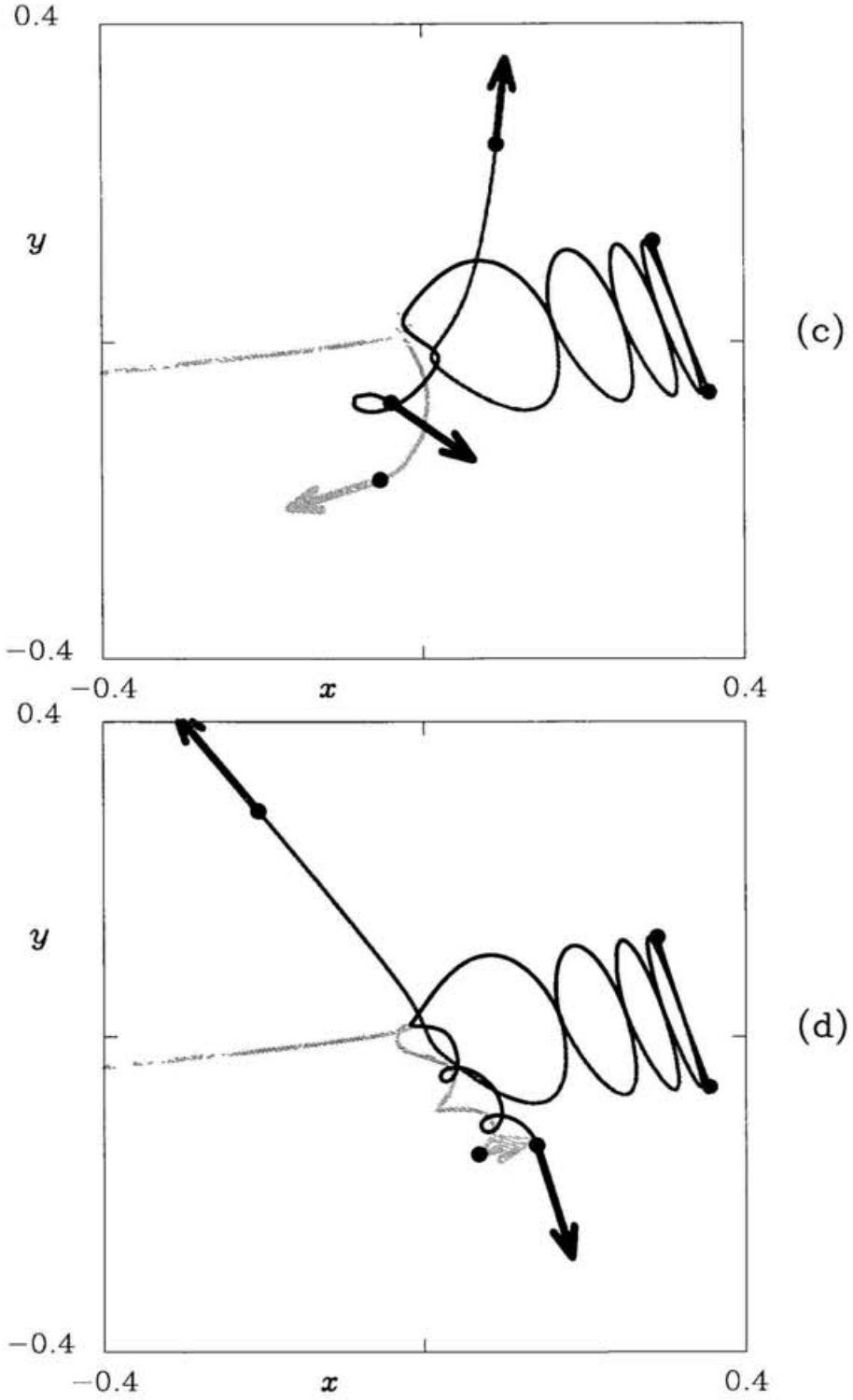

Figure 2.18: (c) An exchange orbit failing in escape after the first triple encounter, although m_3 is ejected at once. The initial value is $(0.430, 0.19)$ located in a blank region between E_5 and S_5. (d) A slingshot orbit leading to escape for m_3. The initial value is $(0.435, 0.19)$ located in the band-like region S_5.

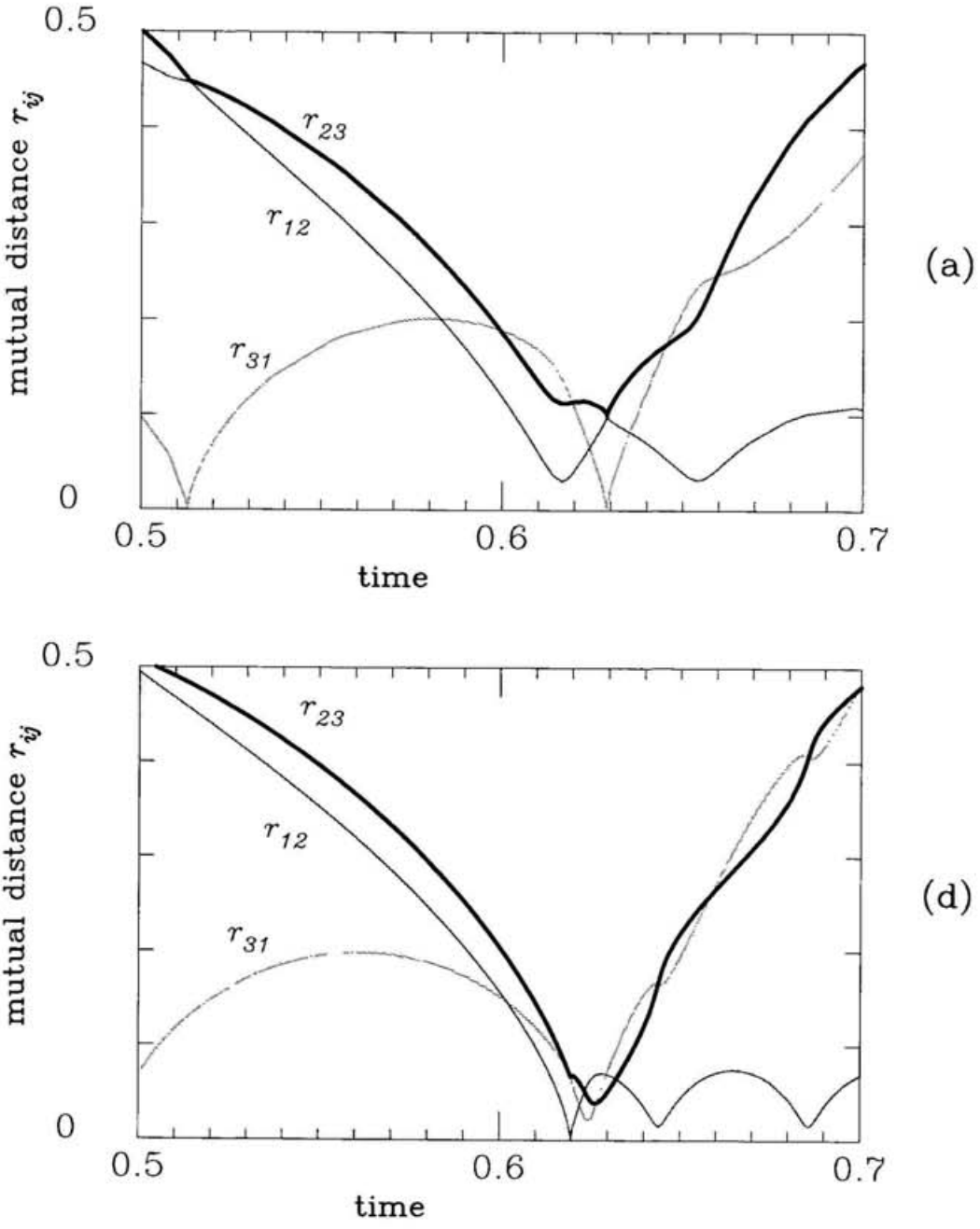

Figure 2.19: The time evolution of mutual distances. A bold curve represents r_{23}, where r_{jk} is the distance between m_j and m_k. The upper figure denoted as (a) shows the evolution of exchange-escape motion starting at the initial value $(0.420, 0.19)$. The lower figure denoted as (d) is the evolution of slingshot-escape motion at $(0.435, 0.19)$.

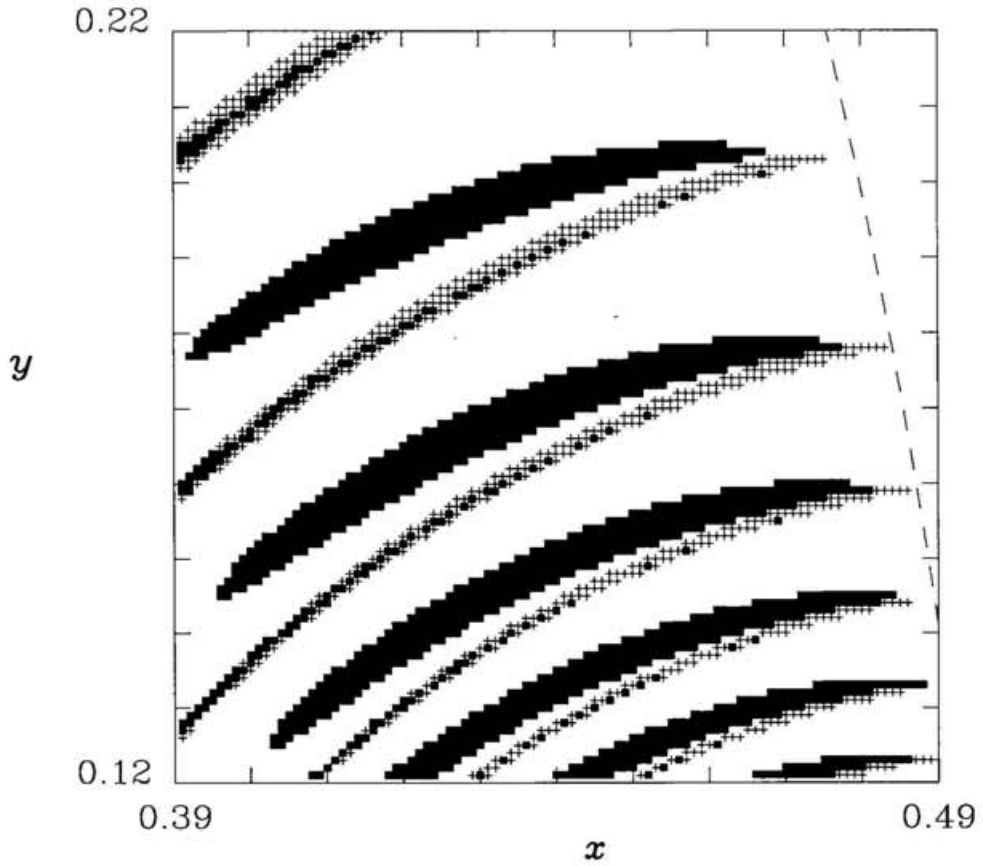

Figure 2.20: Escape regions for m_3. A cross (+) stands for the initial value where the system experience the closest approach between m_2 and m_3. A filled box represents the initial value where the closest approach between m_2 and m_3 does not occur. Distinction between exchange-escape orbit and slingshot-escape one is possible, since the boundary between S_i and E_i appears as a divided curve between crosses and filled boxes.

Chapter 3

Quantitative results

3.1 Introduction

In the present chapter, we analyze binary formation statistically using the free-fall problem. In Section 2.5, we found exchange-escape orbits after the first triple encounter in the free-fall problem with equal masses. In the present chapter, slingshot effect is compared with exchange effect in the evolution of systems. The importance of slingshot is emphasized from the results.

In Section 3.2, escape probabilities due to slingshot and due to exchange are evaluated, and are compared with each other. In Section 3.3, the increments of binding energies of formed binaries due to the respective encounters are evaluated, and are compared with each other. In the final section of the present chapter, favorable configurations of the slingshot encounter leading to escape are investigated statistically.

It is well-known that escape in the three-body problem is one of the important phenomena in the astrophysics. In the system of self-gravitating gas such as a globular cluster, the process of binary formation has a crucial role in the evolution of the system. The binaries can be a significant heat source by increasing their binding energy during encounters with single stars. According to Elson, Hut and Inagaki (1987), even in relaxed globular clusters the three-body interactions may have a global influence on the evolution of the whole system. The interaction among three particles is the fundamental process of binary formation.

The first analytic approximations of energy increments for escape due to exchange were treated by Heggie (1975). Hut (1983) developed more precise analysis of each type. On the other hand, slingshot configuration leading to escape was searched by Agekian

and Anosova (1991) numerically. However, the investigation was incomplete. Recently, Zare and Szebehely (1995) analyzed the mechanism of energy increment for escape due to slingshot by means of analytical methods. Thus the microscopic mechanism to obtain kinetic energy from a binary is clarified roughly. However, there is not any study comparing energy transition due to slingshot with the one due to exchange.

In the free-fall system, the escape probability can be defined simpler. We use the fact that the initial-value space is a two-dimensional surface. In Subsection 3.2.1, we define the escape probability as the ratio of the area of escape region to the area of initial-value space D (see also Anosova, 1986; Anosova, 1991; Umehara and Tanikawa, 1996). Therefore, our attention is concentrated on evaluating the area of escape regions.

In general, it is necessary to know high-dimensional volume of flows leading to escape in order to evaluate the probability. It is a difficult work and much approximation is implemented. The results are not so precise. Keck (1960), Keck and Mansbach (1969) presented a variational theory and they give a least upper bound to the rate of a chemical reaction. Mansbach (1970) expressed analytically the rate of formation of binaries in the three-body system with the aid of Keck's variational theory. The regions which correspond to two particles being gravitationally bound or free are identified in the phase space. The ratio of binary formation is defined as the inward flux of points across a surface which separates these regions. In contrast with the general case, the free-fall problem is easy to derive the probability.

One of our results shows that escape probability due to slingshot relative to total escape probability is about 90%. This large ratio confirms quantitatively that slingshot plays the dominant role in escape phenomena.

The total energies are various on the initial-value space D. In Subsection 3.2.2, the total energies of the systems are normalized for all initial points. The initial-space is transformed to the surface with constant energy in the phase space. By evaluating area leading to escape on the constant-energy surface, the escape probability due to slingshot relative to the escape probability due to exchange is obtained as about 0.4. This small ratio seems to suggests that slingshot does not plays the dominant role in escape phenomena.

Although the slingshot-escape probability is small, it becomes clear that slingshot effect is large in the evolution of systems. Binding-energy transitions after the first triple encounter are evaluated in Section 3.3. In the process, it is shown that the slingshot

encounters can be more energetic that the exchange one. Therefore, slingshot dominates exchange on the evolution of the system.

In Subsection 3.3.1, we evaluate the increment of binding energies of formed binaries and compare the dependence on encounter types. In the case of the exchange type, the binding energy does not increase beyond a certain critical value. On the other hand, in the case of slingshot, the increment may have a large value. The average values of the increment of binding energies due to slingshot and due to exchange are compared with each other. As a result, the ratio of the increment by slingshot escape to the increment by exchange escape is evaluated as approximately 4.0. Therefore, the ratio of the total energy change by slingshot escape to the total energy change by exchange escape is nearly equal to 1.6. Some of slingshot-escape orbits show a large energy change.

Moreover, in Subsection 3.3.2, we search where are initial values of orbits leading to the energetic escape due to slingshot. It is true that slingshot-escape orbits close to a triple-collision orbit are energetic. However, the near-isosceles slingshot is not so energetic in the orbits which are distant from a triple collision orbit. We find that relatively energetic orbits far from triple-collision orbits distribute around the near-isosceles-slingshot orbits. This relatively energetic orbits show that m_2 or m_3 escapes while m_1 escapes in the near-isosceles-slingshot orbits.

Shebalin and Tippens (1996) investigated the time evolution of binding energies between the particles m_1 and m_2, m_2 and m_3, and m_3 and m_1 in the system with small angular momentum where the orbit is close to triple collision. In Subsection 3.3.3, we also observe the time evolution of binding energies between the respective two particles. As a result, the existence of non-escape orbits can be understood between slingshot-escape orbits and exchange-escape orbits. We find that the behavior of the time-dependent binding energies starting in both the slingshot-escape region and the exchange-escape one is different from the behavior of the binding energy starting on the non-escape region in between. The particle m_3 escapes in the exchange-escape region. The same particle m_3 also escapes in the sub-band of the slingshot-escape region neighboring the exchange-escape region. The mechanism is found why m_3 can not obtain enough energy to escape if the system starts on the gap. At the syzygy crossing, the configuration and the velocity-vector directions are not favorable to escape.

Conditions favorable for escape due to slingshot are shown in Section 3.4. The mechanism of acceleration is not clearly understood. In the restricted three-body problem, Sitnikov (1961) shows the mechanism where the massless particle is accelerated by the

receding binary after the syzygy crossing. If all three particles have positive masses, energy-transfer process is more complicated. In the planar-isosceles three-body problem, Zare and Szebehely (1995) suggest a proof that the third particle obtains from the receding binary after the syzygy crossing in the planar-isosceles problem. It is necessary to investigate the condition of slingshot leading to escape in the planar or three-dimensional three-body problem.

In Subsection 3.4.1, we investigate the state at the syzygy crossing of orbits which start in the slingshot-escape regions in the free-fall three-body system. The conclusion is the same as the one in previous works, i.e., the system leads to escape if the particle passes through between two particles when they are receding from each other. However, we find that the radial velocity of the binary components can not characterize the slingshot escape in the planar system. We also find a good measure of the receding. The lower boundary of the measure leading to escape is determined clearly.

Moreover, relations of slingshot encounter and isosceles motion are investigated in the same subsection. We compare the deviation of velocity vectors from the axis of symmetry with the deviation of configuration from the isosceles configuration. The closest syzygy crossing in which the velocity vector is perpendicular to the syzygy line turns out to be more favorable for escape than the crossing which shows the symmetric configuration. If the velocity vector points to the asymmetric direction at the closest syzygy crossing, the configuration of the orbit tends to be symmetric.

In Subsection 3.4.2, we consider why most escape orbits distribute around the near-isosceles-slingshot orbits, using the slingshot-escape condition obtained in Subsection 3.4.1. We find that there are certainly effects of binary collision expected by Tanikawa et al.(1995) in the limiting orbits around the near-isosceles-slingshot ones. Other slingshots which are favorable to escape are shown near the binary-collision orbit of the near-isosceles-slingshot type. When the binary components recede from each other after the close approach, the slingshot effect works on one of the binary components.

In Subsection 3.4.3, we investigate the planar-isosceles (not necessarily free-fall) problem with equal masses in order to understand the behavior of the near-isosceles slingshot. First, escape conditions at the syzygy crossing are evaluated numerically. We take snap shots of escape orbits on the Poincaré section. Second, we superpose the phase points at the syzygy crossing of the near-isosceles-slingshot orbits on the Poincaré section. The one-parameter families of the near-isosceles-slingshot orbits starting in the escape regions S_i for $i \geq 2$ are included in the region of the snap shots leading to escape. Therefore,

in the initial-value space D of the free-fall problem, the binary-collision curves of the near-isosceles-slingshot type in S_i, $i \geq 2$, consist of only escape points and triple-collision points. There does not exist any non-escape point.

3.2 Escape probability due to slingshot and exchange

3.2.1 Area of escape regions on the initial-value space

In the present subsection, escape probabilities due to slingshot and due to exchange are evaluated on the initial-value space D. The initial-value space D is bounded, and so the escape probability is defined as the ratio of the escape region to the area of D.

Umehara et al. (1995) found the similarity of structures between S_1 and S_2, where structure means binary-collision curves and escape sub-regions around the respective triple-collision points in the extended initial-value space $\grave{D}$. Also, they suggested that probability of escape can be computed if there is any scaling law among escaping sub-regions. Umehara and Tanikawa (1996) confirmed the similarity of S_i, $i = 1, 2, \cdots, 6$, and that of E_i, $i = 5, 6$. According to Tanikawa et al. (1995), there is an infinite sequence of the binary-collision curves of *near-isosceles-slingshot type* in D and it converges at the lower-right corner $(0.5, 0)$ of D. This assures the existence of an infinite sequence of S_i and E_i maintaining similarity. We attempt to formulate the areas of escape regions as functions of i.

Before showing the numerical result, some notations are introduced. Recall that i denote the number of close approaches between m_1 and m_3 until the first triple encounter. The initial-value space D is divided into sub-regions for i. The grid-element number of the i-th sub-group of D is denoted by N_i^{D}. The number of the escape points after the first triple encounter is denoted by N^{F}. The samples are also classified into sub-groups for i, and N_i^{F} denotes the element number of escape points after the first triple encounter at the time of the i-th close approach.

The samples of the escape points are also classified into types of triple encounters. Let N^{S} and N^{E} be the numbers of escape points after the first triple encounter due to slingshot and exchange, respectively. Moreover, N_i^{S} and N_i^{F} are the escape-point numbers after the first triple encounter at the i-th close approach due to slingshot and exchange, respectively.

Similarly, the samples are classified into identities of escaping particles. The number of samples where a particle m_j escapes after the first triple encounter at the i-th close approach is denoted by $N_i^{\mathrm{F}\{j\}}$. The sum of $N_i^{\mathrm{F}\{j\}}$ for $i = 1, 2, \cdots$ is denoted by $N^{\mathrm{F}\{j\}}$.

The above definitions give the following relations:

$$N_i^{\mathrm{F}} = N_i^{\mathrm{S}} + N_i^{\mathrm{E}} = \sum_{j=1}^{3} N_i^{\mathrm{F}\{j\}}, \tag{3.1}$$

$$N^{\mathrm{F}} = \sum_{i=1}^{\infty} N_i^{\mathrm{F}}, \tag{3.2}$$

$$N^{\mathrm{S}} = \sum_{i=1}^{\infty} N_i^{\mathrm{S}}, \tag{3.3}$$

$$N^{\mathrm{E}} = \sum_{i=1}^{\infty} N_i^{\mathrm{E}}, \tag{3.4}$$

$$N^{\mathrm{F}} = N^{\mathrm{S}} + N^{\mathrm{E}} = \sum_{j=1}^{3} N^{\mathrm{F}\{j\}}. \tag{3.5}$$

Table 3.1 shows the i-dependence of grid-element numbers of escape points after the first triple encounter. The first column stands for the number i. The second column represents the size of grid elements which is denoted by δx. The grid intervals of x-direction and y-direction are equal, i.e., $\delta x = \delta y$. The size of grid elements is made smaller as i increases. The third, fourth and fifth columns stand for N_i^{F}, N_i^{S} and N_i^{E}, respectively. The sixth, seventh and eighth columns represent $N^{\mathrm{F}\{1\}}$, $N^{\mathrm{F}\{2\}}$ and $N^{\mathrm{F}\{3\}}$, respectively.

The probabilities of escape after the first triple encounter due to slingshot and exchange at the i-th close approach of two particles are denoted by P_i^{S} and P_i^{E}, respectively. The probability of escape for m_j with the i-th close approach is denoted by $P_i^{\mathrm{F}\{j\}}$. The total probability of escape after the first triple encounter is denoted by P_i^F, i.e., $P_i^F = P_i^S + P_i^E$. These probabilities are expressed as

$$P_i^X = \frac{N_i^X \cdot \delta x \cdot \delta y}{D}, \tag{3.6}$$

$$P_i^{F\{j\}} = \frac{N_i^{F\{j\}} \cdot \delta x \cdot \delta y}{D}, \qquad (j = 1, 2, 3), \tag{3.7}$$

where $X \in \{T, S, E\}$, and $D = \pi/6 - \sqrt{3}/8$ is the area of the initial-value space.

The i-dependence of the probabilities P_i^S, P_i^E, and P_i^F are shown in Fig.3.1. An open circle ($\circ$) represents P_i^S. A filled circle ($\bullet$) and a cross ($\times$) stand for P_i^E and P_i^F, respectively. Probabilities P_i^S and P_i^F as functions of i become linear very quickly with increasing i in the log-log plot. Such linear relations are shown as the bold lines in the

figure. Each of the lines is evaluated with the least-squares method from the sampled data between the endpoints of the line. The probabilities as functions of i are given by

$$P_i^{\mathrm{F}} = 0.1765 \cdot i^{-2.125} \quad \text{for } i \in [10, 50], \tag{3.8}$$

$$P_i^{\mathrm{S}} = 0.08892 \cdot i^{-2.191} \quad \text{for } i \in [3, 50], \tag{3.9}$$

The probability for a larger i can be estimated by extrapolation of the above formulae.

The total probability of escape P^F is obtained as

$$P^{\mathrm{F}} = \sum_{i=1}^{\infty} P_i^{\mathrm{F}} = 0.1765 \left\{ \zeta(2.125) - \sum_{i=1}^{9} i^{-2.125} \right\} + \sum_{i=1}^{9} P_i^{\mathrm{F}}, \tag{3.10}$$

where ζ is a zeta function: $\zeta(s) = \sum_{n=1}^{\infty} n^{-s}$ for $s > 1$. For $i = 1, 2, \cdots, 9$, the rule given by eq.(3.8) does not fit the evaluated results from the numerical survey, and so the last term $\sum_{i=1}^{9} P_i^{\mathrm{F}}$ is added from the values evaluated numerically. Therefore,

$$P^{\mathrm{F}} = 0.1765\{1.5416 - 1.4710\} + 0.1065 = 0.1190, \tag{3.11}$$

where $\zeta(2.125) = 1.5416$. Similarly, the probability of escape due to slingshot P^{S} is evaluated as

$$P^{\mathrm{S}} = \sum_{i=1}^{\infty} P_i^{\mathrm{S}} = 0.08892 \left\{ \zeta(2.191) - \sum_{i=1}^{2} i^{-2.191} \right\} + \sum_{i=1}^{2} P_i^{\mathrm{S}} = 0.1055, \tag{3.12}$$

where $\zeta(2.191) = 1.4963$. Since P^{E} does not follow any power law, the probability P^{E} of escape due to exchange is

$$P^{\mathrm{E}} = P^{\mathrm{F}} - P^{\mathrm{S}} = 0.0135. \tag{3.13}$$

The relative probability of escape due to slingshot is

$$P^{\mathrm{S}}/P^{\mathrm{F}} = 0.8866. \tag{3.14}$$

This large ratio confirms quantitatively that slingshot plays the dominant role in escape phenomena.

Next let us discuss the small angular momentum case. The i-dependence of the relative probability of exchange escape to slingshot escape is evaluated as

$$(P_i^{\mathrm{F}} - P_i^{\mathrm{S}})/P_i^{\mathrm{F}} = 1 - 0.504 \cdot n^{-0.07}. \tag{3.15}$$

It increases with increasing i. In the free-fall system with a sufficiently large i, regions of initial values leading to escape after the exchange is larger than that after the slingshot. However, according to Anosova (1992) who added small angular momentum to the

equal-mass system, motion starting from the lower-right part of D is bounded and does not escape. On the other hand, the behavior in the upper part of D is expected not to change with addition of small angular momentum. So we can say that slingshot is more important in the escape phenomena than exchange in small nonzero angular momentum cases.

The total probabilities $P^{\mathrm{F}\{j\}}$ leading to escape for m_j, $j = 2,3$ as functions of i are given by

$$P_i^{\mathrm{F}\{2\}} = 0.04178 \cdot i^{-2.228} \quad \text{for} \quad i \in [3,50], \tag{3.16}$$

$$P_i^{\mathrm{F}\{3\}} = 0.1328 \cdot i^{-2.096} \quad \text{for} \quad i \in [10,50]. \tag{3.17}$$

respectively.

The probabilities $P^{\mathrm{F}\{j\}}$, $j = 2,3$ are

$$P^{\mathrm{F}\{2\}} = \sum_{n=1}^{\infty} P^{\mathrm{F}\{2\}} = 0.04178 \left\{ \zeta(2.228) - \sum_{i=1}^{2} i^{-2.228} \right\} + \sum_{i=1}^{2} P_i^{\mathrm{F}\{2\}} = 0.07815, \tag{3.18}$$

$$P^{\mathrm{F}\{3\}} = \sum_{n=1}^{\infty} P^{\mathrm{F}\{3\}} = 0.1328 \left\{ \zeta(2.096) - \sum_{i=1}^{9} i^{-2.096} \right\} + \sum_{i=1}^{9} P_i^{\mathrm{F}\{3\}} = 0.03927, \tag{3.19}$$

respectively. Note that $\zeta(2.228) = 1.4732$ and $\zeta(2.096) = 1.5633$. The probability of m_1 leading to escape is

$$P^{\mathrm{F}\{1\}} = P^{\mathrm{F}} - P^{\mathrm{F}\{2\}} - P^{\mathrm{F}\{3\}} = 0.0016. \tag{3.20}$$

The relative probabilities are

$$P^{\mathrm{F}\{1\}}/P^{\mathrm{F}} = 0.0134, \quad P^{\mathrm{F}\{2\}}/P^{\mathrm{F}} = 0.6567, \quad P^{\mathrm{F}\{3\}}/P^{\mathrm{F}} = 0.3300. \tag{3.21}$$

The relation among $P^{\mathrm{F}\{j\}}, j = 1,2,3$ is

$$P^{\mathrm{F}\{1\}} < P^{\mathrm{F}\{3\}} < P^{\mathrm{F}\{2\}}. \tag{3.22}$$

Let r_j be the initial distance between m_k and m_l, where $(j,k,l) = (1,2,3)$ or its cyclic permutation. On the initial-space D,

$$r_1 > r_3 > r_2, \tag{3.23}$$

i.e., $P^{\mathrm{F}\{j\}}$ increases with r_j decreasing for $j = 1,2,3$. There is the largest probability of escape for the particle which is not located at endpoints of the shortest side in the initial-configuration triangle of three particles.

Moreover, let ρ_j denote the distance between m_j and the gravity center of m_k and m_l. The following relation is derived easily:

$$\rho_j^2 = \frac{2r_k^2 + 2r_l^2 - r_j^2}{4}. \tag{3.24}$$

We have $\rho_2 > \rho_3 > \rho_1$ since $r_2 < r_3 < r_1$. The escape phenomenon of m_j is more probable as the initial median line ρ_i is longer. It is concluded that an originally distant particle tends to escape.

The particle-identity dependence of the probabilities of each m_j, $j = 1, 2, 3$ leading to escape are shown in Fig. 3.2. A filled circle ($\bullet$), a plus mark ($+$), and a open circle ($\circ$) stand for $P_i^{\mathrm{F}\{1\}}$, $P_i^{\mathrm{F}\{2\}}$, and $P_i^{\mathrm{F}\{3\}}$, respectively.

$$P_i^{\mathrm{F}\{3\}} < P_i^{\mathrm{F}\{1\}} < P_i^{\mathrm{F}\{2\}} \qquad \text{for } i = 1, \tag{3.25}$$

$$P_i^{\mathrm{F}\{1\}} < P_i^{\mathrm{F}\{2\}} < P_i^{\mathrm{F}\{3\}} \qquad \text{for } i \geq 2. \tag{3.26}$$

This means that the most probable particle leading to escape after the first triple encounter is m_3 for a large i. In the lower-right part on the initial-value space D, one of the components of the original binary tends to escape. The escape phenomenon of m_3 is more probable than the escape phenomenon of the incoming particle m_2 in the case of the hierarchical configuration.

3.2.2 Escape probability with constant energy

Derivation of the equi-energy surface

Our numerical survey is executed on the space of initial values where the respective total energies are different. By a suitable scaling of variables and time, the initial-value space can be transformed to the space with constant energy. In the present subsection, we will construct a homeomorphism from the initial-value space D to an equi-energy surface.

Let us introduce the coordinates (r, ρ, θ) in the configuration space of the planar three-body system. Here, r is the mutual distance between the particles m_2 and m_3, ρ is the distance between m_1 and the gravity center of m_2 and m_3, and θ is the angle between the side r and the side ρ. The canonically conjugate momenta to r, ρ, and θ are denoted by p_r, p_ρ, and p_θ, respectively. Hereafter the coordinate system $(r, \rho, \theta, p_r, p_\rho, p_\theta)$ is called the *polar Jacobi system.*

Using the introduced variables, the reduced Hamiltonian of three degrees of freedom

with the zero-angular-momentum and equal-mass case ($m_j = 1, j = 1, 2, 3$) is obtained as

$$H = \left\{ {p_r}^2 + \left(\frac{p_\theta}{r}\right)^2 \right\} + \frac{3}{4}\left\{ {p_\rho}^2 + \left(\frac{p_\theta}{\rho}\right)^2 \right\} - \frac{1}{r} - \frac{1}{r_2} - \frac{1}{r_3}, \tag{3.27}$$

where

$$r_2 = \sqrt{\frac{1}{4}r^2 - r\rho\cos\theta + \rho^2}, \tag{3.28}$$

$$r_3 = \sqrt{\frac{1}{4}r^2 + r\rho\cos\theta + \rho^2}. \tag{3.29}$$

See Appendix A.1 for derivation.

The transformation of the initial-value space is decomposed into the following three procedures:

$$\begin{bmatrix} x_0 \\ y_0 \end{bmatrix} \mapsto \begin{bmatrix} \rho_0 \\ \theta_0 \end{bmatrix} \mapsto \begin{bmatrix} \hat{\rho}_0 \\ \hat{\theta}_0 \end{bmatrix} \mapsto \begin{bmatrix} \hat{r}_0 \\ \hat{\rho}_0 \\ \hat{\theta}_0 \end{bmatrix}. \tag{3.30}$$

The initial-value space D is described by the Cartesian coordinates denoted by (x_0, y_0). The first procedure is the transformation from the Cartesian system to the polar Jacobi system. On D, the largest distance between two particles is adjusted to a unit length, and so the initial value of r is fixed to 1. All initial values of momenta (p_r, p_ρ, p_θ) are zero. Therefore, only two variables ρ and θ are enough to describe the initial-value space D by the polar Jacobi coordinates. These initial values are denoted by (ρ_0, θ_0). The vector (ρ_0, θ_0) indicates the position of m_1 in the polar coordinate system. The composed mapping of the second and the third transformations corresponds to scaling of the variables in order to adjust the energy constant. The second procedure shows a similar transformation on the (ρ, θ)-space. The third one is the projection to the equi-energy surface.

Let us summarize the result of the transformation. The transformation to the surface with constant energy $\hat{h} = \text{const.} < 0$ is given by

$$\hat{r}_0 = \alpha, \qquad \hat{\rho}_0 = \alpha\rho_0, \qquad \hat{\theta}_0 = \theta_0, \tag{3.31}$$

$$\rho_0 = \sqrt{x_0^2 + y_0^2}, \qquad \cos\theta_0 = \frac{x_0}{\rho_0}, \tag{3.32}$$

where

$$\alpha(\rho_0(x_0, y_0), \theta_0(x_0, y_0)) = \frac{1}{-\hat{h}}\left(1 + \frac{1}{r_{20}} + \frac{1}{r_{30}}\right), \tag{3.33}$$

$$r_{20} = \sqrt{\left(x_0 - \frac{1}{2}\right)^2 + y_0^2} = \sqrt{\frac{1}{4} - \rho_0 \cos\theta_0 + {\rho_0}^2}, \tag{3.34}$$

$$r_{30} = \sqrt{\left(x_0 + \frac{1}{2}\right)^2 + y_0^2} = \sqrt{\frac{1}{4} + \rho_0 \cos\theta_0 + {\rho_0}^2}. \tag{3.35}$$

The surface with constant energy is obtained as a function $\hat{r}$ of (ρ_0, θ_0) or (x_0, y_0):

$$\hat{r} = \alpha(\rho_0(x_0, y_0), \theta_0(x_0, y_0)). \tag{3.36}$$

In order to prove that the transformation is homeomorphic, it is sufficient to confirm that the Jacobian matrix of the transformation is regular in the domain of definition on D. The Jacobian determinant of the transformation is denoted by J. It is found that $J \neq 0$ for $(x_0, y_0) \in D$. However, J is undefined at the two points $(x_0, y_0) = (0, 0), (0, 0.5)$. This transformation is not available for the two points. The Jacobian determinant is obtained as

$$J(x_0, y_0) = \frac{d}{-\hat{h}\rho_0} \left\{ \left(\frac{\partial \hat{r}_0}{\partial \hat{\rho}}\right)^2 + \left(\frac{\partial \hat{r}_0}{\partial \hat{\theta}}\right)^2 + 1 \right\}^{1/2}, \tag{3.37}$$

where

$$d = 1 + \frac{1}{2} r_{20}^{-3} \left(\frac{1}{2} - \rho_0 \cos\theta_0\right) + \frac{1}{2} r_{30}^{-3} \left(\frac{1}{2} + \rho_0 \cos\theta_0\right), \tag{3.38}$$

$$\frac{\partial \hat{r}}{\partial \hat{\rho}} = \frac{r_{20}^{-3}(\cos\theta - 2\rho) - r_{30}^{-3}(\cos\theta + 2\rho)}{2d}, \tag{3.39}$$

$$\frac{\partial \hat{r}}{\partial \hat{\theta}} = \frac{\alpha\rho \sin\theta (r_{30}^{-3} - r_{20}^{-3})}{2d}. \tag{3.40}$$

J diverges to ∞ at the points $(x_0, y_0) = (0, 0)$ and $(0.5, 0)$. The transformed surface with constant energy is homeomorphic to the initial-value space D except at the two points. See more detailed derivation of the transformation in Appendix A.2.

In order to evaluate the escape probability with constant energy, it is necessary to evaluate the area of the escape regions on the equi-energy surface. The escape regions are projected to the equi-energy surface. We will derive the change of the escape area. We already know the weight function from the area element in the initial-value space D to the element in the equi-energy surface. At the initial value (x_0, y_0), the weight function is equivalent to the Jacobian determinant $J(x_0, y_0)$ of the transformation. Hence, the area on the equi-energy surface A is given by

$$A = \int_x \int_y J(x, y) dx dy = \sum_{x,y} J(x, y) \delta x \delta y, \tag{3.41}$$

where $\delta x \delta y$ is the grid element of the initial-value space D and the summation $\sum_{x,y}$ runs over our considering region on D.

The distribution of the Jacobian determinant $J(x, y)$ on the initial-value space D is shown in Fig.3.3. Here, J is evaluated from eq.(3.37) where energy constant $\hat{h}$ is fixed at -1. The darkness in the figure increases with increasing J and is proportional to $\log_{10} J$. A gray scale varies linearly as the logscale of J. If the initial configuration is the equilateral triangle, $J(0, \sqrt{3}/2)$ is equal to $\sqrt{7}$ on the equi-energy surface with $\hat{h} = -1$. If the initial configuration is the collinear central one, $J(0, 0)$ tends to infinity as explained above. $J(0.5, 0)$ also diverges to infinity.

Evaluation of escape regions on the equi-energy surface

The equi-energy surface transformed from the initial-value space D is not bounded, and so the escape probability can not be defined as the ratio of the escape region to the total area of the surface. Thus we will evaluate the relative probability.

Let us consider the area-sequence of conditional escape as well as that of escape where the escape criterion is satisfied. Recall that the conditional escape is defined as the ejected particle recedes from a binary to the distance $20 d_{\rm unit}$ without satisfying the escape criterion, where $d_{\rm unit}$ denotes the mean harmonic separation between particles in virial equilibrium (see the flow-chart of the integration until the i-th triple encounter in Section 2.2).

Before showing the numerical result, some notations are necessary. On the equi-energy surface, $A_i^{\rm D}$ denotes the area of the region where the triple encounter occurs at the i-th close approach between m_1 and m_3. Let $A_i^{\rm F}$ denote the area of the escape region after the first triple encounter at the time of the i-th close approach. The areas of the escape regions due to slingshot and exchange at the i-th close approach are denoted by $A_i^{\rm S}$ and $A_i^{\rm E}$, respectively. For $X \in \{S, E, F\}$, the conditional-escape region after the first triple encounter at the time of the i-th close approach is denoted by $\bar{A}_i^X$. Note that

$$A_i^{\rm D} > \bar{A}_i^{\rm F} = \bar{A}_i^{\rm S} + \bar{A}_i^{\rm E} > A_i^{\rm F} = A_i^{\rm S} + A_i^{\rm E}, \qquad \bar{A}_i^{\rm S} > A_i^{\rm S}, \qquad \bar{A}_i^{\rm E} > A_i^{\rm E}, \tag{3.42}$$

The i-dependences of areas $A_i^{\rm D}$, $A_i^{\rm S}$, $\bar{A}_i^{\rm S}$, $A_i^{\rm E}$, $\bar{A}_i^{\rm E}$, $A_i^{\rm F}$, $\bar{A}_i^{\rm F}$ are shown in Fig.3.4. The data-plot sequences on dotted lines stand for the conditional-escape regions $\bar{A}_i^{\rm F}$, $\bar{A}_i^{\rm S}$ and $\bar{A}_i^{\rm E}$. Open triangles represent the data plots for $A_i^{\rm F}$ and $\bar{A}_i^{\rm F}$. Filled circles and open circles show $A_i^{\rm S}$, $\bar{A}_i^{\rm S}$ and $A_i^{\rm E}$, $\bar{A}_i^{\rm E}$. A sequence of open squares stands for $A_i^{\rm D}$.

We find that all area sequences A_i^X, $X \in \{S, \bar{S}, E, \bar{E}, F, \bar{F}, D\}$ decrease with increasing i on the equi-energy surface. Moreover, Figure 3.4 suggests the following analytical relation

$$\log f(i) = p_1 \log i + p_2 + \frac{p_3}{\log i}, \qquad \text{for} \qquad f(i) \in \{A_i^S, \bar{A}_i^S, A_i^F, \bar{A}_i^F, A_i^D\}. \tag{3.43}$$

The slingshot-escape areas A_i^S and $\bar{A}_i^S$ follow the power laws, i.e., the functions of the areas become linear very quickly in the log-log plot. The areas A_i^F, $\bar{A}_i^F$ and A_i^D seem to approach the respective straight lines asymptotically. Thus a linear equation with a non-linear term which tends to zero as $i \to \infty$ is used for fitting the evaluated plots.

Bold curves in Fig.3.4 represent the function curves of eq.(3.43) where the parameters p_1, p_2 and p_3 are evaluated with the least-squares method from the sample data for $i \in \{19, 26, \ldots, 30, 36, \ldots, 40, 50\}$. The respective parameters are obtained as follows:

area	p_1	p_2	p_3
A_i^D	-0.3184	-0.06113	0.2883
$\bar{A}_i^F$	-0.3640	0.02528	-0.1600
A_i^F	-0.3897	0.05061	-0.2489
$\bar{A}_i^S$	-0.3389	-0.6026	0.03124
A_i^S	-0.3257	-0.7004	0.07588

(3.44)

Let $X \in \{D, \bar{F}, F, \bar{S}, S\}$. Let p_j^X, $j = 1, 2, 3$ denote the parameter p_j of the function for the areas A_i^D, $\bar{A}_i^F$, A_i^F, $\bar{A}_i^S$, A_i^S, respectively. The results in Fig.3.5 assure us the following relation:

$$p_1^D \simeq p_1^S \simeq \bar{p}_1^S. \tag{3.45}$$

Let $I = \{1, \cdots, 19, 26, \cdots, 30, 36, \cdots, 40, 50\}$. We have the data of the area for $i \in I$. Let $p_j^X(i)$ denote the parameter p_j^X evaluated from the plot data X_k, $k \in ([i, 50] \subset I)$ for $i \in [5, 19]$. For example, $p_j^X(19)$ is evaluated from X_k, $k = \{19, 26, \cdots, 30, 36, \cdots, 40, 50\}$. Figure 3.5 shows the i-dependence of $p_j^X(i)$, $j = 1, 2, 3$. The ordinate in the upper figure is $p_1^X(i)$. The middle and the lower figures represent $p_2^X(i)$ and $p_3^X(i)$, respectively. A data-plot sequence on a bold line stands for parameters which are evaluated from escape regions, i.e., $p_j^F(i)$ and $p_j^S(i)$. A data-plot sequence on a dotted line represents a parameter for conditional-escape regions, i.e., $\bar{p}_j^F(i)$ and $\bar{p}_j^S(i)$. Open triangles show $p_j^F(i)$ and $\bar{p}_j^F(i)$. Filled circles represent $p_j^S(i)$ and $\bar{p}_j^S(i)$.

For a linear term, parameters of slingshot-escape $p_1^S(i)$ and $\bar{p}_1^S(i)$ are nearly equal to $p_1^D(i)$ although the fluctuations of the data sequences are large. On the other hand,

total-escape parameters $p_1^{\mathrm{F}}(i)$ and $\bar{p}_1^{\mathrm{F}}(i)$ tend to p_1^{D} asymptotically with increasing i. The sequence gap at $i = 15$ may be caused by coarse sampling of the grid elements, and so it is conjectured that the fluctuation of the sequence becomes small if we sample more grid elements.

From the observed relation (3.45), we can conclude the following:

$$p_1^{\mathrm{X}} \simeq p_1^{\mathrm{D}}, \qquad X \in \{S, \bar{S}, F, \bar{F}\}. \tag{3.46}$$

It is noticed that

$$A_i^{\mathrm{S}} \leq A_i^{\mathrm{X}} \leq A_i^{\mathrm{D}}, \qquad X \in \{\bar{S}, F, \bar{F}\}, \tag{3.47}$$

for $i \geq 5$. If $p_1^{\mathrm{X}} > p_1^{\mathrm{D}}$, then A_i^{X} exceeds A_i^{D} for a sufficiently large i. It contradicts eq.(3.42). On the other hand, if $p_1^{\mathrm{X}} < p_1^{\mathrm{D}}$, then $p_1^{\mathrm{X}} < p_1^{\mathrm{S}}$. It suggests that A_i^{X} becomes smaller than A_i^{S} for a sufficiently large i. It also contradicts eq.(3.42).

From the above observation, we fix the linear parameter p_1 as

$$p_1 = \frac{p_1^{\mathrm{D}}(19) + \bar{p}_1^{\mathrm{S}}(19) + p_1^{\mathrm{S}}(19)}{3} = -0.328. \tag{3.48}$$

We will describe a modified function as

$$\log f(i) = p_1 \log i + q_2 + \frac{q_3}{\log i}, \quad p_1 = -0.328, \tag{3.49}$$

for $f(i) \in \{A_i^{\mathrm{S}}, \bar{A}_i^{\mathrm{S}}, A_i^{\mathrm{F}}, \bar{A}_i^{\mathrm{F}}, A_i^{\mathrm{D}}\}$ with parameters q_2 and q_3. In Fig.3.6, the function curves expressed by eq.(3.43) with $p_1 = -0.328$ are fitted to the data-plot sequences A_i^{X}, $X \in \{D, \bar{F}, F, \bar{S}, S\}$. Bold curves in Fig.3.6 represent the function curves of eq.(3.49) where the parameters p_1, p_2 and p_3 are evaluated with the least-squares method from the sample data for $i \in \{19, 26, \cdots, 30, 36, \cdots, 40, 50\}$. The respective parameters are obtained as the following:

area	q_2	q_3
A_i^{D}	-0.03263	0.2673
$\bar{A}_i^{\mathrm{F}}$	-0.08103	-0.08191
A_i^{F}	-0.1317	-0.1150
$\bar{A}_i^{\mathrm{S}}$	-0.6349	0.05491
A_i^{S}	-0.6785	0.05974

(3.50)

It is shown that q_j^{X} is not influenced by the choice of sampling data. A parameter $q_j^{\mathrm{X}}(i)$ is defined similarly as $p_j^{\mathrm{X}}(i)$. Let $q_j^{\mathrm{X}}(i)$ denote the parameter q_j^{X}, $j = 2, 3$ evaluated

from the plot data X_k, $k \in ([i, 50] \subset I)$ for $i \in [5, 19]$. Figure 3.7 shows the i-dependence of $p_j^{\mathrm{X}}(i)$, $j = 1, 2, 3$. The ordinates in the upper figure and in the lower figure are $q_2^{\mathrm{X}}(i)$ and $q_3^{\mathrm{X}}(i)$, respectively. A data-plot sequence on a bold line stands for parameters evaluated from escape regions, i.e., $q_j^{\mathrm{F}}(i)$ and $q_j^{\mathrm{S}}(i)$, $j = 2, 3$. A data-plot sequence on a dotted line represents a parameter for conditional-escape regions, i.e., $\bar{q}_j^{\mathrm{F}}(i)$ and $\bar{q}_j^{\mathrm{S}}(i)$. Open triangles show $q_j^{\mathrm{F}}(i)$ and $\bar{q}_j^{\mathrm{F}}(i)$. Filled circles represent $q_j^{\mathrm{S}}(i)$ and $\bar{q}_j^{\mathrm{S}}(i)$. From the figure, we find that the fluctuation of each parameter curve $q_j^{\mathrm{X}}(i)$ is almost zero. Moreover, we notice that each $q_j^{\mathrm{X}}(i)$ is almost constant with respect to i.

From the parameters evaluated in the result (3.50), we can derive relative probabilities. For a sufficiently large i, the escape probability after the first triple encounter at the i-th close approach of the original binary is evaluated as

$$\frac{A_i^{\mathrm{F}}}{A_i^{\mathrm{D}}} \to 10^{q_2^{\mathrm{F}} - q_2^{\mathrm{D}}} = 0.796. \tag{3.51}$$

If the system starts on the hierarchical configuration with zero initial velocities, 80% of the system escapes without shrinking after the first triple encounter. Moreover,

$$\frac{\bar{A}_i^{\mathrm{F}}}{A_i^{\mathrm{D}}} \to 10^{\bar{q}_2^{\mathrm{F}} - q_2^{\mathrm{D}}} = 0.895. \tag{3.52}$$

If the conditional escape is considered, 90% of the system escapes after the first triple encounter. The other relative probabilities are obtained as

$$\frac{A_i^{\mathrm{S}}}{A_i^{\mathrm{D}}} \to 10^{(q_2^{\mathrm{S}} - q_2^{\mathrm{D}})} = 0.226, \tag{3.53}$$

$$\frac{\bar{A}_i^{\mathrm{S}}}{A_i^{\mathrm{D}}} \to 10^{(\bar{q}_2^{\mathrm{S}} - q_2^{\mathrm{D}})} = 0.250. \tag{3.54}$$

About a quarter of the orbit experiencing the triple encounter at the i-th close approach leads to escape due to slingshot after the first encounter for each i.

About 30% of the escape orbits after the first triple encounter is due to slingshot since

$$\frac{A_i^{\mathrm{S}}}{A_i^{\mathrm{F}}} \to 10^{q_2^{\mathrm{S}} - q_2^{\mathrm{F}}} = 0.284, \tag{3.55}$$

and

$$\frac{\bar{A}_i^{\mathrm{S}}}{\bar{A}_i^{\mathrm{F}}} \to 10^{\bar{q}_2^{\mathrm{S}} - \bar{q}_2^{\mathrm{F}}} = 0.279. \tag{3.56}$$

The ratio of the slingshot-escape probability to the exchange-escape probability is less than a half:

$$\frac{A_i^{\mathrm{S}}}{\mathrm{E}_i} = \frac{A_i^{\mathrm{S}}}{A_i^{\mathrm{F}} - A_i^{\mathrm{S}}} \to 0.397, \tag{3.57}$$

and

$$\frac{\bar{A}_i^{\mathrm{S}}}{\bar{A}_i^{\mathrm{E}}} = \frac{\bar{A}_i^{\mathrm{S}}}{\bar{A}_i^{\mathrm{F}} - \bar{A}_i^{\mathrm{S}}} \to 0.387. \tag{3.58}$$

The ratio of the complete escape to the conditional escape is considered.

$$\frac{A_i^{\mathrm{F}}}{\bar{A}_i^{\mathrm{F}}} \to 10^{q_2^{\mathrm{F}} - \bar{q}_2^{\mathrm{F}}} = 0.890, \tag{3.59}$$

It implies that the error of evaluating escape regions on the equi-energy surface is 10%. Moreover, the ratio of the complete escape to the conditional escape due to slingshot and exchange are evaluated, respectively, as

$$\frac{A_i^{\mathrm{S}}}{\bar{A}_i^{\mathrm{S}}} \to 10^{q_2^{\mathrm{S}} - \bar{q}_2^{\mathrm{S}}} = 0.904, \tag{3.60}$$

$$\frac{A_i^{\mathrm{E}}}{\bar{A}_i^{\mathrm{E}}} = \frac{A_i^{\mathrm{F}} - A_i^{\mathrm{S}}}{\bar{A}_i^{\mathrm{F}} - \bar{A}_i^{\mathrm{S}}} \to \frac{10^{q_2^{\mathrm{F}}} - 10^{q_2^{\mathrm{S}}}}{10^{\bar{q}_2^{\mathrm{F}}} - 10^{\bar{q}_2^{\mathrm{S}}}} = 0.884. \tag{3.61}$$

The ratio due to slingshot is larger than the one due to exchange. It implies that the escape criterion works on the slingshot-escape orbit better than the exchange-escape orbit.

Table 3.1: The numbers of grid elements of escape points.

i	grid size	N_i^{F}	N_i^{S}	N_i^{E}	$N_i^{\mathrm{F}\{1\}}$	$N_i^{\mathrm{F}\{2\}}$	$N_i^{\mathrm{F}\{3\}}$	N_i^{D}
1	1.0×10^{-3}	18175	18175	0	199	17787	189	98894
2		6641	6641	0	157	2881	3603	123061
3		2518	2518	0	47	1116	1355	34835
4		1318	1318	0	20	581	717	15512
5		1209	804	405	11	358	840	8608
6		988	539	449	11	234	743	5391
7		766	380	386	8	161	597	3660
8		604	285	319	8	118	478	2633
9	5.0×10^{-4}	1943	884	1059	14	391	1538	7888
10		1583	705	878	9	325	1249	6104
11	2.0×10^{-4}	8136	3524	4602	42	1557	6537	29119
12		6847	2929	3918	38	1270	5539	24434
13		5816	2470	3346	39	1054	4723	20138
14		4896	1995	2901	23	885	3988	16426
15		4359	1841	2518	22	779	3558	14409
16		3816	1600	2216	21	685	3110	12378
17		3354	1392	1962	19	597	2738	10696
18		2957	1225	1732	14	514	2429	9343
19		2635	1077	1558	10	465	2160	8220
26	1.0×10^{-4}	5389	2165	3224	25	901	4463	15697
27		4936	1982	2954	18	829	4089	14361
28		4588	1839	2749	16	760	3812	13187
29		4254	1690	2564	18	700	3536	12150
30	5.0×10^{-5}	15852	6364	9488	72	2642	13138	44853
36		10720	4318	6402	54	1759	8907	29535
37		10087	4058	6029	46	1634	8407	27717
38		9536	3852	5684	32	1553	7951	26058
39		8979	3596	5383	30	1454	7495	24542
40		8472	3400	5072	33	1384	7055	23095
50	2.0×10^{-5}	32200	12734	19466	123	5182	26895	84778

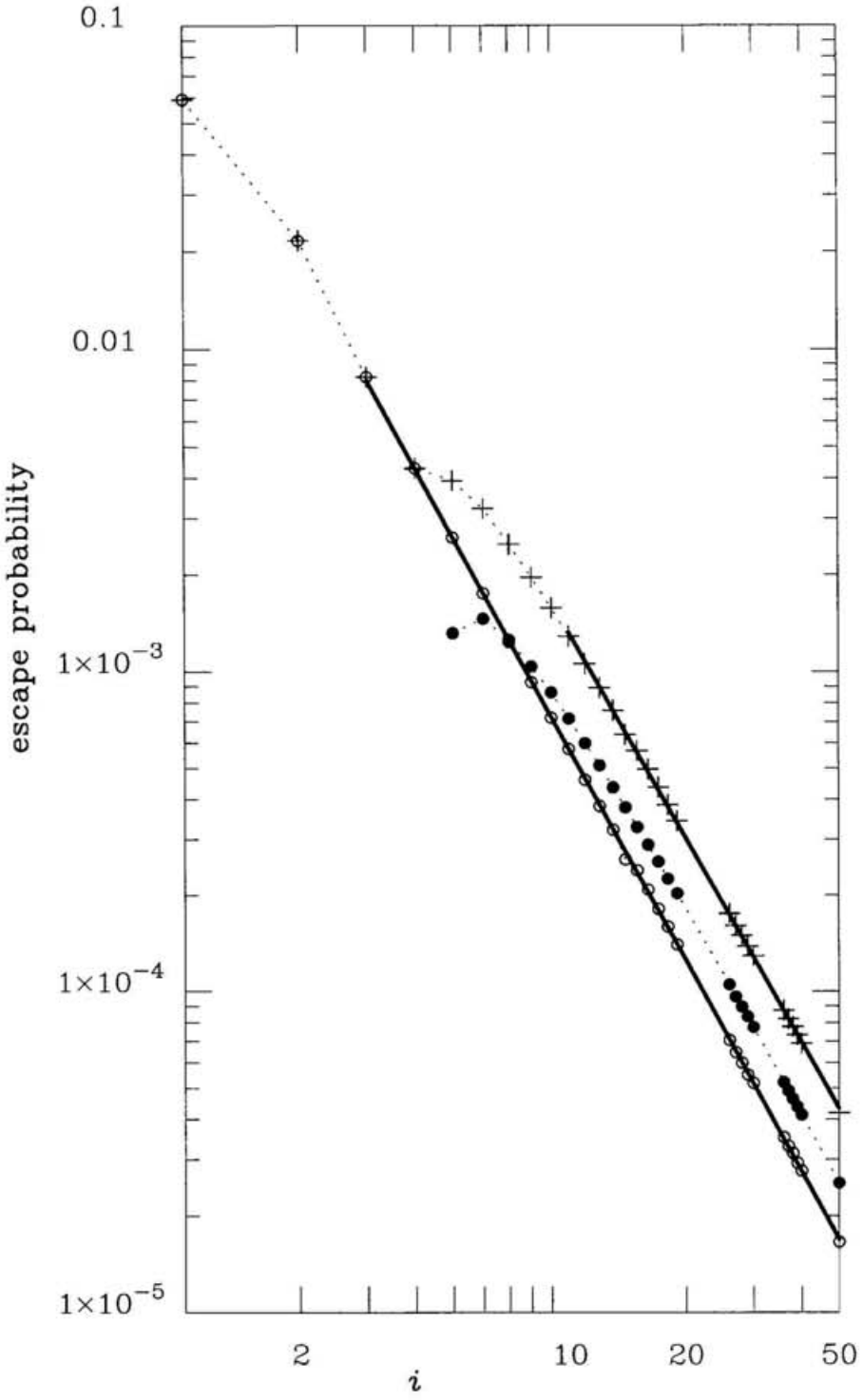

Figure 3.1: The i-dependence of the escape probabilities after the first triple encounter with the i-th close approach. The abscissa is i. The ordinate is the escape probability as a function of i. The escape probability due to slingshot is denoted by P_i^{S} and is represented by open curcles (○). The exchange-escape probability is denoted by P_i^{E} and is shown by filled circles (●). The total-escape probability is denoted by P_i^{F} and is shown by crosses (×). Here, it is considered that the escape probability is proportional to the area of escape region.

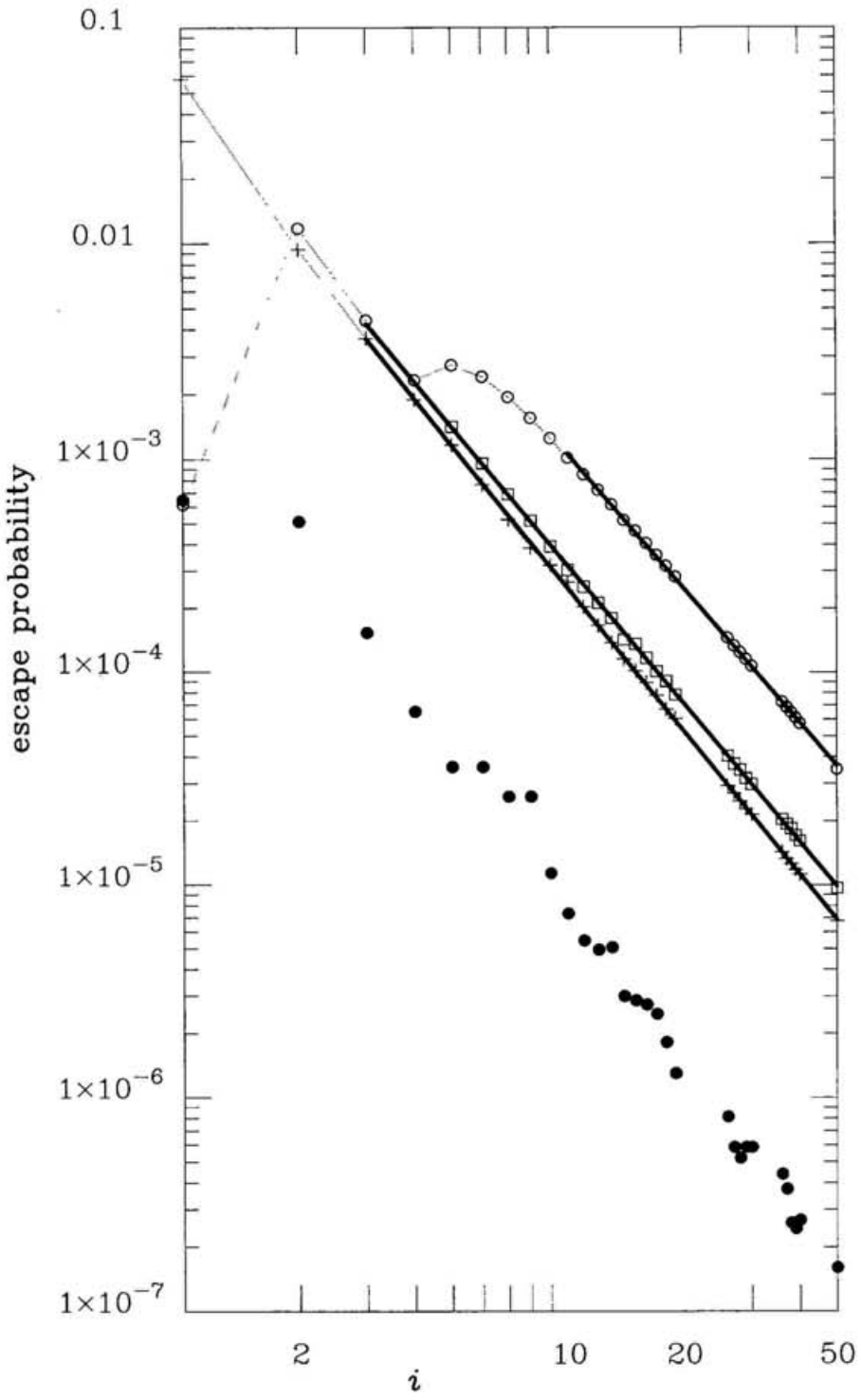

Figure 3.2: The i-dependence of the probabilities of m_i, $i = 1, 2, 3$ leading to escape. The abscissa is i. The ordinate is the escape probability as a function of i. A filled circle (•), a plus mark (+), and a open circle (○) stand for $P_i^{\mathrm{F}\{1\}}$, $P_i^{\mathrm{F}\{2\}}$, and $P_i^{\mathrm{F}\{3\}}$, respectively.

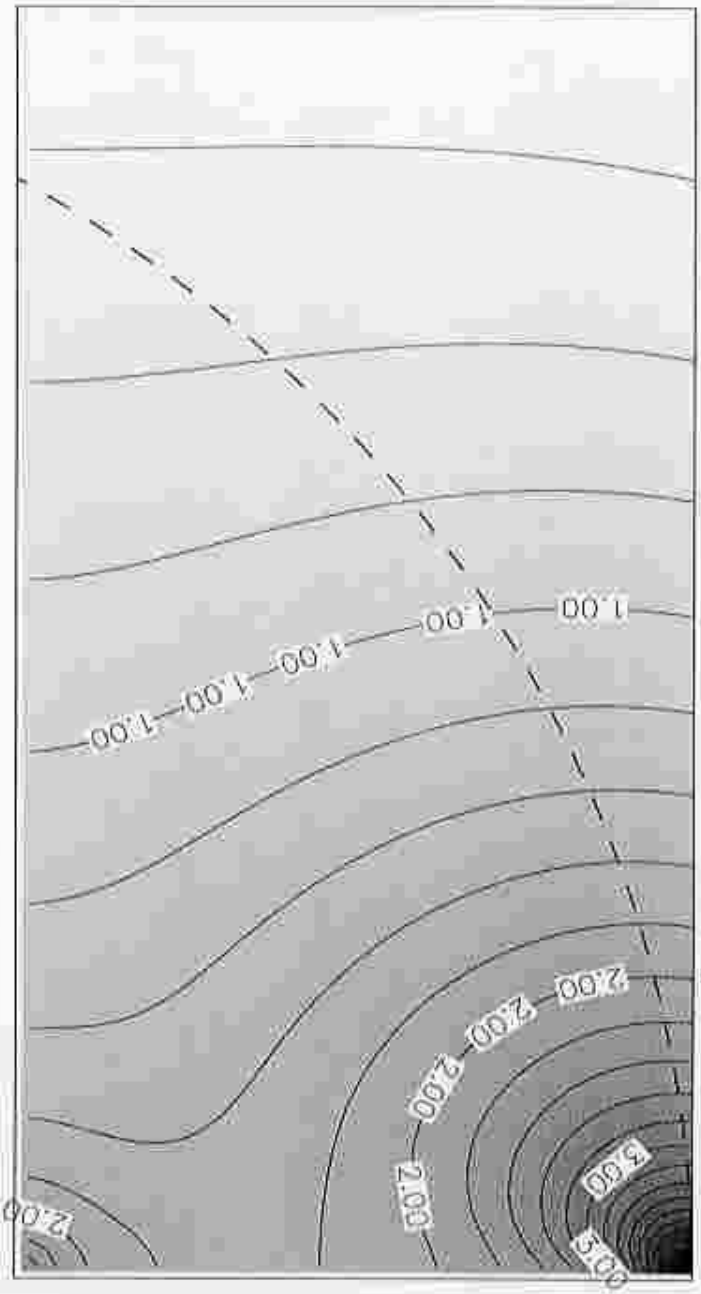

Figure 3.3: The Jacobian determinant $J(x, y)$ of the transformation from the initial-value space D to the equi-energy surface where the total energy is equal to -1. The darkness is directly proportional to $\log_{10} J$.

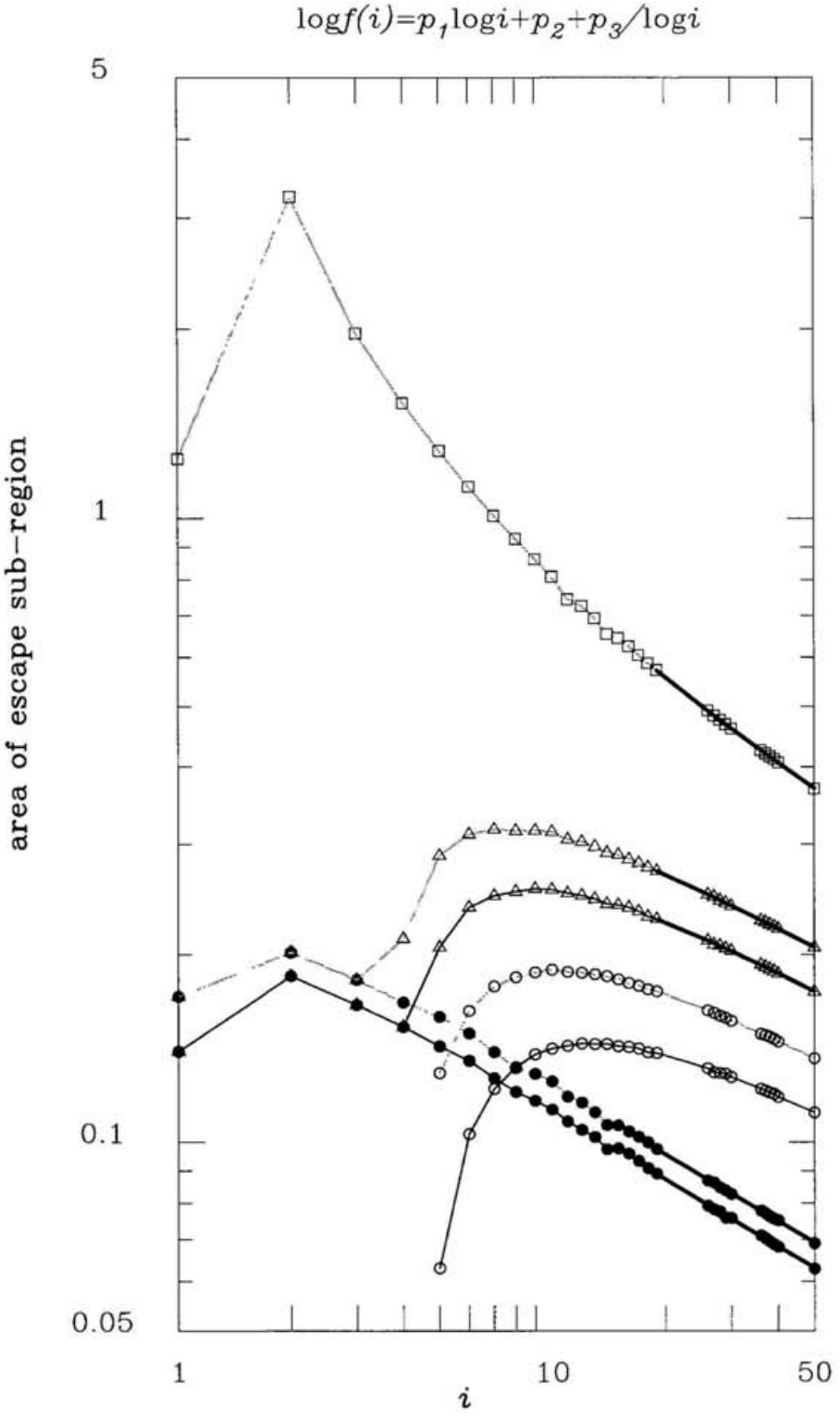

Figure 3.4: Area of the first escape regions on the equi-energy surface as a function of i. The abscissa is i which is the number of close approach between two particles until the triple encounter. The ordinate is the area of escape sub-regions. A bold curve stands for the analytic function $\log f(i) = p_1 \log i + p_2 + p_3/\log i$ which fits the i-dependence data of the area. Parameters p_1, p_2, and p_3 are obtained with the least-square method.

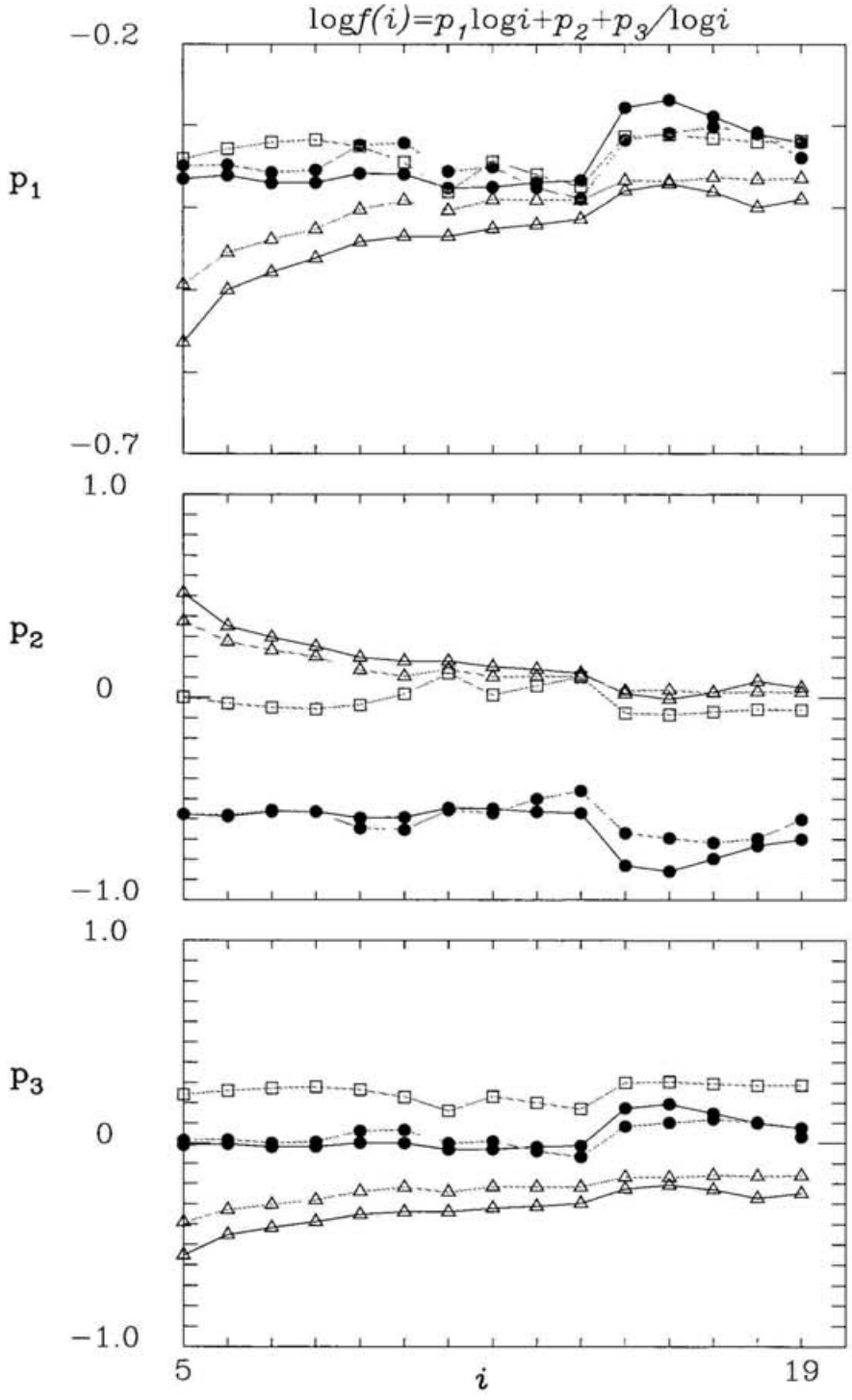

Figure 3.5: The sampling-dependence of the parameters $(i, p_j(i))$, $j = 1, 2, 3$ evaluated with the least-square method. The function form is $\log f(i) = p_1 \log i + p_2 + p_3/\log i$. Here $p_j(i)$ is a parameter as a result of fitting the data points between i and 50 in the samples $i \in \{5, \ldots, 19, 26, \cdots, 30, 36, \cdots, 40, 50\}$.

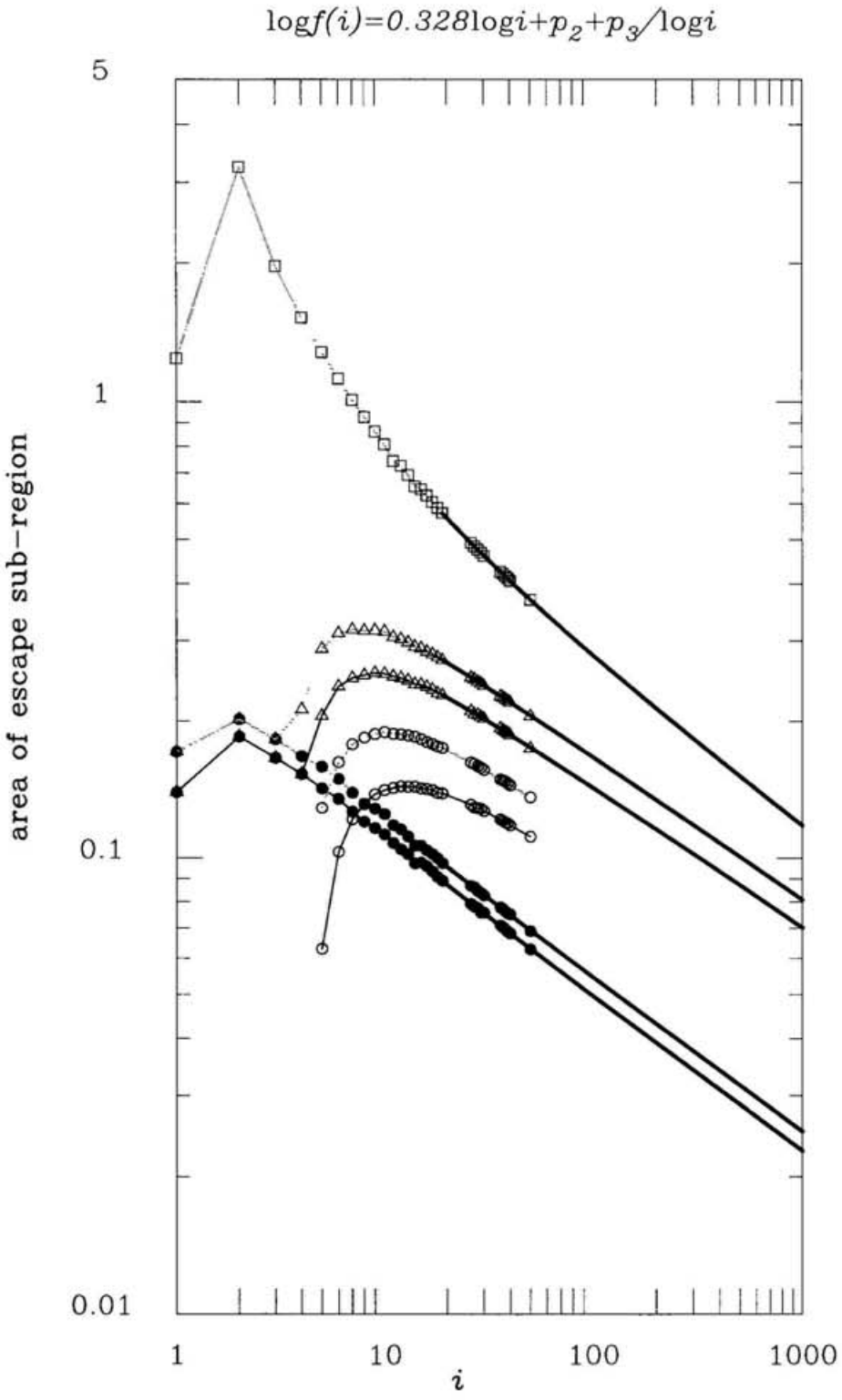

Figure 3.6: Analytic-function curves fitted to the data sequences. A bold curve stands for the function $\mathrm{nlog}\, f(i) = 0.328 \log i + q_2 + q_3/\log i$, where parameters q_2 and q_3 are obtained with the least-square method.

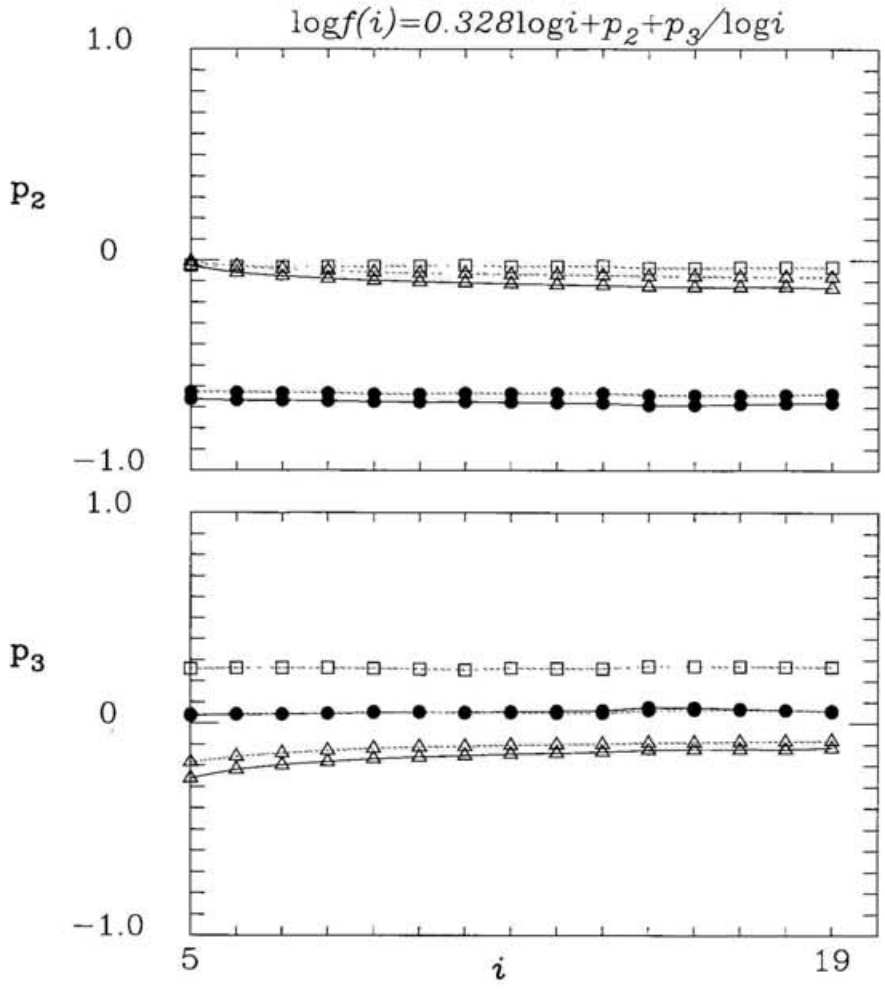

Figure 3.7: The sampling-dependence of the parameters $(i, q_j(i))$, $j = 2, 3$ evaluated with the least-square method. The function form is $\log f(i) = 0.328 \log i + q_2 + q_3/\log i$. Here $q_j(i)$ is a parameter as a result of fitting the data points between i and 50 in the samples $i \in \{5, \cdots, 19, 26, 27, \cdots, 30, 36, \cdots, 40, 50\}$.

3.3 Relative change of binding energy

3.3.1 Energy transfer in slingshot and exchange

In the present subsection, we will compare physical features of slingshot and exchange encounters. The respective energy transfers between an escaping particle and a binary due to slingshot and exchange will be evaluated. In the free-fall three-body problem, we will introduce the change of binding energy defined originally by Heggie (1975) in the scattering three-body problem. According to Heggie (1975), the relative change of binding energy is defined as the increase in binding energy normalized by the original binding energy. Heggie and Hut (1993) formulated the relative change of binding energy between initial and final binaries systematically with the aid of numerical investigation in an extensive initial-value space of the scattering problem.

As a first step in the present subsection, we will confirm that this relative change is also available for the free-fall three-body problem. The binding energy of the binary is the difference of the kinetic energy of the two components and the potential energy between them. The relative-coordinate system in the binary components is adopted in order to define the binding energy. Let r_{ij} denote the mutual distance between the particle m_i and m_j. The binding energy ε_{ij} between m_i and m_j is defined as

$$\varepsilon_{ij} = \frac{m_i m_j}{r_{ij}} - \frac{1}{2}\frac{m_i m_j}{m_i + m_j}\dot{r_{ij}}^2. \tag{3.62}$$

Suppose the scattering three-body problem. Initially, the incoming particle approaches from a large distance so that the binding energy of the binary may be approximately constant at a value ε_0. Moreover, if the third particle recedes to a large distance after the triple encounter, then the new binding energy of the binary becomes approximately constant again around a value ε_1. The relative change of binding energy Δ is

$$\Delta = \frac{\varepsilon_1 - \varepsilon_0}{\varepsilon_0}. \tag{3.63}$$

Next we make sure that the above assumptions in the scattering problem are also available for the free-fall three-body problem. In any case of the free-fall problem, the inequality $r_{23} \geq r_{12} \geq r_{31}$ is satisfied at the initial state. Thus m_2 is regarded as an incoming particle, and m_1 and m_3 are as components of a binary. However, the initial distance between the incoming particle and the gravity center of the binary is not so large relative to the separation of the binary. It may imply that the two-body approximation is useless, and so we expect that both initial binding energy and final binding energy fluctuate widely.

We investigate how wide the fluctuation of binding energy is. Let us show one orbit in the escape region S_2. The system starting in S_2 experiences the triple encounter earlier than any system in the other regions S_i, $i = 3, 4, \cdots$ and E_i, $i = 5, 6, \cdots$. Thus we expect that the width of the fluctuation starting in S_2 is largest in the escape regions except in S_1.

An escape orbit is drawn in Fig.3.8(a). The initial value is $(0.291, 0.327)$. A cross stands for an initial position of a particle. A bold, a middle-gray and a light-gray curves represent the respective trajectories of m_1, m_2 and m_3. A filled circle shows a position at $t = 0.617007$ when the escape criterion by Yoshida (1972, 1974) is satisfied. A close approach between m_1 and m_3 occurs before the time is 0.2. The triple encounter occurs in a period $t \in (0.5, 0.6)$. After that, the particles m_3 and m_1 form a binary and m_2 escapes.

The time-dependent binding energies between two particles are shown in Fig.3.8(b). A bold curve stands for $\varepsilon_{23}/\varepsilon_0$. A middle-gray and a light-gray curves represent $\varepsilon_{31}/\varepsilon_0$ and $\varepsilon_{12}/\varepsilon_0$, respectively. A vertical line at $t = 0.617007$ shows the time when the escape criterion is satisfied.

It is clear that ε_{31} is approximately constant just before the triple encounter, while the other energies ε_{12} and ε_{23} diverge to negative infinity at the close approach between m_1 and m_3 around $t \simeq 0.2$. The third particle m_2 does not affect the value of the binding energy of the binary even if m_2 exists near the binary. Therefore, ε_0 can safely be considered as the initial potential energy between m_1 and m_3 in the free-fall three-body problem.

Also after the triple encounter, the binding energy of the formed binary converges to a constant value very quickly. In the case shown in Fig.3.8(a), three particles stay around a gravity center of the system when the escape criterion is satisfied. However, the binding energy is already steady.

Let us define $\Delta(t)$ as $(\varepsilon(t)-\varepsilon_0)/\varepsilon_0$. Table 3.2 shows the systematical result that the fluctuation of $\Delta(t)$ after the triple encounter can be ignored in any system starting in S_2. Let t_1 be the time when the escape criterion is satisfied, and t_2 denotes the time when the condition of the conditional escape is satisfied, i.e., when an escaping particle is ejected from a binary to the distance $20d_{\rm unit}$. (see eq.(??) for $d_{\rm unit}$).

We evaluate the change of $\Delta(t)$ normalized by $\Delta(t_1)$,

$$\delta = \frac{|\Delta(t_2)-\Delta(t_1)|}{\Delta(t_1)}, \tag{3.64}$$

in the system starting on S_2. Approximately, δ denotes the fluctuation of $\Delta(t)$. The relative distribution of δ is shown in Table 3.2. We investigate all initial values in S_2, i.e., 6641 samples. All samples satisfy $\delta < 0.1$. There are not so large fluctuations by as much as the order of Δ. More exactly, the maximum value of the fluctuation δ in S_2 is 0.036. The relative fluctuation δ is limited within 3.6%. Note that the system where δ becomes maximum is shown in Fig.3.8(a) and (b). We can directly observe that the fluctuation is small after the time when the escape criterion is satisfied from Fig.3.8(a) and (b).

The distance between an ejected particle and the gravity center of a formed binary is denoted by $\rho(t)$ at a given time t. If $\rho(t_2)$ is not so larger than $\rho(t_1)$, the above statistics does not have any significance. Table 3.3 shows the result that $\rho(t_2)$ is large enough. The $\rho(t_2)/\rho(t_1)$-distributions are expressed as a function of $\rho(t_1)$ in Table 3.3. The lines classify the ranges of $\rho(t_2)/\rho(t_1)$. The columns identify the ranges of $\rho(t_1)$. We notice that 67% of the samples satisfy $\rho(t_2) \geq 100\rho(t_1)$. Moreover, almost all samples (except 0.03% systems) satisfy $\rho(t_2) \geq 10\rho(t_1)$.

The $\rho(t_1)$-distribution shows that 98.7% of the samples are judged escape within $\rho(t_1) < 1$. This distance is comparable to the initial size since the maximum of initial distance is equal to 1. An escaping particle is not so distant from a binary at the judgement of escape. However, the relative fluctuation δ is sufficiently small after the judgement, and so $\Delta(t)$ is almost constant. Thus ε_1 can be regarded as the binding energy of the binary at the time of satisfaction of the escape criterion.

Observation 3.1. *The time-dependent $\varepsilon(t)$ is not so fluctuating around the initial time and the time when the escape criterion satisfies although the third particle is not so far from the formed binary. Therefore, the relative change of binding energy which is formulated in eq.(3.63) is available for the free-fall three-body problem.*

Let us observe the difference of the relative change of the binding energy in the respective triple encounters, slingshot and exchange. The numerical result of i-dependence of Δ is shown in Table 3.4 and Fig.3.9. Similar to evaluating the escape probabilities in Subsections 3.2.1 and 3.2.2, the initial-value space D is divided into a grid with elements, and an orbital integration starting from each vertex of the elements is performed. The grid sizes are the same as the ones in Table 3.1. Recall that the numbers of grid elements of initial values after slingshot and exchange will be denoted by N_i^S and N_i^E, respectively, for each i. A maximum of the relative changes of binding energies for a given i is denoted by $\max \Delta_i$. An average and a minimum of Δ for a given i are $\langle \Delta_i \rangle$ and $\min \Delta_i$, respectively. The suffices S and E represent the types of triple encounter, slingshot and exchange, respectively. For example, $\max \Delta_i^E$ is the maximum value of Δ-samples where initial values lies in the region E_i. Recall that there is not any initial value leading to escape after the first triple encounter of exchange type for $i \leq 4$ in the initial-value space D.

Here, the average is weighted by the magnification ratio due to the projection of the grid elements to the initial-value surface with constant energy. Let $\Delta(x_i^X, y_i^X)$ be Δ of the system starting at the initial point (x_i^X, y_i^X) in the escape region S_i or E_i, where $X \in \{S, E\}$. The weight function at the initial value (x_i^X, y_i^X) is equivalent to the Jacobian determinant $J(x_i^X, y_i^X)$ of the transformation in eq.(3.37) in Subsection 3.2.2. The average is evaluated as

$$\langle \Delta_i^X \rangle = \frac{\sum_{x,y} \Delta(x_i^X, y_i^X) J(x_i^X, y_i^X)\ \delta x_i^X \delta y_i^X}{\sum_{x,y} J(x_i^X, y_i^X)\ \delta x_i^X \delta y_i^X}, \qquad X \in \{S, E\}, \tag{3.65}$$

where the summations $\sum_{x,y}$ run over all the grid elements sampled in the escape region S_i or E_i.

In Fig.3.9, a bold and a dotted lines with filled circles ($\bullet$) stand for $\max \Delta_i^S$ and $\max \Delta_i^E$, respectively. A bold and a dotted lines with open circles ($\circ$) represent $\langle \Delta_i^S \rangle$ and $\langle \Delta_i^E \rangle$, respectively. A mark $+$ and a $\times$ show $\min \Delta_i^S$ and $\min \Delta_i^E$, respectively.

The following is found.

Observation 3.2. $\max \Delta_i^E \ll 10$, $i \geq 5$. *In other words, there exist no escape orbits due to the exchange type such that the systems increase an order of magnitude in the free-fall three-body problem.*

This is in contrast with slingshot encounter. In the case of slingshot, $\max \Delta_i^S > 10$, $i \geq 2$. Note that we did not consider the samples of orbits starting in S_1.

On the other hand, minimum values of Δ_i due to slingshot and exchange are equal to each other. Moreover,

$$\min \Delta_i^S \cong \min \Delta_i^E < 1 \quad \text{for each} \quad i \geq 4. \tag{3.66}$$

It means that the increment of the order of binding-energy increment does not vary in the case experiencing $\min \Delta_i^{\{S,E\}}$. We confirmed that for $i = 5, 6, 7, 8$ initial values where the systems satisfy $\min \Delta_i^S$ are near the boundaries of the escape region. There is a great variety of values of relative changes in slingshot type. In such a sense, the slingshot is different from the exchange. For slingshot, $(\max \Delta_i^S - \min \Delta_i^S)$ is much greater than 1, whereas $(\min \Delta_i^E - \min \Delta_i^E)$ is less than 1. Slingshot encounter causes $\Delta > 100$ as well as $\Delta < 1$.

The existence of much energetic slingshot is shown in the above result. Here, we compare total increments of the binding energies due to slingshot and exchange with each other. It is found that the total influence on the evolution of the system due to slingshot is comparable to the one due to exchange. The total-energy change of the binding energies in the escape orbits after the first triple encounter at the i-th binary-close approach are derived as

$$\sum_{x,y} \Delta(x_i^X, y_i^X) J(x_i^X, y_i^X)\, \delta x_i^X \delta y_i^X, \qquad X \in \{S, E\}. \tag{3.67}$$

Recall that J is the weight function as a result of the transformation to the equi-energy surface, and that the summations $\sum_{x,y}$ run over all the grid elements sampled in the escape region S_i or E_i. Using eq.(3.65), the ratio of the total-energy change due to slingshot escape to the one due to exchange escape is given by

$$\frac{\sum_{x,y} \Delta(x_i^S, y_i^S) J(x_i^S, y_i^S) \delta x_i^S \delta y_i^S}{\sum_{x,y} \Delta(x_i^E, y_i^E) J(x_i^E, y_i^E) \delta x_i^E \delta y_i^E} = \frac{\langle \Delta_i^S \rangle}{\langle \Delta_i^E \rangle} \cdot \frac{A_i^S}{A_i^E}. \tag{3.68}$$

Figure 3.9 shows that average values of the relative changes $\langle \Delta_i^S \rangle$ and $\langle \Delta_i^E \rangle$ for each i are different from each other by factor 4. More precisely,

$$\frac{\langle \Delta_{10}^S \rangle}{\langle \Delta_{10}^E \rangle} = 4.37, \qquad \frac{\langle \Delta_{30}^S \rangle}{\langle \Delta_{30}^E \rangle} = 4.04, \qquad \frac{\langle \Delta_{50}^S \rangle}{\langle \Delta_{50}^E \rangle} = 4.25. \tag{3.69}$$

See Table 3.4 again. On the other hand, the result in Subsection 3.2.2 shows that the ratio of the escape-region area due to slingshot to the one due to exchange is nearly equal to 0.4 on the equi-energy surface (see in eq.(3.57)). Therefore, the ratio of the total-energy changes are given by

$$\frac{\langle \Delta_i^S \rangle}{\langle \Delta_i^E \rangle} \cdot \frac{A_i^S}{A_i^E} \cong 1.6. \tag{3.70}$$

The order of the change due to slingshot is the same as the one due to exchange. In terms of total-energy change, the slingshot escape is more effective than the exchange escape by a factor.

Finally, we consider the possibility to distinguish the type of escape (i.e., whether slingshot or exchange). It is shown that we can judge the types by the detected value Δ in most cases. Let R_i is defined as the ratio for the grid elements of initial values leading to escape due to slingshot exceeding Δ_i^S over $\max \Delta_i^E$. For each i, the excess ratio R_i is derived in the last column in Table 3.4. Although R_i decreases with increasing i, we have a chance of assurance that an escape orbit is due to slingshot with possibility 64.8% only by referring to the value Δ_n, even if $i = 8$. Referring to the relative change of binding energy results in a separating method of slingshot and exchange with large probability. The most important cause of decreasing the ratio R_i with i is that $\max \Delta_E$ increases with increasing n. Is there any possibility that Δ_E due to exchange becomes as large as due to slingshot, in the case of large i? This problem is still open.

3.3.2 Collisions and binding energy

Triple collision and binding energy

The i-dependence of $\max \Delta_i^S$ is not regular in Fig.3.9. At $i = 12, 16$, $\max \Delta_i^S$ is larger than the maximum values for the other i. It is caused by the sampling method of the initial points. Every vertex of a grid element on the initial space D is located at a finite distance from triple collision points.

Let us consider only the systems experiencing $\max \Delta_i^S$. We conjecture that the orbit of the system approaches a triple-collision orbit with increasing $\max \Delta_i^S$ of the system. We observe the normalized minimal moment of inertia $\hat{I}_{\min}$ in the systems experiencing $\Delta = \max \Delta_i^S$ for respective i. Figure 3.10 shows the result. A filled circle stands for $\hat{I}_{\min}$ as a function of $\max \Delta_i^S$. A number in a vicinity of each filled circle represents i. In almost every case, $\hat{I}_{\min}$ decreases with increasing $\max \Delta_i^S$ of a system. Thus, if $\max \Delta_i^S$ of the system is large, the orbit of the system approaches a triple-collision orbit. A binary formation increasing the binding energy strongly is detected from the orbit close to triple collision.

The inverse is not true. There are slingshot-escape systems where $\max \Delta_i^S$ is small even if $\hat{I}_{\min}$ is small. The samples of slingshot-escape orbits starting in S_5, S_{11}, S_{30}, and S_{50} will be considered. There are the results of the relations between $\hat{I}_{\min}$ and Δ_i^S for

$i = 5, 11, 30$, and 50 in Fig.3.11(a), (b), (c), and (d), respectively. On a logarithmic-scale graph, a dot stands for $(\hat{I}_{\min}, \Delta_i^S)$-relation for each sample starting in slingshot-escape region S_i. Each of four figures shows that there is a maximal value of Δ_i^S for a given $\hat{I}_{\min}$. Let $f(\hat{I}_{\min})$ be its maximal value. For each i, f is a continuous function of $\hat{I}_{\min}$. In other words, the existence region of the dots $(\hat{I}_{\min}, \Delta_i^S)$ is bounded from below, and so the boundary forms a continuous curve of the function $\Delta_i^S = f(\hat{I}_{\min})$. The function f decreases monotonically with increasing $\hat{I}_{\min}$. If $\hat{I}_{\min}$ is large, Δ_n^S must be small. If $\hat{I}_{\min}$ is small, there is a sample which Δ_i^S is large. Even if $\hat{I}_{\min}$ is small, there is also a sample which Δ_i^S is small.

Moreover, we observe that the function f tends to approach the following form for lower $\hat{I}_{\min}$:

$$\log f = -\frac{1}{2} \log \hat{I}_{\min} + \text{const.} \tag{3.71}$$

It means that the samples in lower $\hat{I}_{\min}$ satisfy the enequality,

$$\Delta_i^S \leq C_i \left(\hat{I}_{\min}\right)^{-1/2}, \tag{3.72}$$

where C_i is a constant depending on i. From the numerical survey, $C_5 = -0.952$, $C_{11} = -1.19$, $C_{30} = -1.48$, $C_{50} = -1.63$. These boundaries are drawn as fine lines in Fig.3.11.

Next, we consider whether the binding-energy change due to exchange-escape type has relation to triple collision or not. As a result, $\max \Delta_i^E$ bears no relation to triple collision for each i. It is different from the slingshot-escape type. Figure 3.12(a), (b), (c), and (d) show the results of $(\hat{I}_{\min}, \Delta_i^E)$-distributions of all exchange-escape samples for $i = 5, 11, 30$, and 50, respectively. The boundary of an existence region of the dots forms a continuous curve. However, each boundary curve is not monotonically decreasing in contrast to the slingshot-escape case. The system experiencing $\max \Delta_i^E$ is not a minimum of $\hat{I}_{\min}$ for samples in E_i. There is no exchange-escape orbit such that motion is sufficiently close to triple collision and the system evolves with sufficiently large transition of binding energy. In other words, it becomes clear that there is no exchange-escape orbit close to a triple-collision orbit in the free-fall problem with equal masses.

Near-isosceles slingshot and binding energy

Let us consider orbits far from a triple-collision orbit. An orbit whose binding energy changes strongly also exists far from triple-collision orbits. Where are the initial

values of these orbits? We find that such initial points lies in the escape sub-bands which are different from the narrow region including the binary collision curve of near-isosceles-slingshot type. These initial points distribute close to the near-isosceles-slingshot curve in the escape sub-bands.

The relative changes of the binding energies are evaluated in the systems starting on a segment $y = 0.4$ which is parallel to the x-axis in the slingshot-escape region S_2. The size of grids in the x-direction is 1×10^{-4}. Figure 3.13 shows the result of the survey. A boundary curve of a gray region stands for the relative change of binding energy $\Delta_2^S(x)$ as a function of initial value x. Three lines below the x-axis show the sections of three sub-bands of a slingshot-escape region. The identity of an escaping particle is represented as the level of three lines.

The system experiencing the maximum of the binding-energy change $\Delta_2^S(x)$ starts in the escape region which is different from the region including the binary-collision curve of the near-isosceles-slingshot type. It is true that the function $\Delta_2^S(x)$ has an extremum at the binary-collision curve of the near-isosceles-slingshot type in an interval where m_1 escapes. However, $\Delta_2^S(x)$ has a maximum in m_3-escaping region. More exactly, the maximal point is located at the initial value neighboring m_1-escaping region.

Let us explain how the formed binary obtain the large amount of the binding energy. The system experiences the maximum of Δ_2^S at the initial point on the segment $y = 0.4$ in S_2 is $(0.3590, 0.4)$. The oribt starting at this initial point is shown in Fig.3.14(a). The time evolution of the binding energies between respective two particles during the triple encounter represents three curves in Fig.3.14(b). Each of three vertical lines stands for the time of syzygy crossing during the triple encounter. Figures 3.14(c), (d), and (e) show the configurations and velocity vectors of three particles at the successive syzygy crossings.

The first stage of syzygy crossing during the triple encounter occurs at $t = 0.6161$. At this stage, m_2 and m_3 become weakly bound. In Fig.3.14(b), we see that the binding energy ε_{23} between m_2 and m_3 decreases. Figure 3.14(c) shows that m_1 passes through between m_2 and m_3 which are approaching each other. Until the second stage of syzygy crossing, the trajectory of m_1 is deflected to the direction of the m_2's position. After that, m_2 passes through between m_3 and m_1. Its motion is represented in Fig.3.14(d). The figure shows that m_3 and m_1 approach each other at the second syzygy crossing. It results in decreasing of ε_{31} as we can observe it at the second vertical line in Fig.3.14(b), and so m_3 and m_1 become wider. At this stage, m_3 is regarded to be weakly bound from both

m_1 and m_2. After that, m_3 passes through between m_1 and m_2. Figure 3.14(e) shows that m_1 and m_2 are receding from each other at the third syzygy crossing. The particle m_3 obtains the kinetic energy from the other two particles. Since m_3 gets weakly bound from both m_1 and m_2, m_3 is easy to escape. Therefore, it is assured that the binding between m_1 and m_2 becomes strong intensively.

3.3.3 Non-escape orbits between slingshot and exchange orbits

In the present subsection, we will explain a process of failure in escape after the first triple encounter if the orbit starts in the non-escape region between the band-like region S_i and the tongue-like region E_i. Hereafter, this non-escape region will be called a *gap region*. A brief summary is here. By the syzygy crossing of m_1 near the gravity center between m_2 and m_3, the norms and directions of velocity vectors for m_2 and m_3 become nearly equal to each other. Motions of m_2 and m_3 are parallel to each other temporarily. Therefore, m_2 and m_3 become harder during the successive close approach in the exchange encounter, and so m_3 fails in getting enough kinetic energy to escape after the exchange encounter.

The particle m_3 escapes in both sides of the gap region: the tongue-like region E_i and the sub-band of S_i neighboring E_i. Four orbits in and around the gap region are already shown in Fig.2.18 in Subsection 2.5. A typical exchange orbit in E_5 is Fig.2.18(a). Orbits (b) and (c) fail in escape. These initial values lie in the gap region. Orbit (d) represents the behavior near the boundary of D_5 neighboring E_5. The successive close approaches between two particles take place during exchange encounter: first, m_1 and m_2; second, m_1 and m_3.

The particle m_3 can not obtain enough kinetic energy to escape if the system starts in the gap region. In Fig.2.18(b) and (c), m_3-velocities become slower after the triple encounter than the other cases (a) and (d). The upper figure of Fig.3.15 shows the time evolution of the absolute value of the velocity for m_3. This value is denoted as v_3. The darkest curve of the four curves stands for $v_3(t)$ of Orbit (a) which leads to escape due to exchange. The lightest curve is $v_3(t)$ of Orbit (d) leading to escape due to slingshot. The other gray curves are ones of (b) and (c). Surely, after $t > 0.65$, the m_3-velocities in (b) and (c) become slower than ones in escape orbits (a) and (d). We observe similar phenomena in the middle figure of Fig.3.15 which represents the time evolution of v_2 (the velocity for m_2). During $t \in (0.64, 0.67)$, peaks of v_2-evolutions (a) and (d) are higher

than ones of (b) and (c).

From the observation of v_2 and v_3 evolutions, it becomes clear that the kinetic energies of the two particles are lost just after the second close approach in exchange encounter. In each of the four systems, m_2 experiences a peak speed around $t \simeq 0.62$. After that v_3 becomes maximal around $t \simeq 0.63$. The particle m_1 approaches m_2 and m_3 successively, so v_2 and v_3 increase once.

The velocity v_2 decreases with the initial value x increasing until a peak of v_2. At $t = 0.61$, for example, the relation $v_2^{(a)} < v_2^{(b)} < v_2^{(c)} < v_2^{(d)}$, where a velocity v_2 of Orbit (χ) is denoted by $v_2^{(\chi)}$, $\chi = \{a,b,c,d\}$. Similarly, v_3 increases with increasing x until a peak of v_3. In both cases, after the peak of v_3, inequality relations change to $v_j^{(b)}, v_j^{(c)} < v_j^{(a)}, v_j^{(d)}$, $j = 2, 3$.

Why the inequality relations among velocities change around the time of peak speed? Both m_2 and m_3 can not obtain enough kinetic energy to escape in a non-escape orbit. It is expected that the binding energy $\varepsilon_{23}(t)$ between m_2 and m_3 becomes large temporarily. Here, we observe the time evolution of $\varepsilon_{23}(t)$. The darkness of curves stands for the four systems (a), (b), (c) and (d). The four curves are lighter in alphabetical order. It is the same as the upper and middle figures in Fig.3.15, i.e., the darkest curve of the four curves stands for $\varepsilon_{23}(t)$ of Orbit (a) and the lightest curve is the one of Orbit (d).

In each of the four systems, $\varepsilon_{23}(t)$ becomes maximal during $t \in (0.62, 0.63)$. This time interval lies between the peak times of v_2 and v_3. In other words, m_2 and m_3 become tight temporarily during the successive close approaches. Moreover, we must notice that maximal values of the systems (b) and (c) are larger than ones of (a) and (d). Inequality relations of ε_{23} among the four systems change before and after the first close approach between m_1 and m_2. Let $\varepsilon_{23}^{(\chi)}$ denote ε_{23} of the system (χ), where $\chi = \{a,b,c,d\}$. Just before the first close approach, $\varepsilon_{23}^{(a)} < \varepsilon_{23}^{(b)} < \varepsilon_{23}^{(c)} < \varepsilon_{23}^{(d)}$; whereas $\varepsilon_{23}^{(a)}, \varepsilon_{23}^{(d)} < \varepsilon_{23}^{(b)}, \varepsilon_{23}^{(c)}$ just after the first close approach. Therefore, it is considered that temporary increasing the binding energy causes failure in escape.

In the final part of the present section, we will explain why m_2 and m_3 become harder during the successive close approaches if the system starting in the gap region between D_n and E_n. Let us give attention to the system (c) whose initial value is $(0.430, 0.19)$. The upper figure of Fig.3.16 shows the time evolutions of binding energies between respective particles. A bold curve stands for $\varepsilon_{23}(t)$. The lightest gray and a middle-gray

curves represent $\varepsilon_{31}(t)$ and $\varepsilon_{12}(t)$, respectively. There is a peak of $\varepsilon_{23}(t)$ around $t \simeq 0.6204$ marked with a vertical line. The configuration and velocities at this stage are shown in the lower figure of Fig.3.16. Three particles are filled-circle positions at $t = 0.6204$. Three arrows represent velocity vectors of the respective particles. A bold curve stands for the trajectory of m_1. The lightest and a middle-gray curves represent ones of m_2 and m_3, respectively.

Notice that the velocity vectors of m_2 and m_3 are almost parallel. Moreover, the respective norms of the vectors are comparable. Thus the relative velocity between m_2 and m_3 are almost zero at the time of ε_{23}'s peak. By the definition of the binding energy, if the distance between m_2 and m_3 is determined, ε_{23} tends large with the absolute value of the relative velocity decreasing.

Furthermore, the syzygy crossing of m_1 just after $t = 0.6204$ is also remarkable. At $t = 0.6226$, the particle m_1 passes through the thin line connecting the positions of m_2 and m_3 in the figure. The figure shows that m_1 passes through near the gravity center of the m_2-m_3 system. This syzygy-crossing configuration is close to isosceles one. In Subsection 2.4.1, we found the near-isosceles motion tends to escape. However, this syzygy crossing can not result in escape since the velocity vectors are far from isosceles motion in the velocity-coordinate system.

Conversely, the following is conjectured: when m_1 passes through near the gravity center between m_2 and m_3, they obtain the comparable kinetic energies and the velocity vectors of m_2 and m_3 tend to be parallel. It results in increasing phenomenon of the binding energy between m_2 and m_3.

Note that Aarseth et al. (1994) concluded by the numerical works that the isosceles configuration at the triple encounter is more important for escape than the symmetry of the velocity-vector directions. However, this case in Fig.3.16 is a counter-example. In Subsection 3.4.1, it will be clear that the directions of the velocities are more important for escape than the configurations of the three particles in the free-fall problem.

Table 3.2: The $|\Delta(t_2) - \Delta(t_1)|/\Delta(t_1)$-distribution. Here, t_1 denotes the time when the escape criterion is satisfied, and t_2 is the time when the distance between an escaping particle and a gravity center of a binary becomes $20d_{\rm unit}$. The mean harmonic separation between particles in virial equilibrium is denoted by $d_{\rm unit}$. The first column is the range of $|\Delta(t_2) - \Delta(t_1)|/\Delta(t_1)$. The second column shows the distribution of samples where the systems satisfy the respective range denoted in the first column.

$\lvert\Delta(t_2) - \Delta(t_1)\rvert/\Delta(t_1)$	distribution
$[0, 10^{-6})$	0
$[10^{-6}, 10^{-5})$	0.0021
$[10^{-5}, 10^{-4})$	0.0128
$[10^{-4}, 10^{-3})$	0.1006
$[10^{-3}, 10^{-2})$	0.6632
$[10^{-2}, 10^{-1})$	0.2212
$[10^{-1}, \infty)$	0

Table 3.3: The dependence of $\rho(t_2)/\rho(t_1)$ ratio on $\rho(t_1)$. Here, $\rho(t_1)$ denotes the distance between the position of an escaping particle and the gravity center of a binary when the escape criterion by Yoshida (1972, 1974) is satisfied, and $\rho(t_2)$ is the distance when the distance becomes $20d_{\rm unit}$.

$\rho(t_2)/\rho(t_1)$ \ $\rho(t_1)$	$[10^{-2}, 10^{-1})$	$[10^{-1}, 10^{0})$	$[10^{0}, 10^{1})$
$[10^{2}, 10^{3})$	0.0002	0.6702	0.0000
$[10^{1}, 10^{2})$	0.0000	0.3162	0.0131
$[10^{0}, 10^{1})$	0.0000	0.0000	0.0003

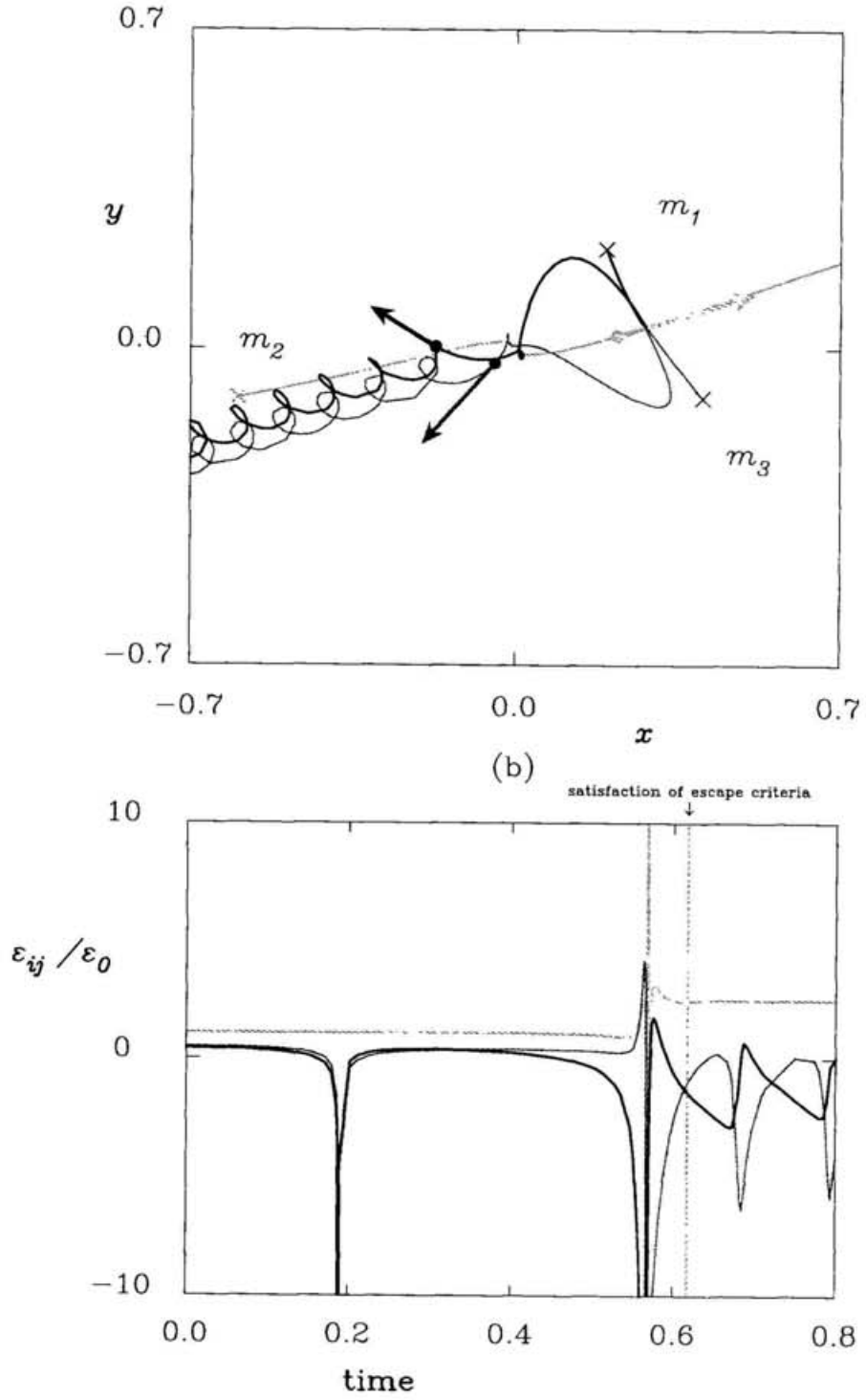

Figure 3.8: (a) The orbit in the band-like escape region S_2. The initial value is $(0.291, 0.327)$. Bold, light-gray, and middle-gray curves stand for trajectories of m_1, m_2, and m_3, respectively. Three filled circles and the respective arrows show the positions and velocity vectors of three particles at the time when the escape criterion by Yoshida (1972, 1974) is satisfied. (b) The time-dependence of binding energies in the system (a). Bold, light-gray and middle-gray curves represent binding energies between m_2 and m_3, m_3 and m_1, and m_1 and m_2, respectively. A vertical line indicates the time when the escape criterion is satisfied.

Table 3.4: The i-dependence of relative change of binding energies Δ_S and Δ_E corresponding to slingshot and exchange escapes, respectively. The number of samples is indicated as N. The maximum, minimum, and average of the relative changes of binding energies for each i are indicated as $\max \Delta_i$, $\min \Delta_i$, and $\langle \Delta_i \rangle$, respectively. The suffices represent the type of triple encounter. S and E mean slingshot and exchange, respectively. The ratio of samples of Δ^S which is more than $\max \Delta^E$ to the all samples of Δ^S are indicated as R_i for the respective i.

	N_i^S	N_i^E	$\max \Delta_i^S$	$\max \Delta_i^E$	$\min \Delta_i^S$	$\min \Delta_i^E$	$\langle \Delta_i^S \rangle$	$\langle \Delta_i^E \rangle$	R_i
S_2	6641		165		0.783		2.75		
S_3	2518		122		0.586		2.49		
S_4	1318		56.2		0.472		2.37		
S_5 E_5	804	405	25.8	0.547	0.405	0.417	2.22	0.484	0.889
S_6 E_6	539	449	172	0.628	0.350	0.368	2.37	0.484	0.789
S_7 E_7	380	386	37.0	0.672	0.321	0.332	2.12	0.483	0.739
S_8 E_8	285	319	16.4	0.706	0.290	0.298	1.96	0.478	0.648
S_9 E_9	884	1059	42.5	0.737	0.259	0.269	1.96	0.471	0.646
S_{10} E_{10}	705	878	32.4	0.760	0.245	0.251	2.04	0.467	0.631
S_{11} E_{11}	3534	4602	73.6	0.779	0.229	0.234	1.98	0.462	0.615
S_{12} E_{12}	2929	3918	281	0.796	0.215	0.220	2.08	0.438	0.554
S_{13} E_{13}	2470	3346	53.3	0.812	0.203	0.209	1.75	0.432	0.525
S_{14} E_{14}	1995	2901	56.8	0.823	0.195	0.196	1.85	0.426	0.532
S_{15} E_{15}	1841	2518	51.6	0.837	0.185	0.188	1.65	0.422	0.490
S_{16} E_{16}	1600	2216	795	0.847	0.178	0.179	1.95	0.417	0.477
S_{17} E_{17}	1392	1962	30.0	0.856	0.169	0.172	1.69	0.412	0.476
S_{18} E_{18}	1225	1732	47.0	0.863	0.163	0.165	1.64	0.411	0.480
S_{19} E_{19}	1077	1558	30.3	0.870	0.159	0.160	1.57	0.405	0.466
S_{30} E_{30}	6364	9488	50.9	0.929	0.115	0.116	1.53	0.379	0.401
S_{50} E_{50}	12734	19466	109	0.975	0.0817	0.0820	1.52	0.358	0.370

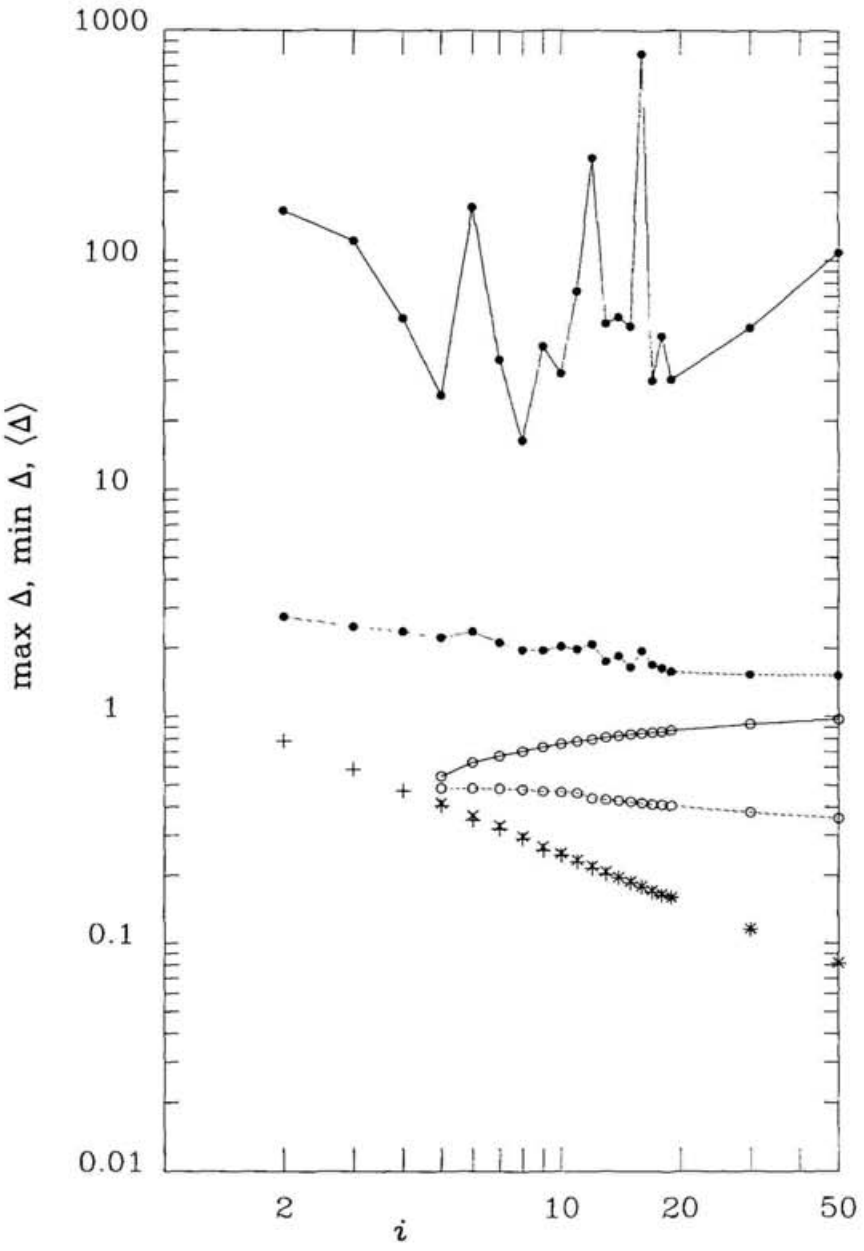

Figure 3.9: The maximum, the average and the minimum of relative changes of binding energy Δ_i for the respective i. A filled circle (•) stands for the relative change due to slingshot: Δ_i^S. An open circle (○) represents the relative change due to exchange: Δ_i^E. A bold line and a dotted line show a maximum and an average of $\Delta_i^{\{S,E\}}$, respectively. Crosses + and × correspond to minimum values of Δ_i^S and Δ_i^E, respectively.

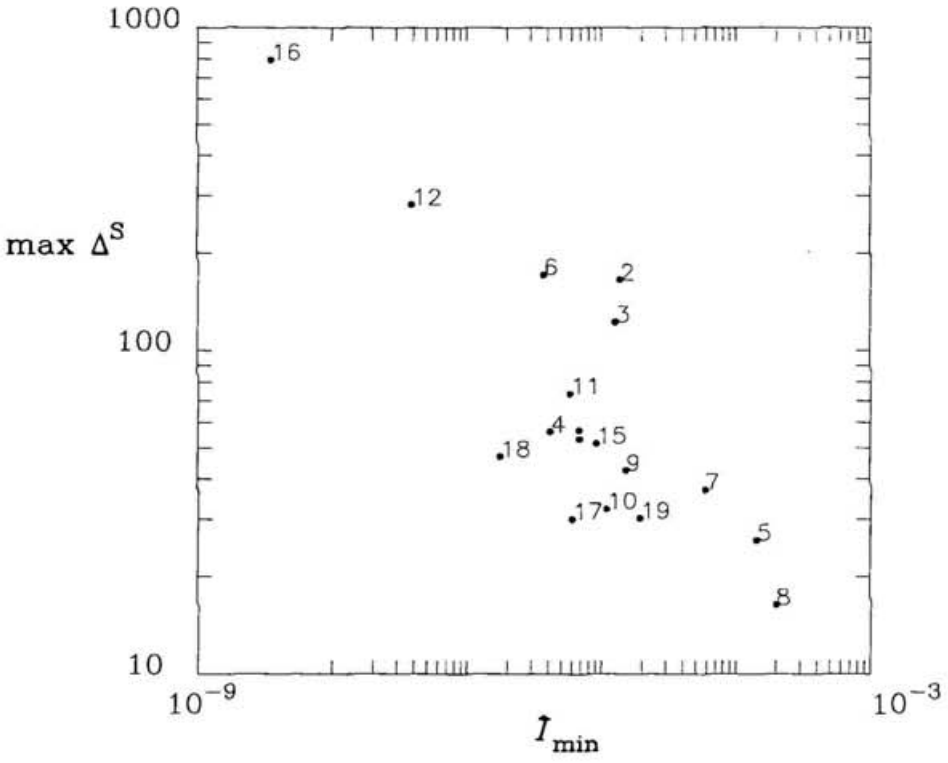

Figure 3.10: Dependence of max Δ_i^S on $\hat{I}_{\min}$. A filled circle stands for $\hat{I}_{\min}$-max Δ_i^S relation in the system experiencing max Δ_i^S. A number in a vicinity of each filled circle represents i.

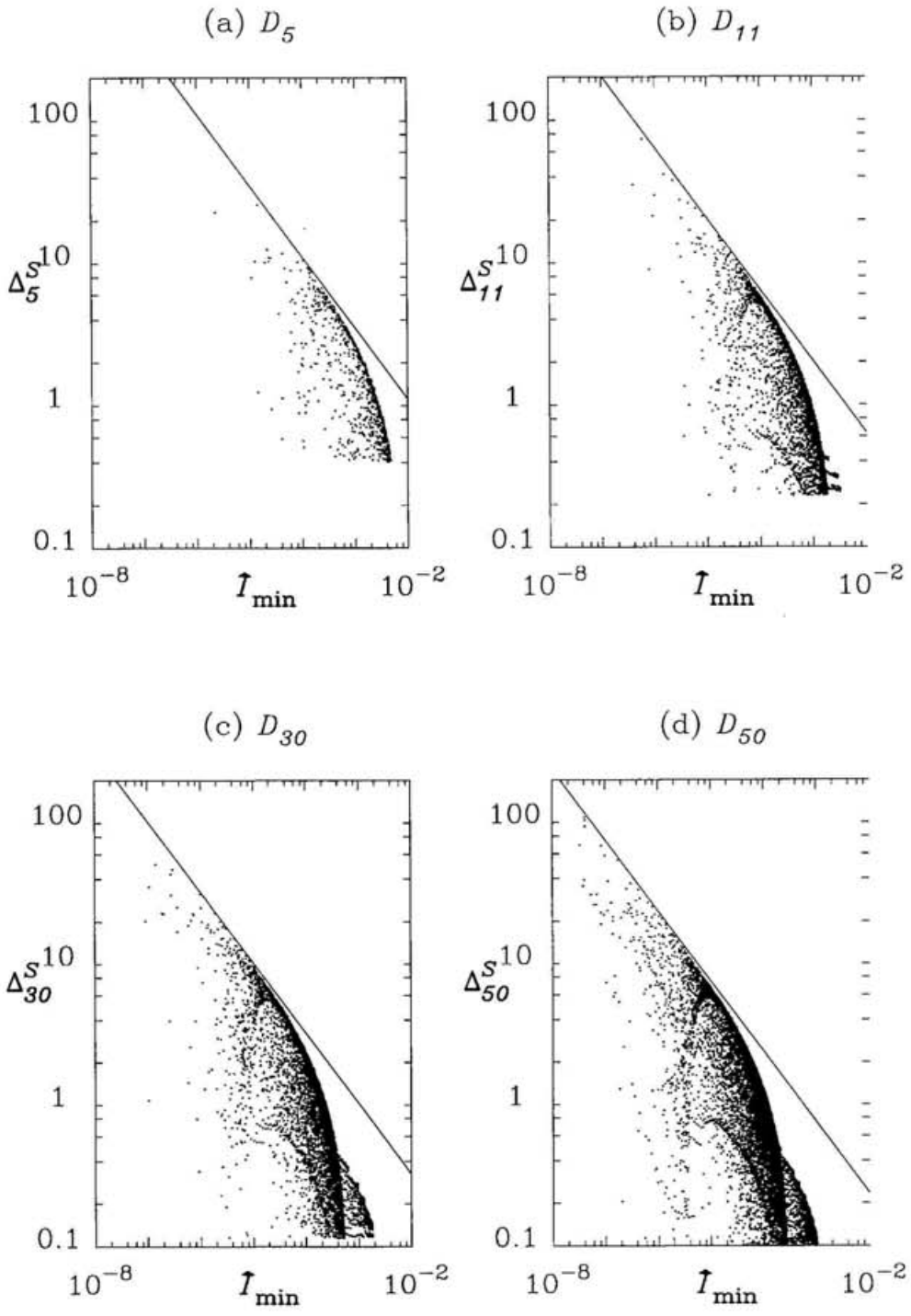

Figure 3.11: Dependence of Δ_i^S on $\hat{I}_{\min}$. A dot stands for $(\hat{I}_{\min}, \Delta_i^S)$ distribution of all samples of a slingshot-escape region S_i. A line represents $\Delta_i^S = C_i \left(\hat{I}_{\min}\right)^{-1/2}$ which is tangent to an existence region of dots, where C_i is a constant. Four figures (a), (b), (c) and (d) represent samples for $i = 5, 11, 30$ and 50.

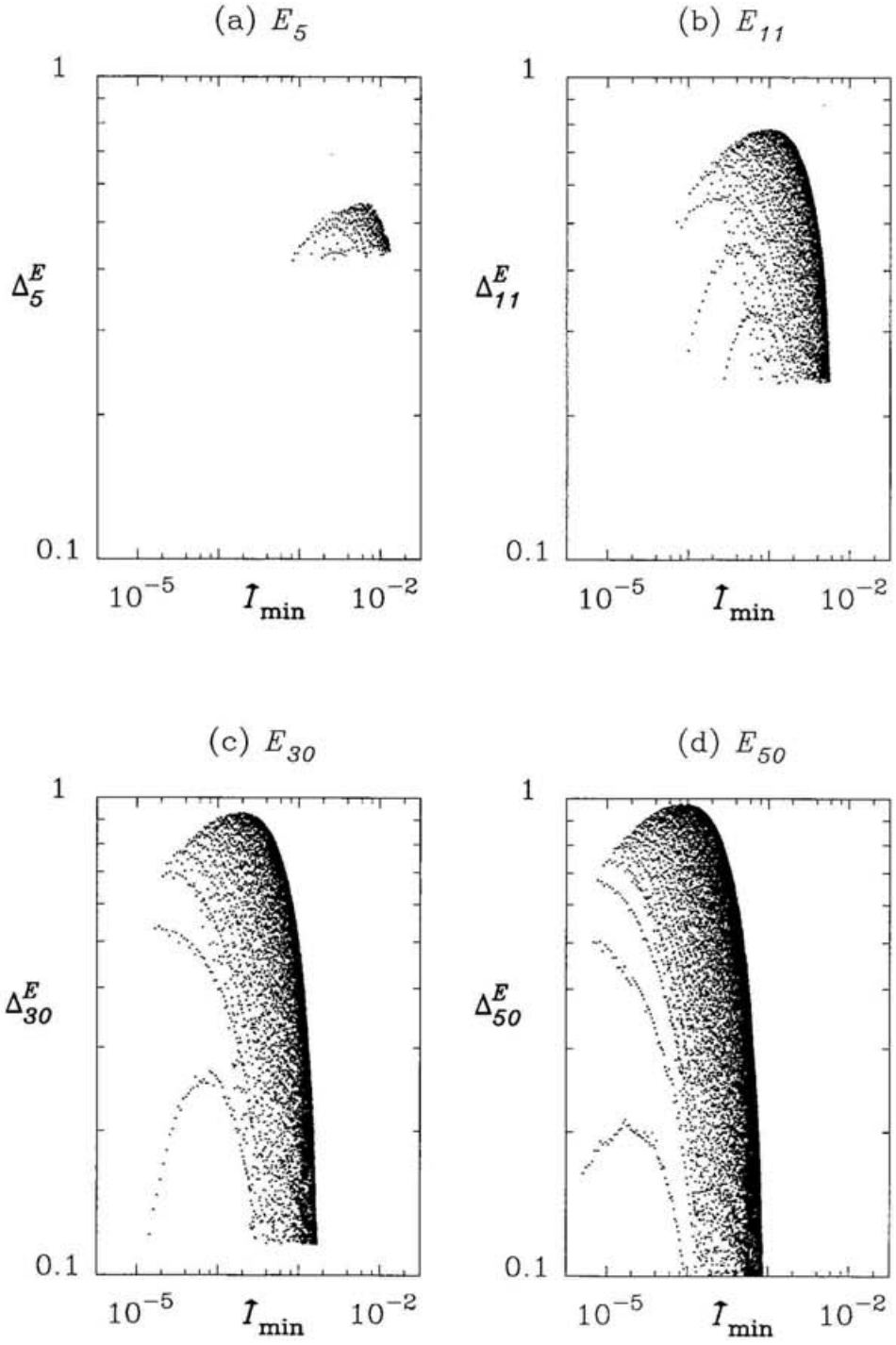

Figure 3.12: Dependence of Δ_i^E on $\hat{I}_{\min}$. A dot stands for $(\hat{I}_{\min}, \Delta_i^E)$ distribution of all samples of an exchange-escape region E_i. Four figures (a), (b), (c) and (d) represent samples for $i = 5, 11, 30$ and 50.

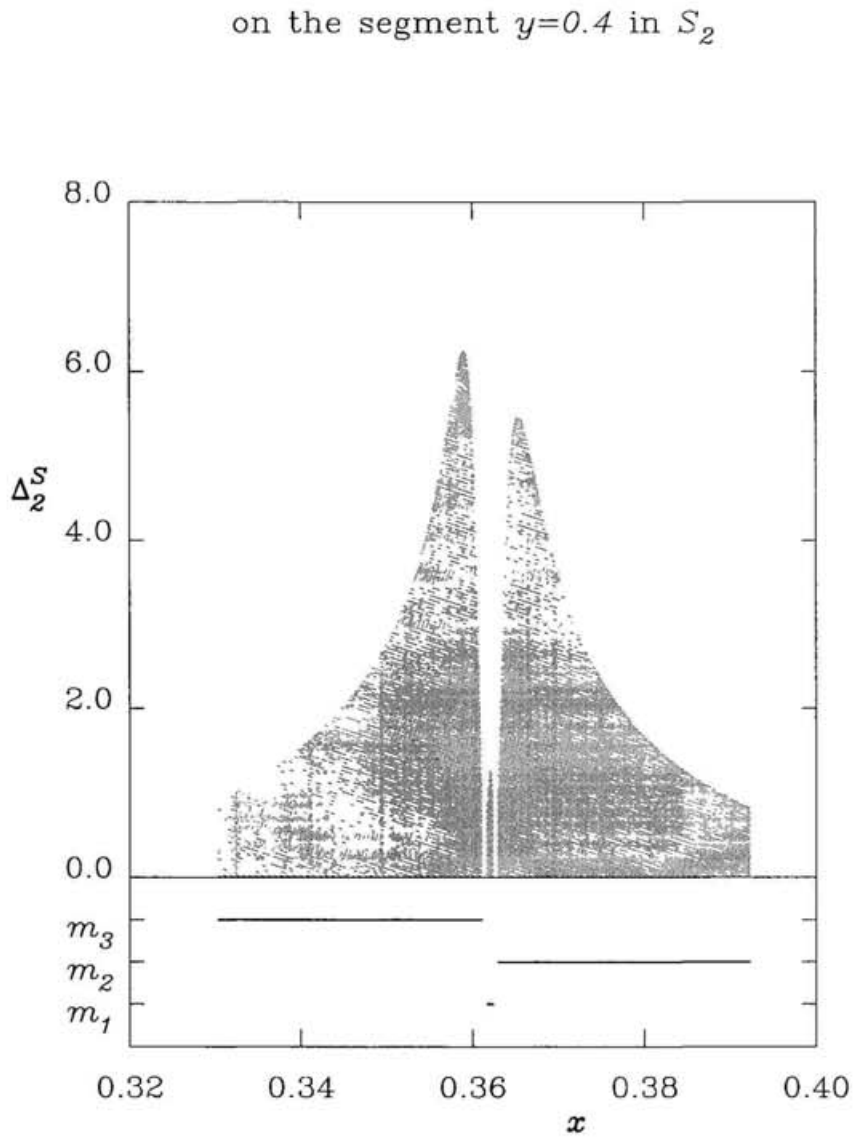

Figure 3.13: The relative change of binding energy on the segment $y = 0.4$ in S_2. The value of the upper edge of a gray region is Δ at x on $y = 0.4$. Three lines below the x-axis show the sections of three escape sub-bands. Escape particles are written outside the frame.

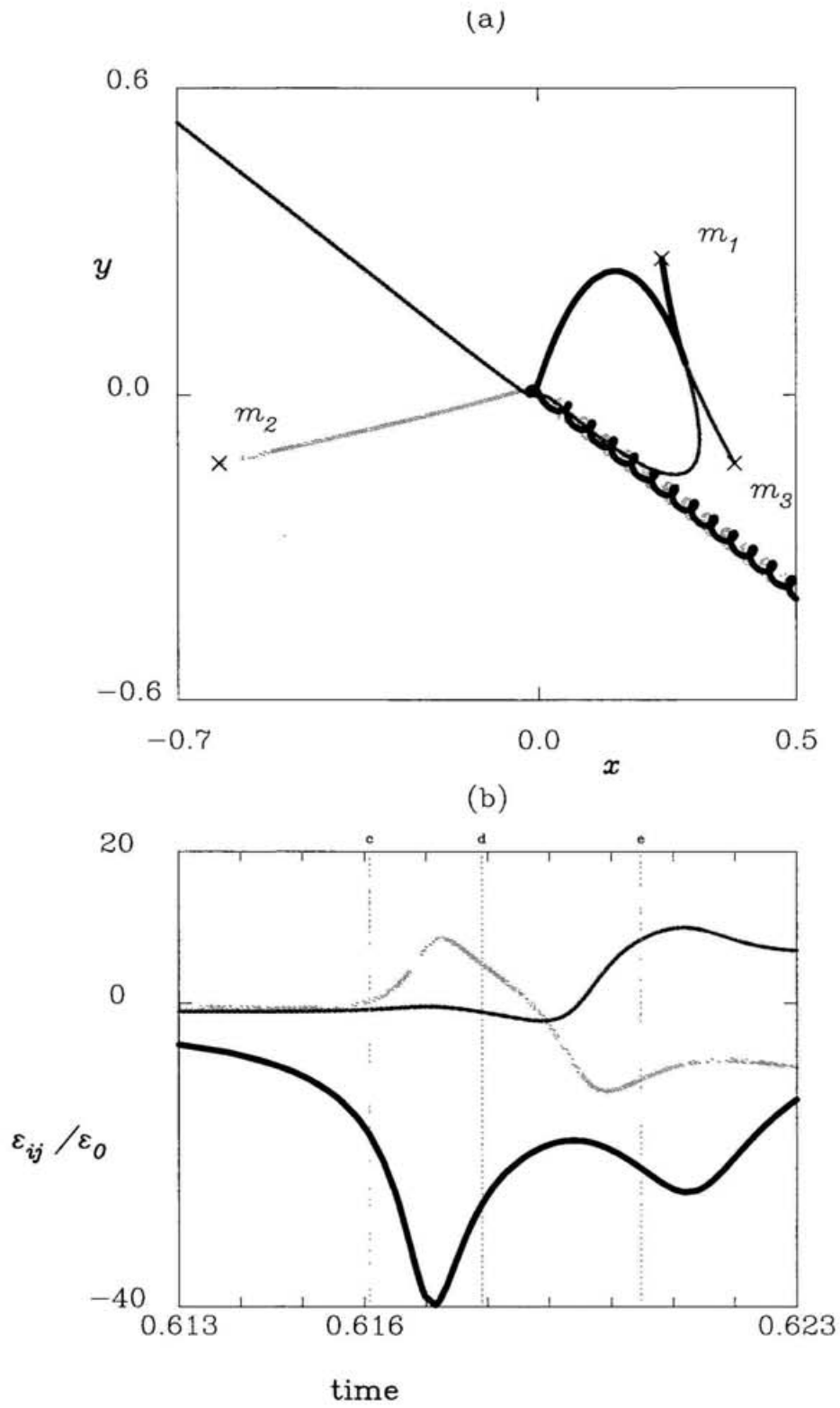

Figure 3.14: Behavior starting at $(0.359, 0.4)$ which is the initial value of maximum change of $\Delta_2^S(x)$ on $y = 0.4$ in S_2. (a) The orbit. The particle m_3 leads to escape. (b) The time-dependence of three binding energies. Three vertical lines indicate the times at syzygy crossings.

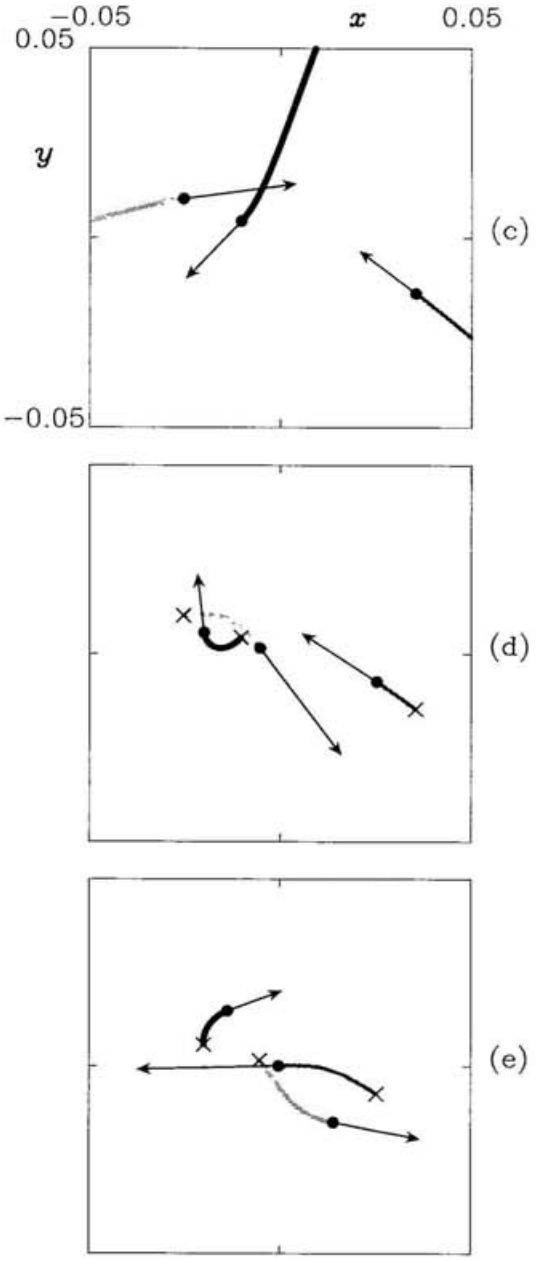

Figure 3.14: (c) The orbit until the first syzygy crossing during the triple encounter. The filled circles are the positions of the particles at the time of the syzygy crossing $t = 0.6161$ corresponding to the left vertical line in (b). The arrow represents the velocity vectors. The length of each arrow is reduced to 0.003 times as the scale of the axis. The particle m_1 passes through between m_2 and m_3 which are approaching each other. (d) The orbit from the first syzygy crossing to the second crossing at $t = 0.6179$ corresponding to the middle vertical line in (b). The particle m_2 passes through between m_3 and m_1 which are approaching each other. (e) The third syzygy crossing at $t = 0.6204$ corresponding to the right vertical line in (b). The particle m_3 passes through between m_1 and m_2 which are receding to each other.

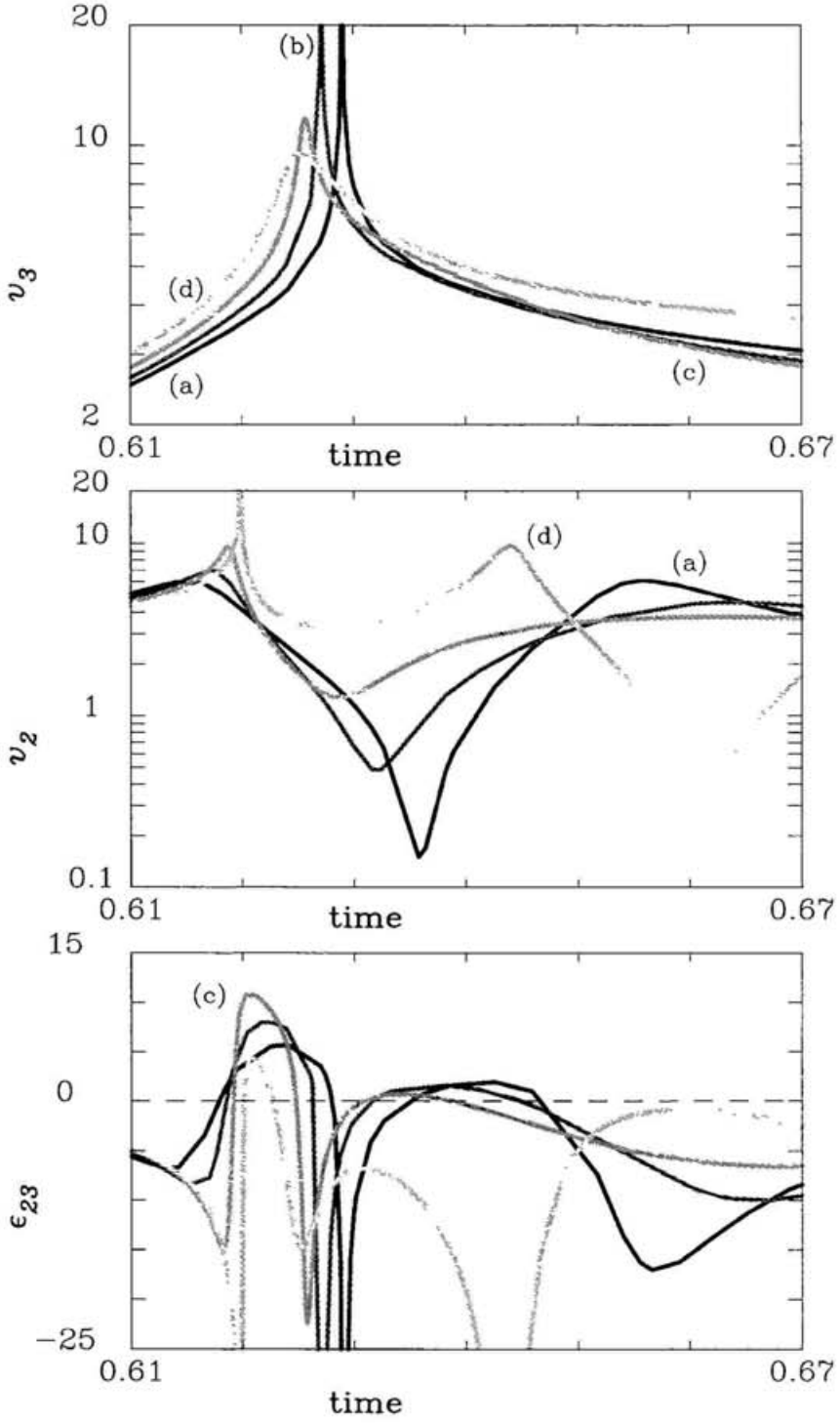

Figure 3.15: The time evolutions of the velocity for m_3, one for m_2 and the binding energy between m_2 and m_3 in the four system (a), (b), (c) and (d). The system (a) leads to escape for m_3 due to exchange. The system (d) leads to escape for m_3 due to slingshot. The systems (b) and (c) fail in escape after the first triple encounter. The initial values are $(0.420, 0.19)$, $(0.425, 0.19)$, $(0.430, 0.19)$ and $(0.435, 0.19)$ in alphabetical order.

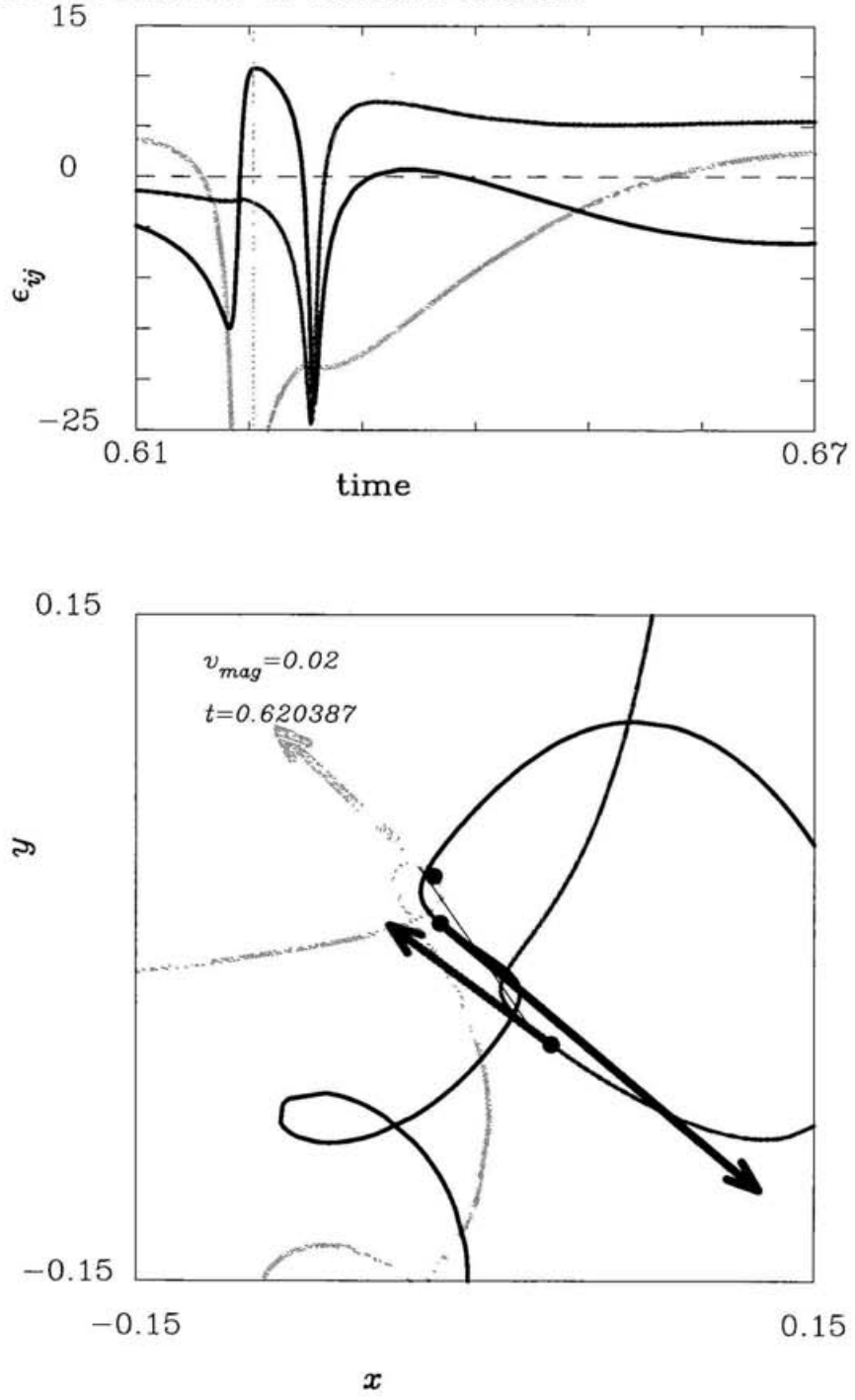

Figure 3.16: The upper figure: the time evolutions of binding energies between the respective particles in the system (c) starting at $(0.430, 0.19)$ in the gap region between D_5 and E_5. A bold curve stands for ε_{23}. The lightest gray and middle gray curves represent $\varepsilon_{31}(t)$ and $\varepsilon_{12}(t)$, respectively. The lower figure: the orbit of the system (c). A bold curve stands for the trajectory of m_1. The lightest and middle gray curves represent ones of m_2 and m_3, respectively.

3.4 Slingshot-escape conditions

3.4.1 Behavior of syzygy crossing leading to escape

The conditions of syzygy-crossing motion leading to escape are investigated in the present section which consists of two parts. First, we will investigate the relation between the configuration and the velocity vectors at the syzygy crossing, and search for the restricting conditions of the slingshot leading to escape. Second, we will consider the relation between the isosceles motion and the syzygy-crossing motion, and search for conditions of slingshot favorable for escape.

Velocity vectors at the syzygy crossing

It is well-known that a triple system tends to escape if the third particle passes through between components of the binary which are receding from each other. We will consider the physical meaning of *receding binary* in the first half part of the present subsection. We will define the *receding* strictly.

Aarseth et al. (1994b) investigated the conditions of triple encounter leading to escape numerically. They evaluated the physical states at the closest triple encounter in the free-fall system with equal masses. Here, the *closest triple encounter* is defined as a state at the time when the system experiences minimum moment of inertia, provided the perimeter of the triangle spanned by the three particles is smaller than a certain value. The sampling number of escape orbits was 5000.

One of parameters evaluated by Aarseth et al. (1994b) is the relative velocity of the radial motion of the binary components, u. According to them, the majority of the escape orbits are due to slingshot. The ratio is about 75%. They conjectured that exchange escape takes place in the other case (25%).

However, we concluded in Subsection 3.2.1 that escape due to exchange is more infrequent than exchange escape mentioned by Aarseth et al. (1994b). The relative probability of escape due to exchange is only about 10% (see eq.(3.14)). We expect that the

slingshot-escape orbits satisfying $u < 0$ exist. We ask whether the receding phenomena of the two components at the closest triple encounter is really a slingshot-escape condition.

We concentrate on the escape orbits starting in the band-like region S_2. The sampling number from our numerical results is 6641. Suppose that a particle leading to escape is m_l and the other particles are m_j and m_k. Let u_{jk} be the relative radial velocity of m_j and m_k. We evaluate u_{jk} at the time of *the closest syzygy crossing* instead of the time of the closest triple encounter. Here, the *closest syzygy crossing* is defined as a state where m_l passes through a line connecting m_j and m_k just after the closest triple encounter. We already know that the closest syzygy crossing takes place at the last stage of slingshot encounters leading to escape (see Subsection 2.4.2). In both cases of forward and backward slingshots, m_l leads to escape without passing through between m_j and m_k after m_l experiences the closest syzygy crossing.

Figure 3.17(a) is the histogram of u-distribution. The abscissa is u. This bin size is 0.4. The ordinate is the relative-distribution frequency of u. Here, the distribution is weighted by the magnification ratio due to the projection of the grid elements to the initial-value space with constant energy -1. Let the relative distribution frequency of u satisfying $u \in [u_{(i)}, u_{(i+1)}]$ be denoted by $f_i(u)$ for each integer i. The sequence $u_{(i)}$ composes the arithmetic progression. The bin size means $(u_{(i+1)} - u_{(i)})$. So the relative-distribution frequency with weight is described as

$$f_i(u) = \frac{\sum_{x,y} g(x,y)J(x,y)\ \delta x \delta y}{\sum_{x,y} J(x,y)\ \delta x \delta y}, \tag{3.73}$$

where $g(x,y) = 1$ if the system starting at the initial-value element (x,y) leads to syzygy crossing satisfying $u \in [u_{(i)}, u_{(i+1)})$, and $g(x,y) = 0$ otherwise. The weight at the initial value (x,y) is $J(x,y)$. The explicit expression of J is shown in eq.(3.37) of Subsection 3.2.2. The summation $\sum_{x,y}$ runs over all the grid elements sampled in S_2. The data points outside the range of abscisa are summed up in the respective corner entries.

We see that u is less than 0 in 23% systems of the band-like region. It means that about a quarter of the systems leading to slingshot escape shows the backward slingshot if the receding binary is defined as $u < 0$. This result is similar to the result by Aarseth et al. (1994b). How behave the escape orbits experiencing $u < 0$ at the closest syzygy crossing? In order to know the initial-value distribution of the orbits with $u < 0$, the initial-y dependence of u at the closest syzygy crossing is shown in Fig.3.17(b). The maximum value of the ordinate 0.4284 is the y-coordinate of the triple-collision point T_2 (Tanikawa et al., 1995). A cross (+) stands for u at the syzygy crossing of m_1. In this case, m_1 leads

to escape. A dot ($\cdot$) represents u at the syzygy crossing of m_2 or m_3. In this case, m_2 or m_3 leads to escape. There is a syzygy crossing with $u < 0$ in the system starting in $y < 0.34$ and leading to escape for m_2 or m_3 although the closest syzygy crossing of m_1 satisfies $u > 0$ if m_1 escapes.

An escape orbit showing $u < 0$ at the closest syzygy crossing is shown in Fig.3.18(a). The initial value is $(0.24, 0.25)$. A bold curve stands for the trajectory of m_1. The lightest and a middle-gray curves represent ones of m_2 and m_3, respectively. Three filled circles and arrows show the positions and velocities at the closest syzygy crossing. The scale of the arrow is reduced to 0.003 of the configuration scale. The particle m_1 comes from the upper side. It passes through between m_2 and m_3 which are approaching each other, and so m_1 is decelerated. The trajectory of m_1 is deflected. In the meantime, m_2 passes through between m_3 and m_1. Just after that, the closest syzygy crossing of m_3 takes place as we see in the figure.

The position and velocity vectors of particles m_j, $j = 1, 2, 3$ are denoted by $\boldsymbol{q}_j \in \mathbf{R}^2$ and $\boldsymbol{v}_j \in \mathbf{R}^2$, respectively, in the barycentric-coordinate system. Let $\boldsymbol{r}_{jk}$ be $\boldsymbol{q}_k - \boldsymbol{q}_j$. The norm of $\boldsymbol{v}_j$ is denoted by v_j. Let $\theta_1 \in [0, \pi]$ be the angle between $\boldsymbol{r}_{12}$ and $\boldsymbol{v}_1$. Similarly, θ_2 denote the angle between $\boldsymbol{r}_{12}$ and $\boldsymbol{v}_2$.

The relative radial velocity u_{jk} of the binary components is expressed as

$$u_{jk} = v_k \cos\theta_k - v_j \cos\theta_j. \tag{3.74}$$

Figure 3.18(b) shows the vectors $\boldsymbol{r}_{12}$ and $\boldsymbol{v}_2 - \boldsymbol{v}_1$ at the closest syzygy crossing occured in Fig.3.18(a). It is shown that u_{jk} is negative in this case.

However, the velocity vectors $\boldsymbol{v}_1$ and $\boldsymbol{v}_2$ spread each other. Therefore, we will define new parameter Φ_{jk} as

$$\Phi_{jk} = v_j v_k \sin(\theta_j - \theta_k). \tag{3.75}$$

Note that $|\Phi_{jk}|$ is equal to an absolute value of the exterior product of $\boldsymbol{v}_j$ and $\boldsymbol{v}_k$. The meaning of the sign (plus or minus) of $|\Phi_{jk}|$ is as follows: $\Phi_{jk} > 0$ if the velocity vectors of the temporary binary m_j and m_k spread from each other; on the other hand, $\Phi_{jk} < 0$ if the velocity vectors of m_j and m_k face each other. In the case with parallel velocity vectors, $\Phi_{jk} = 0$. We will call Φ_{jk} a *velocity-vector product.*

Figure 3.19(a) shows the histogram of the velocity-vector products Φ at the closest syzygy crossing. The abscissa is Φ. This bin size is 4.0. The ordinate is the relative

frequency. The distribution is normalized to energy -1 as in Fig.3.17(a). The entries at both sides include proportion of the systems having values exceeding the lower and upper bounds. Notations are same as Fig.3.19(a).

Notice that most of the parameter Φ distribute in the positive area. The ratio of the evaluated distribution with positive Φ is 99.86%. At the closest syzygy crossing, the velocity vectors of the two particles spread from each other.

The initial-y dependence of Φ at the closest syzygy crossing is shown in Fig.3.19(b). Notations are same as Fig.3.17(b). There are the initial values showing negative Φ in $y < 0.15$, and so it is necessary to investigate such a lower region in further detail. However, the present thesis does not concentrate on orbits starting around lower y. The detail observation of these orbits will be done in a future paper.

Tanikawa et al. (1995) found that a sequence of the triple-collision points lies on the binary-collision curve of type 1 in S_i according to Fig.2 of them. A triple-collision point neighboring T_2 on the binary-collision curve of type 1 is located at $(0.196978, 0.1342)$. The vertical line in Fig.3.17(b) represents the initial y of this triple-collision point. It is expected that various orbits exist around the triple-collision point on lower y. Thus, it is possible that the system determines escape at another syzygy crossing after the closest syzygy crossing. The closest syzygy crossing may not correspond to the last stage of triple encounter.

We have found that the velocity-vector products of samples are larger than a positive value except several ones in the lower region. Let us magnify the ordinate of Fig.3.19(b). The result is shown in Fig.3.20(a). Almost all samples in $y \in (0.1342, 0.4284)$ which is the interval between two triple-collision points T_2 and its neighbor satisfy

$$\Phi_{jk} > 2, \qquad (j,k) = (1,2), (2,3), (3,1). \tag{3.76}$$

We found that this inequality is established in other band-like regions S_i. Figures 3.20(b), (c), and (d) show similar results in S_5, S_9, and S_{11}, respectively. The sample numbers are 804 in S_5, 884 in S_9, and 3534 in S_{11}. The vertical line in the figure (b) represents the initial y of the triple-collision point which is the neighbor of T_5 (see Fig.2 of Tanikawa and Umehara, 1998). In S_9 and S_{11}, there is no evaluated result of triple collision points which are neighbor of T_i. The meaning of the lower boundary $\Phi_{jk} = 2$ will be discussed in a future paper.

Deviation from isosceles motion at the syzygy crossing

We will continue to study the syzygy-crossing condition leading to escape. Many authors consider the slingshot maintaining isosceles configuration as the ideal motion of the slingshot with the equal-mass case (Anosova, 1986, 1991; Aarseth et al., 1994b; Zare and Szebehely, 1995; Umehara and Tanikawa, 1997). In Section 2.4, it is found that the binary collision maintaining isosceles configuration nearly dominate the escape orbits. Thus, it is natural to consider the relation between isosceles motion and triple encounter leading to escape.

Recall that a particle leading to escape was denoted by m_l and the other particles are called m_j and m_k. Aarseth et al. (1994b) defined the indices representing the deviations from the isosceles motion as the following values:

(1) the ratio of distance

$$\delta = |r_{jl} - r_{kl}|/(r_{jl} + r_{kl}) \in [0, 1], \tag{3.77}$$

where r_{jl} is the distance between m_j and m_l,

(2) the angle $\psi \in [0, \pi/2]$ between the velocity vector of the escaper and the syzygy line connecting with the two other particles.

The phase space can be divided into two subspaces: the configuration subspace and the velocity subspace. The distance ratio δ is equal to zero if the system becomes isosceles in the configuration subspace. If the velocity become symmetric in the velocity subspace, $\cos\psi$ is also equal to zero. If the motion maintains isosceles configuration for all time, the two parameters are $\delta = \cos\psi = 0$.

Aarseth et al. (1994b) concluded that the isosceles configuration at triple encounter is more important for escape than the direction of velocity vector by observing distributions of the above indices in the 5000 systems with zero initial velocities and equal masses. According to their statistical results of escape orbits, δ must tend to be zero at the time of the closest triple encounter whereas distribution of ψ must be somewhat flat.

However, the conclusion by Aarseth et al. (1994b) has a problem with respect to the procedure of sampling the data. Let us consider the case that m_j and m_k approach closely each other at the minimum moment of inertia. In this case, r_{jk} and r_{kl} are comparable to each other inevitably. Thus, even if the configuration is not symmetrical, δ is nearly equal to zero. On the other hand, the fluctuation of ψ tends to be large since the interaction between m_j and m_k is large and the directions of the velocity vectors change quickly.

Moreover, ψ is undefined in the limit case that the binary collision occurs between m_j and m_k at the minimum moment of inertia.

Therefore, we will evaluate δ and ψ at the time of the closest syzygy crossing in order to sample the values when the system does not experience the close approach between two particles except an escaper. We found a remarkable result. Figures 3.21, 3.22, and 3.23 suggest the opposite conclusion to Aarseth et al. (1994b).

Figure 3.21 shows the distribution of the systems with respect to δ and $\cos\psi$, The sampled systems are as in Fig.3.17. The 6641 initial values belong to S_2. Moreover, Figures 3.22 and 3.23 show the $(\delta, \cos\psi)$-distributions in the systems whose initial values belong to S_5 and S_{11}, respectively. The sample numbers are 804 in S_5 and 3534 in S_{11}. In the gray-scale figure, the darkness of a grid element is directly proportional to the distribution frequency. The distribution on the darkest element includes ratio more than 0.01. Here, the distribution is normalized to the equi-energy surface. The following is found from the surveyed $(\delta, \cos\psi)$-map.

Observation 3.3. *On the $(\delta, \cos\psi)$-map, most of grid elements of the 20×20 mesh where the probability distribution exceeds 1% lies in the lower part $\cos\psi < 0.2$. Hence, the symmetric direction of the escape velocity is more important than the symmetric configuration at the time of the closest syzygy crossing.*

According to Aarseth et al. (1994b), the peak showing the large distribution must tends to the left side. It is true that there is a large distribution in the lower-left part of Fig.3.21 ($\cos\psi < 0.4$ and $\delta < 0.2$). However, many samples also exist in the lower-right part ($\delta \in [0.9, 1.0]$ and $\cos\psi \in [0.0, 0.1]$). Therefore, the system tends to escape if the escape-velocity direction is nearly perpendicular to the syzygy line. Many systems lead to escape even if the configuration is not close to the isosceles one.

This phenomenon is more evident with large i of S_i. See Figs.3.22 and 3.23. In this region, the escape-velocity directions of most systems are confined to $\cos\psi < 0.2$ whereas the distribution of the distance-ratio δ spreads in all interval. Although a blank region exists in $\{(\delta, \cos\psi) | \cos\psi < 0.1 \text{ and } \delta \in [0.3, 0.6]\}$ of S_2, such a non-existence region does not exist in the lower part on the distribution map of S_5 and S_{11}. Our results are summarized as follows.

Observation 3.4. *In* $\cos\psi \geq 0.2$ *on the* $(\delta, \cos\psi)$*-map, most of grid elements of the* 20×20 *mesh where the probability distribution exceeds* 0.4% *lie in the region* $\{(\delta, \cos\psi)|\delta \in [0.1, 0.5], \cos\psi \in [0.2, 0.6]\}$. *Hence, if the escape-velocity direction is not symmetric, the configurations of many slingshot-escape orbits tend to be symmetric at the time of the closest syzygy crossing.*

There are few orbits satisfying small δ and large $\cos\psi$ in the region $\{(\delta, \cos\psi)|\delta \in [0.1, 0.5], \cos\psi \in [0.2, 0.6]\}$. The dark peak of distributed elements shifts to the upper-right instead of the upper-left corner. If the escape velocity deviates from the symmetric direction, the configuration of the three particles also tends to deviate from the isosceles configuration.

In the upper part of the $(\delta, \cos\psi)$-map, the distribution probability is found to be nearly zero.

Observation 3.5. *Almost all samples satisfy the following inequality at the closest syzygy crossing:*

$$\cos\psi < 0.9 \qquad (|\psi| \gtrsim 30°). \tag{3.78}$$

The result shows that the system fails to escape if the velocity vector of the crossing particle is nearly parallel to the syzygy line. It seems that the angle of the escape-velocity direction seldom becomes close to zero whether the system leads to escape or not. If the configuration continues oblate before and after the syzygy crossing, the incoming particle must approach a particle of the temporary-binary components before the syzygy crossing. In most cases of such a situation, the orbital path of the incoming particle is bent, and so the incoming direction tends to be perpendicular to the syzygy line.

The distribution of the lower-right elements $(\delta, \cos\psi) \simeq (1, 0)$ is large. The distribution satisfying $\delta \in [0.9, 1.0]$ and $\cos\psi \in [0.0, 0.1]$ is 9.0%. The initial values in these elements lies in $y \in [0, 0.15]$, the lower part of S_2. It is expected that the exchange encounter occurs. Behavior in this part is not well investigated, and so it is discussed in a future paper. Each binding-energy transfer in the systems corresponding to these elements is small ($\Delta \in (0.8, 2.7)$). Thus the role in the systems of these elements does

not seem to be crucial to the evolution.

There are several systems in the right parts, for example $(\delta, \cos\psi) \simeq (1, 0.5)$. The distribution satisfying $\delta \in [0.9, 1.0]$ and $\cos\psi \in [0.5, 0.6]$ is 0.12%. The initial values in these elements lies in $y \in [0.14, 0.18]$ which is also the lower part of S_2. The binding-energy transfer in the systems corresponding to these elements are large ($\Delta \in (15, 27)$). We can not ignore these systems since it may be crucial to the evolution.

Therefore, finally let us investigate an orbit which enters in these elements at the closest syzygy crossing. We have found that the type of these orbits is also slingshot. See Fig.3.24. In this case, an escaping particle passes through near one of binary components at the syzygy crossing. The initial value is $(0.209, 0.176)$. The system experiences $(\delta, \cos\psi) = (0.901, 0.528)$ at the closest syzygy crossing. Notations are same as Fig.3.18(a). The scale of an arrow representing a velocity vector is reduced by a factor of 0.002 relative to the configuration scale.

After coming from the upper side, m_1 passes through between m_2 and m_3 approaching each other, and so m_1 is decelerated. The trajectory of m_1 is deflected. In the meantime, m_2 is decelerated by the inverse-slingshot effect by m_1 and m_3. After that, m_3 approaches m_1, and m_3 passes through near the position of m_1 on a line connecting m_1 and m_2. This is the closest syzygy crossing leading to escape for m_3. In the figure, filled circles and arrows representing the positions and velocities of three particles show the state just before the closest syzygy crossing.

Notice that the escaper m_1 never approaches m_2 before m_3 approaches m_1 at the syzygy crossing. Thus the type of triple encounter is not exchange. If exchange encounter occurs in the system, the system experiences the following successive close approaches. Before the close approach between the escaper and one particle (so-called the *intermediate particle*), the close approach occurs between the intermediate particle and the other particle. Since m_3 is an escaper in this case, m_1 must approach m_2 before m_1 approaches m_3, provided exchange encounter. However, such a phenomenon is not seen. Hence the classification of triple encounter in this case is slingshot.

Let us summarize the results in the present subsection. Slingshot escape needs the state where the escaping particle passes through between other particles receding from each other. Here, the receding phenomenon is not equivalent to the positive value of radial velocity between the two particles. We introduced new parameter *velocity-vector*

product described by eq.(3.75), and derived the confinement of the parameter for leading to escape as eq.(3.76). Moreover, relations between slingshot encounter and isosceles motion are found as Observations 3.3, 3.4, and 3.5. The symmetric direction of the escape velocity is more important than the symmetric configuration at the time of the closest syzygy crossing. If the system leading to escape due to slingshot experiences the asymmetric direction of the escape velocity at the closest syzygy crossing, the configuration of the orbit tends to symmetric. Finally, the confinement of the velocity direction eq.(3.78) is obtained.

3.4.2 Behavior close to near-isosceles slingshot

Slingshot-escape regions distribute around a binary-collision curve where the near-isosceles slingshot occurs. They mainly consist of three sets with respect to the three components of escape particles. We can understand the reason why most escape orbits distribute around the near-isosceles slingshot, according to a scenario by the expectation by Tanikawa et al. (1995) and the numerical results obtained in Subsection 3.4.1.

Tanikawa et al. (1995) expected that slingshot works on one component of the temporary binary for the orbits in the vicinity of the binary collision, and that escape orbits distribute around the binary-collision orbit. This prediction is suggested from the following behavior. Let $m_{\rm b}^{(1)}$ and $m_{\rm b}^{(2)}$ be the particles experiencing the binary collision. There is a system in a neighborhood of the initial value of the binary-collision orbit such that $m_{\rm b}^{(1)}$ passes through the syzygy between $m_{\rm b}^{(2)}$ and the third particle (say $m_{\rm in}$) in the system. At the time of the syzygy crossing, $m_{\rm b}^{(2)}$ and $m_{\rm in}$ are receding from each other. Furthermore, they expected as the above result that the binary-collision curve divides two sets of initial values corresponding to the escapes of $m_{\rm b}^{(1)}$ and $m_{\rm b}^{(2)}$, respectively, in the initial-value space.

We have found that in the initial-value space the binary-collision curve due to near-isosceles slingshot divide the escape regions for m_2 and m_3. It suggests that the expectation by Tanikawa et al. (1995) is correct. Around the near-isosceles slingshot orbits, however, there is a phenomenon which is not mentioned by them. In S_i for $i \geq 2$, the near-isosceles-slingshot orbits themselves lead to escape for m_1, and the escape orbits for m_1 exist in the initial points close to the near-isosceles slingshot orbits.

The following is the reason why Tanikawa et al. (1995) did not expect the existence of the escape region on and around the binary-collision curve. They assumed that the third particle is far away from the colliding particles and moving slowly. In the case with

near-isosceles slingshot, however, the third particle is approaching the colliding particles and leads to escape passing through the gravity center of the other particles.

According to our results of numerical survey, there is a straight segment parallel to x-axis in the escape region S_2 such that one endpoint is located on the binary-collision curve of type 1 and the other endpoint is included in the sub-region where m_3 escapes. The segment is composed from the following three intervals: the right interval where m_1 escapes, the intermediate interval where the system shrinks again, and the left interval where m_3 escapes. Let us observe the orbits starting on the three intervals. The results are shown in Figs.3.25(a), (b), (c), and (d). Figures (a) and (b) show the orbits starting on the right interval where m_1 escapes. Figure (a) corresponds to the binary-collision orbit of the near-isosceles-slingshot type. Figure (c) and (d) represent the orbits starting on the intermediate interval and the left interval, respectively. Each figure consists of two views. The time shifts from the upper view to the lower one. Three filled circles (•) and arrows represent the positions and the velocity vectors of the particles at a certain time. The scale of velocity vector is reduced by a factor of 0.002 relative to the scale of configuration.

Let $(x_{\rm col}, y_{\rm col})$ be the initial value experiencing the near-isosceles slingshot which starts from the binary-collision curve of type 1. We choose $x_{\rm col} = 0.2702483$ and $y_{\rm col} = 0.3$ from the table IIa of Tanikawa et al. (1995). Figure 3.25(a) illustrates a binary collision between m_2 and m_3 from the above initial value. The motion in Fig.3.25(a) corresponds to the one in Fig.3.26(b) illustrated schematically. The final motions in Fig.3.26(b) is the escape of m_1. We can see that the particle m_1 passes through the close-approaching particles which are receding from each other immediately after the binary collision.

We observe the change of behavior as a result of small perturbation for the binary collision in the left direction. We shift the initial point of m_1 to the left direction from the one experiencing the near-isosceles slingshot. In Fig.3.25(b), the initial point is located at $(x_b, y_{\rm col})$, $x_b = 0.2701 < x_{\rm col}$. The final motion in Fig.3.25(b) is the escape of m_1 as in Fig.3.25(a). The third particle m_1 approaches the other particles during binary encounter occurs. Therefore, the third particle and one component m_2 can not form a receding binary when the other particle m_3 passes through between them. This phenomenon is beyond the expectation by Tanikawa et al. (1995). The approaching m_1 passes through close to the gravity center of the other particles which are receding from each other after the binary encounter. As a result, m_1 leads to escape.

Let the initial values be shifted further left on the initial-value space. Figures

3.25(c) and (d) show results of a larger perturbation for the binary-collision orbit. In Fig.3.25(c) and (d), the initial values are set at $(x_c, y_{\rm col})$ and $(x_d, y_{\rm col})$, respectively, where $x_d = 0.2694 < x_c = 0.2698 < x_b$. We can observe from the respective figures that the position of m_1 at the syzygy crossing between m_2 and m_3 tends to shift to the left position of m_2 as m_1 is initially located at the left position of the initial value leading to near-isosceles slingshot. These phenomena occur as a result of a perturbation to the head-on collision.

Since the particle m_2 approaches m_3 passing the upper side of m_1, the orbital path of m_2 is bent downward. As the initial position of m_1 shifts to the further left, the bending of m_2 tends to be large. In the respective lower figures of (a), (b), (c), and (d), the following phenomena are observed: m_2 can not approach m_3 after m_1 passes through downwards the syzygy between m_2 and m_3 because of bending by m_1, and m_3 does not turn around m_2 sharply Thus, m_3 passes through closer to the mid-point of the syzygy between m_1 and m_2 than the case (b) (see the lower figure of Fig.3.25(c)). However, m_3 fails to escape since the lower figure shows that m_3 passes through the syzygy when the other components are approaching. It does not satisfy eq.(3.76) obtained by the statistical observation.

Does m_1 escape in this case? The particle m_1 can not pass through near the mid-point of the syzygy between m_2 and m_3 since m_3 is attracted by m_1 more strongly than the case (b) and the orbital path of m_1 is bent to the position of m_3. As a result, m_1 can not escape. No particles do not escape after the first triple encounter and the system shrinks again.

Figure 3.25(d) shows that the larger perturbation results in escape of m_3. The trajectory of m_3 becomes straight since m_2 can not approach m_3 due to the existence of m_1. As a result, the velocity vector of the escaping particle at the syzygy crossing is not perpendicular to the syzygy line, and m_3 passes through near the mid-point between m_2 and m_1 which are receding each other. According to Observation 3.4 in Subsection 3.4.1, if the escape-velocity vector deviates from the perpendicular direction, a slingshot-escape orbit tends to symmetric configuration at the syzygy crossing. For many escape orbits, the escaping particle passes through near the mid-point of the other two particles. Thus m_3 leads to escape.

We have found that the behavior in Fig.3.25(d) is the same as the schematical one in Fig.3.26(b). In the vicinity of the binary-collision orbit, the slingshot effect works on one component of the receding binary. We have verified that the expectation by Tanikawa et

al. (1995) is correct in the neighborhood of the binary-collision orbit due to near-isosceles slingshot.

We could understand that the escape region for m_1 is distributed around the binary-collision curve due to near-isosceles slingshot, and that the escape region for m_3 is located on the left side of binary-collision curve of near-isosceles slingshot. By right shifting of the initial values, we can also understand the existence of an escape region for m_2 similar to the left shifting case.

In the collisional case except near-isosceles slingshot, the expectation by Tanikawa et al. (1995) is not realized. There does not exist any escape orbit around the orbits on the binary-collision curve of type 3 which is far from the triple-collision point. Escape regions exist on the right side of the binary-collision curve of type 3. We can describe such phenomena as follows.

Fig.3.27(a) shows the binary-collision orbits of type 3 where escape does not occur. Arrows represent the velocity vectors reduced by a factor of 0.05 with respect to the scale of position. Other notations are the same as Fig.3.25. Let $(x_{\rm col}, y_{\rm col})$ be the initial value experiencing binary collision of type 3. We choose $x_{\rm col} = 0.2451897$ and $y_{\rm col} = 0.3$ from the table IIb of Tanikawa et al. (1995). The main difference between type 1 and type 3 is the direction of incoming particles at the time of binary collision. The velocity vector of m_3 is not perpendicular to the direction of each velocity of the colliding particles. As a result of the asymmetrical repulsion, the distance between m_1 and m_3 is shorter than the distance between m_2 and m_3. Thus m_3 passes through the point away from the mid-point on the syzygy line connecting m_1 and m_2. Moreover, escape-velocity direction of m_3 is not perpendicular to the syzygy line at the closest syzygy crossing. In such a case, escape hardly occurs according to the results in Subsection 3.4.1.

Figure 3.27(b) shows the case that the initial value is shifted to the right direction. As a result of a perturbation for the binary collision, m_2 is turned clockwise and tends to approach m_3 compared to the collisional case of type 3. Thus m_3 passes through near the mid-point of the line connecting the other particles. Such a case is easy to lead to escape, according to the results in Subsection 3.4.1. Note that closer triple encounter in this case can be realized than the one in the case (a). It is also the reason of escape.

With respect to type 2, there are no escape orbits for $i \leq 4$; on the other hand, tongue-like regions where m_3 escapes exist for $i \geq 5$. However, there is only one escape

region and the binary-collision curve of type 2 does not divide two sets.

3.4.3 Slingshot escape in the planar isosceles subsystem

In the present subsection, the behavior of slingshot in the planar-isosceles problem is considered in order to understand the behavior of the system starting on the near-isosceles-slingshot orbits in the free-fall problem.

According to 2.4.1, the narrow region around the near-isosceles-slingshot curve belonging to the escape region S_i for $i = 2, 3, \ldots$, seems not terminated. The convergence point in the upper direction is the triple collision T_i. The lower-convergence point seems another triple-collision point. It is in contrast to the escape region S_1. There exists an interval on the y-axis where m_1 returns after the first triple encounter although the syzygy crossing occurs between the receding components of binary. The y-axis corresponts to the isosceles curve running the center of the narrow escape region. As a result, the narrow region around the near-isosceles-slingshot curve belonging to the escape region S_1 is terminated.

In order to answer the above question, we will make clear the condition of escape by slingshot after the syzygy crossing of a receding binary in the planar isosceles subsystem. This subsystem has two degrees of freedom, and so the structure of the phase space is easy to comprehend. Because of the energy integral, the motion is restricted to the three-dimensional equi-energy subspace. Hence, we can define a two-dimensional surface of section where a flux consisting of phase trajectories crosses transversally.

We will evaluate the condition of escape by slingshot numerically. Although we will restrict the system to the case of equal masses (i.e., $m_1 = m_3 = 1$), the initial values are not restricted to the system with zero velocities. Let us study the case where the total energy is negative. After a suitable scaling of variables and time, we restrict ourselves to the energy level $h = -1$. We will start at the syzygy crossing with a receding binary, i.e., $y(0) = 0$ and $\dot{x}(0) > 0$. By the symmetry of motion, we investigate only the case with $\dot{y}(0) > 0$. By the existence of the invariance $h = -1$, one value $x(t)$ is determined from the other variables. Then the initial-value space is $(\dot{x}(0), \dot{y}(0))$.

In Fig.3.28(a), the initial points resulting in escape without any return are represented by dots $(\cdot)$. The other points represent initial points where the third particle returns after the ejection. The ordinate is the logscale of $\dot{x}(0)$ and the abscissa is the logscale of $\dot{y}(0)$. There is one curve which runs along the boundary of the set of initial

values leading to escape. There is a curve of the initial values where each motion returns until one hundred times of binary collision. Thus, the initial values leading the parabolic-elliptic escape should exist between the boundary and this curve.

Figure 3.28(b) shows the initial values of $x(0)$ at the respective initial points. According to this figure, $x(0)$ is smaller on the upper and right parts in the initial-value space than the lower-left part.

Three bold curves in the Fig.3.28(a) represent the sets of cross points where the near-isosceles slingshot of the free-fall system starting in S_1, S_2 and S_3 passes through the surface of section. The orbits of the near-isosceles slingshot in S_i for $i = 2, 3, \cdots$ does not maintain isosceles configuration exactly; however, we approximate the motion as the isosceles. In the three U-shape curves, the outside one is the section of trajectories starting in S_1, and the inside one is in S_3. The result shows that the respective binary-collision orbits form a sequence of one-parameter families since the shapes of the section are similar. We conjecture that the U-shape tends to narrow as the i of S_i increases.

Furthermore, the results give us information of a near-isosceles slingshot condition. Only the section belonging to S_1 goes out of the escape region on the surface. It verifies the existence of the initial-value interval where the system does not escape immediately after the syzygy crossing of a receding binary.

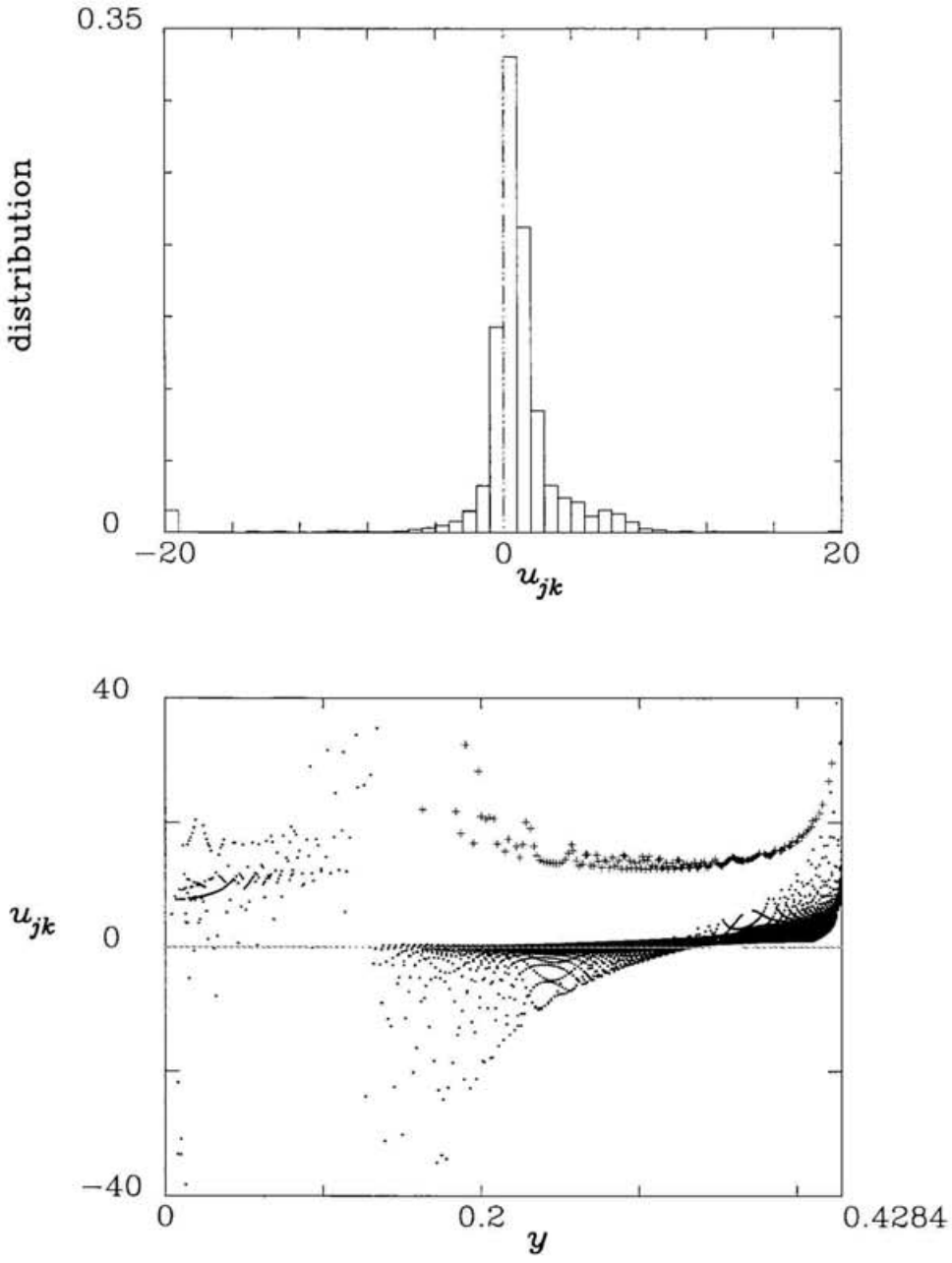

Figure 3.17: Relative velocity of the radial motion of the binary components u_{jk} at the closest syzygy crossing. (a) Distribution of u_{jk} with weight by the magnification ratio due to projection of the initial-value elements to the space with constant energy. (b) Initial-value dependence of u_{jk}.

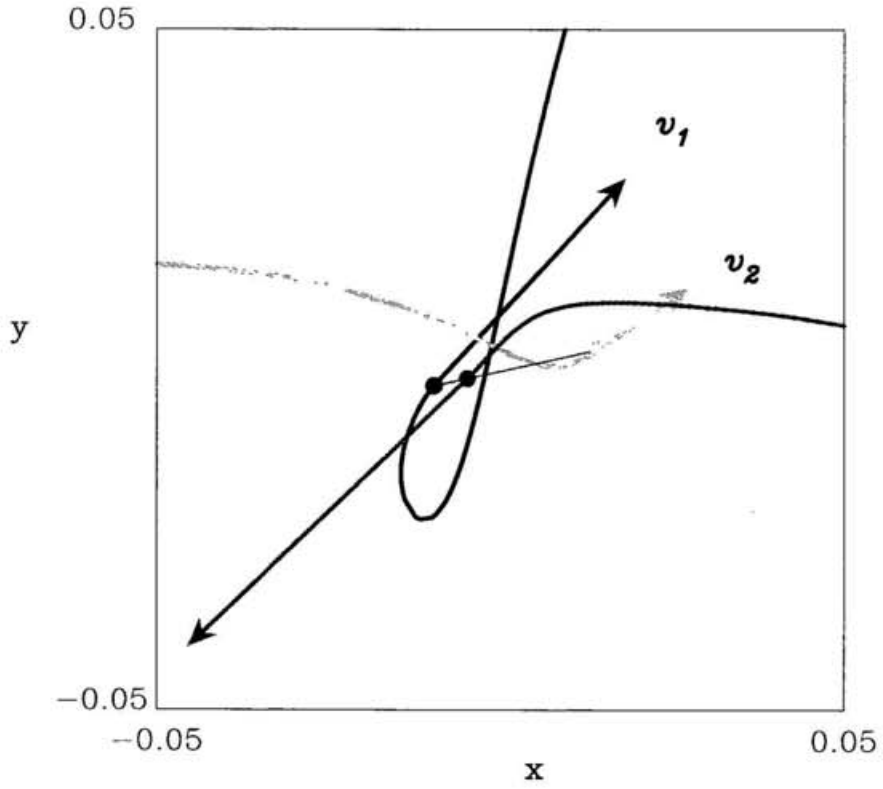

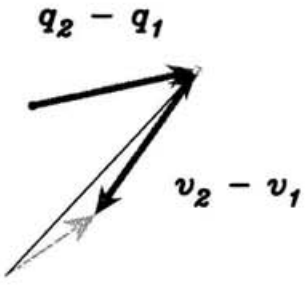

Figure 3.18: A slingshot-escape orbit showing $u_{12} < 0$ at the closest syzygy crossing although the velocity vectors $\mathbf{v}_1$ and $\mathbf{v}_2$ spread each other.

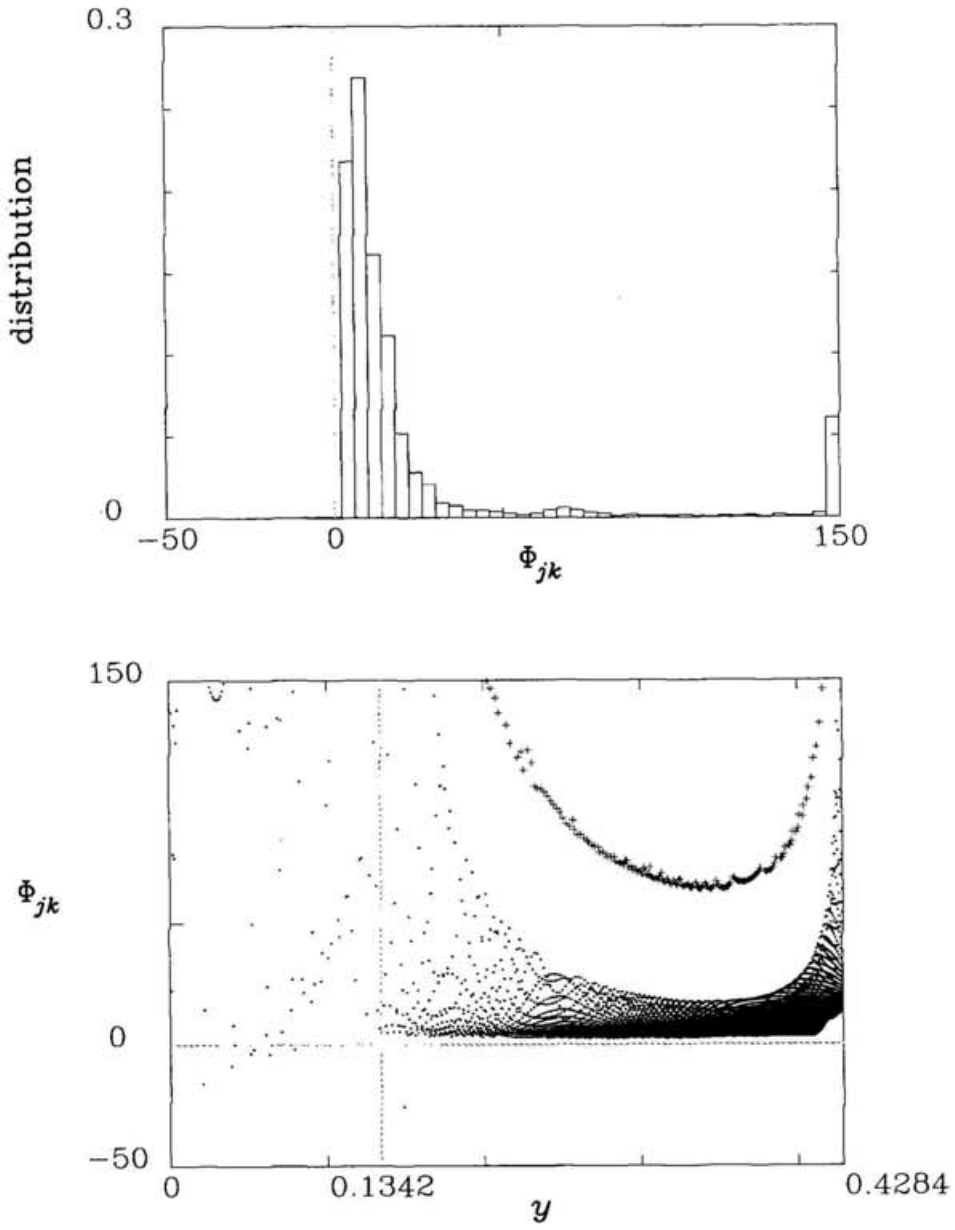

Figure 3.19: Velocity-vector product of the radial motion of the binary components Φ_{jk} at the closest syzygy crossing. (a) Distribution of Φ_{jk} with weight by the magnification ratio due to projection of the initial-value elements to the space with constant energy. (b) Initial-value dependence of Φ_{jk}.

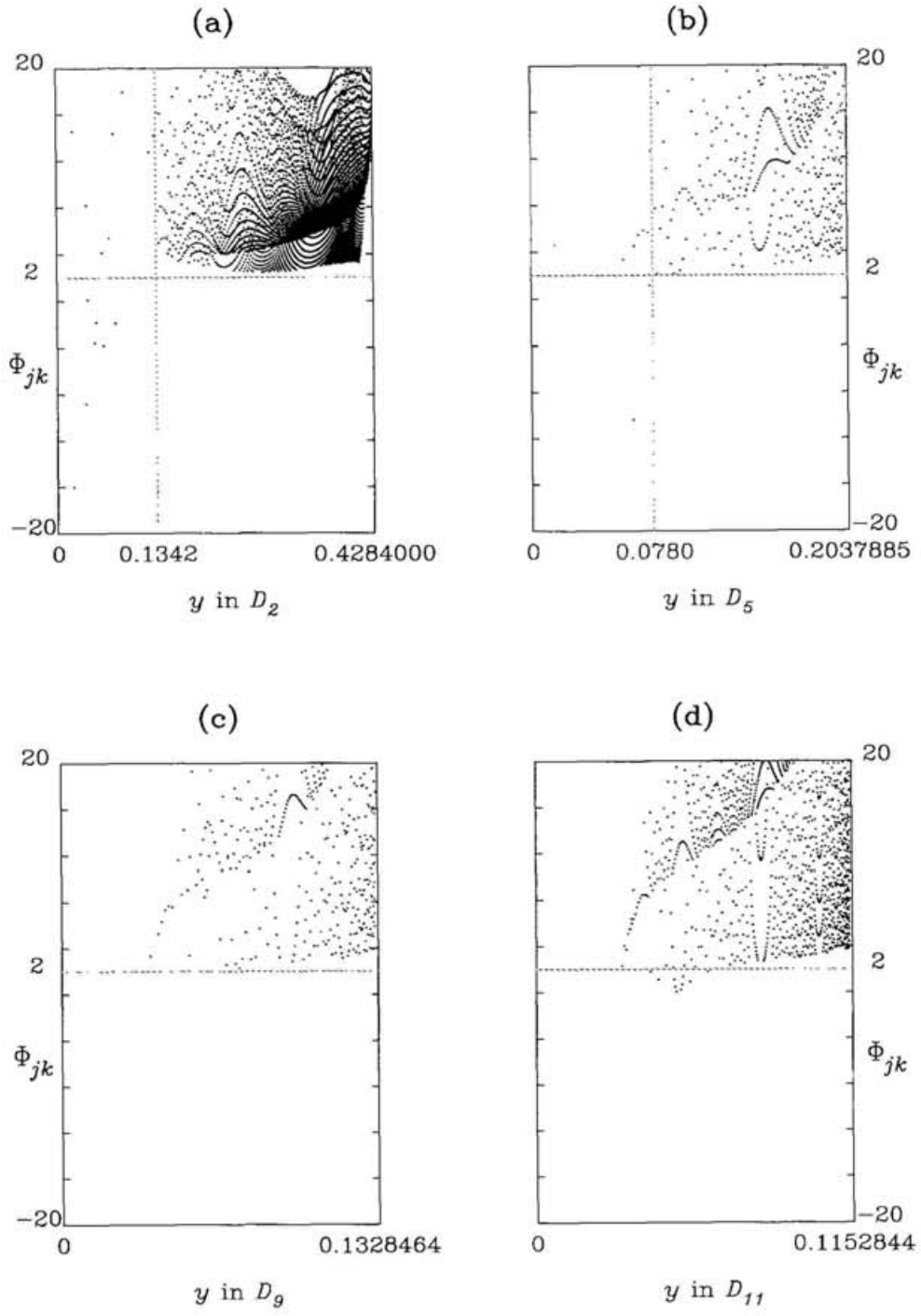

Figure 3.20: Distribution of velocity-vector product Φ_{jk} at the closest syzygy crossing with weight by the magnification ratio due to projection of the initial-value elements to the space with constant energy in the four slingshot-escape regions. (a) in S_2, (b) in S_5, (c) in S_9 and (d) in S_{11}.

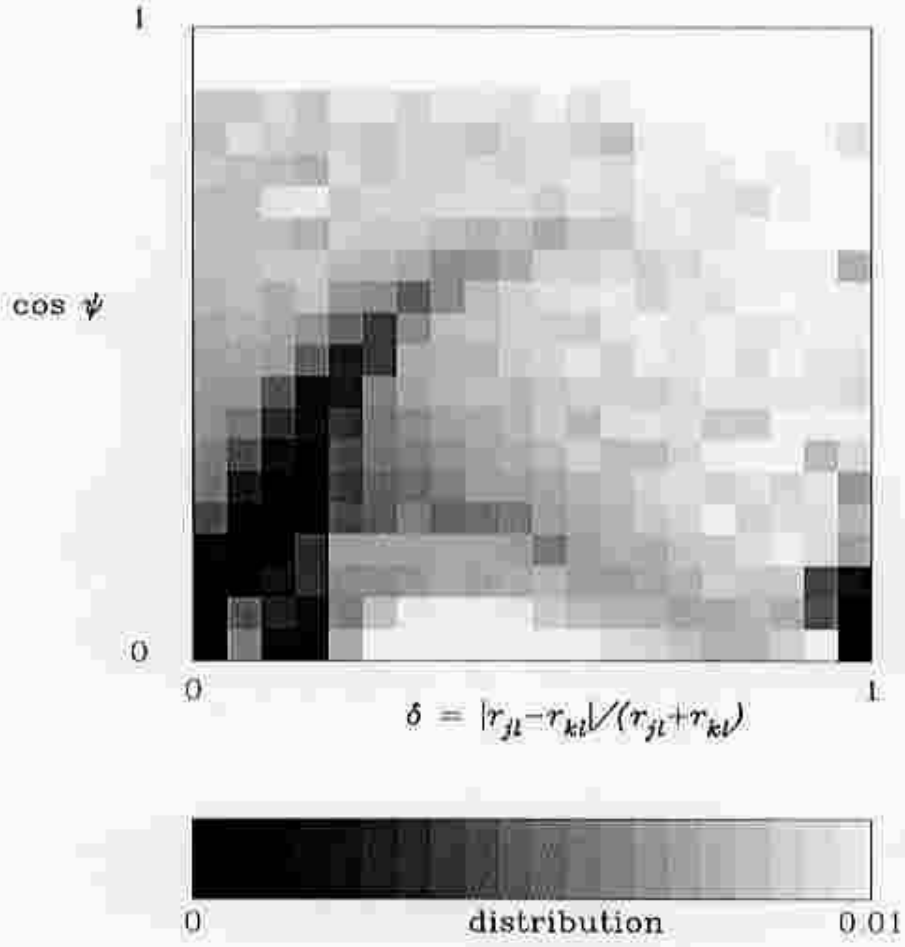

Figure 3.21: Distribution of distance ratio (δ) and cosine of escape-velocity direction ($\cos\psi$) at the closest syzygy crossing in S_2.

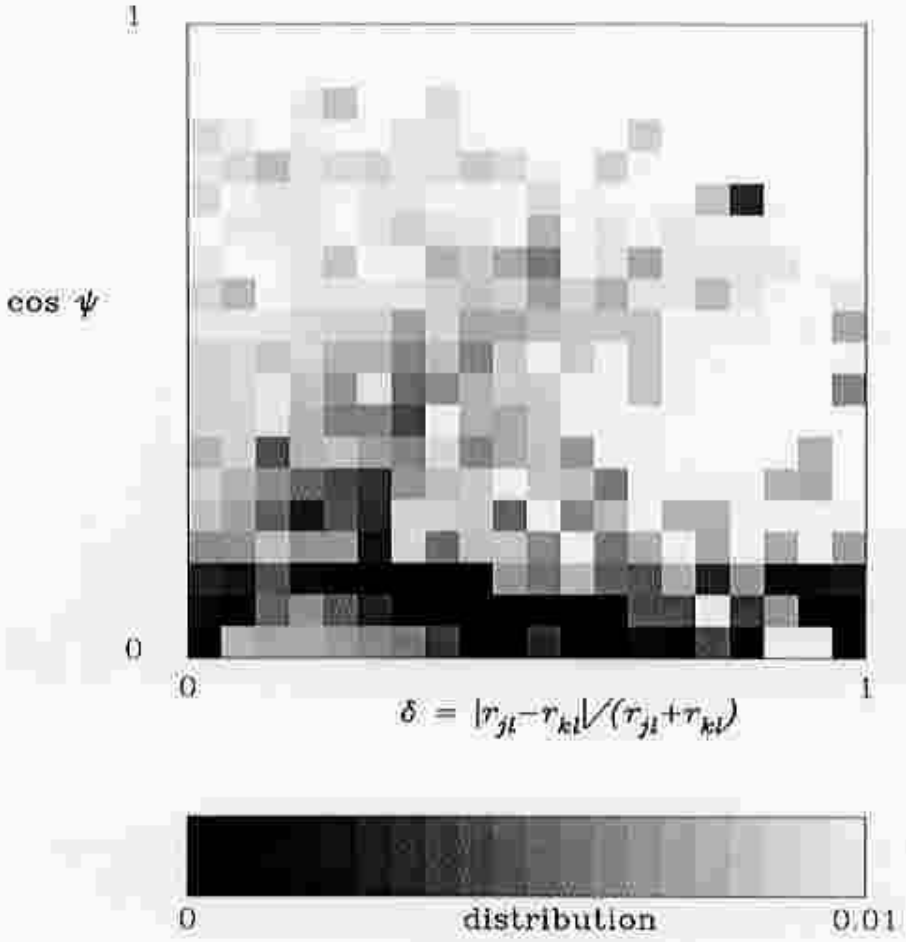

Figure 3.22: Distribution of distance ratio (δ) and cosine of escape-velocity direction ($\cos\psi$) at the closest syzygy crossing in S_5.

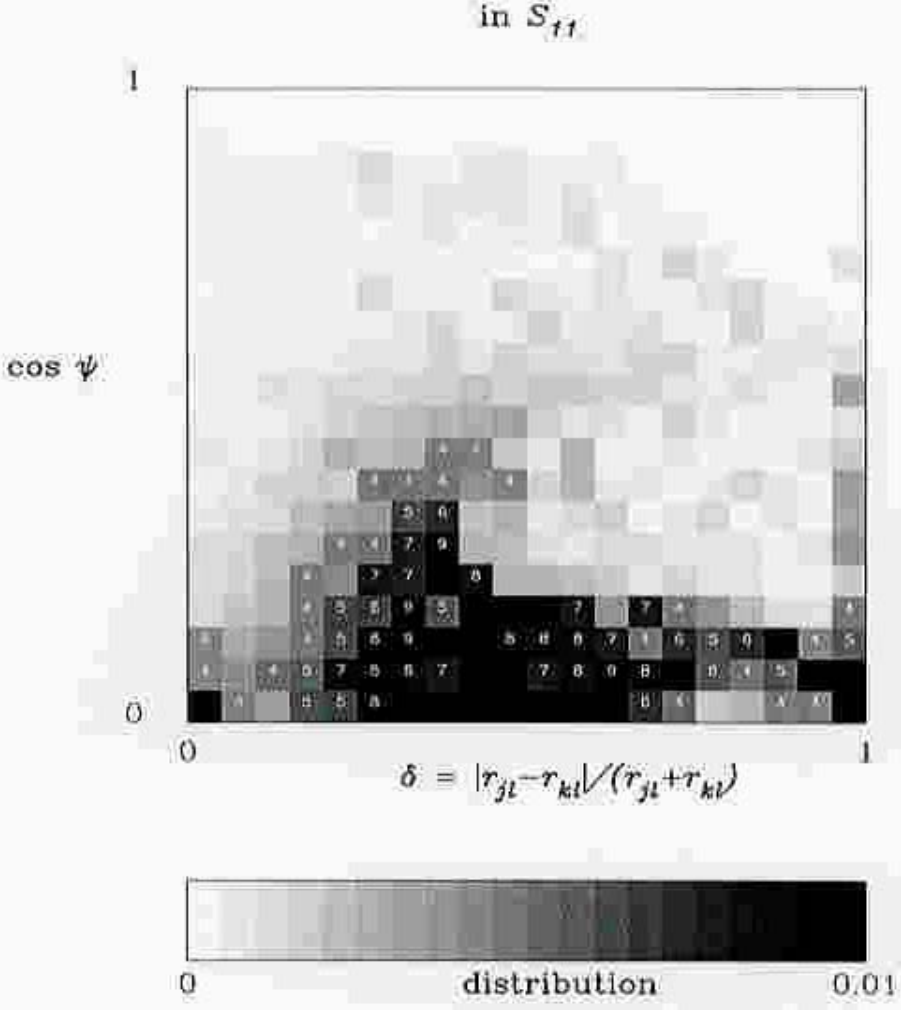

Figure 3.23: Distribution of distance ratio (δ) and cosine of escape-velocity direction ($\cos\psi$) at the closest syzygy crossing in S_{11}.

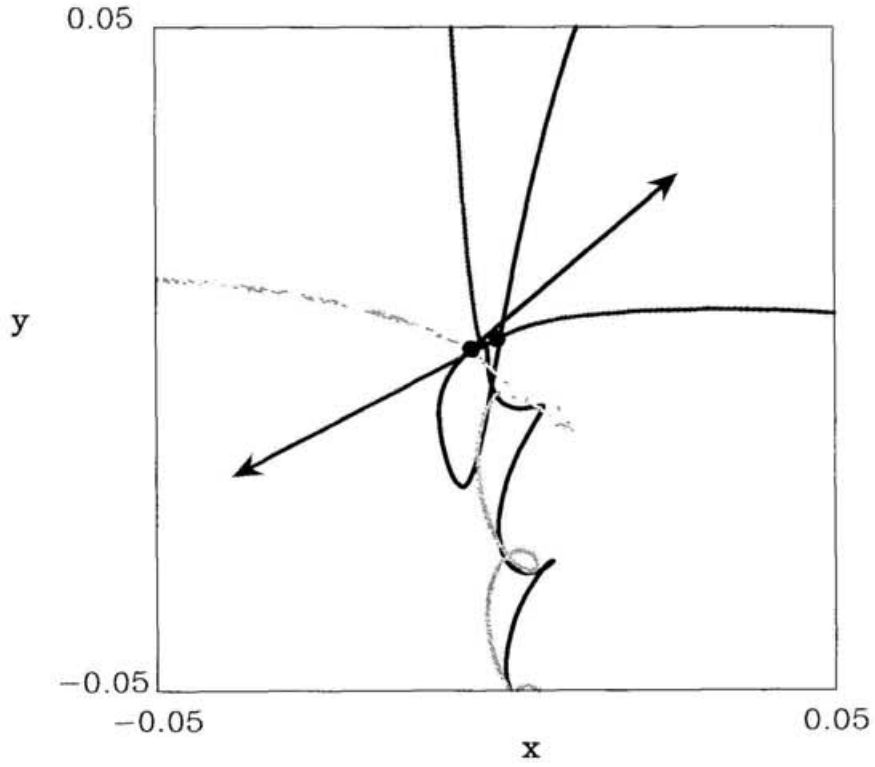

Figure 3.24: A strange slingshot-escape. The escaping particle passes near one of the other components, i.e., away from the isosceles configuration.

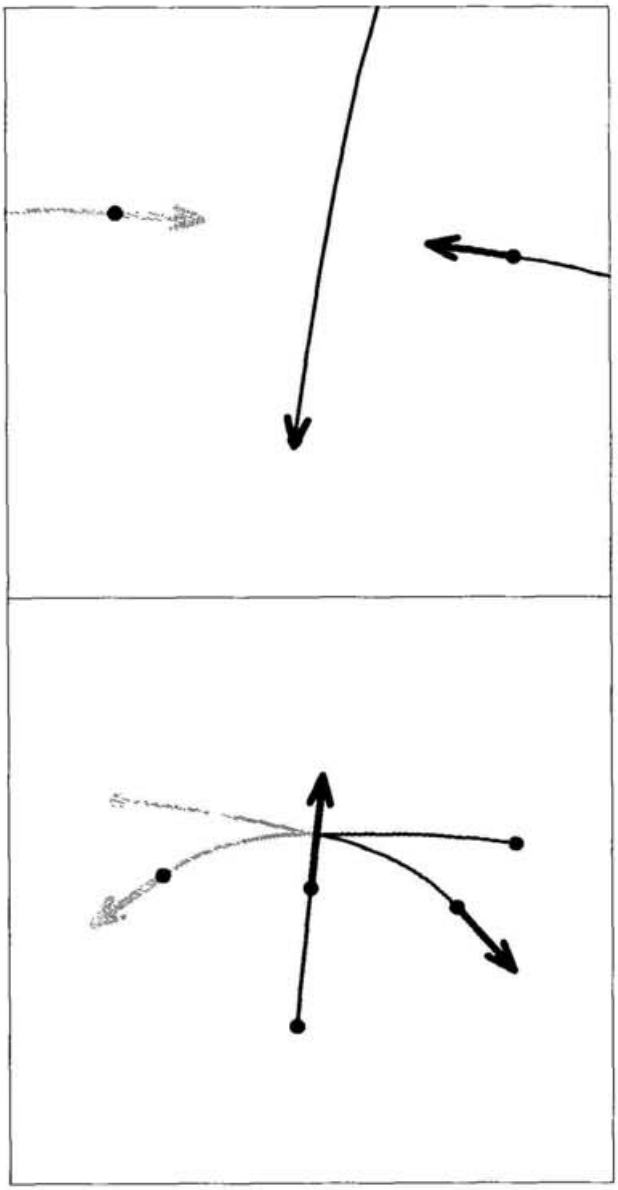

Figure 3.25: The slingshot orbits close to the near-isosceles slingshot. (a) The orbit of the near-isosceles slingshot on the binary-collision curve of type 1. The particle m_1 escapes. The initial value is $(0.2702483, 0.3)$.

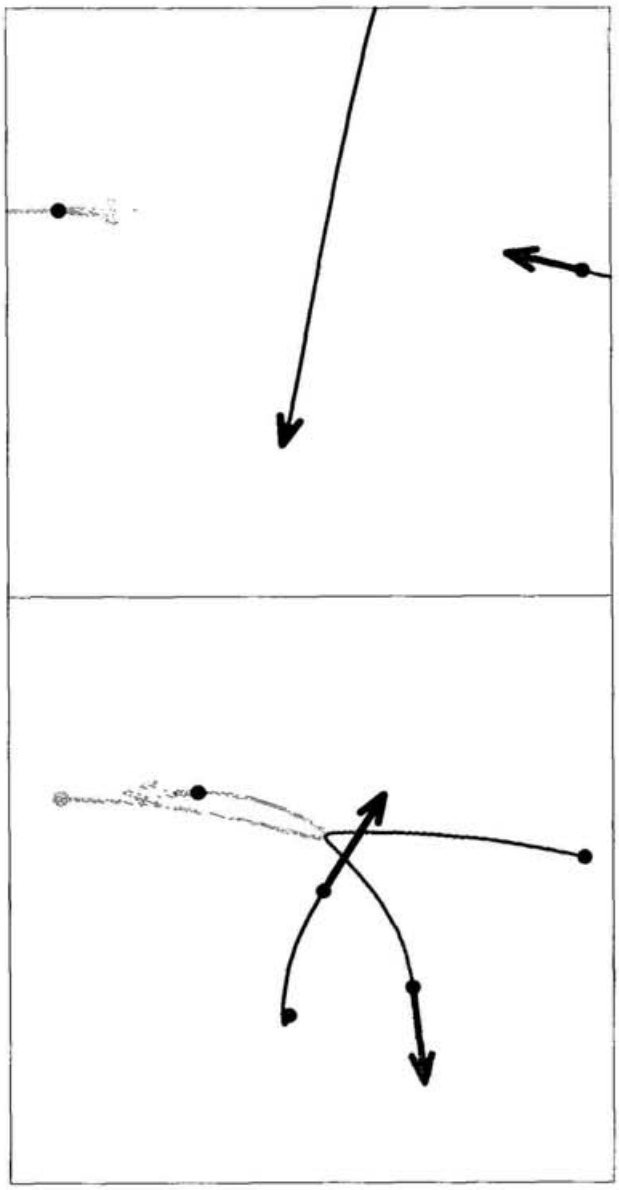

Figure 3.25: (b) The result of the small deviation from the near-isosceles slingshot. The particle m_1 escapes. The initial value is $(0.2701, 0.3)$.

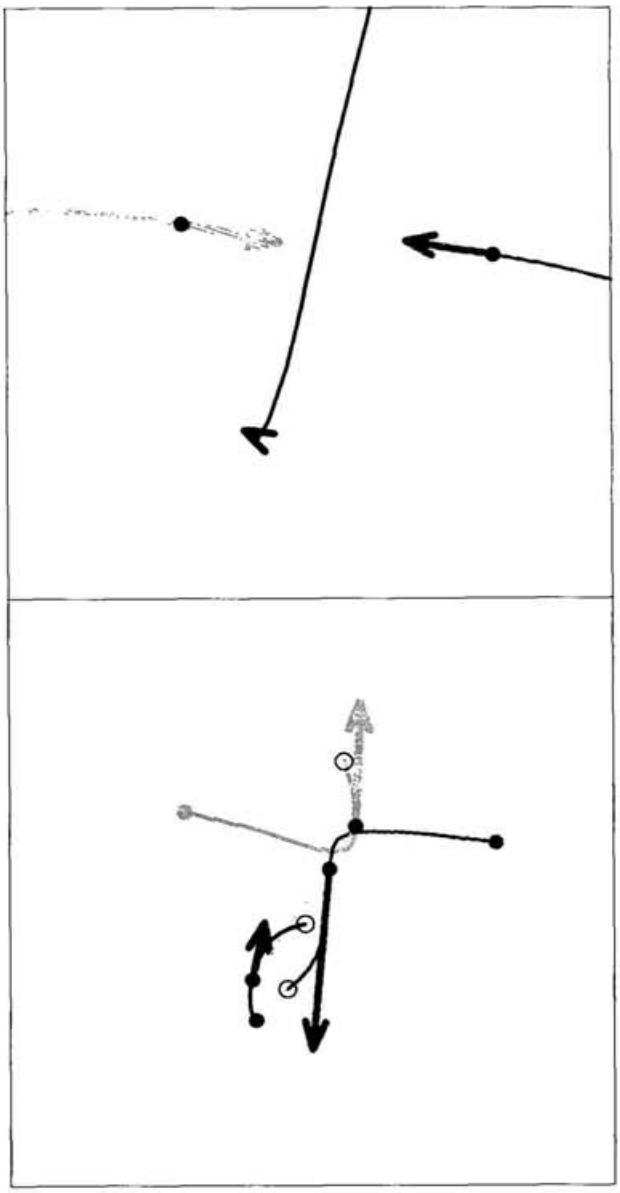

Figure 3.25: (c) The result of the further deviation. The particle m_1 can not escape after the first triple encounter since the syzygy crossing occurs when binary components approach each other. Also m_3 can not escape. The initial value is $(0.2698, 0.3)$.

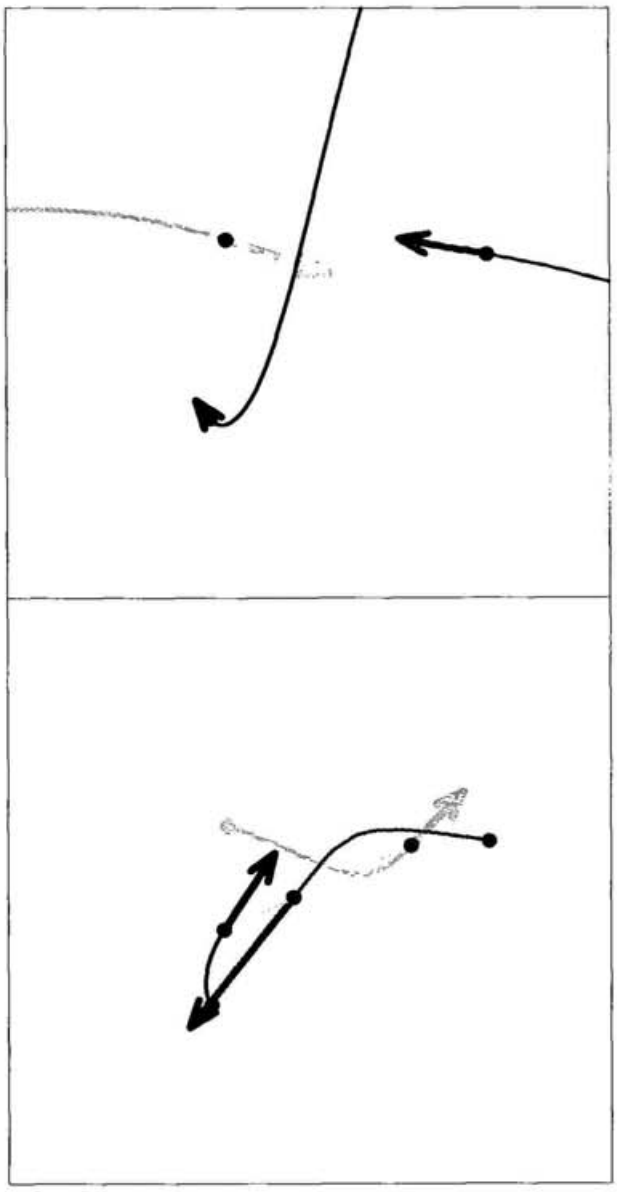

Figure 3.25: (d) The result of the largest deviation of the four figures. The particle m_3 passes through the syzygy of the receding binary. The initial value is $(0.2694, 0.3)$.

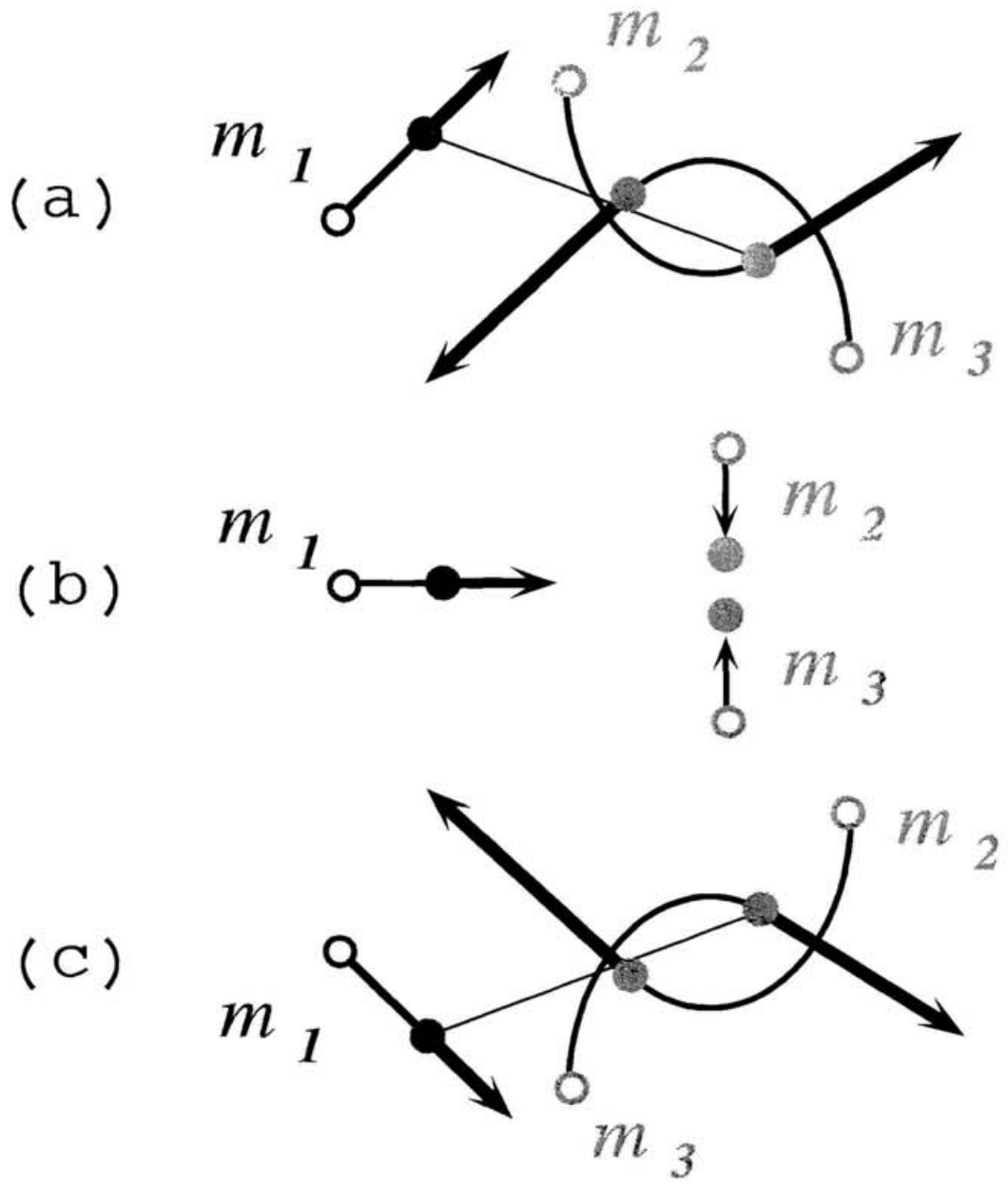

Figure 3.26: Schematical figures representing the relation between a binary collision and slingshots. The middle figure (b) illustrates the binary-collision orbit of the near-isosceles-slingshot type. The figures (a) and (c) correspond to the results of two opposite perturbations to the near-isosceles slingshot.

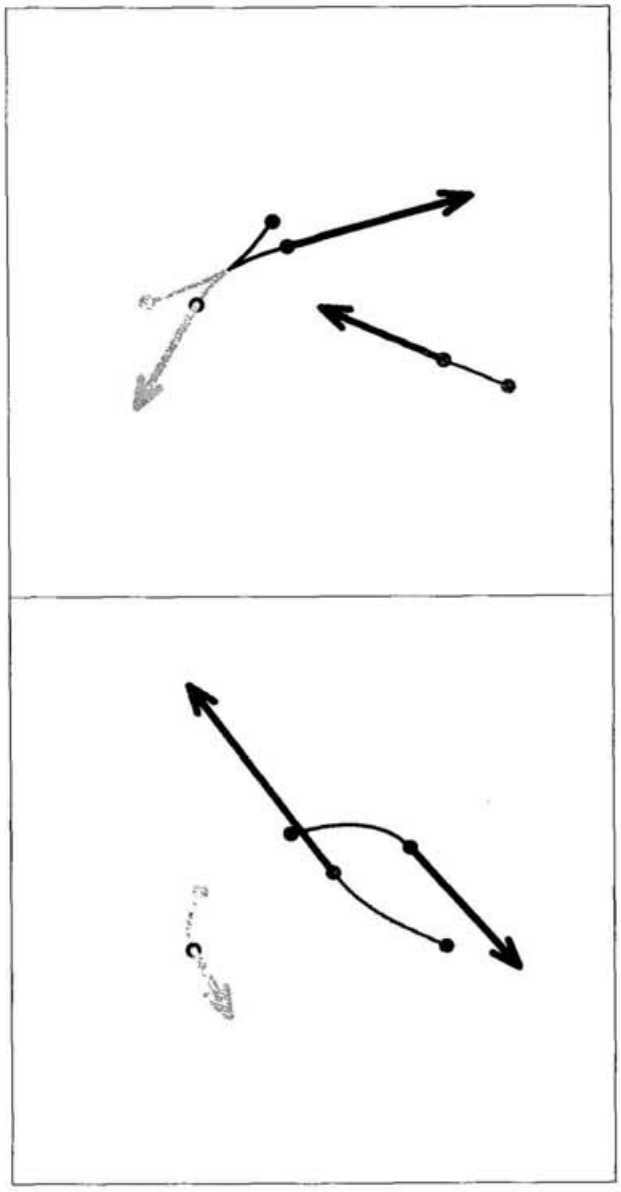

Figure 3.27: (a) The slingshot-escape orbit starting on the binary-collision curve of type 3. At the present initial point, the system results in escape after the first triple encounter.

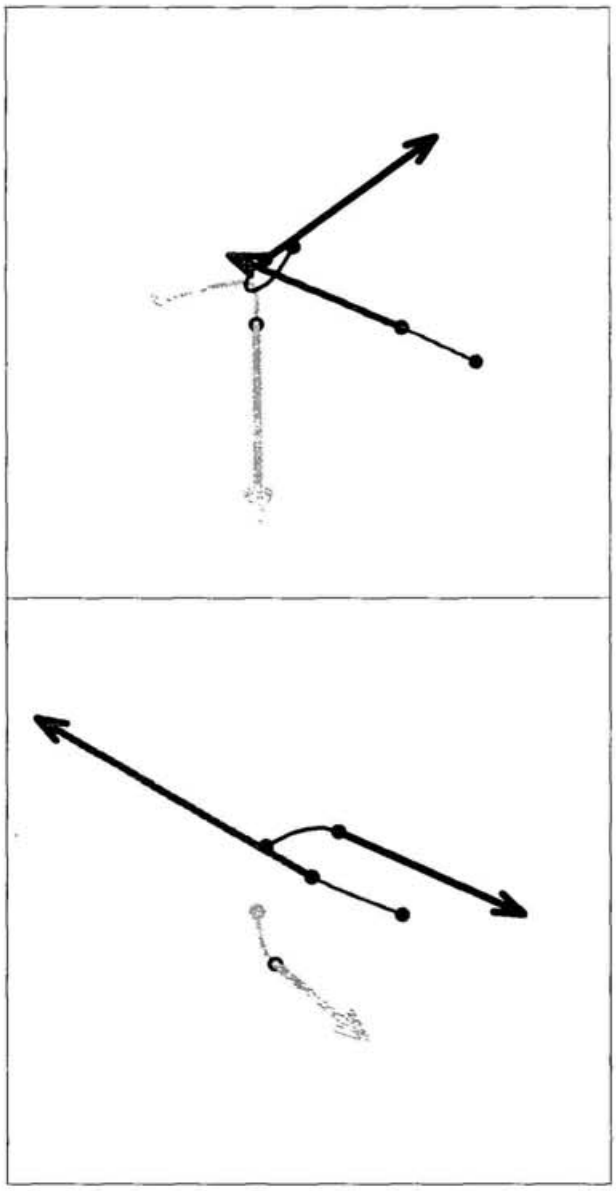

Figure 3.27: (b) The slingshot orbits near the binary collision of type 3. It is the result of perturbation in the right direction from the binary-collision orbit. The particle m_3 escapes.

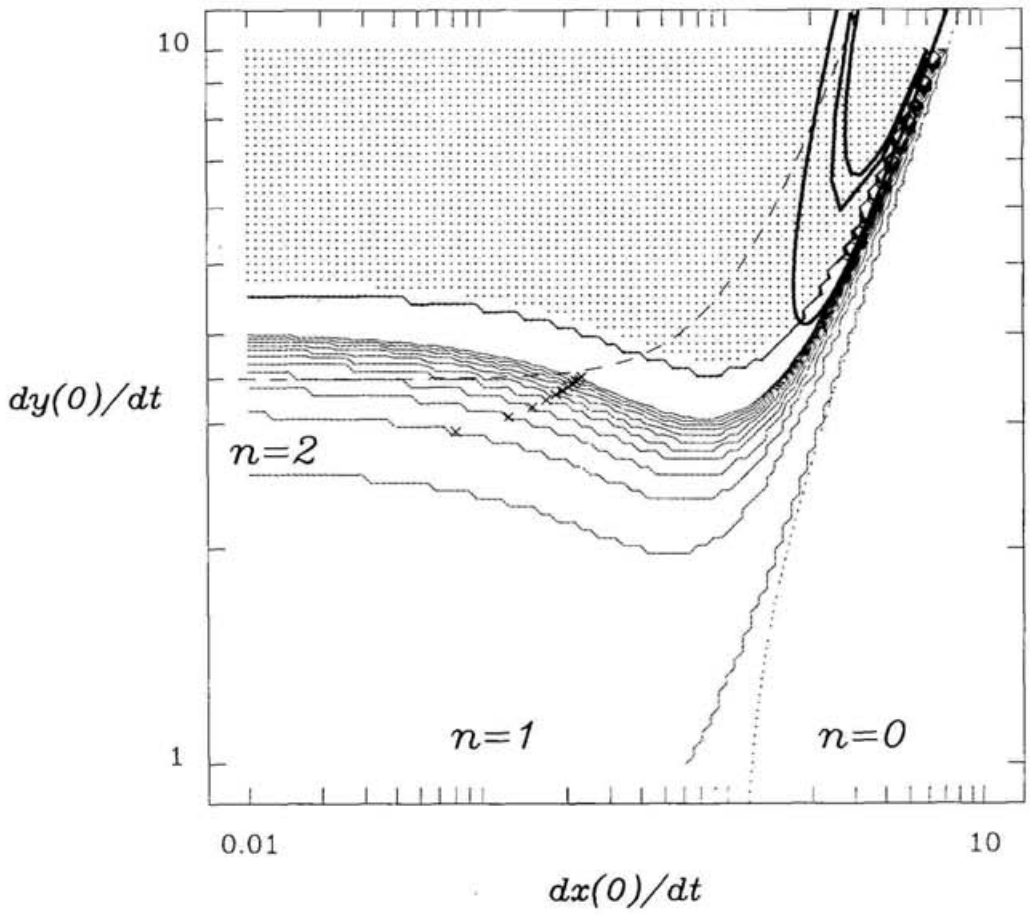

Figure 3.28: (a) The slingshot condition in the planar isosceles system. The dotted region shows the initial values of the syzygy crossing leading to escape without returning.

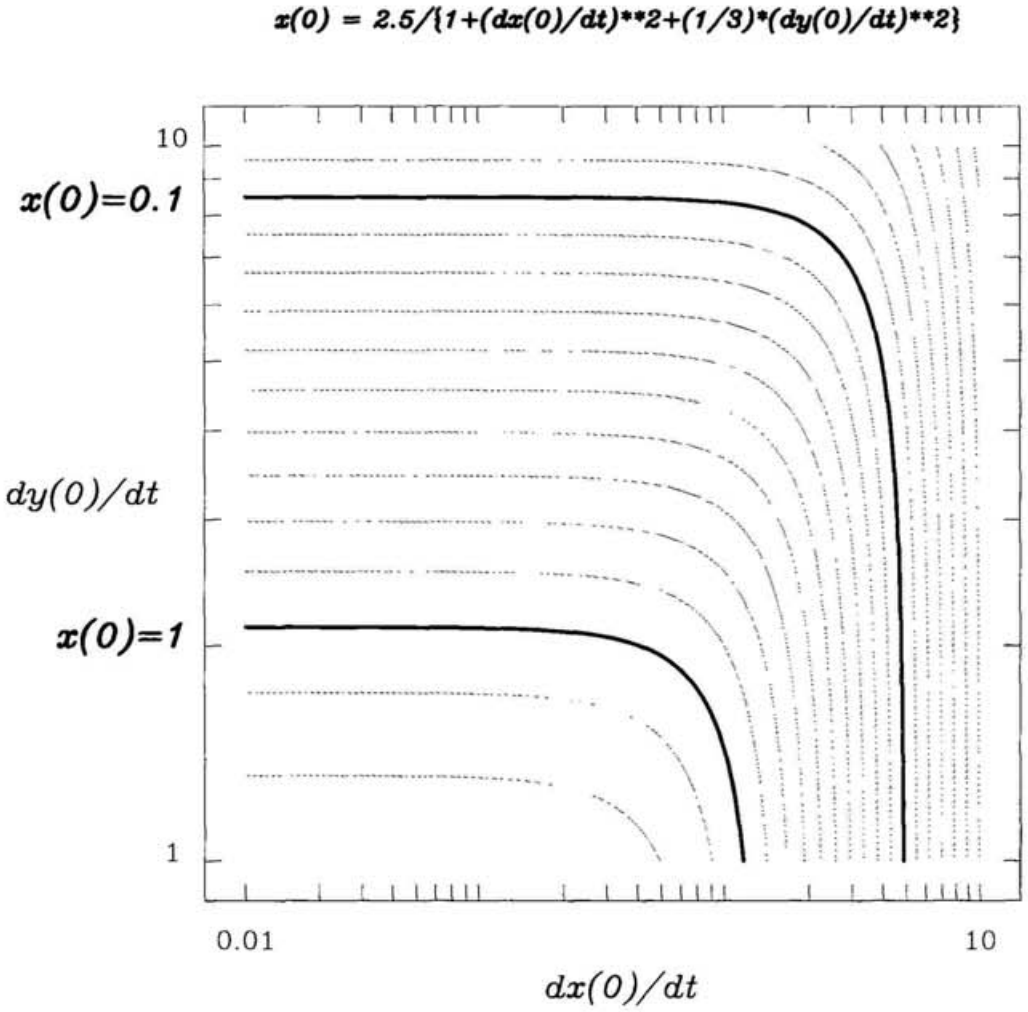

Figure 3.28: (b) The initial value of x in the system with the total energy being -1.

Chapter 4

Analytical and geometrical results

4.1 Introduction

Collision singularities are crucial to the evolution of the three-body systems. In particular, the singularity of triple collision is considered as the origin of chaos in the theory of the three-body problem. In the collinear three-body problem, McGehee (1974) developed a method which blows up the triple-collision singularity to the two-dimensional invariant manifold, known as the triple-collision manifold, in the three-dimensional phase space. There are equilibrium points on the invariant manifold, and the sets of triple collision and triple-expansion orbits are interpreted as the stable and unstable manifolds of the equilibrium points, respectively.

In 1980s, the analysis of triple collision has been progressed in the isosceles problem by McGehee's blow-up method (Devaney, 1980; Simó, 1980; Simó and Martínez, 1988). One of their remarkable results in the collinear and the isosceles problems is that one particle may get an arbitrarily large velocity as an orbit approaches triple-collision singularity. This suggests a close relation between triple collision and escape.

Investigations of the planar problem by the blow-up method also started in 1980s (Waldvogel, 1982; Moeckel, 1983; Simó and Susín, 1989; Susín and Simó, 1991). Waldvogel (1982) introduced another type of blow-up variables in the planar problem. Moeckel (1983) investigated the existence of the connection of the stable and unstable manifolds among various equilibrium points, and made a list of possible motions passing near triple collision. There are escape phenomena for the respective three particles after the close triple encounter in the list.

In the above theoretical works, however. it is not well-known how escape orbits distribute around a triple-collision orbit in the planar problem. It is also uncertain whether

non-escape orbits exist in an arbitrary neighborhood of a triple-collision orbit. Numerical works show the initial-value distribution of escape orbits in the free-fall three-body problem which is the special planar case with zero initial velocities (Agekyan and Anosova, 1968; Anosova and Zavalov, 1989; Tanikawa et al., 1995; Umehara et al., 1995; Zare and Szebehely, 1995; Broucke, 1995; Umehara and Tanikawa, 1996). Tanikawa et al. (1995) found many triple-collision orbits of Lagrange type in the free-fall system with equal masses. Umehara et al. (1995), and Umehara and Tanikawa (1996) numerically showed that escape orbits and non-escape orbits are distributed around triple-collision orbits. However, one can not see the orbital distribution *arbitrarily* close to the triple-collision orbit from numerical works since the precision in numerical integration is limited.

The purpose of the present chapter is to clarify the orbital distribution in an *arbitrary* small neighborhood of triple-collision orbits in the planar problem with equal masses. In Section 4.2 and 4.3, we consider distributions of orbits around the triple-collision points T_1 and T_2, respectively. Around T_1, taking the previous numerical results into account, we will analytically verify such distribution beyond the limit of numerical integrations. Around T_2, the similar distribution as around T_1 is shown with the aid of numerical results investigated by the blow-up variables.

Before detailed proofs, in Subsection 4.2.1, we summarize the procedure to verify the existence of both escape and non-escape orbits in an arbitrary neighborhood of $T_1(0, \sqrt{3}/2)$, i.e., the homothetic equilateral collision orbit. Here, we assume two lemmas which will be proved in the subsequent subsections.

There are three planar-isosceles subsystems in a neighborhood of the homothetic equilateral solution. The distribution of escape orbits in the free-fall three-body problem is determined from the disposition of the three isosceles subspaces in the phase space and orbital behavior in the planar-isosceles subsystem. These results imply that non-escape orbits also exist in an arbitrary neighborhood of the triple-collision orbit. It turns out that the isosceles subsystem has an important role on escape phenomena as the triple collision has.

In Subsection 4.2.2, we first prove one lemma, i.e., the isolation of the homothetic equilateral triple-collision orbit from other triple-collision orbits in the free-fall three-body problem with equal masses. We will prove that no other triple-collision orbit exists in a sufficiently small neighborhood of the homothetic equilateral orbit in this case as far as the triple collision at the first triple encounter concerns.

In Subsection 4.2.3, we analyze the case of the planar-isosceles problem. Here, we prove the other lemma, i.e., an orbit passing sufficiently close to triple-collision singularity results in escape. If a particle experiencing syzygy crossing gets high kinetic energy by passing close to triple-collision singularity, the other two particles also obtain kinetic energy. Thus it is not apparent that the syzygy-crossing particle always leads to escape. We will adapt the derivation of the escape criterion of Yoshida (1972) to the planar-isosceles case and translate it to the words of blow-up variables.

In Section 4.3, we investigate numerically the behavior another triple-collision orbit starting at T_2 with the aid of the blow-up analysis. The numerical work by Tanikawa and Umehara (1998) shows various triple-collision orbits in the free-fall three-body problem. If orbits are restricted to the free-fall case, there are not all three kinds of isosceles orbits around the individual orbits ending in triple collision except the homothetic equilateral orbit. According to numerical results by Umehara et al.(1995) showing the similarity of orbital distributions around triple-collision orbits, binary-collision orbits instead of isosceles orbits dominate escape orbits. Escape orbits seem to be distributed around a one-parameter family of binary-collision orbits. The proofs of orbital distributions around other triple-collision orbits may be based on the lemmas in the present paper. These proofs will be given in a future paper.

4.2 motions arbitrarily close to triple collision

4.2.1 Geometric analysis of orbital distributions

In the present section, our attention is concentrated to the initial-value dependence of solutions in a neighborhood of the initial value $T_1(0, \sqrt{3}/2)$ corresponding to the equilateral configuration. Hereafter, this homothetic equilateral triple-collision point T_1 will be called a *homothetic equilateral point.*

Theorem 4.1. *Arbitrarily close to $T_1(0, \sqrt{3}/2)$, at least six first-hyperbolic regions exist and the six first-hyperbolic regions are located around the respective isosceles curves on the initial-value space $\grave{D}$ of the free-fall three-body problem with equal masses. The non-escape points after the triple encounter also exist arbitrarily close to T_1.*

Recall that the initial-value space $\grave{D}$ and the isosceles curve are defined in Subsection

1.3.1, and that the first-hyperbolic region and the first-non-escape point are defined in Subsection 2.3.1.

The triple encounter is defined by Triple-encounter criterion in Subsection 2.2. The formulation of this definition is complicated since it is improved to be applied even in the case of triple encounter with wide configuration. However, in the present section we will consider only orbits close to triple collision, and so another definition reviewed in Subsection 2.2 is suitable for these orbits. One of blow-up variables is related with the moment of inertia as we will introduce them later. Thus it is favorable for the blow-up analysis that the triple-encounter criterion is defined using the moment of inertia. Therefore, we adopt Definition 2.3 developed by J.Yoshida, 1997. See also the following.

Triple-encounter criterion (J.Yoshida, 1997) *The near-triple-collision orbit with negative energy is called to be in triple encounter if* $I < I_0$, *where*

$$I_0 = \frac{M_*^3}{4Mh^2}, \tag{4.1}$$

and $M = m_1 + m_2 + m_3$ *and* $M_* = m_1m_2 + m_2m_3 + m_3m_1$. *When* $I(t)$ *is equal to* I_0 *with increasing, the system is called to survive the triple encounter.*

The following two lemmas are necessary in order to verify the above theorem.

Lemma 4.1 *There is no initial point ending in triple collision during the first triple encounter in a sufficiently small neighborhood of* T_1 *on the initial-value space* $\grave{D}$ *except* T_1.

Lemma 4.2 *On the isosceles curves of the initial-value space, all initial points in a sufficiently small neighborhood of* T_1 *except* T_1 *are the first hyperbolic-elliption points.*

In the final part of the present subsection, we will prove Theorem 4.1 assuming the above two lemmas. The statement of the first half of Theorem 4.1 is that

> at least six first-hyperbolic regions exist in an arbitrarily close to T_1 and the six first-hyperbolic regions are located around the respective isosceles curves.

Proof of the first half of Theorem 4.1. By the continuous dependence of solutions on the initial values except at triple-collision points, there is a hyperbolic region around

a hyperbolic point. From Lemma 4.2, there are hyperbolic points not only on the six isosceles curves but also around the curves in a sufficiently small neighborhood of T_1 except T_1, and so these hyperbolic points compose open regions on the initial-value space. □

The second half of Theorem 4.1 is proved as the following. The statement is that

> there is also a non-escape point after the first triple encounter in an arbitrarily close to T_1.

Proof of the second half of Theorem 4.1. Suppose the contrary. From Lemma 4.1, there is no triple-collision point during the first triple encounter in this neighborhood of T_1 except T_1. Thus, all initial points in a sufficiently small neighborhood of T_1 except T_1 are hyperbolic or parabolic points after the first triple encounter. According to Lemma 4.2, however, three kinds of escape points exist where the escaping particles are m_1, m_2, and m_3, respectively, in a sufficiently small neighborhood of T_1. Therefore, there is a common point of the first escape points for m_j and m_k, $j \neq k$, even if the closure of the escape region for m_j contacts with the region for m_k. At the common point, both m_j and m_k leads to parabolic or hyperbolic scape after the first triple encounter. This contradicts the fact that the number of escaping particle is at most one in the system with negative energy. Hence, a non-escape point after the first triple encounter exists arbitrarily close to T_1. □

The above proof shows the existence of at least six escape regions. We can not prove that each escape region form a wedge at the triple-collision point T_1 as the numerical result shows in Fig.2.12(a). We can not also assert the non-existence of escape regions other than the six considered in the above. If such a region exists, a region consisting of non-escape points does not form a wedge. According to the numerical result, however, each non-escape region seems to form a wedge at T_1.

Theorem 4.1 implies a remarkable distribution of orbits close to the homothetic equilateral triple-collision singularity.

Corollary 4.2. *In any small neighborhood of the triple-collision orbit corresponding to the homothetic equilateral solution, all types of orbits exist such that the system leads to hyperbolic-elliptic escape, parabolic-elliptic escape, and non-escape, respectively, after the first triple encounter.*

In Sections 4.2.2 and 4.2.3, we will prove Lemma 4.1 and Lemma 4.2, respectively.

4.2.2 Initial-value distribution ending in triple collision

Outline of the proof

In the present section, we will prove Lemma 4.1 using the blow-up variables developed by Waldvogel (1982). There are equilibrium points corresponding to triple collision in the blow-up phase space, and a set of triple collision orbits is transformed into a stable manifold of an equilibrium point. Thus an intersection of the stable manifold and the initial-value space with zero-initial velocities is a set of initial values leading to triple collision in the free-fall three-body problem.

The phase space of the planar three-body problem with a given energy is a five-dimensional manifold. The equilibrium point corresponding to triple collision of the equilateral-triangle type has a three-dimensional stable manifold. The initial-value space with zero-initial velocities is a two-dimensional manifold. Therefore, the intersection is a zero-dimensional manifold, i.e., points, if the stable manifold and the initial-value space are transversal. However, it is difficult to prove the transversality. It is also hard to distinguish whether initial values leading to triple collision are isolated points or not. The results of Tanikawa and Umehara (1998) investigating the initial-value instability until the third triple encounter suggest a fractal distribution of initial values leading to triple collision in the initial-value space.

Nevertheless, if we restrict ourselves to the behavior of orbits up to and including the first triple encounter, we can prove the isolation of the initial values leading to triple collision. In order to avoid the difficulty of proving transversality, we will consider the position of a phase point released with zero-initial velocities with respect to the stable manifold of the equilibrium point when the phase point approaches the equilibrium point. Further, we only consider the case of the homothetic equilateral solution.

First, we introduce blow-up variables, and derive tools necessary for the proof: a tangent space of an equilibrium point corresponding to triple collision, the homothetic equilateral solution, and the variation of the homothetic equilateral solution. After that, a necessary condition for a solution approaching the equilibrium point to be included in the local stable manifold of the equilibrium point is established in Lemma 4.3.

Second, we will set up two lemmas. In Lemma 4.4, we will prove that any solution curve starting sufficiently close to the initial point of the homothetic equilateral solution

on the initial-value space is not included in the local stable manifold of the equilibrium point when the solution curve passes close to the equilibrium point for the first time. In Lemma 4.5, we will show that if such a near-homothetic-equilateral solution is included in a global stable manifold of a certain equilibrium point, it ends in triple collision after surviving the first triple encounter. From this result, it is easy to prove Lemma 4.1.

blow-up variables by Waldvogel

Let us introduce blow-up variables in the planar three-body problem. In the present paper, we consider only the case of zero angular momentum. Let $q_j \in \mathbf{C}$, $j = 1,2,3$ be the complex Cartesian coordinates of the mass m_j in the center-of-mass system. The canonically conjugate momenta are $p_j = m_j \cdot dq_j/dt \in \mathbf{C}$ where t is the time. Let $a_j \in [0,\infty)$ and $\phi_j \in [0,2\pi]$, $j = 1,2,3$ be defined as follows:

$$q_l - q_k = a_j e^{i\phi_j}, \tag{4.2}$$

where (j,k,l) is $(1,2,3)$ or its cyclic permutation. Let $b_j \in \mathbf{R}$, $j = 1,2,3$ be defined as

$$p_j = b_k e^{i\phi_k} - b_l e^{i\phi_l}. \tag{4.3}$$

Note that a_j is the mutual distance between particles m_k and m_l. We consider the equal-mass case: $m_j = 1$, $j = 1,2,3$. According to van Kampen and Wintner (1937), the Hamiltonian of the system with zero angular momentum is written by a_j and b_j as

$$\mathcal{H} = \frac{1}{2}\sum_{jkl}\left(b_k^2 + b_l^2 + b_k b_l \frac{a_k^2 + a_l^2 - a_j^2}{a_k a_l}\right) - \sum_{j=1}^{3}\frac{1}{a_j}. \tag{4.4}$$

The equations of motion are

$$\frac{da_j}{dt} = \frac{\partial \mathcal{H}}{\partial b_j}, \quad \frac{db_j}{dt} = -\frac{\partial \mathcal{H}}{\partial a_j}, \qquad j = 1,2,3. \tag{4.5}$$

The system is of three degrees of freedom and admits the energy integral

$$\mathcal{H} = h = \text{const.} \tag{4.6}$$

There are two kinds of singularities in the phase space: $a_j = 0$ for each of $j = 1,2,3$ corresponding to binary collisions, and $a_1 = a_2 = a_3 = 0$ corresponding to triple collision.

Let us introduce blow-up variables $\tilde{\alpha}_j$ which also regularize the binary collision singularity. These are related to the mutual distances a_j as follows:

$$\tilde{a}_j = \tilde{\alpha}_k^2 + \tilde{\alpha}_l^2. \tag{4.7}$$

with

$$a_j = r\tilde{a}_j, \tag{4.8}$$

where r is defined by the square root of the moment of inertia:

$$r = \sqrt{\frac{1}{3}\sum_{j=1}^{3} a_j^2}. \tag{4.9}$$

The variables $\tilde{\beta}_j$ are introduced by

$$\tilde{\beta}_j = 2r^{\frac{1}{2}}\tilde{\alpha}_j(b_k + b_l). \tag{4.10}$$

Scaling the time by

$$\frac{dt}{d\tau} = r^{\frac{3}{2}}\tilde{a}_1\tilde{a}_2\tilde{a}_3, \tag{4.11}$$

we get the following seven equations from eqs.(4.5):

$$\begin{aligned}
\frac{dr}{d\tau} &= \frac{r}{2}\tilde{a}_1\tilde{a}_2\tilde{a}_3\tilde{v}, \\
\frac{d\tilde{\alpha}_j}{d\tau} &= \frac{1}{4}\{2(\tilde{a}_j^2 + \tilde{a}_j\tilde{\alpha}_j^2 - \tilde{\alpha}_k^2\tilde{\alpha}_l^2)\tilde{\beta}_j - \tilde{a}_l\tilde{\alpha}_j\tilde{\alpha}_k\tilde{\beta}_k - \tilde{a}_k\tilde{\alpha}_j\tilde{\alpha}_l\tilde{\beta}_l - \tilde{a}_1\tilde{a}_2\tilde{a}_3\tilde{v}\tilde{\alpha}_j\}. \\
\frac{d\tilde{\beta}_j}{d\tau} &= -\frac{1}{2}\{\tilde{a}_j\tilde{\alpha}_j\tilde{\beta}_j^2 + \tilde{\alpha}_j(2\tilde{\alpha}_j^2 + \tilde{a}_j)(\tilde{\beta}_k^2 + \tilde{\beta}_l^2)\} + \frac{\tilde{\beta}_j}{4}\{(2\tilde{\alpha}_j^2 + \tilde{a}_l)\tilde{\alpha}_k\tilde{\beta}_k + (2\tilde{\alpha}_j^2 + \tilde{a}_k)\tilde{\alpha}_l\tilde{\beta}_l\} \\
&+ 2\tilde{\alpha}_j(2\tilde{a}_j + \tilde{a}_k + \tilde{a}_l) + 2hr\tilde{\alpha}_j\tilde{a}_j(\tilde{a}_k + \tilde{a}_l),
\end{aligned} \tag{4.12}$$

for $j = 1, 2, 3$, where

$$\tilde{v} = \sum_{j}^{3} \tilde{\alpha}_j\tilde{\beta}_j. \tag{4.13}$$

They admit the following invariant relations:

$$\frac{1}{8}\sum_{jkl}\tilde{a}_j[(\tilde{\alpha}_1^2 + \tilde{\alpha}_2^2 + \tilde{\alpha}_3^2)\tilde{\beta}_j^2 + (\tilde{\alpha}_k\tilde{\beta}_l - \tilde{\alpha}_l\tilde{\beta}_k)^2] - \sum_{jkl}\tilde{a}_k\tilde{a}_l \;-\; hr\tilde{a}_1\tilde{a}_2\tilde{a}_3 = 0, \tag{4.14}$$

and

$$\sum_{j}^{3}\tilde{a}_j^2 = 3. \tag{4.15}$$

These invariant relations correspond to the energy conservation and scale normalization, respectively.

Let $\tilde{M}(h)$ and $\tilde{M}_0$ denote a blow-up phase space with a given energy h and its subset satisfying $r = 0$, respectively. Both subsets constitute invariant submanifolds for the

vectorfield (4.12). These have dimensions five and four, respectively. The orbits in $\tilde{M}_0$ have no direct physical meaning. Their behavior, however, reflects the behavior of orbits in $\tilde{M}(h) \setminus \tilde{M}_0$ while these are close to triple collision.

The initial-value space in the blow-up coordinate system will be considered instead of the initial-value space $\grave{D}$ defined in the preceding section. In the free-fall problem, initial values of b_j are equal to zero for $j = 1, 2, 3$, and so $\tilde{\beta}_j(0) = 0$. The initial-value space with zero-initial velocities in $\tilde{M}(h)$ can be defined as $(\tilde{\alpha}_1, \tilde{\alpha}_2, \tilde{\alpha}_3)$ where eq.(4.15) holds. Therefore, any of the two-dimensional surfaces $(\tilde{\alpha}_i, \tilde{\alpha}_j)$, $1 \leq i < j \leq 3$ can be used as an initial value space. Let us denote them by S_{ij}.

Let H_0 be the initial point on S_{12} corresponding to $T_1(0, \sqrt{3}/2)$ on $\grave{D}$. Surfaces S_{12} around H_0 and $\grave{D}$ around T_1 are topologically equivalent. Indeed the Jacobian determinant of the transformation $(x, y) \mapsto (\tilde{\alpha}_1, \tilde{\alpha}_2)$ is $-y\tilde{a}_1(\tilde{a}_1 + \tilde{a}_2)/(24r^4\tilde{\alpha}_1\tilde{\alpha}_2\tilde{a}_2\tilde{a}_3)$ and the variables $y, \tilde{a}_j, \tilde{\alpha}_1$ and $\tilde{\alpha}_2$ are positive around H_0, and so the Jacobian determinant keeps negative. This property holds in the other S_{ij}.

The homothetic equilateral solution

Let us describe the homothetic equilateral solution which starts at the initial point H_0 with zero-initial velocities. The configuration of this solution maintains equilateral triangle, and so the equalities $\tilde{\alpha}_1(\tau) = \tilde{\alpha}_2(\tau) = \tilde{\alpha}_3(\tau) = \tilde{\alpha}(\tau)$ and $\tilde{\beta}_1(\tau) = \tilde{\beta}_2(\tau) = \tilde{\beta}_3(\tau) = \tilde{\beta}(\tau)$ always hold with appropriate functions $\tilde{\alpha}(\tau)$ and $\tilde{\beta}(\tau)$. Thus the solution has the form

$$\boldsymbol{\psi}_{\text{homo}}(\tau) = (r(\tau), \tilde{\alpha}(\tau)\mathbf{e}, \tilde{\beta}(\tau)\mathbf{e})^T, \tag{4.16}$$

where $\mathbf{e} = (1, 1, 1)$, and $\tilde{\alpha}(\tau)$, $\tilde{\beta}(\tau)$ and $r(\tau)$ are described explicitly as

$$\tilde{\alpha}(\tau) = \frac{1}{\sqrt{2}},$$

$$\tilde{\beta}(\tau) = \frac{4}{\sqrt{3}} \cdot \frac{1 - \exp(\sqrt{6}\tau)}{1 + \exp(\sqrt{6}\tau)}, \tag{4.17}$$

$$r(\tau) = 1 - \frac{3}{16}\tilde{\beta}^2(\tau) = \frac{4\exp(\sqrt{6}\tau)}{\{1 + \exp(\sqrt{6}\tau)\}^2}.$$

The fact that $\tilde{\alpha}(\tau)$ is constant is obtained from the invariance (4.15). The variable $\tilde{\beta}(\tau)$ is obtained from the following differential equation:

$$\frac{d\tilde{\beta}}{d\tau} = -\frac{3}{4}\sqrt{2}\left(\tilde{\beta}^2 - \frac{16}{3}\right) + 2\sqrt{2}rh = \frac{3}{8}\sqrt{2}\left(\tilde{\beta}^2 - \frac{16}{3}\right). \tag{4.18}$$

This equation is derived using the third equation of the system (4.12). The latter equality is derived from the energy integral (4.14). Note that $h = -3$ in this case.

Next let us derive the variational equations along $\boldsymbol{\psi}_{\text{homo}}$. We introduce a variation $\delta\boldsymbol{\psi}_{\text{homo}}$ in the tangent space to $\mathbf{R}^7$. Let a 3×3 matrix $J[x, y]$ be

$$\begin{bmatrix} x & y & y \\ y & x & y \\ y & y & x \end{bmatrix}. \tag{4.19}$$

Then

$$\frac{d}{d\tau}\begin{bmatrix} \delta r(\tau) \\ \delta\tilde{\boldsymbol{\alpha}}(\tau) \\ \delta\tilde{\boldsymbol{\beta}}(\tau) \end{bmatrix} = \begin{bmatrix} \frac{3}{2\sqrt{2}}\tilde{\beta}(\tau) & \frac{7}{2}\left(1 - \frac{3}{16}\tilde{\beta}^2(\tau)\right)\mathbf{e} & \frac{1}{2\sqrt{2}}\left(1 - \frac{3}{16}\tilde{\beta}^2(\tau)\right)\mathbf{e} \\ \mathbf{o}^T & J_{\tilde{\alpha},\tilde{\alpha}} & J_{\tilde{\alpha},\tilde{\beta}} \\ -6\sqrt{2}\mathbf{e}^T & J_{\tilde{\beta},\tilde{\alpha}} & J_{\tilde{\beta},\tilde{\beta}} \end{bmatrix}\begin{bmatrix} \delta r(\tau) \\ \delta\tilde{\boldsymbol{\alpha}}(\tau) \\ \delta\tilde{\boldsymbol{\beta}}(\tau) \end{bmatrix} \tag{4.20}$$

where $\mathbf{o} = (0, 0, 0)$,

$$\tilde{\boldsymbol{\alpha}} = (\tilde{\alpha}_1, \tilde{\alpha}_2, \tilde{\alpha}_3)^T, \qquad \tilde{\boldsymbol{\beta}} = (\tilde{\beta}_1, \tilde{\beta}_2, \tilde{\beta}_3)^T, \tag{4.21}$$

and

$$\begin{aligned} J_{\tilde{\alpha},\tilde{\alpha}} &= J\left[-\tfrac{5}{2\sqrt{2}}\tilde{\beta}(\tau),\ -\tfrac{1}{4\sqrt{2}}\tilde{\beta}(\tau)\right], & J_{\tilde{\alpha},\tilde{\beta}} &= J\left[\tfrac{1}{2},\ -\tfrac{1}{4}\right], \\ J_{\tilde{\beta},\tilde{\alpha}} &= J\left[\tfrac{3}{2}\tilde{\beta}^2(\tau) - 12,\ \tfrac{21}{8}\tilde{\beta}^2(\tau) - 12\right], & J_{\tilde{\beta},\tilde{\beta}} &= J\left[0,\ -\tfrac{3}{2\sqrt{2}}\tilde{\beta}(\tau)\right]. \end{aligned} \tag{4.22}$$

The conditions so that the variations belong to $\tilde{M}(h)$ are

$$\sum_j^3 \delta\tilde{\alpha}_j(\tau) = 0, \qquad \delta r(\tau) = -\frac{1}{8}\tilde{\beta}(\tau)\sum_j^3 \delta\tilde{\beta}_j(\tau). \tag{4.23}$$

Local stable manifold of Lagrangian equilibrium point

In the blow-up phase space, a solution ending in triple collision approaches asymptotically an equilibrium point. We will derive a position of the equilibrium point and vectors spanning the stable manifold of the equilibrium point. Let E_h be the equilibrium point which $\boldsymbol{\psi}_{\text{homo}}(\tau)$ tends to approach as $\tau \to \infty$. The local stable manifold of E_h in an ε-neighborhood of E_h is denoted by $W^s_{\text{loc}}(E_h)$ where ε is a small positive number. Similarly, $W^u_{\text{loc}}(E_h)$ denotes the local unstable manifold of E_h. The tangent space to a manifold M at a point P is denoted by $T_P M$.

The position of E_h in the phase space is

$$(r^{\text{eq}}, \tilde{\boldsymbol{\alpha}}^{\text{eq}}, \tilde{\boldsymbol{\beta}}^{\text{eq}})^T = \{(r, \tilde{\alpha}\mathbf{e}, \tilde{\beta}\mathbf{e})^T | r = 0, \tilde{\alpha} = \frac{1}{\sqrt{2}}, \tilde{\beta} = -\frac{4}{\sqrt{3}}\}, \tag{4.24}$$

since r and $\tilde{\beta}$ tend 0 and $-4/\sqrt{3}$, respectively, as $\tau \to \infty$. Therefore, variational equations at E_h are obtained by substituting $\tilde{\beta} = -4/\sqrt{3}$ in eq.(4.20).

We obtain $T_{E_h} W^s_{\rm loc}(E_h)$ as the following three-dimensional subspace:

$$\begin{bmatrix} \delta r^{\rm eq} \\ \delta\tilde{\alpha}_1^{\rm eq} \\ \delta\tilde{\alpha}_2^{\rm eq} \\ \delta\tilde{\alpha}_3^{\rm eq} \\ \delta\tilde{\beta}_1^{\rm eq} \\ \delta\tilde{\beta}_2^{\rm eq} \\ \delta\tilde{\beta}_3^{\rm eq} \end{bmatrix} = \zeta_1 \begin{bmatrix} 1 \\ 0 \\ 0 \\ 0 \\ \frac{2}{\sqrt{3}} \\ \frac{2}{\sqrt{3}} \\ \frac{2}{\sqrt{3}} \end{bmatrix} + \zeta_2 \begin{bmatrix} 0 \\ 1 \\ 0 \\ -1 \\ \kappa_- \\ 0 \\ -\kappa_- \end{bmatrix} + \zeta_3 \begin{bmatrix} 0 \\ 0 \\ 1 \\ -1 \\ 0 \\ \kappa_- \\ -\kappa_- \end{bmatrix}, \tag{4.25}$$

for any real numbers ζ_1, ζ_2 and ζ_3, where

$$\kappa_- = -\frac{\sqrt{6}(5+\sqrt{13})}{3}. \tag{4.26}$$

See Appendix for the derivation. From the above expression, we can derive the following lemma.

Lemma 4.3. *If a variation at E_h is included in $T_{E_h} W^s_{\rm loc}(E_h)$, then*

$$\delta\tilde{\beta}_i^{\rm eq} - \delta\tilde{\beta}_j^{\rm eq} = \kappa_- \left(\delta\tilde{\alpha}_i^{\rm eq} - \delta\tilde{\alpha}_j^{\rm eq}\right), \tag{4.27}$$

where $(i,j) = (1,2), (2,3)$ and $(3,1)$.

Variation with zero initial velocities

In order to prove Lemma 4.4 that follows, we transform the variational equations (4.20) and examine the behavior of solutions. Although this system is five dimensional, we can independently solve the two-dimensional subsystem $(q(\tau), p(\tau))$ definded by

$$q(\tau) = \delta\tilde{\alpha}_1(\tau) - \delta\tilde{\alpha}_2(\tau), \quad p(\tau) = \delta\tilde{\beta}_1(\tau) - \delta\tilde{\beta}_2(\tau). \tag{4.28}$$

From eq.(4.20) we obtain

$$\begin{aligned} q'(\tau) &= -\tfrac{9}{4\sqrt{2}}\tilde{\beta}(\tau)q(\tau) + \tfrac{3}{4}p(\tau) \\ p'(\tau) &= -\tfrac{9}{8}\tilde{\beta}^2(\tau)q(\tau) + \tfrac{3}{2\sqrt{2}}\tilde{\beta}(\tau)p(\tau), \end{aligned} \tag{4.29}$$

and so

$$\begin{aligned} z' &= -\tfrac{3}{4}z^2 + \tfrac{15}{4\sqrt{2}}\tilde{\beta}(\tau)z - \tfrac{9}{8}\tilde{\beta}^2(\tau) \\ \rho' &= \left\{\tfrac{3\sqrt{2}}{4}\tilde{\beta}(\tau)z^2 + \left(\tfrac{3}{4} - \tfrac{9}{8}\tilde{\beta}^2(\tau)\right)z - \tfrac{9}{4\sqrt{2}}\tilde{\beta}(\tau)\right\}\rho\cos^2(\arctan z), \end{aligned} \tag{4.30}$$

where a prime (′) means differentiation with respect to τ, and

$$\rho = \sqrt{q^2+p^2}, \tag{4.31}$$

$$z = \frac{p}{q} \quad (\text{if } \rho \neq 0). \tag{4.32}$$

Let $\varphi(\tau)$ be a solution $z(\tau)$ with the initial value $z(0)=0$ corresponding to zero velocities in the first equation of the system (4.30). We assume $\rho(0) > 0$. The origin is the fixed point showing isosceles motion including the homothetic equilateral solution. Thus $\rho(\tau) \neq 0$ for $\tau > 0$, and so $\varphi(\tau)$ is well-defined.

We will investigate the behavior of $\varphi(\tau)$. On the (τ, z)-plane, there are two boundaries satisfying $z'(\tau)=0$ represented as

$$z = \left\{ \zeta_\pm(\tau) \middle| \ \zeta_\pm = \frac{5 \pm \sqrt{13}}{2\sqrt{2}} \tilde{\beta}(\tau) \right\}. \tag{4.33}$$

Note that $\zeta_+(\tau) \leq \zeta_-(\tau) \leq 0$. The equality holds if and only if $\tau = 0$. We have $z' > 0$ if $\zeta_+(\tau) < z(\tau) < \zeta_-(\tau)$, and $z' < 0$ if $z(\tau) < \zeta_+(\tau)$ or $z(\tau) > \zeta_-(\tau)$. The solution $\varphi(\tau)$ stays in the region $\{z | z \geq \zeta_-\}$. Indeed $\varphi(\Delta) > \zeta_-(\Delta)$ for a sufficiently small $\Delta > 0$, and if there is a $\tau > \Delta$ such that $\varphi(\tau)$ reaches the boundary $z = \zeta_-(\tau)$, then $\varphi'(\tau)$ becomes 0. Since the boundary $z = \zeta_-(\tau)$ is monotone decreasing with respect to τ, $\varphi(\tau)$ returns to the region $\{z(\tau) | z > \zeta_-(\tau)\}$. As a result, the relations $\varphi(\tau) \geq \zeta_-(\tau)$ and $\varphi'(\tau) \leq 0$ hold for $\tau \geq 0$. Hence, for $\tau_0 \in [0, \infty)$

$$\varphi(\tau_0) > \lim_{\tau \to \infty} \varphi(\tau) = \kappa_- + \frac{2\sqrt{78}}{3}. \tag{4.34}$$

With respect to τ, $\rho(\tau)$ along $\varphi(\tau)$ is monotone increasing. For, the second equation of (4.30) shows that on the (τ, z)-plane there are two boundaries satisfying $\rho'(\tau) = 0$ represented as

$$z = \left\{ \varpi_\pm(\tau) \middle| \ \varpi_\pm = \frac{3\tilde{\beta}^2(\tau) - 2 \pm \sqrt{9\tilde{\beta}^4(\tau) + 36\tilde{\beta}^2(\tau) + 4}}{4\sqrt{2}\tilde{\beta}(\tau)} \right\}. \tag{4.35}$$

We have $\rho' > 0$ for any $\tau > 0$ since $\varpi_+(\tau) < \varphi(\tau) < \varpi_-(\tau)$.

In the above, we assumed $\rho(0) > 0$. If $\rho(0) = 0$, we will define $q = \delta\tilde{\alpha}_2 - \delta\tilde{\alpha}_3$ and $p = \delta\tilde{\beta}_2 - \delta\tilde{\beta}_3$ instead of the above. Then we again obtain the relation (4.34) for $\rho(0) \neq 0$, $\delta\tilde{\alpha}_1(0) \neq 0$. It is not necessary to consider the case $\delta\tilde{\alpha}_1(0) = \delta\tilde{\alpha}_2(0) = 0$ since this solution is ψ_{homo} itself.

Finally, let us estimate the direction of $W^s_{\text{loc}}(E_h)$ on the (q,p)-plane at $H(\tau_0)$. From

eq.(4.25), $W^s_{\rm loc}(E_h)$ has dimension three in $\tilde{M}(h)$. According to Devaney (1980) an intersection between $W^s_{\rm loc}(E_h)$ and the isosceles subspace has dimension two. Isosceles orbits are degenerated at the origin on the (q,p)-plane. Therefore, $T_{H(\tau_0)}W^s_{\rm loc}(E_h)$ has at most one-dimensional direction σ on the (q,p)-plane. From Lemma 4.3, a direction of $T_{H(\tau_0)}W^s_{\rm loc}(E_h)$ formally tends $z \to \kappa_-$ as $\tau_0 \to \infty$. Since $W^s_{\rm loc}(E_h)$ is a real analytic manifold, for an any $\chi > 0$ there is a sufficiently small $\varepsilon > 0$ (i.e., a sufficiently large τ_0) such that the direction of $T_{H(\tau_0)}W^s_{\rm loc}(E_h)$ is limited to

$$\kappa_- - \chi < \sigma < \kappa_- + \chi. \tag{4.36}$$

Now we can establish the following lemma. Let $N_d(P)$ denote a d-neighborhood of a point P. Let $\boldsymbol{\psi}(\tau, \boldsymbol{\psi}_0)$ be a solution starting at the initial value $\boldsymbol{\psi}_0 \in \tilde{M}(h)$ in the system (4.20). τ_0 is the time τ when $\boldsymbol{\psi}_{\rm homo}(\tau)$ enters $N_\varepsilon(E_h)$ for the first time.

Lemma 4.4. *No solution $\boldsymbol{\psi}$ starting in a sufficiently small neighborhood of H_0 on the initial-value space S_{12} except H_0 itself belongs to $W^s_{\rm loc}(E_h)$ when $\boldsymbol{\psi}$ enters an ε-neighborhood of E_h for the first time.*

Proof. Suppose the contrary. Then, there is an infinite sequence of points $P_n \in S_{12}$ converging to H_0 such that the direction of $\{\boldsymbol{\psi}(\tau_0, P_n) - \boldsymbol{\psi}_{\rm homo}(\tau_0)\}$ on the (q,p)-plane tends to σ of eq.(4.36) as $n \to \infty$. However, it contradicts eq.(4.34). Hence, there is a $d > 0$ such that $\boldsymbol{\psi}(\tau_0, \{N_d(H_0) \cap S_{12} \setminus H_0\}) \not\subset W^s_{\rm loc}(E_h)$. □

In this stage, the following transversality is shown easily:

Corollary 4.2. *The stable manifold of E_h intersect the initial-value space transversally at T_1.*

In fact, any solution curve crossing the initial-value space is perpendicular to the initial-value space. Lemma 4.4 says that all solutions starting sufficiently close to T_1 except T_1 are not included in the local stable manifold of E_h. The stable manifold and the initial-value space are three- and two-dimensional manifolds, respectively, in the five-dimensional phase space.

Behavior of near-collision solutions after bypassing the equilibrium point

Once $\psi(\tau, \{N_d(H_0) \cap S_{12} \setminus H_0\})$ leaves the equilibrium point E_h, variational equations are invalid. Let E_x be any equilibrium point corresponding to triple collision including E_h. It is possible that the solution enters the stable manifold of E_x eventually. If it happens, there is an initial point leading to triple collision in a sufficiently small neighborhood of the point H_0. In this case, however, we can prove that such a solution survives the first triple encounter.

In order to prove it, it is sufficient to show that the system experience a minimal value of the moment of inertia $I(t)$ at least once even if the system starting near T_1 ends in triple collision. If $I(t)$ becomes minimal, $I(t)$ continues to be concave during $I(t) < I_{\rm enc}$, where $I_{\rm enc}$ is introduced in eq.(2.2). In this time interval, $I(t)$ does not have any other minimal value. From the definition of triple encounter, it implies that the system survives the first triple encounter.

The global stable and unstable manifolds of E_h are defined by

$$W^s(E_h) = \bigcup_{\tau \le 0} \psi(\tau, W^s_{\rm loc}(E_h)), \tag{4.37}$$

$$W^u(E_h) = \bigcup_{\tau \ge 0} \psi(\tau, W^u_{\rm loc}(E_h)), \tag{4.38}$$

respectively. From Lemma 4.4, $\psi(\tau, \{N_d(H_0) \cap S_{12} \setminus H_0\})$ flows away from E_h along $W^u(E_h)$ since the equilibrium point E_h is of a hyperbolic type.

Lemma 4.5. *If a solution starting in any small neighborhood of H_0 on S_{12} except H_0 itself is included in $W^s(E_x)$, then the system survives the first triple encounter.*

Proof. It will be shown that for any small $d > 0$, $\psi(\tau, \{N_d(H_0) \cap S_{12} \setminus H_0\})$ experiences the minimal value of the moment of inertia. It means that the system survives the first triple encounter by the definition of triple encounter.

From the equations of motion (4.12), we have $r' < 0$ if $\tilde{v} < 0$, and $r' > 0$ if $\tilde{v} > 0$. Recall that $r^2(\tau)$ is the moment of inertia of the system. According to Waldvogel (1982), motions in $\tilde{M}_0$ are gradient-like with respect to $\tilde{v}$. Since $W^u(E_h)$ lies in $\tilde{M}_0$, $\tilde{v}$ increases along any non-stationary solution curves in $W^u(E_h)$.

First consider a solution curve which lies in $W^u(E_h)$. There is a $\tau_1 > 0$ such that $\tilde{v}(\tau_1) = 0$ and $\tilde{v}(\tau) > 0$ during $\tau \in (\tau_1, \infty)$ along every $\psi(\tau, W^u_{\rm loc}(E_h))$ since there is no equilibrium point between E_h and a section $\tilde{v} = 0$ in $\tilde{M}_0$. Any equilibrium point E_x

corresponding to triple collision satisfies $\tilde{v} < 0$. All the equilibrium configurations are classified in only two types: the collinear central configuration and the equilateral triangle one. Let $\tilde{v}^{\mathrm{C}}$ and $\tilde{v}^{\mathrm{T}}$ be values of $\tilde{v}$ at the equilibrium points of the collinear type and the equilateral-triangle type, respectively. Then $\tilde{v}^{\mathrm{C}} < \tilde{v}^{\mathrm{T}} < 0$. Thus, $W^u(E_h)$ is not connected to any E_x.

Next consider a solution curve $\boldsymbol{\psi}(\tau, \{N_d(H_0) \cap S_{12} \setminus H_0\})$. Since $\boldsymbol{\psi} \not\subset W^s_{\mathrm{loc}}(E_h)$ when $\boldsymbol{\psi}$ passes close to E_h from Lemma 4.4, $\boldsymbol{\psi}$ follows $W^u(E_h)$. Thus $\boldsymbol{\psi}$ passes through the section $\tilde{v} = 0$ around τ_1. The non-decreasing value $\tilde{v}(\tau)$ of $\boldsymbol{\psi}$ changes sign from negative to positive for the first time. The moment of inertia of $\boldsymbol{\psi}$ begins to increase. It survives the first triple encounter by the definition. □

From the above lemma, the system survives the first triple encounter if there is an initial point leading to triple collision in a sufficiently small neighborhood of the point H_0 on S_{12}. The initial-value space S_{12} is topologically equivalent to the initial-value space $\grave{D}$. Therefore, Lemma 4.1 follows at once.

4.2.3 Escape in the planar isosceles subsystem

In the present section, we will prove Lemma 4.2 using the blow-up variables developed by Devaney (1980). Here, the planar isosceles three-body problem is considered in order to investigate the distribution of escape orbits which start on the isosceles curves I_j, $j = 1, 2, 3$. We will prove the following theorem.

Theorem 4.2. *In the planar isosceles problem with sufficiently equal masses ($\epsilon \cong 1$), all systems of initial points sufficiently close to the initial point where the system ends in triple collision of equilateral type lead to escape of hyperbolic-elliptic type.*

Notice that an initial point in the above theorem is not restricted in the initial-value of the free-fall problem. This theorem is established at any initial point in the phase space in the planar isosceles problem. Moreover, triple-collision systems means the cases that each configuration tends to be equilateral triangle.

After the above theorem is proved, it is easy to understand that the distribution of escape regions around the triple-collision point in the initial-value space of the free-fall problem. In other words, the proof of Lemma 4.2 is easy. It is enough to reduce the phase space applicable in the theorem to the space with zero velocities. In order to prove that

an orbit leads to escape if it passes sufficiently close to triple collision singularity, we will first formulate an escape criterion in the planar isosceles problem and confirm that the large ejection velocity satisfies the escape criterion.

Let us consider the isosceles configuration with $a_2 = a_3$, i.e., with base m_2m_3. This assumption can be done without any loss of generality since other isosceles cases with base m_1m_2 and m_3m_1 will be considered similarly. Recall that we defined a_j as the mutual distance between particles m_k and m_l. We assume $m_2 = m_3 = 1$ and $m_1 = \epsilon$. Let x_1 denote a_1, i.e., the distance between the particles m_2 and m_3, and x_2 be the signed distance of the particle m_1 and the gravity center of the binary m_2 and m_3. The gravity center of all masses is fixed at the origin in the configuration space, and the suitable velocities of three particles are taken in order to maintain the isosceles configuration. The Hamiltonian of the system is given by the following function:

$$\mathcal{H} = \frac{\dot{x}_1^2}{4} + \frac{\epsilon}{2+\epsilon}\dot{x}_2^2 - \frac{1}{x_1} - \frac{4\epsilon}{(x_1^2 + 4x_2^2)^{1/2}}, \tag{4.39}$$

where a dot ($\dot{}$) denotes the differentiation with respect to time t. The system is of two degrees of freedom and admits the energy integral

$$\mathcal{H} = h = \text{const.} \tag{4.40}$$

Let us introduce the following quantity before formulating the criterion in the planar isosceles problem.

Definition 4.2. *The energy of the two-body approximation is defined as*

$$\bar{h}(t) \quad = \quad \frac{1}{2}\dot{x}_2(t)^2 - \frac{2+\epsilon}{|x_2(t)|}. \tag{4.41}$$

We consider the case of upward escape, i.e., $x_2 > 0$ and $\dot{x}_2 > 0$. The downward case ($x_2 < 0$ and $\dot{x}_2 < 0$) can be treated similarly. The following lemma is the simplified version of Yoshida's criterion (1972) which is adapted to the planar isosceles case. See Appendix for the proof.

Lemma 4.6. *Let $h < 0$. If the following inequalities are satisfied at time $t = t_0$:*

$$x_2(t_0) \neq 0 \qquad \text{and} \qquad \bar{h}(t_0) > 0, \tag{4.42}$$

then $\dot{x}_2(t) > 0$ *for any* $t \geq t_0$, *i.e., the orbit leads to hyperbolic-elliptic escape as* $t \to \infty$.

The escape criterion can be applied to any orbit except at syzygy crossing, even when it stays close to triple collision singularity. This feature is advantageous to the analysis of the planar isosceles problem. Usual criteria in the general three-body problem can be only effective after a particle is ejected beyond a certain distance (Standish, 1971; Yoshida, 1972, Laskar and Marchal, 1984).

In order to consider whether an orbit arbitrarily close to triple collision leads to escape or not, we describe the escape criterion by the blow-up variables in the planar isosceles problem developed by Devaney (1980). In the isosceles problem, the blow-up variables by Devaney (1980) are more suitable for the proof than the ones by Waldvogel (1982) since we know many results obtained with Devaney's variables (Devaney, 1980; Simó and Martínez, 1988).

Let us introduce some notations: $\boldsymbol{x} = (x_1, x_2)^T, A = \mathrm{diag}(1/2, 2\epsilon/(2+\epsilon))$. New variables $r, \boldsymbol{s}, v, \boldsymbol{u}, \theta, u, w$ are defined by

$$\begin{aligned}
&r = (\boldsymbol{x}^T A \boldsymbol{x})^{1/2}, \\
&\boldsymbol{s} = r^{-1}\boldsymbol{x} = A^{-1/2}(\cos\theta, \sin\theta)^T, \qquad \theta \in \left[-\tfrac{\pi}{2}, \tfrac{\pi}{2}\right], \\
&v = r^{1/2}(\boldsymbol{s}^T A \dot{\boldsymbol{x}}), \\
&\boldsymbol{u} = r^{1/2}\dot{\boldsymbol{x}} - v\boldsymbol{s} = uA^{-1/2}(-\sin\theta, \cos\theta)^T, \\
&w = u\cos\theta/\sqrt{W(\theta)},
\end{aligned} \tag{4.43}$$

where

$$V(\theta) = -\frac{1}{\sqrt{2}\cos\theta} - \frac{4\epsilon^{3/2}}{(2\epsilon + 4\sin^2\theta)^{1/2}}, \qquad W(\theta) = -\cos\theta \cdot V(\theta). \tag{4.44}$$

Scaling the time by $dt/d\tau = r^{3/2}\cos\theta/\sqrt{W(\theta)}$, we have the equations of motion as

$$\begin{aligned}
r' &= rv\tfrac{\cos\theta}{\sqrt{W(\theta)}}, \\
v' &= \sqrt{W(\theta)}\left(1 - \tfrac{\cos\theta(v^2 - 4rh)}{2W(\theta)}\right), \\
\theta' &= w, \\
w' &= \sin\theta\left(-1 + \tfrac{\cos\theta(v^2-2rh)}{W(\theta)}\right) - vw\tfrac{\cos\theta}{2\sqrt{W(\theta)}} + \left(\cos\theta - \tfrac{w^2}{2}\right)\tfrac{W'(\theta)}{W(\theta)},
\end{aligned} \tag{4.45}$$

where a prime ($'$) denotes the differentiation with respect to τ, except in $W'(\theta)$ which represents $dW/d\theta$. The energy integral becomes

$$\frac{w^2}{2} = \cos\theta + \frac{\cos^2\theta}{W(\theta)}\left(rh - \frac{v^2}{2}\right). \tag{4.46}$$

The energy of the two-body approximation $\bar{h}$ which depends on x_2 and $\dot{x}_2$ is related to x_1 and $\dot{x}_1$ via the binding energy between the base particles m_2 and m_3. Let h_b denote the binding energy, i.e.,

$$h_b = \frac{1}{x_1} - \frac{1}{4}\dot{x}_1^2. \tag{4.47}$$

Then

$$\bar{h} \leq \frac{1}{2}\dot{x}_2^2 - \frac{2+\epsilon}{(x_1^2/4 + x_2^2)^{1/2}} = \frac{2+\epsilon}{2\epsilon}(h + h_b). \tag{4.48}$$

The last quantity of eq.(4.48) corresponds to the energy function for m_1 (Zare and Szebehely, 1995). The equality holds if and only if $x_1 = 0$, i.e., $\theta = \pm\pi/2$.

From eq.(4.48), the escape criterion in the blow-up coordinate system can be described as follows.

Lemma 4.7. *Let $h < 0$. If the following inequalities are satisfied at time $\tau = \tau_1$ when $\theta = \pm\frac{\pi}{2}$:*

$$v^2 > \frac{8\epsilon^{3/2}}{\sqrt{2(2+\epsilon)}}, \tag{4.49}$$

then the orbit leads to hyperbolic-elliptic escape as $\tau \to \infty$.

Proof. Simó and Martínez (1988) described the binding energy h_b at the time of binary collision (i.e., $\theta = \pm\pi/2$) by the blow-up variables. According to Lemma 5.1 of Simó and Martínez (1988),

$$h_b\rfloor_{\theta=\pm\frac{\pi}{2}} = \frac{1}{r}\left(\frac{v^2}{2} - \frac{4\epsilon^{3/2}}{\sqrt{2(2+\epsilon)}}\right) - h. \tag{4.50}$$

Note that the fact $w = 0$ at $\theta = \pm\pi/2$ is used from eq.(4.46). From eq.(4.48) we obtain

$$\bar{h}\rfloor_{\theta=\pm\frac{\pi}{2}} = \frac{2+\epsilon}{2\epsilon}(h + h_b) = \frac{2+\epsilon}{2\epsilon r}\left(\frac{v^2}{2} - \frac{4\epsilon^{3/2}}{\sqrt{2(2+\epsilon)}}\right). \tag{4.51}$$

If $\bar{h}$ is positive at the time of the binary collision, the escape criterion is satisfied. Hence if $v^2 > 8\epsilon^{3/2}/\sqrt{2(2+\epsilon)}$ holds at the same time, then the system leads to hyperbolic-elliptic escape. □

From the above lemma, escape can be judged only by monitoring the behavior of

v at the time of binary collision. Now we can prove Theorem 4.2. We will keep notations $\tilde{M}(h)$, $\tilde{M}_0$, H_0, E_h, $W^s_{\rm loc}(E_h)$, and $W^u(E_h)$ defined in the planar system (see Section 4.2.2). In the planar isosceles problem, blow-up phase space $\tilde{M}(h)$ with a given energy h and its subset $\tilde{M}_0$ satisfying $r = 0$ have dimensions three and two, respectively.

Proof of Theorem 4.2. Let T denote an initial value of the orbit ending in triple collision of equilateral type. The equilibrium point corresponding to the equilateral triple collision is represented by E. Let $\boldsymbol{\psi}$ be a solution of the system (4.45) starting in $N_d(T)\backslash T$ for a sufficiently small $d > 0$. From the continuous dependence of solutions, there is a sufficiently small $d > 0$ such that $\boldsymbol{\psi}$ enters in $N_\varepsilon(E)$ for any $\varepsilon > 0$.

According to Devaney (1980), motions in $\tilde{M}_0$ are gradient-like with respect to v. Since $W^u(E_h)$ lies in $\tilde{M}_0$, v increases along any non-stationary solution curves on $W^u(E_h)$. According to Simó and Susín (1989), $W^u(E_h)$ stretches towards $v \to \infty$ with nealy equal masses, i.e., $m_1 \cong m_2 = m_3 = 1$. Therefore, there is a $\delta > 0$ such that v of $\boldsymbol{\psi}$ starting in $N_\delta(E) \setminus E$ becomes larger than the critical value satisfying the escape criterion at a time when $\theta = \pm\pi/2$. It results in hyperbolic-elliptic escape.

We can choose a sufficiently small d such that the inequality $\varepsilon < \delta$ holds for positive numbers d, ε, and δ which satisfy the above conditions. □

In this stage, Lemma 4.2 is easily proved. Let the initial value of $\boldsymbol{\psi}$ be located in $N_d(H_0) \cap I_j \setminus H_0$, $j = 1, 2, 3$. Recall that I_j denotes the isosceles curve which means a set of initial points in the planar isosceles problem with zero initial velocities. A suitable $d > 0$ satisfying the above lemma is found. In fact, from Lemma 4.4, $\boldsymbol{\psi}$ is not included in $W^s_{\rm loc}(E_h)$ when $\boldsymbol{\psi}$ enters in $N_\varepsilon(E_h)$. In other words, $\boldsymbol{\psi}$ lies in $N_\varepsilon(E_h) \setminus E_h$ for a time interval. Thus $\boldsymbol{\psi}$ passing close to E_h follows $W^u(E_h)$, and so the system of $\boldsymbol{\psi}$ satisfies the escape criterion.

Lemma 4.2 is established on both segments on I_j with respect to T_1. The respective phase trajectories starting on both segments run away along respective branches of the one-dimensional $W^u(E_h)$ on $\tilde{M}_0$ in opposite directions each other. After passing close to E_h, the trajectory moves away towards each side of $\tilde{M}_0$ along the $W^u(E_h)$. If the near-homothetic trajectory $\boldsymbol{\psi}$ exists around one branch of $W^u(E_h)$, m_1 escapes forward with respect to the incoming direction. We will call such a branch the *branch* B_+. On the other hand, m_1 escapes backward if the trajectory exists around the other branch, which

we will call the *branch* B_-.

Dynamically, the branches of $W^u(E_h)$ can be interpreted in the following way. A triple collision can be regarded to occur when where m_1 crosses the syzygy of the base m_2 and m_3 at the time of binary collision between m_2 and m_3. The one branch B_+ of $W^u(E_h)$ corresponds to the limit orbit of what the syzygy crossing occurs just after the binary collision. The particle m_1 passes through the syzygy of the binary when the components are receding from each other and is accelerated by the gravity of the binary. On the other branch B_-, the syzygy crossing occurs just before the binary collision. The particle m_1 passes through the approaching binary and is decelerated strongly. Immediately after that, m_1 returns and crosses the syzygy again, while the binary collision occurs and the components of the binary repel from each other. As a result, m_1 is accelerated by the gravity of the receding binary at the second syzygy crossing.

4.3 Motions close to asymmetrical triple collisions

The purpose of the present section is to verify that escape regions exist arbitrarily close to triple collision point T_2 as well as close to T_1 although we will use the numerical integrations. We will show that such escape regions contain binary-collision curves around T_2 as well as around T_1.

In order to do this, it is necessary to show that on the binary-collision curves, all initial points close to T_2 are escape points. If a binary-collision curve is equivalent to one of the isosceles curves, it is already clear that this statement is correct from Lemma 4.2. Such a binary-collision curve crossing T_2 is only the curve which is of type 2. On the curves of type 1 and type 3, the motion does not maintain isosceles configurations.

Let us concentrate our attention to the binary-collision orbits of type 1 and type 3 in the present section. With the aid of the numerical computations, we will show that the orbit experiencing binary collision tends to maintain the isosceles configuration approximately as the orbit passes close to the equiliblium point corresponding triple collision. Such a statement is summarized in Observation 4.1. If it is assured, the proof of the existence of non-escape points around T_2 on the binary-collision curves is easy. So we will prove it assuming Observation 4.1.

Moreover, the existence of non-escape points arbitrarily close to T_2 can be proved as well as the existence around T_1. In this stage, it is clear the similar structures of escape

regions around the respective triple collision points. These existence and similarity are shown in 4.3.2.

In Subsection 4.3.3, we will compare the behavior of non-escape orbits after the first triple encounter with one of escape orbits starting on the binary-collision curves.

4.3.1 Behavior of binary collision orbits

Since we consider the case that three masses are equal, we have three combinations of (k,l) such that the equality $a_k = a_l$ holds forever, where a_l is the mutual distance between the particle m_j and m_k. Recall that $(j,k,l) = (1,2,3), (2,3,1)$, or $(3,1,2)$. If the equality $a_k = a_l$ maintains forever, then

$$|\tilde{\alpha}_k| = |\tilde{\alpha}_l| \qquad \text{and} \qquad |\tilde{\beta}_k| = |\tilde{\beta}_l|. \tag{4.52}$$

In the phase space of the blow-up coordinate system $(r, \tilde{\alpha}_j, \tilde{\alpha}_k, \tilde{\alpha}_l, \tilde{\beta}_j, \tilde{\beta}_k, \tilde{\beta}_l)$, the above equalities represent isosceles subspace with $a_k = a_l$.

We chose a phase point P and consider the distance from P to the isosceles subspace. We restrict attention to the five-dimensional subspace which is defined by the two invariances of eqs.(4.14) and (4.15) in the seven-dimensional phase space. From the two invariances, the two variables $\tilde{\alpha}_j$ and $\tilde{\beta}_j$ for $j = 1, 2$ or 3 can be eliminated. The five-dimensional subspace $(r, \tilde{\alpha}_k, \tilde{\alpha}_l, \tilde{\beta}_k, \tilde{\beta}_l)$ will be called the phase space simply from here. We assume that the five variables are orthogonal. We project the point P and the isosceles subspace to the configuration subspace $(\tilde{\alpha}_k, \tilde{\alpha}_l)$ which is embedded in the phase space. Let a point P' be the projected point of the phase point P. The length of the shortest perpendicular segment is $\left||\tilde{\alpha}_k| - |\tilde{\alpha}_l|\right|/\sqrt{2}$. Let a point Q' be the foot of a perpendicular. Similarly we consider the complementary subspace $(r, \tilde{\beta}_k, \tilde{\beta}_l)$ to the configuration subspace. Let a point P'' and Q'' be the projected point of the phase point P and the shortest foot of a perpendicular from P'' to the isosceles subspace, respectively. The length of the perpendicular segment is $\overline{P''Q''} = \left||\tilde{\beta}_k| - |\tilde{\beta}_l|\right|/\sqrt{2}$. Notice that the isosceles subspace is independent of the component r. Therefore, we can measure the distance from the phase point to the isosceles subspace as follows:

$$d_j = \sqrt{\overline{P'Q'}^2 + \overline{P''Q''}^2} = \sqrt{\frac{(|\tilde{\alpha}_k| - |\tilde{\alpha}_l|)^2}{2} + \frac{(|\tilde{\beta}_k| - |\tilde{\beta}_l|)^2}{2}}. \tag{4.53}$$

First, we observe the trajectories experiencing the binary collision axsof type 1. we

measure the distances to the isosceles subspace d_j at the following four instances: (1) approaching an equilateral triangle, (2) the first syzygy crossing, (3) becoming the minimal moment of inertia, and (4) the second syzygy crossing.

In general, any triple-collision orbit tends to either a collinear or an equilateral triangle central configuration. At the triple-collision point T_2 the configuration approaches an equilateral one. Thus all the configurations in the vicinity of the triple-collision point becomes close to an equilateral triangle when three particles approach each other. See Appendix A.5, where several time-evolutions of triple and binary collision orbits are shown in the blow-up-coordinate system.

We briefly explain how to know the time of approaching an equilateral triangle. The equilateral triangle has the largest area, provided that a perimeter of the triangle is constant. Let S be the area of the triangle. Then

$$S = \sqrt{\tilde{\alpha}^2(\tilde{\alpha}^2 - \tilde{a}_1)(\tilde{\alpha}^2 - \tilde{a}_2)(\tilde{\alpha}^2 - \tilde{a}_3)} = \tilde{\alpha}\tilde{\alpha}_1\tilde{\alpha}_2\tilde{\alpha}_3, \tag{4.54}$$

where $\tilde{\alpha}^2 = \tilde{\alpha}_1^2 + \tilde{\alpha}_2^2 + \tilde{\alpha}_3^2 = (\tilde{a}_1 + \tilde{a}_2 + \tilde{a}_3)/2$, which is a half of a perimeter of the triangle. We scale the length by $\tilde{\alpha}^2$ and so the normalized area is $S/\tilde{\alpha}^4$. The time when $S/\tilde{\alpha}^4$ is maximal means the time of approaching an equilateral triangle.

In Fig.4.1, numerical results of the minimum distance to the isosceles subspace are shown. We have measured only d_1, the distance to the isosceles subspace with $\tilde{a}_2 = \tilde{a}_3$, since eventually m_1 escapes and so $\tilde{\alpha}_2$ and $\tilde{\alpha}_3$ are nearly equal. The abscissa is the x component of the initial value on the binary-collision curve of type 1, and the ordinate is the logscale of the distance d_1. The position of the triple-collision point T_2 is $x = 0.4035896$ taken from Tanikawa et al. (1995). An important result is that at all four instances the distance d_1 decreases as the binary-collision point approaches T_2. This means that the motion tends to be close to the isosceles one with decreasing the initial distance to the triple-collision point during triple encounter. The distance during the period of approach to an equilateral triangle is rather longer than those at the time of the other events. This is because the initial points around T_2 are distributed close to isosceles configuration with $\tilde{a}_1 = \tilde{a}_3$.

Second, we investigate a binary-collision orbit of type 3 around the triple-collision orbit. Since the syzygy crossing occurs once, we have measured d_3 at the following three instances: (1) approaching an equilateral triangle, (2) becoming the minimal moment of inertia, and (3) the syzygy crossing. In Fig.4.2. numerical results of type 3 are shown similarly as type 1. The notations are the same as Fig.4.1. At the all three instances, the distance d_3 decreases as the binary-collision point approaches T_2. This means that

the motion tends close to the isosceles one with decreasing the initial distance to the triple-collision point.

The above results are restricted during the triple encounter, and so there is no result after the triple encounter. From the above observation, we can not understand whether the phase trajectory corresponding binary collision continues to wander in an neighborhood of the isosceles subspaces. Now we will observe the several phase trajectories which experiences binary collision of type 1 where the phase space is projected to the $\tilde{\alpha}_2$-$\tilde{\alpha}_3$ space and the $\tilde{\beta}_2$-$\tilde{\beta}_3$ space. In order to translate the isosceles subspaces in the horizontal and vertical directions, the axes are rotated with 45 degrees. Thus on the rotated $\tilde{\alpha}_2$-$\tilde{\alpha}_3$ space the abscissa is $(\tilde{\alpha}_2 - \tilde{\alpha}_3)/\sqrt{2}$ and the ordinate is $(\tilde{\alpha}_2 + \tilde{\alpha}_3)/\sqrt{2}$, and on the rotated $\tilde{\beta}_2$-$\tilde{\beta}_3$ space the abscissa is $(\tilde{\beta}_2 - \tilde{\beta}_3)/\sqrt{2}$ and the ordinate is $(\tilde{\beta}_2 + \tilde{\beta}_3)/\sqrt{2}$. Note that the origin of the former space represent the binary collision between m_2 and m_3. The equilibrium points are located at $(-1,0),(1,0),(0,-1),(0,1)$ on the rotated $\tilde{\alpha}_2$-$\tilde{\alpha}_3$ space, and $(-4\sqrt{6}/3,0),(4\sqrt{6}/3,0),(0,-4\sqrt{6}/3),(0,4\sqrt{6}/3)$ on the rotated $\tilde{\beta}_2$-$\tilde{\beta}_3$ space.

Figs.4.3(a), (b) and (c) show three phase trajectories which start at the points along the binary-collision curve, on the rotated $\tilde{\alpha}_2$-$\tilde{\alpha}_3$ space. We set the initial value of each figure tending to approach triple-collision point in alphabetical order. Each trajectory enters the frame of the graph from the upper side, when it begins to flow apart from the equilibrium point. After the first syzygy crossing, the trajectory passes through the origin corresponding binary collision. After the second syzygy crossing, the trajectory runs away from the isosceles subspace downwards for a moment, and spirals to a certain simple closed curve encircling the origin. The spiraling phenomenon corresponds to binary formation, since it means that the distance $\tilde{a}_1 = \tilde{\alpha}_2^2 + \tilde{\alpha}_3^2$ between binary components oscillate around a small value.

A remarkable result is that the three trajectories have the same form. However, one must notice that the scale length of the ordinate tends small with decreasing the distance between the initial point and the triple-collision point. The scales of the abscissas are equal to each other. As far as we see the subspace corresponding to the configuration $\tilde{\alpha}_j$, the motion of the binary-collision orbit tends to the isosceles approximately as the initial point on the binary-collision curve approaches the triple-collision point.

With respect to the subspace corresponding to the velocity $\tilde{\beta}_j$, the same result are obtained, which shows in Figs.4.4(a), (b), and (c). As the same manner as Figs.4.3(a), (b), and (c), we put initial value of each figure tending to approach triple-collision point in

alphabetical order. We have also found that the forms of the three trajectories agree with each other if the scales of the abscissas are normalized appropriately. Each trajectory enters the frame of the graph from the lower side. The first syzygy crossing, minimum moment of inertia, and the second syzygy crossing occur successively. Eventually the trajectory revolve around the origin. Notice that the revolution tends oblate, as the initial point approaches the triple-collision point. Also in the subspace corresponding to $\tilde{\beta}_j$, the motion of the binary-collision orbit tends isosceles approximately as the initial point on the binary-collision curve approach the triple-collision point.

The above is the result on the binary-collision curve of type 1. Figures.4.5 and 4.6 are the result on type 3, which we have obtained the same as type 1. Now we can summarize the numerical observation.

Observation 4.1. *If an initial point on a binary-collision curve which does not accord with any isosceles line is located sufficiently close to the triple-collision point, the phase trajectory wanders in an arbitrary neighborhood of the isosceles subspace forever during and after the triple encounter.*

How does the trajectory behave if the binary-collision point approaches the triple-collision point furthermore? It seems that, if the ordinates are normalized in an appropriate manner, the form of trajectories on this binary-collision curve tends to some definite one as the scale of the abscissa tends to zero. We can conjecture that the limit trajectory corresponds to the isosceles motion on the triple-collision manifold $\tilde{M}_0$. The phase trajectory experiencing binary collision which is close to triple collision may flow along the invariant manifold of the unstable manifold of the equilibrium point on $\tilde{M}_0$.

4.3.2 Similar structure of escapes and collisions

In the present subsection, it will be shown that the structures of triple-collision points, binary-collision curves, escape regions are similar around the respective triple-collision points T_i, $i = 1, 2$. Recall that T_i denotes the triple-collision point on the isosceles line $(x + 0.5)^2 + y^2 = 1$ where triple collision occurs at the i-th close approach between m_1 and m_3. The structures around T_1 is analyzed strictly with the proofs in Section 4.2. We will establish the successive conjectures in the present subsection which shows the similar structures between S_1 and S_2 around T_1 and T_2, respectively.

Let as verify Observation 2.1 in Subsection 2.4.2 as follows. In $\check{M}(h)$, the stable manifold of the equilibrium point which is of Lagrange type has three dimension. This stable manifold corresponds the set of triple-collision orbits in the original phase space. The zero velocities means $\tilde{\beta}_j = 0$ for $j = 1, 2, 3$, and initial values of r and one of $\tilde{\alpha}_j$ is determined from the others $\tilde{\alpha}_k$ and $\tilde{\alpha}_l$ by eqs.(4.14), (4.15). Thus, the initial-value space in the free-fall problem has two dimension. The phase space $\tilde{M}(h)$ is the five-dimensional manifold. Thus, in general, the dimension of the intersection of the three-dimensional stable manifold and the two-dimensional initial-value space is 0 if the transversality of the stable manifold and the initial-value space is proved.

Conjecture 4.1. *In the free-fall three-body problem, the initial point leading to triple collision of Lagrange type is a point in the initial-value space.*

The proof of the transversality is one of the future works.

Let us accept the assumption without rigorous proofs that the set of binary-collision points forms a Jordan arc on the initial-value space, and that the set of triple-collision points is a point of which dimension is zero. They are the results obtained by Tanikawa et al. (1995). Furthermore, Tanikawa et al. (1995) observed that at least three binary-collision curves of different types meet at a triple-collision point. It is also assumed. Although we have no rigorous proof of such observations, we assume them and will clarify the behavior of binary-collision orbits close to triple collision. Morever, we also assume the following.

Assumption 4.1. *Three binary-collision curves meet at a triple-collision point. For any amll $\epsilon > 0$, there exists a circle with radius ϵ of which center is the triple-collision point such that the circle crosses the binary-collision curves in the following order: type 1, type 2, type 3, type 1, type 2, type 3.*

This connection has not been proved; however, we use this observation as an assumption without proofs. In the verification of Conjecture 4.3, we will use such a connection of binary-collision curves at a triple-collision point.

How escape regions distribute around a triple-collision point? To answer this question, at the beginning we confirm that the an escape point on the binary-collision curve

exists arbitrarily close to triple-collision point.

We now turn our attention to the behavior of binary-collision orbits close to triple collision of which does not maintain the isosceles configuration. In Observation 4.1 in Subsection 4.3.1, we showed numerically that the orbit experiencing binary-collision tends to maintain the isosceles configuration approximately as the orbit passes close to the equilibrium point corresponding to triple collision. In other words, the orbit experiencing binary-collision tends to maintain the isosceles configuration approximately as the orbit passes close to the equilibrium point corresponding to triple collision. The following statement will be utilized for convergence of an escape region to a triple-collision point along a binary-collision curve.

Conjecture 4.2. *On an binary-collision curve, all initial points in a sufficiently small neighborhood of the triple-collision point T_i except T_i itself are hyperbolic-elliptic points for $i = 1, 2$.*

This conjecture is correct around T_1 since binary-collision curves accord with isosceles curves. See Lemma 4.2 in Section 4.2.3.

We suggest the proof around T_i, $i \neq 1$. Let B be the flow experiencing binary-collision which passes sufficiently close to the equilibrium point corresponding to triple collision. From Observation 4.1 in Subsection 4.3.1, as the flow B passes close to the equilibrium point, B tends to approaches a flow which maintains isosceles configuration exactly. We call this isosceles flow the *flow* I. If B does not maintain the isosceles configuration, the isosceles flow I does not pass through the zero-velocities surface.

Since the flow B passes close to the equilibrium point, the flow I also passes close to the equilibrium point. The flow I runs away along the unstable manifold for an arbitrarily long time. This phenomenon corresponds to escape of one particle. Since the continuous dependence of the solution on initial values is established in the blow-up coordinate system, the flow B which lies arbitrarily close to the flow I also leads to escape. □

In the sequel, the orbit which starts on a binary-collision curve arbitrarily close to a triple-collision point runs along the isosceles unstable manifold during an arbitrarily long period, after passing near the equilibrium point.

In this stage, we will consider the initial points around the binary-collision curves

near the triple-collision points. The next conjecture indicates the existence of escape regions including a binary-collision curve in any close to triple-collision point. On the respective binary-collision curve, there is an escape point arbitrarily close to the triple-collision point. Moreover, the remarkable distribution of non-escape orbits after the first triple encounter has been evident. The existence of the non-escape region arbitrarily close to the triple-collision point have been verified.

Conjecture 4.3. *Each of six escape regions which is located around the respective binary-collision curve close to T_i forms a wedge at T_i, $i = 1, 2, \cdots$. Moreover, for any small $\varepsilon > 0$, non-escape points after the first triple encounter exist in an ε-neighborhood of T_i, $i = 1, 2, \cdots$.*

This conjecture shows the topological similarities of escape regions around T_1 and around T_2. The above conjecture implies the following distribution of orbits close to the equilateral triple-collision singularity which is Lagrange type:

Corollary 4.2. *Arbitrarily close to the triple-collision orbits of Lagrange type, all types of orbits exist such that the system leads to hyperbolic-elliptic escape, parabolic-elliptic escape, and non-escape, respectively, after the first triple encounter.*

Hitherto, the question remained how escape orbits distribute around a triple-collision orbit although the following blow-up analysis explored. Moeckel (1983) investigated the connection of flows between equilibrium point on the triple-collision manifold $\tilde{M}_0$, and made a list of the existence of a topologically transverse intersection of an unstable manifold and a stable manifold of equilibrium points with the aid of topological technique. As a result, possible behavior after the close triple encounters had been clarified, respectively. In advance of his classification, Simó (1980) shown that in the case of equal masses the unstable manifold of an equilibrium point corresponding to Lagrange type extends three types of ω-limit points where two particles coincide together, numerically. The combinations of two particles are all of three. The proof by Moeckel (1983) verifying the possibilities of respective escape phenomena for three particles around triple-collision orbits is based on the numerical work by Simó (1980).

4.3.3 Behavior of the ejection orbits close to triple collision

In the previous section, we have conjectured that a returning region without escape after the first triple encounter exists in an any neighborhood of the triple collision point. In the present section, we will show how the returning orbit tends to behave as it approach triple collision singularity.

We draw an artificial line on the initial-value space such that its directional vector is $(0.4020 - x_t, 0.4299 - y_t)$, where (x_t, y_t) is the position of the triple collision point T_2, i.e., $x_t = 0.4035896$ and $y_t = 0.4284000$. This line is out of the escape regions after the first triple encounter. It lies between the small escape region for m_2 and large escape region for m_3. Typical behavior of the orbits starting on the artificial line is the following. After the close approach between m_1 and m_3, the configuration tends equilateral as three particles approach each other. At the beginning of the triple encounter, the particle m_2 passes through the syzygy between m_3 and m_1 which are approaching each other. While m_3 and m_1 are turning around the center of two masses and receding from each other, m_2 is decelerated suddenly and returns, and passes through the syzygy again. At the second syzygy crossing, the particles m_1 and m_3 are receding from each other; however, the particle m_2 returns without escape. In this case m_2 can not obtain enough energy from the binary to escape.

We will measure the deviation of these trajectories from the isosceles subspace as the deviation of binary-collision trajectories are measured in the preceding section. Since the syzygy crossing occur twice during the triple encounter, the distances at the four instances will be measured: (1) approaching an equilateral triangle, (2) the first syzygy crossing, (3) becoming the minimal moment of inertia, and (4) the second syzygy crossing. We will attention to only d_2 which is the distance to the isosceles subspace with $\tilde{a}_3 = \tilde{a}_1$, since this artificial line lies near the isosceles line where $\tilde{a}_3 = \tilde{a}_1$ and the configuration is closer to the isosceles triangle with $\tilde{a}_3 = \tilde{a}_1$ than the other isosceles ones apparently.

In Fig.4.8, numerical results of the distance d_2 are shown. The abscissa is the x-component of the initial value on the artificial line, and the ordinate is the logscale of the distance d_2.

During a period approaching the equilateral triangle configuration, the distance d_2 decreases with decreasing the distance between an initial point and the triple-collision point T_2 on the initial-value space. It means that at first the system tends to be the isosceles configuration as the initial point are located in an arbitrarily small neighborhood of the triple collision point. On each initial point, d_2 at the remaining three instances is

larger than d_2 at the staying the equilateral triangle. This shows that all trajectories begin to recede from the isosceles subspace as the configuration recedes from the equilateral triangle. The different behavior from that of the binary collision orbit has been shown at the remaining instances: at the syzygy crossings and at the minimal moment of inertia. The distance d_2 increases at each three instance with decreasing the initial distance to T_2, unlike on the binary collision curves. The phase trajectory tends to recede from the isosceles subspace in the phase space $\tilde{M}(h)$, as the initial point approaches the triple collision point.

We could detect the difference between the escape and the return motions. The isosceles motion has an important role on the escape phenomena in near-triple-collision orbits.

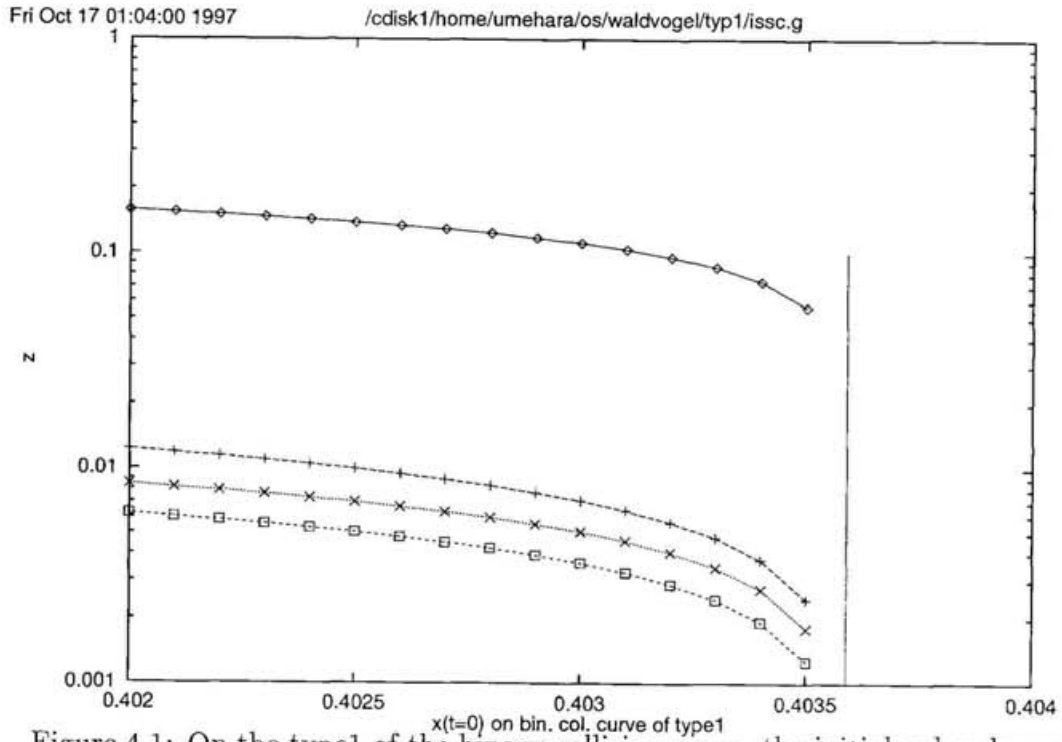

Figure 4.1: On the type1 of the binary collision curve, the initial-value dependence of the distance to the isosceles subspaces with base m_2-m_3 which is denoted by d_1. The ordinate is the logscale of the distance d_1. The abscissa is the x component of the initial value on the binary-collision curve of type1. The distances are measured at the following four steps: (1) approaching an equilateral triangle represented as a diamond square ($\diamond$), (2) the first syzygy crossing as a plus-type cross ($+$), (3) becoming the minimal moment of inertia as a square ($\square$), and (4) the second syzygy crossing as a cross ($\times$). The x position at a vertical line shows an initial value ending in triple collision.

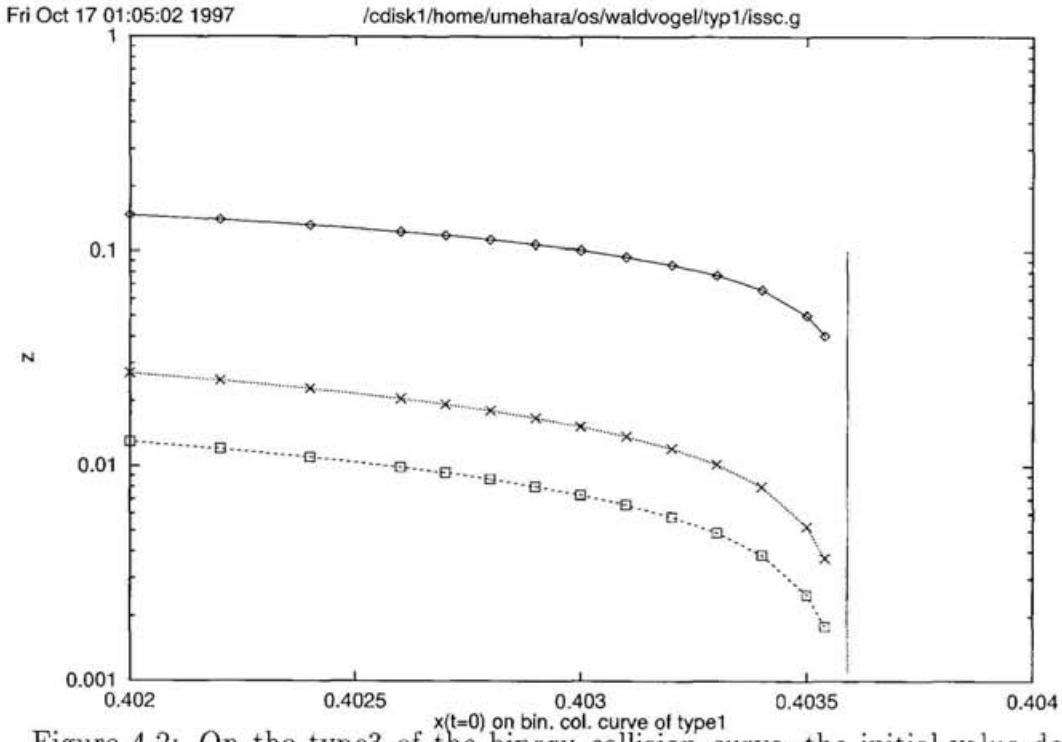

Figure 4.2: On the type3 of the binary collision curve. the initial-value dependence of the distance to the isosceles subspaces. with base m_1-m_2 which is denoted by d_3. The distances are measured at the following three steps: (1) approaching an equilateral triangle represented as a diamond square ($\diamond$), (2) becoming the minimal moment of inertia as a square ($\square$), and (3) the second syzygy crossing as a cross ($\times$). The x position at a vertical line shows an initial value ending in triple collision.

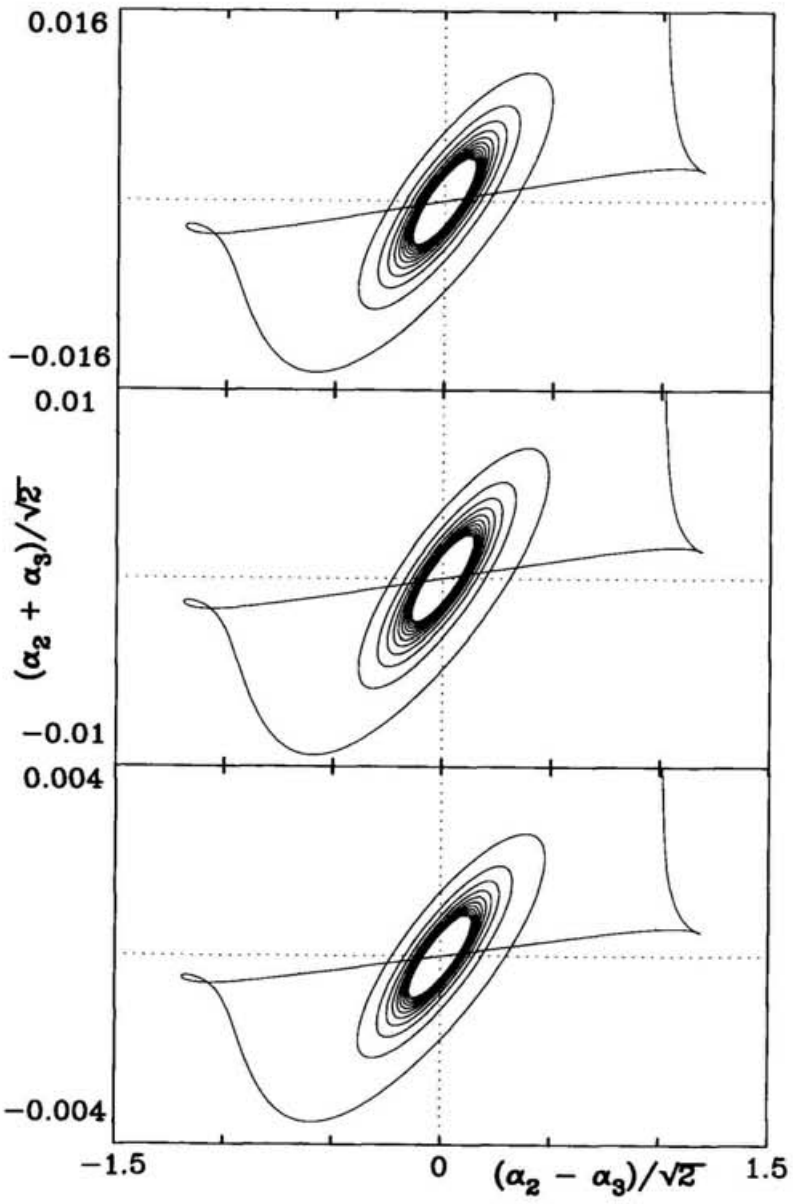

Figure 4.3: The projection of the phase trajectorys to the $(\tilde{\alpha}_2, \tilde{\alpha}_3)$ plane starting on the binary collision curve of type1.

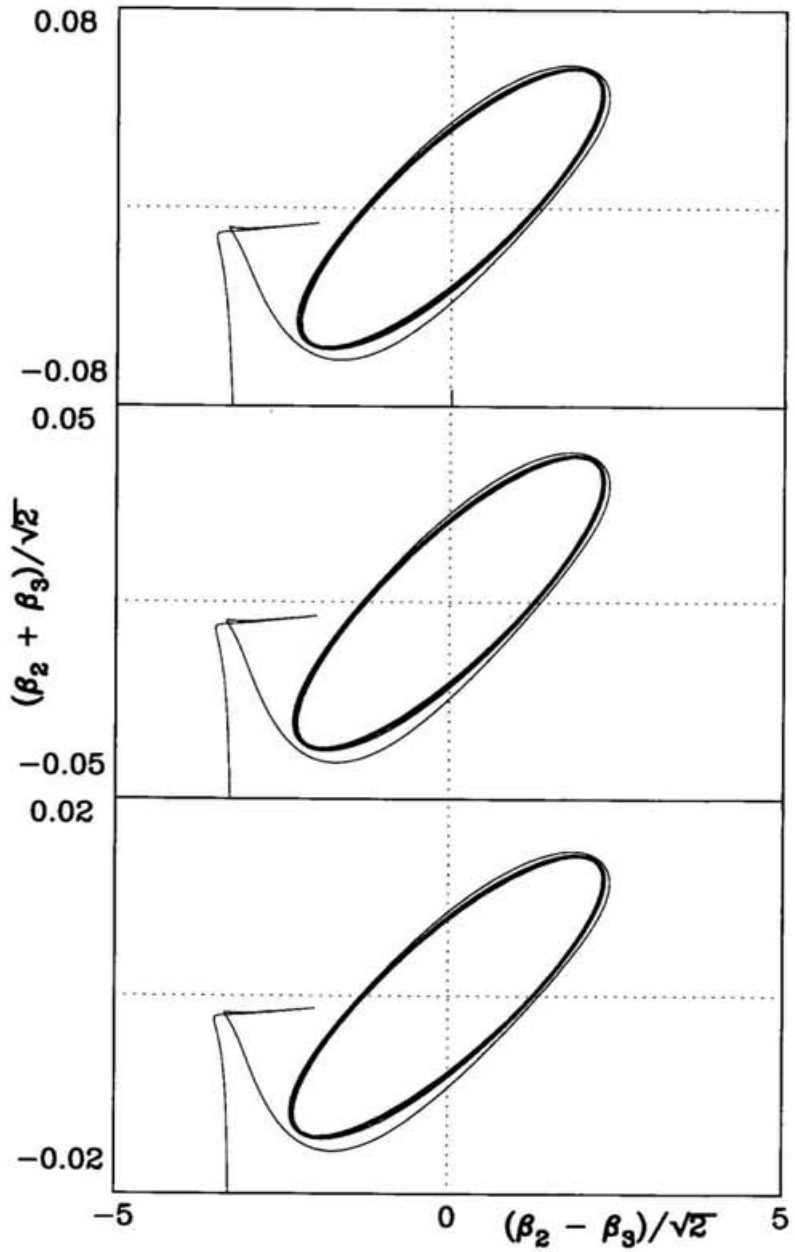

Figure 4.4: The projection of the phase trajectorys to the $(\tilde{\beta}_2, \tilde{\beta}_3)$ plane starting on the binary collision curve of type1.

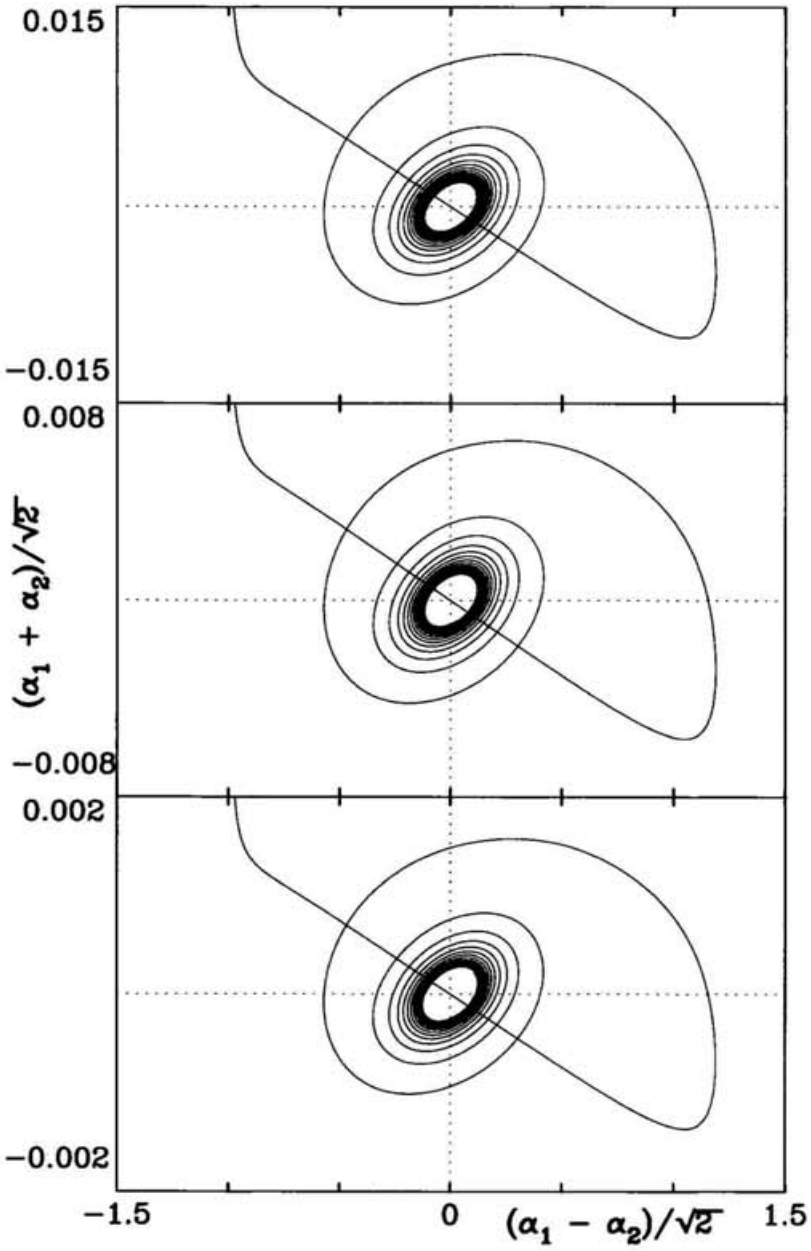

Figure 4.5: The projection of the phase trajectorys to the $(\tilde{\alpha}_1, \tilde{\alpha}_2)$ plane starting on the binary collision curve of type3.

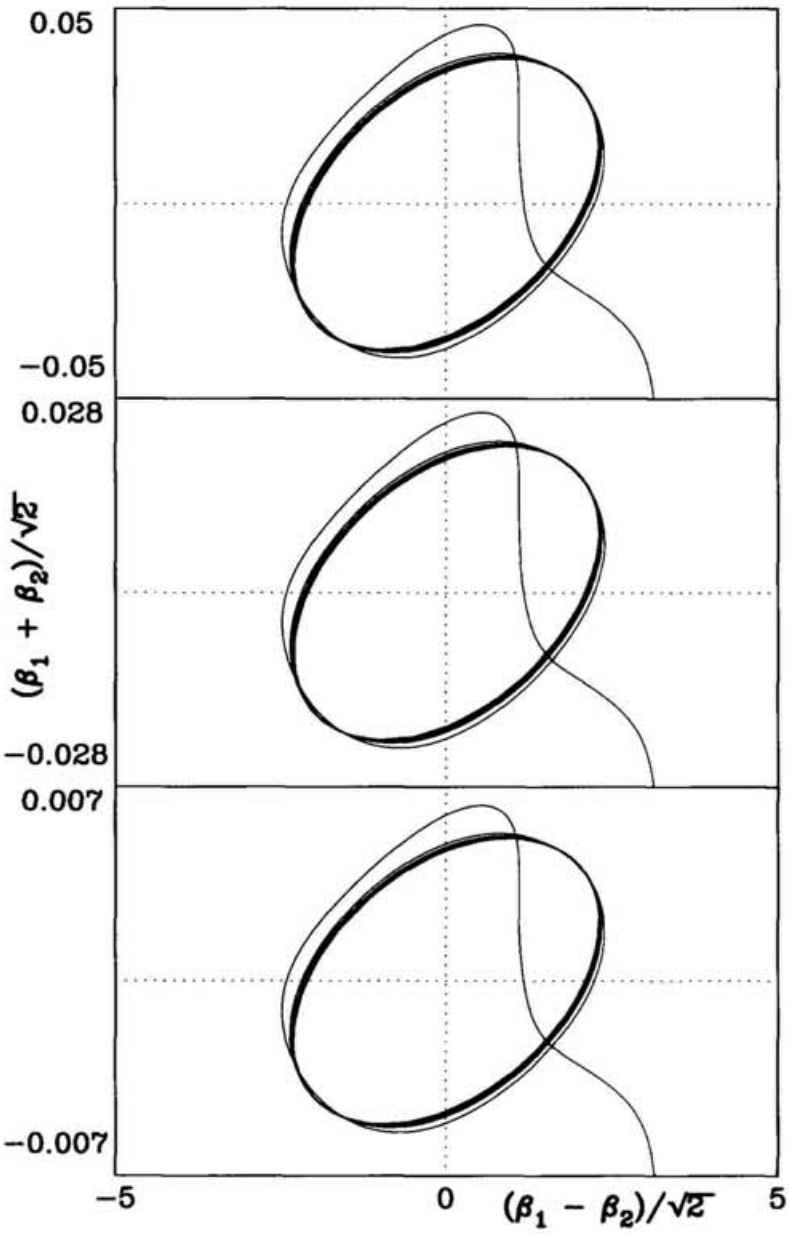

Figure 4.6: The projection of the phase trajectorys to the $(\tilde{\beta}_1, \tilde{\beta}_2)$ plane starting on the binary collision curve of type3.

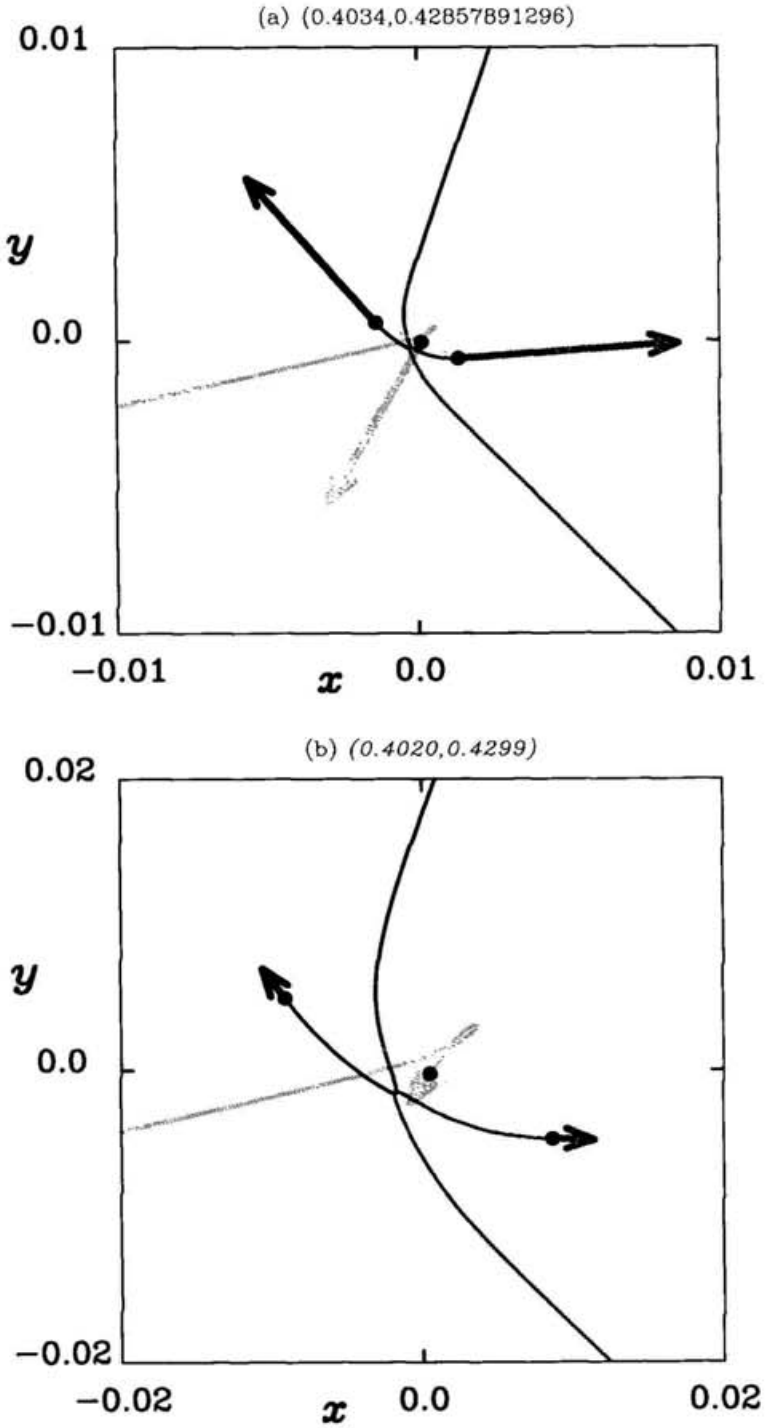

Figure 4.7: The returning orbits without escape after the first triple encounter starting on the artificial line passing throught the triple collision point T_2. The initial point of the case (a) is closer to T_2 than the case (b).

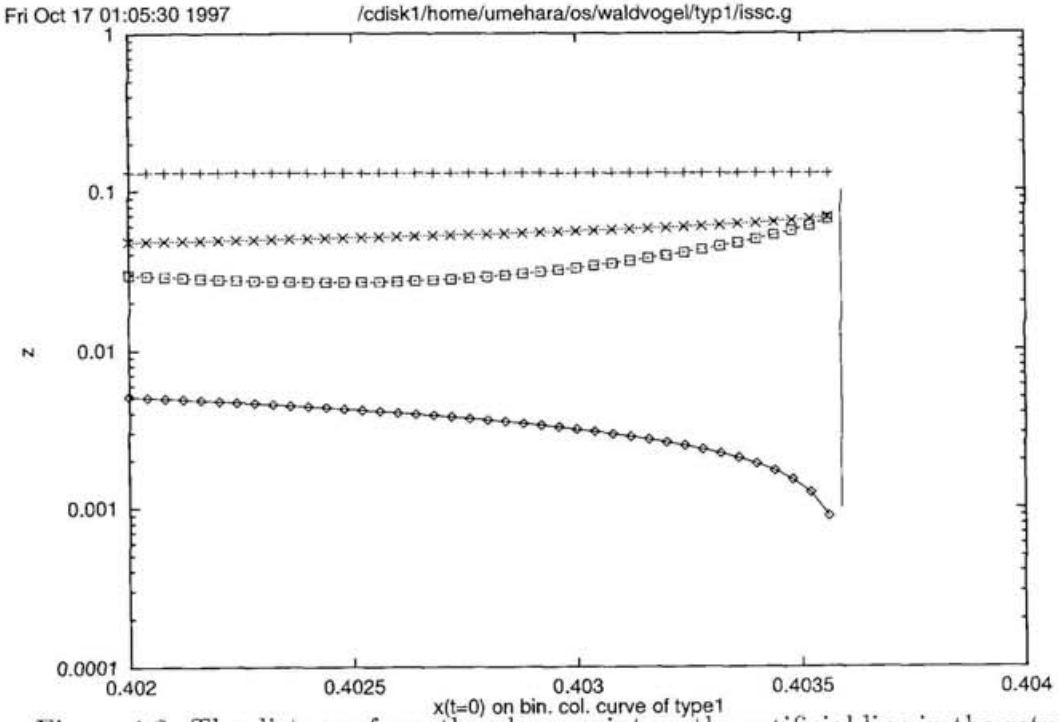

Figure 4.8: The distance from the phase point on the artificial line in the returning region to the isosceles subspace with base m_3-m_1 which is denoted by d_2. The ordinate is the logscale of the distance d_2. The abscissa is the x component of the initial value on the artificial line. The distances are measured at the following four steps: (1) approaching an equilateral triangle represented as a diamond square ($\diamond$), (2) the first syzygy crossing as a plus-type cross ($+$), (3) becoming the minimal moment of inertia as a square ($\square$), and (4) the second syzygy crossing as a cross ($\times$). The x position at a vertical line shows an initial value ending in triple collision.

Chapter 5

Discussion

The extension of such a systematical observation and analysis to the other three-body systems, for example non-zero angular momentum system, is our future work. We predict that most of binary collision orbits do not disappear even if we add small angular momentum on the equal-mass system, although triple collision orbits vanish. Close encounter of stars may be not rare and give a large probability to the formation of a binary or a multiplet.

We also should find out that the relation between escape and collision in the system *with unequal masses*. There are the planar-isosceles subspaces which are invariant in the phase space of the free-fall problem with equal masses. In the several proofs of the present thesis, we found that the binary-collision motions which are dominant to escape phenomena are close to the planar-isosceles motions, and so we used the fact to verify the importance of binary collision to escape phenomena. Therefore, we expect that the planar-isosceles subsystem is also crucial to escape phenomena.

In order to clarify that the binary-collision orbits dominate the planar-isosceles subsystem, it is necessary to investigate *the free-fall system where three masses are different* from each other. In this system, the planar-isosceles subspace do not exist in the phase space. In the free-fall system with unequal-mass case, Broucke (1995) investigated the initial-value distribution of escape after the first triple encounter. Note that the mass-ratio is $3 : 4 : 5$. In the figures of the results by Broucke, we can recognize that several escape regions converge to a point in the initial-value space, and that non-escape regions after the first triple encounter also converge to the point. We conjecture that this point is a triple-collision point. Moreover, we expect that the respective escape regions include the binary-collision curve since binary-collision orbits exist even in the unequal-mass system.

Appendix A

Derivations

A.1 Canonical reduction to the Jacobi coordinate

Let (q_1, q_2), (q_3, q_4) be the Jacobi coordinates, where (q_1, q_2) is a vector from m_1 to m_2, and (q_3, q_4) from the center of mass of m_1 and m_2 to m_3. Let p_k for $k = 1, 2, 3, 4$ be the conjugate momentum of the Jacobi coordinates, q_k for $k = 1, 2, 3, 4$. The Hamiltonian is the following:

$$\begin{aligned} H &= \frac{1}{2}\left(\frac{1}{m_1}+\frac{1}{m_2}\right)({p_1}^2+{p_2}^2)+\frac{1}{2}\left(\frac{1}{m_1+m_2}+\frac{1}{m_3}\right)({p_3}^2+{p_4}^2) \\ &- \frac{m_1 m_2}{({q_1}^2+{q_2}^2)^{\frac{1}{2}}} - \frac{m_1 m_3}{\left\{\left(q_3+\frac{m_2}{m_1+m_2}q_1\right)^2+\left(q_4+\frac{m_2}{m_1+m_2}q_2\right)^2\right\}^{\frac{1}{2}}} \\ &- \frac{m_2 m_3}{\left\{\left(q_3-\frac{m_1}{m_1+m_2}q_1\right)^2+\left(q_4-\frac{m_1}{m_1+m_2}q_2\right)^2\right\}^{\frac{1}{2}}}. \end{aligned} \tag{A.1}$$

Let the original Hamiltonian system be transformed from (q_k, p_k) for $k = 1, 2, 3, 4$ to $(r, p_r), (\rho, p_\rho), (\theta, p_\theta), (\phi, p_\phi)$ by the contact-transformation

$$q_k = \frac{\partial W}{\partial p_k} \text{ for } k = 1, 2, 3, 4, \qquad p_r = \frac{\partial W}{\partial r}, \quad \cdots, \tag{A.2}$$

where

$$W \stackrel{\text{def}}{=} r\cos\phi \cdot p_1 + r\sin\phi \cdot p_2 + \rho\cos(\theta+\phi)\cdot p_3 + \rho\sin(\theta+\phi)\cdot p_4. \tag{A.3}$$

The relation of variables are the following:

$$\begin{aligned}
q_1 &= r_1\cos\theta_2 && \text{(a)},\\
q_2 &= r_1\sin\theta_2 && \text{(b)},\\
q_3 &= r_2\cos(\theta_1+\theta_2) && \text{(c)},\\
q_4 &= r_2\sin(\theta_1+\theta_2) && \text{(d)},\\
p_{r_1} &= \cos\theta_2\cdot p_1{}' + \sin\theta_2\cdot p_2{}' && \text{(e)},\\
p_{r_2} &= \cos(\theta_1+\theta_2)\cdot p_3{}' + \sin(\theta_1+\theta_2)\cdot p_4{}' && \text{(f)},\\
p_{\theta_1} &= -r_2\sin(\theta_1+\theta_2)\cdot p_3{}' + r_2\cos(\theta_1+\theta_2)\cdot p_4{}' && \text{(g)},\\
p_{\theta_2} &= -r_1\sin\theta_2\cdot p_1{}' + r_1\cos\theta_2\cdot p_2{}' \\
&\quad -r_2\sin(\theta_1+\theta_2)\cdot p_3{}' + r_2\cos(\theta_1+\theta_2)\cdot p_4{}' && \text{(h)},
\end{aligned} \tag{A.4}$$

Using eqs.(A.4 g),(A.4 h)

$$p_{\theta_2} - p_{\theta_1} = -r_1\sin\theta_2\cdot p_1{}' + r_1\cos\theta_2\cdot p_2{}' \text{—(A.4 i)}.$$

The respect both sides of eqs.(A.4 e) and (A.4 i) is transformed by $[(\mathrm{e})^2 + \{(\mathrm{i})/r_1\}^2]$ to

$$p_{r_1}{}^2 + \left(\frac{p_{\theta_2} - p_{\theta_1}}{r_1}\right)^2 = p_1{}'^2 + p_2{}'^2, \tag{A.5}$$

Similarly, respect both sides of eqs.(A.4 f) and (A.4 g) is transformed by $[(\mathrm{f})^2 + \{(\mathrm{g})/r_2\}^2]$ to

$$p_{r_2}{}^2 + \left(\frac{p_{\theta_1}}{r_2}\right)^2 = p_3{}'^2 + p_4{}'^2. \tag{A.6}$$

On substitution in H of the new variables for the old, ϕ does not occur in H; therefore $p_\phi = c$ is the integral, where c is a constant. This corresponds to the angular momentum of the system. The Hamiltonian for the new variables is given by

$$\begin{aligned}
H &= \frac{1}{2}\left(\frac{1}{m_1}+\frac{1}{m_2}\right)\left\{p_r{}^2 + \left(\frac{p_\theta - c}{r}\right)^2\right\} + \frac{1}{2}\left(\frac{1}{m_1+m_2}+\frac{1}{m_3}\right)\left\{p_\rho{}^2 + \left(\frac{p_\theta}{\rho}\right)^2\right\} \\
&- \frac{m_1m_2}{r_1} - \frac{m_1m_3}{\left\{\left(\frac{m_2}{m_1+m_2}\right)^2 r_1{}^2 + \frac{2m_2}{m_1+m_2}r_1r_2\cos\theta_1 + r_2{}^2\right\}^{\frac{1}{2}}} \\
&- \frac{m_2m_3}{\left\{\left(\frac{m_1}{m_1+m_2}\right)^2 r_1{}^2 - \frac{2m_1}{m_1+m_2}r_1r_2\cos\theta_1 + r_2{}^2\right\}^{\frac{1}{2}}}.
\end{aligned} \tag{A.7}$$

A.2 Transformation to the equi-energy surface

Let us derive the equations of the transformation and the Jacobian determinant for each of successive transformations (3.30). The Jacobian determinants of the first, second

and third transformations are denoted by J_1, J_2, and J_3, respectively. We have

$$J = J_1 J_2 J_3. \tag{A.8}$$

The first mapping is the transformation from the Cartesian coordinates to the polar coordinates given by

$$x_0 = \rho_0 \cos\theta_0, \qquad y_0 = \rho_0 \sin\theta_0. \tag{A.9}$$

The domain of definition on D is expressed by the inequalities:

$$x_0 \geq 0, \qquad y_0 \geq 0, \qquad \left(x_0 + \frac{1}{2}\right)^2 + y_0^2 \leq 1. \tag{A.10}$$

Thus the range of the function $(\rho_0(x_0, y_0), \theta_0(x_0, y_0))$ satisfies

$$0 \leq \theta_0 \leq \frac{\pi}{2}, \qquad \rho_0 \geq 0, \qquad {\rho_0}^2 + \rho_0 \cos\theta \leq \frac{3}{4}. \tag{A.11}$$

The Jacobian determinant of the transformation $(x_0, y_0) \mapsto (\rho_0, \theta_0)$ is

$$J_1 = \frac{1}{\rho_0}, \tag{A.12}$$

and so the Jacobian matrix of the transformation is not defined for $\rho_0 = 0$. The range of the function includes $\rho_0 = 0$. Therefore, we must exclude $\rho_0 = 0$ which is equivalent to $x_0 = y_0 = 0$.

Next let us consider the second mapping corresponding to the scaling. The above canonical variables and the time are scaled by the factor α. The equations of motion is invariant under the following transformations:

$$(r, \rho, \theta, p_r, p_\rho, p_\theta) \mapsto (\hat{r}, \hat{\rho}, \hat{\theta}, \hat{p}_r, \hat{p}_\rho, \hat{p}_\theta), \tag{A.13}$$

where

$$\hat{r} = \alpha r, \qquad \hat{\rho} = \alpha \rho, \qquad \hat{\theta} = \theta, \tag{A.14}$$

$$\hat{p}_r = \alpha^{-1/2} p_r, \qquad \hat{p}_\rho = \alpha^{-1/2} p_\rho, \qquad \hat{p}_\theta = \alpha^{1/2} p_\theta. \tag{A.15}$$

These transformations result in the shift of the energy constant from h to $\hat{h}$. The Hamiltonian $H(\hat{r}, \hat{\rho}, \hat{\theta}, \hat{p}_r, \hat{p}_\rho, \hat{p}_\theta)$ of the scaled system is equal to a constant energy $\hat{h}$. Using the scaling relations (A.14), we obtain

$$H(\hat{r}, \hat{\rho}, \hat{\theta}, \hat{p}_r, \hat{p}_\rho, \hat{p}_\theta) = \alpha^{-1} H(r, \rho, \theta, p_r, p_\rho, p_\theta), \qquad \text{i.e.,} \qquad \hat{h} = \alpha^{-1} h. \tag{A.16}$$

Since the system starts from the zero-initial velocities with equal masses, the total energy of the system is

$$h = -\sum_{j=1}^{3} \frac{1}{r_j(t=0)} = -\left(\frac{1}{r} + \frac{1}{r_{20}} + \frac{1}{r_{30}}\right). \tag{A.17}$$

From Eqs.(A.16) and (A.17), α is obtained as in eq.(3.33).

The scaling equations (A.14) show that $\hat{\rho}$ is a function of ρ and θ whereas $\hat{\theta}$ is a function only of θ. Hence,

$$d\hat{\rho} = \left(\frac{\partial\hat{\rho}}{\partial\rho}\right) d\rho + \left(\frac{\partial\hat{\rho}}{\partial\theta}\right) d\theta, \qquad d\hat{\theta} = d\theta, \tag{A.18}$$

and so the Jacobian determinant of the transformation $(\rho_0, \theta_0) \mapsto (\hat{\rho}_0, \hat{\theta}_0)$ is

$$J_2 = \frac{\partial\hat{\rho}_0}{\partial\rho_0} = \frac{d(\rho_0, \theta_0)}{-\hat{h}}. \tag{A.19}$$

On the domain of the definition (A.11),

$$\frac{1}{4} - \rho_0\cos\theta_0 + \rho_0^2 \leq 1 - 2\rho_0\cos\theta_0. \tag{A.20}$$

Hence,

$$d(\rho_0, \theta_0) \geq 1 + \frac{1}{2}r_{30}^{-3}\left(\frac{1}{2} + \rho_0\cos\theta_0\right) + \frac{1}{2}\frac{1}{\sqrt{1 - 2\rho_0\cos\theta_0}} > 0. \tag{A.21}$$

The Jacobian determinant of the transformation is not zero in the domain of the definition (A.11). However, this determinant is not defined for ρ_0 satisfying

$$\frac{1}{4} - \rho_0\cos\theta_0 + \rho_0^2 = 0. \tag{A.22}$$

The region where the above equation is satisfied is a point $(\rho_0, \theta_0) = (0.5, 0)$ in the domain of the definition (A.11). We must exclude this point which is equivalent $x_0 = 0.5$, $y_0 = 0$.

Finally let us consider the third transformation. It corresponds to the projection to an equi-energy surface. The equation of the projection is derived easily as eq.(3.36) with eq.(3.33). It is also proved easily that this projection is a homeomorphism. The Jacobian determinant of the projection is equivalent to $\sqrt{\det(g_{ij})}$, $i, j = 1, 2$, where g_{ij} is a metric of the equi-energy surface $\hat{r} = \hat{r}(\hat{\rho}, \hat{\theta})$. The matrix form $[g_{ij}]$ of the metric is given by

$$[g_{ij}] = \begin{bmatrix} 1 + \left(\frac{\partial\hat{r}}{\partial\hat{\rho}}\right)^2 & \frac{\partial\hat{r}}{\partial\rho}\frac{\partial\hat{r}}{\partial\theta} \\ \frac{\partial\hat{r}}{\partial\rho}\frac{\partial\hat{r}}{\partial\theta} & 1 + \left(\frac{\partial\hat{r}}{\partial\hat{\theta}}\right)^2 \end{bmatrix}. \tag{A.23}$$

Therefore, the Jacobian determinant J_3 is obtained as

$$J_3 = \left\{\left(\frac{\partial\hat{r}_0}{\partial\hat{\rho}}\right)^2 + \left(\frac{\partial\hat{r}_0}{\partial\hat{\theta}}\right)^2 + 1\right\}^{1/2}. \tag{A.24}$$

The Jacobian determinant of the transformation is not zero in the domain of the definition (A.11). However, this determinant is not defined for the point $(\rho, \theta) = (0.5, 0)$.

In order to derive the above differentials, the implicit-function theorem is used. Let a function f is defined as

$$f(\hat{r}, \hat{\rho}, \hat{\theta}) = \{H(\hat{r}, \hat{\rho}, \hat{\theta}, \hat{p}_r, \hat{p}_\rho, \hat{p}_\theta) - \hat{h} \mid \hat{p}_r = \hat{p}_\rho = \hat{p}_\theta = 0\}. \tag{A.25}$$

There is a $(\hat{r}_0, \hat{\rho}_0, \hat{\theta}_0) \in (\hat{r}, \hat{\rho}, \hat{\theta})$ such that the function f sasisfies $f(\hat{r}_0, \hat{\rho}_0, \hat{\theta}_0) = 0$ and $f_{\hat{r}}(\hat{r}_0, \hat{\rho}_0, \hat{\theta}_0) \neq 0$ except at $(\rho, \theta) = (0.5, 0)$, where $f_{\hat{r}} = \partial f / \partial \hat{r}$. Note that the explicit expression of $f_{\hat{r}}$ is

$$\frac{\partial f}{\partial \hat{r}} = -\frac{d(\rho, \theta)}{\alpha^2}. \tag{A.26}$$

The function d is not defined at $(0, 5, 0)$, and so $f_{\hat{r}}$ is also not defined at the point. Hence, the implicit-function theorem is available except the point $(0.5, 0)$. It results in

$$f_{\hat{\rho}} + f_{\hat{r}} \frac{\partial \hat{r}}{\partial \hat{\rho}} = 0, \tag{A.27}$$

$$f_{\hat{\theta}} + f_{\hat{r}} \frac{\partial \hat{r}}{\partial \hat{\theta}} = 0, \tag{A.28}$$

where $f_{r\hat{h}o} = \partial f / \partial \hat{\rho}$ and $f_{\hat{\theta}} = \partial f / \partial \hat{\theta}$. The differentials $f_{\hat{\rho}}$ and $f_{\hat{\theta}}$ are described in eqs.(3.39) and (3.40).

A.3 Escape criterion in the planar isosceles problem

We rewrite Lemma 4.6 which is the escape criterion in the planar isoscles three-body problem. The escape criterion in the general three-dimensional three-body problem developed by Yoshida (1972) is adapted to the following lemma. We consider the case of upward escape, i.e., $x_2 > 0$ and $\dot{x}_2 > 0$. The downward case ($x_2 < 0$ and $\dot{x}_2 < 0$) can be treated similarly.

Lemma 4.6. *Let $h < 0$. If the following inequalities are satisfied at time $t = t_0$:*

$$x_2(t_0) \neq 0 \qquad \text{and} \qquad \bar{h}(t_0) > 0, \tag{A.29}$$

then $\dot{x}_2(t) > 0$ for any $t \geq t_0$, i.e., the orbit leads to hyperbolic-elliptic escape as $t \to \infty$, where

$$\bar{h}(t) = \frac{1}{2}\dot{x}_2(t)^2 - \frac{2 + \epsilon}{|x_2(t)|}. \tag{A.30}$$

Proof. As long as $x_2 \neq 0$, the only possible collision is the binary collision between m_2 and m_3. Since the binary collision can always be prolonged analytically, $x_2(t)$ is a smooth function and $x_1(t)$ is a continuous function of t. So from the assumption eq.(A.29), there is a t_1 ($t_1 > t_0$) such that for any $t \in [t_0, t_1]$

$$x_2(t) > 0 \quad \text{and} \quad \dot{x}_2(t) > 0. \tag{A.31}$$

Suppose that the following τ is a finite value:

$$\tau = \sup\{t \mid x_2(t) > 0 \quad \text{and} \quad \dot{x}_2(t) > 0\}. \tag{A.32}$$

Then at the time $t = \tau$, the following equality holds:

$$x_2(\tau) = 0 \quad \text{or} \quad \dot{x}_2(t) = 0. \tag{A.33}$$

The equation of motion about x_2 are transformed as

$$\ddot{x}_2 = -\frac{Mx_2}{(x_1^2 + x_2^2)^{3/2}} \geq -\frac{M}{x_2^2}. \tag{A.34}$$

Here, $\dot{x}_2(t)$ is greater than or equal to 0 for $t \in [t_0, \tau]$. Multiplying the above inequality by $\dot{x}_2(t)$ and integrating the product from t_0 to t ($\leq \tau$), we have

$$\frac{1}{2}\dot{x}_2^2(t) - \frac{1}{2}\dot{x}_2^2(t_0) \geq \frac{M}{x_2^2(t)} - \frac{M}{x_2^2(t_0)}. \tag{A.35}$$

Therefore, the following inequality is derived:

$$\dot{x}_2(t) \geq \sqrt{2}\sqrt{\left(\frac{1}{2}\dot{x}_2^2(t_0) - \frac{M}{x_2(t_0)}\right) + \frac{M}{x_2(t)}} > \sqrt{2\left(\frac{1}{2}\dot{x}_2^2(t_0) - \frac{M}{x_2(t_0)}\right)} > 0. \tag{A.36}$$

In other words, $\dot{x}_2(t)$ and $x_2(t)$ are positive for $t \in [t_0, \tau]$, and so $\dot{x}_2(\tau) > 0$ and $x_2(\tau) > 0$. It contradicts eq.(A.33). Hence the inequalities $x_2(t) > 0$ and $\dot{x}_2(t) > 0$ hold for $t \in [t_0, \infty)$.

Finally, the feature of hyperbolic-elliptic escape, $x_2(t) = O(t)$, is derived by integrating the inequality (A.36) with t from t_0 to t. We have

$$x_2(t) > \left[\sqrt{2\left(\frac{1}{2}\dot{x}_2^2(t_0) - \frac{M}{x_2(t_0)}\right)}\right] t + x_2(t_0), \tag{A.37}$$

for any $t \geq t_0$. □

A.4 Tangent space to the blow-up stable manifold

The tangent space to the stable manifold of the equilibrium point $T_{E_h}W^s_{\rm loc}(E_h)$ will be evaluated as follows. Recall that the variational equations at E_h are obtained by substituting $\tilde{\beta} = -4/\sqrt{3}$ in eq.(4.20). The vector

$$(\delta r, \delta\tilde{\boldsymbol{\alpha}}, \delta\tilde{\boldsymbol{\beta}})^T = (1, \mathbf{o}, \frac{2}{\sqrt{3}}\mathbf{e})^T, \tag{A.38}$$

is an eigenvector of the Jacobian matrix defined in these equations for the eigenvalue $-\sqrt{6}$. This eigenvector is perpendicular to the tangent space to $\tilde{M}_0$, since from eq.(4.23) the tangent space to $\tilde{M}_0$ satisfies

$$\delta r = 0, \qquad \sum_j \delta\tilde{\alpha}_j = 0, \qquad \sum_j \delta\tilde{\beta}_j = 0. \tag{A.39}$$

Following Devaney (1979) and Moeckel (1983), we will compute the remaining eigenspaces. Since the dimension of the tangent space to $\tilde{M}_0$ is reduced by one, the remaining eigenvectors lie in the tangent space to $\tilde{M}_0$ at the equilibrium point. Thus we can restrict attention to the lower right 6×6 submatrix:

$$X = \begin{bmatrix} J_{\alpha,\alpha} & J_{\alpha,\beta} \\ J_{\beta,\alpha} & J_{\beta,\beta} \end{bmatrix}, \tag{A.40}$$

where 3×3 matrices $J_{\alpha,\alpha}$, $J_{\alpha,\beta}$, $J_{\beta,\alpha}$ and $J_{\beta,\beta}$ are described in eq.(4.22) with $\tilde{\beta} = -4/\sqrt{3}$. Let μ be the eigenvalues of X, and $\lambda_{\alpha,\alpha}$, $\lambda_{\alpha,\beta}$, $\lambda_{\beta,\alpha}$ and $\lambda_{\beta,\beta}$ be the eigenvalues of the respective 3×3 submatrices $J_{\alpha,\alpha}$, $J_{\alpha,\beta}$, $J_{\beta,\alpha}$ and $J_{\beta,\beta}$. The respective eigenvectors are obtained as $\mathbf{e}^T$ and $u_1(1,0,-1)^T + u_2(0,1,-1)^T$ for any $u_1, u_2 \in \mathrm{R}$, since y is not equal to 0 in the form $J[x,y]$. Note that respective eigenvalues are $(x+2y)$ and $(x-y)$. Suppose that $\delta\tilde{\boldsymbol{\alpha}} \in \mathbf{R}^3$ is an eigenvector of the four matrices $J_{\alpha,\alpha}$, $J_{\alpha,\beta}$, $J_{\beta,\alpha}$ and $J_{\beta,\beta}$. Then $(\delta\tilde{\boldsymbol{\alpha}}, \kappa\delta\tilde{\boldsymbol{\alpha}})^T \in \mathbf{R}^6$ is an eigenvector of X, provided

$$\begin{cases} \lambda_{\alpha,\alpha} + \lambda_{\alpha,\beta}\kappa &= \mu, \\ \lambda_{\beta,\alpha} + \lambda_{\beta,\beta}\kappa &= \kappa\mu. \end{cases} \tag{A.41}$$

These equations are derived from

$$\begin{bmatrix} J_{\alpha,\alpha} & J_{\alpha,\beta} \\ J_{\beta,\alpha} & J_{\beta,\beta} \end{bmatrix} \begin{bmatrix} \delta\tilde{\boldsymbol{\alpha}} \\ \kappa\delta\tilde{\boldsymbol{\alpha}} \end{bmatrix} = \mu \begin{bmatrix} \delta\tilde{\boldsymbol{\alpha}} \\ \kappa\delta\tilde{\boldsymbol{\alpha}} \end{bmatrix}. \tag{A.42}$$

The vector $(\mathbf{e}, \kappa\mathbf{e})^T$ is perpendicular to the tangent space to $\tilde{M}_0$ (eq.(A.39)) and so it does not lie in the tangent space to $\tilde{M}_0$. The eigenvalues of the 3×3 matrices corresponding

to the eigenvector $u_1(1,0,-1)^T + u_2(0,1,-1)^T$ are computed as follows:

$$\lambda_{A\alpha} = \frac{3}{2}\sqrt{6}, \quad \lambda_{A\beta} = \frac{3}{4}, \quad \lambda_{B\alpha} = -6, \quad \lambda_{B\beta} = -\sqrt{6}. \tag{A.43}$$

Therefore, from eq.(A.41) the eigenvalues of X are evaluated as

$$\mu_- = \frac{\sqrt{6}(1-\sqrt{13})}{4}, \text{ and } \mu_+ = \frac{\sqrt{6}(1+\sqrt{13})}{4}. \tag{A.44}$$

Their corresponding eigenvectors are evaluated from eq.(A.41) as follows:

$$\delta\tilde{\alpha}_1(1,0,-1,\kappa_-,0,-\kappa_-)^T + \delta\tilde{\alpha}_2(0,1,-1,0,\kappa_-,-\kappa_-)^T, \tag{A.45}$$

and

$$\delta\tilde{\alpha}_1(1,0,-1,\kappa_+,0,-\kappa_+)^T + \delta\tilde{\alpha}_2(0,1,-1,0,\kappa_+,-\kappa_+)^T, \tag{A.46}$$

where

$$\kappa_- = -\frac{\sqrt{6}(5+\sqrt{13})}{3}, \text{ and } \kappa_+ = -\frac{\sqrt{6}(5-\sqrt{13})}{3}. \tag{A.47}$$

From eqs.(A.38),(A.45), $T_{E_h}W^s_{\rm loc}(E_h)$ is

$$\begin{bmatrix} \delta r_{\rm eq.} \\ \delta\tilde{\alpha}_1^{\rm eq.} \\ \delta\tilde{\alpha}_2^{\rm eq.} \\ \delta\tilde{\alpha}_3^{\rm eq.} \\ \delta\tilde{\beta}_1^{\rm eq.} \\ \delta\tilde{\beta}_2^{\rm eq.} \\ \delta\tilde{\beta}_3^{\rm eq.} \end{bmatrix} = \zeta_1 \begin{bmatrix} 1 \\ 0 \\ 0 \\ 0 \\ \frac{2}{\sqrt{3}} \\ \frac{2}{\sqrt{3}} \\ \frac{2}{\sqrt{3}} \end{bmatrix} + \zeta_2 \begin{bmatrix} 0 \\ 1 \\ 0 \\ -1 \\ \kappa_- \\ 0 \\ -\kappa_- \end{bmatrix} + \zeta_3 \begin{bmatrix} 0 \\ 0 \\ 1 \\ -1 \\ 0 \\ \kappa_- \\ -\kappa_- \end{bmatrix}, \tag{A.48}$$

for any real numbers ζ_1, ζ_2 and ζ_3.

A.5 Collisional solutions in the blow-up space

We will show several solutions in the blow-up-coordinate system. First of all, the two solutions leading to triple collision which start at the triple-collision points T_1 and T_2 are observed, respectively. We derived the expression for the solution starting at T_1 explicitly. See eq.(4.17). In Fig.A.1, the time-dependence of respective variables are shown. In the two figures, the upper ordinate represents $\tilde{\alpha}_j$, and the lower ordinate shows r and $\tilde{\beta}_j$ for $j = 1, 2, 3$. The absissas of both figures are the regularized time τ.

A bold curve in the upper figure shows the time-dependent $\tilde{\alpha}_j(t)$, $j = 1, 2, 3$. A bold curve in the lower figure shows the time-dependent $\tilde{\beta}_j(t)$, $j = 1, 2, 3$. A broken curve in the lower figure represents $r(t)$. Here, we observe the homothetic equilateral solution. Thus

$$\tilde{\alpha}_j(t) = \text{const.} \quad , \quad \tilde{\alpha}_1 = \tilde{\alpha}_2 = \tilde{\alpha}_3, \tag{A.49}$$

$$\tilde{\beta}_j(t) = \text{const.} \quad , \quad \tilde{\beta}_1 = \tilde{\beta}_2 = \tilde{\beta}_3. \tag{A.50}$$

Dotted horizontal straight lines stand for the equilibrium values:

$$\tilde{\alpha}_j^{\text{eq}} = \pm\frac{1}{\sqrt{2}}, \qquad \tilde{\beta}_j^{\text{eq}} = \pm\frac{4}{\sqrt{3}}, \qquad r^{\text{eq}} = 0. \tag{A.51}$$

This figure shows that all values approach the equilibrium values asymptotically.

Next, we will show the time evolution which starts at the triple-collision T_2 in the Fig.A.2. In this case, the solution curves of $j = 1$ and $j = 3$ always accord with each other. Two dark-bold curves in the upper figure and in the lower one stand for $\tilde{\alpha}_1(t) = \tilde{\alpha}_3(t)$ and $\tilde{\beta}_1(t) = \tilde{\beta}_3(t)$, respectively. Two light-bold curves represent $\tilde{\alpha}_2(t)$ and $\tilde{\beta}_2(t)$, respectively. A broken curve in the lower figure represents $r(t)$.

At $\tau = 0.807$, the curve representing the time evolution of $\tilde{\alpha}_1$ and $\tilde{\alpha}_3$ crosses τ-axis, which corresponds to a binary collision between m_1 and m_3. This figure also shows that all values approaches the equilibrium values asymptotically.

Next, we will show the numerical solutions of the planar isosceles problem. In the general planar three-body problem, if at least two masses of the particles are equal, there is an invariant subset of the system consisting of solutions whose configuration is always an isosceles triangle. One isosceles curve includes the triple collision point T_n for $n = 1, 2, \cdots$. In this case, $\tilde{\alpha}_1 = \tilde{\alpha}_3$ always holds. We will observe two of isosceles solutions where the initial points are located around the triple collision point T_2. One is the initial value of which the configuration starts a thinner triangle than a triangle spanned by the initial value of T_2, and the other is the fatter configuration. The time evolutions of the thinner and the fatter triangle are shown in Fig.A.3 and Fig.A.4, respectively. Notations in the respective figures are the same as in Fig.A.2.

In the case of the thinner triangle, the syzygy crossing occurs only once during the triple encounter. After a binary collision at $\tau = 0.806$, the solution approaches the equilibrium point. The solution stays close to the equilibrium point during a period $2 < \tau < 4$, and begins to recede. Immediately after that, at $\tau = 4.512$ the second binary collision

occurs, and the syzygy crossing of m_2 occurs at $\tau = 5.529$. The particle passes through the gravity center of the remnant particles. The particle m_2 undergoes the effect of slingshot, and so escape to infinity. See the moment of inertia increasing monotonically after the triple encounter.

In the case of the fatter triangle, the syzygy crossing occurs twice during the triple encounter. The time evolution until staying the equilibrium point is similar as the thinner triangle, although the binary collision occurs at $\tau = 0.807$. In the case, however, the syzygy crossing occurs before the second binary collision. See the light bold curve crosses before the dark curve crosses again. At the respective times $\tau = 4.492$ and at $\tau = 5.645$, the syzygy crossing and the binary collision occur. The second syzygy crossing occurs at $\tau = 6.775$. After that, the particle m_2 escapes.

The above two solutions corresponds to motions along both sides of the unstable manifold on the triple collision manifold. Unlike the blow-up variables by Devaney (1980), we can not distinguish whether the binary is receding or approaching at the syzygy crossing in the coordinate system by Waldvogel (1982).

Finally, we will show the solutions experiencing binary collision which does not maintain isosceles configuration, i.e., type 1 and type 3. Typical behavior of binary collision orbit which is of type 1 in the escape region D_2 are following. The three particles start at the initial value with zero velocities. After binary encounter between the particle m_1 and m_3 occurs once, the configuration of the three particles tends to equilateral triangle as three particles approach each other. During the triple encounter, the particle m_1 crosses the syzygy between m_2 and m_3. The m_1 ejecting downwards shortly returns and crosses the syzygy again. In that period, binary collision occurs and the moment of inertia becomes to be minimum. As a result, m_1 escapes upwards and m_2 and m_3 form a binary.

The time evolution of the solution of type 1 is shown in Fig.A.5. In the upper figure, a dark-bold curve, a light-bold curve and a fine curve stand for the time evolutions of $\tilde{\alpha}_1$, $\tilde{\alpha}_2$ and $\tilde{\alpha}_3$, respectively. In the lower figure, the same kinds of curves stand for $\tilde{\beta}_1$, $\tilde{\beta}_2$ and $\tilde{\beta}_3$, respectively, and a broken curve represents r.

In the case of the binary collision of type 1, the particle m_1 passes through the syzygy between m_2 and m_3 before collision. It means that the flow in $\tilde{M}(h)$ passes through the $\tilde{\alpha}_1$-axis (i.e., $\tilde{\alpha}_2 = \tilde{\alpha}_3 = 0$) after crossing the plane where $\tilde{\alpha}_1 = 0$. Since the flow which starts on an neighborhood of the triple collision T_2 approaches the equilibrium point at $\tilde{\boldsymbol{\alpha}}_{\rm eq} = \frac{1}{\sqrt{2}}(-1, 1, -1)^T$, the flow crosses the plane $\tilde{\alpha}_1 = 0$ in a positive direction from the

region of $\tilde{\alpha}_1 < 0$. Thus the flow passes through the $\tilde{\alpha}_1$-axis where $\tilde{\alpha}_1 > 0$ at the successive binary collision.

Typical behavior of binary collision orbit which is of type 3 in the escape region D_2 is following. After close approach between the particle m_1 and m_3 occurs once, the configuration of the three particles tends to equilateral triangle as three particles approach each other. During the triple encounter, the moment of inertia becomes to be minimum and the particle m_3 crosses the syzygy between m_1 and m_2. As a result, m_3 escapes without returning and m_1 and m_2 form a binary.

The time evolution of the solution of type 3 is shown in Fig.A.6. The notations in the present figure are the same as in Fig.A.5. In the case of the binary collision of type 3, the syzygy crossing of the particle m_3 does not occur from the beginning of the triple encounter until the binary collision. Thus the binary collision of type 3 corresponds to crossing the $\tilde{\alpha}_3$-axis where $\tilde{\alpha}_3 < 0$.

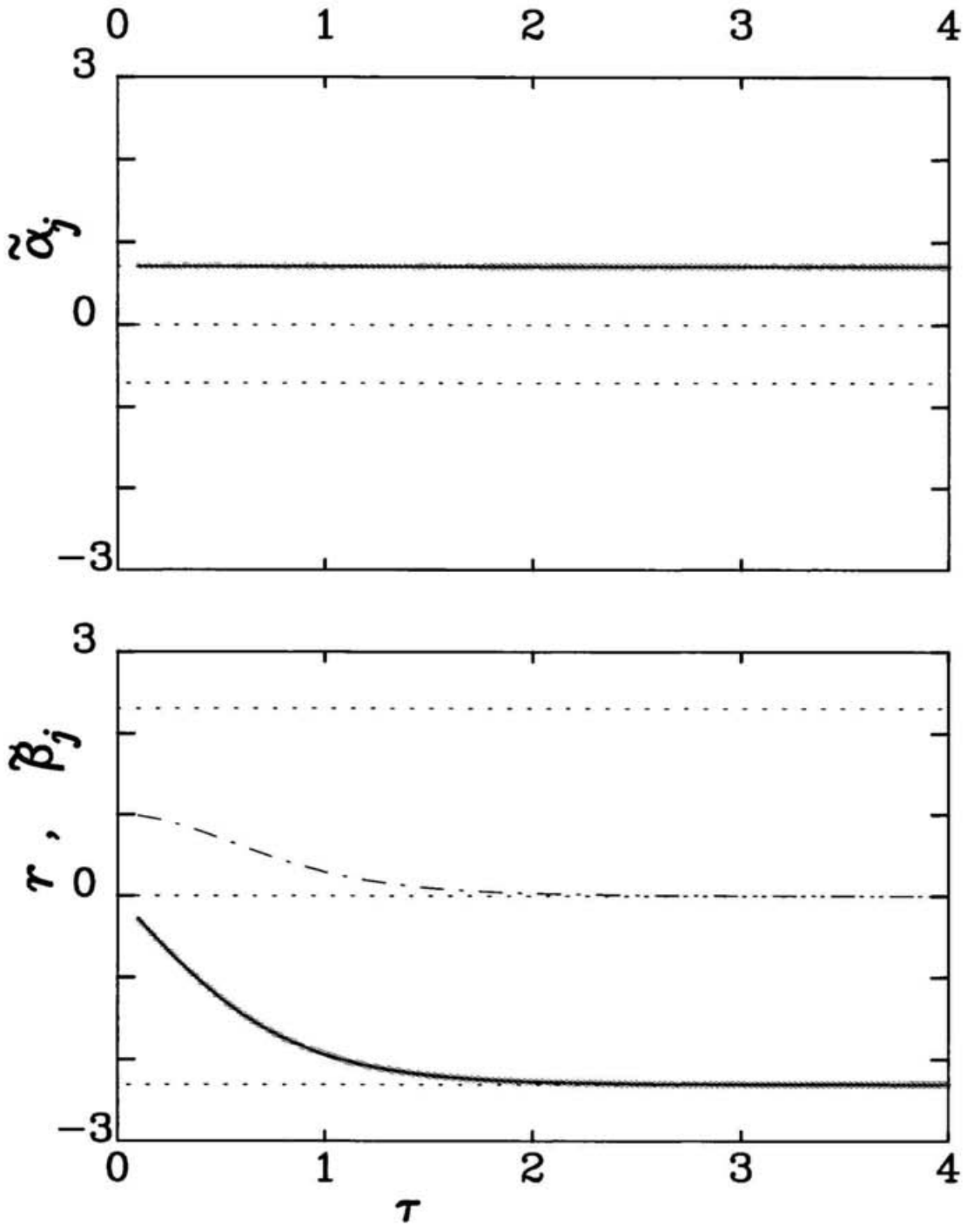

Figure A.1: In the blow-up coordinate system the time evolution of the solution leading to triple collision which starts at T_1.

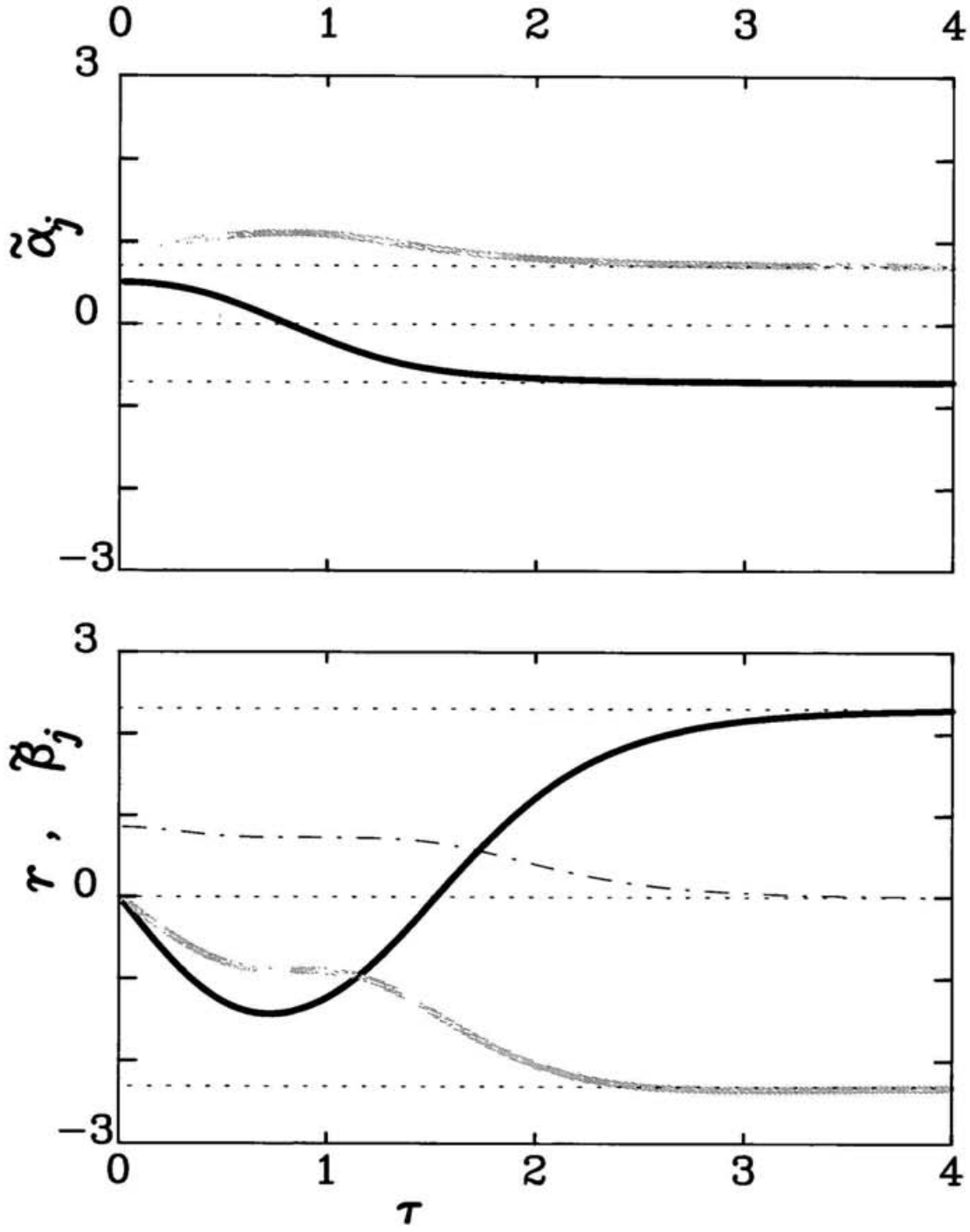

Figure A.2: In the blow-up coordinate system the time evolution of the solution leading to triple collision which starts at T_2.

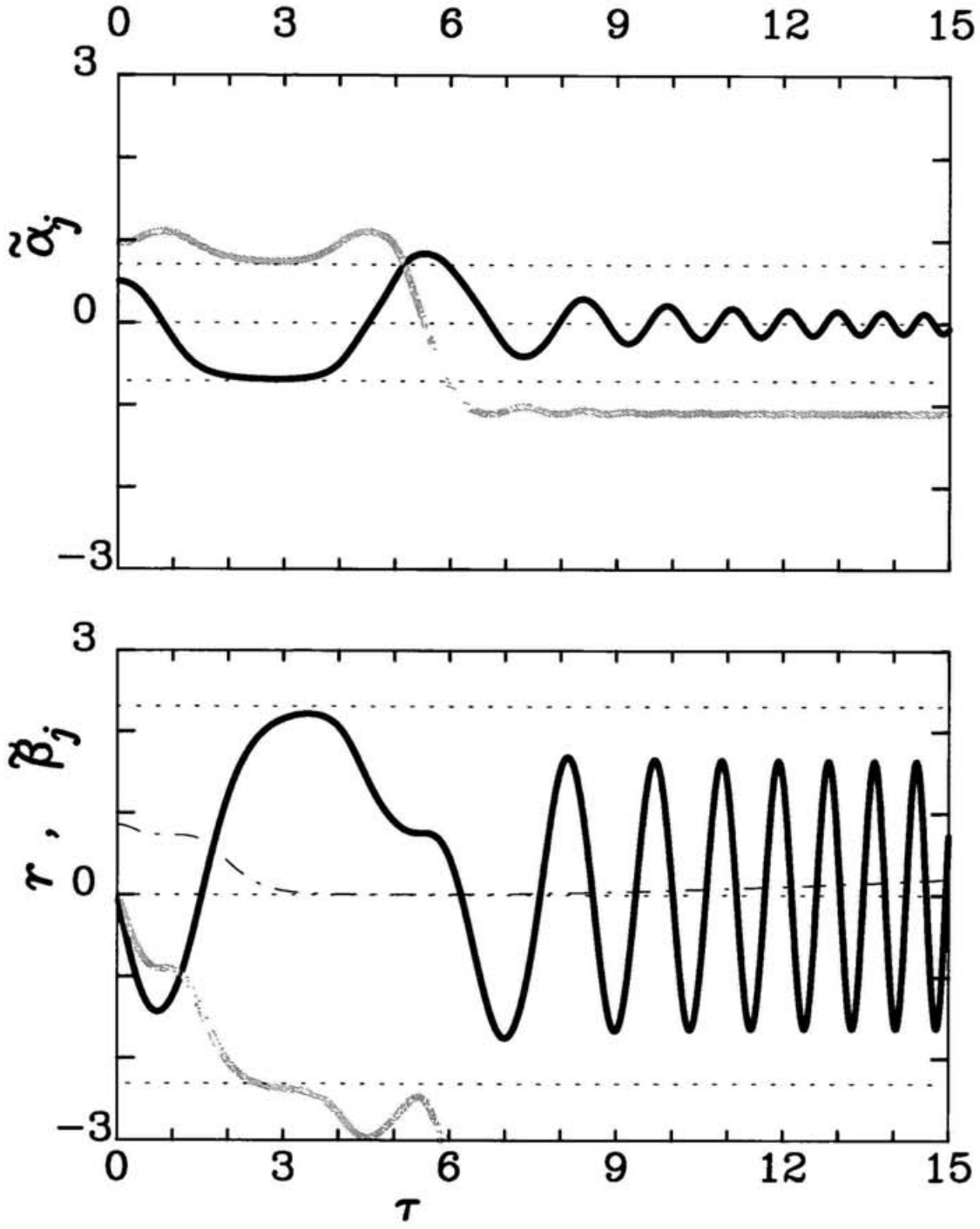

Figure A.3: In the blow-up coordinate system the time evolution of the solution on the isosceles line: the thinner triangle near T_2.

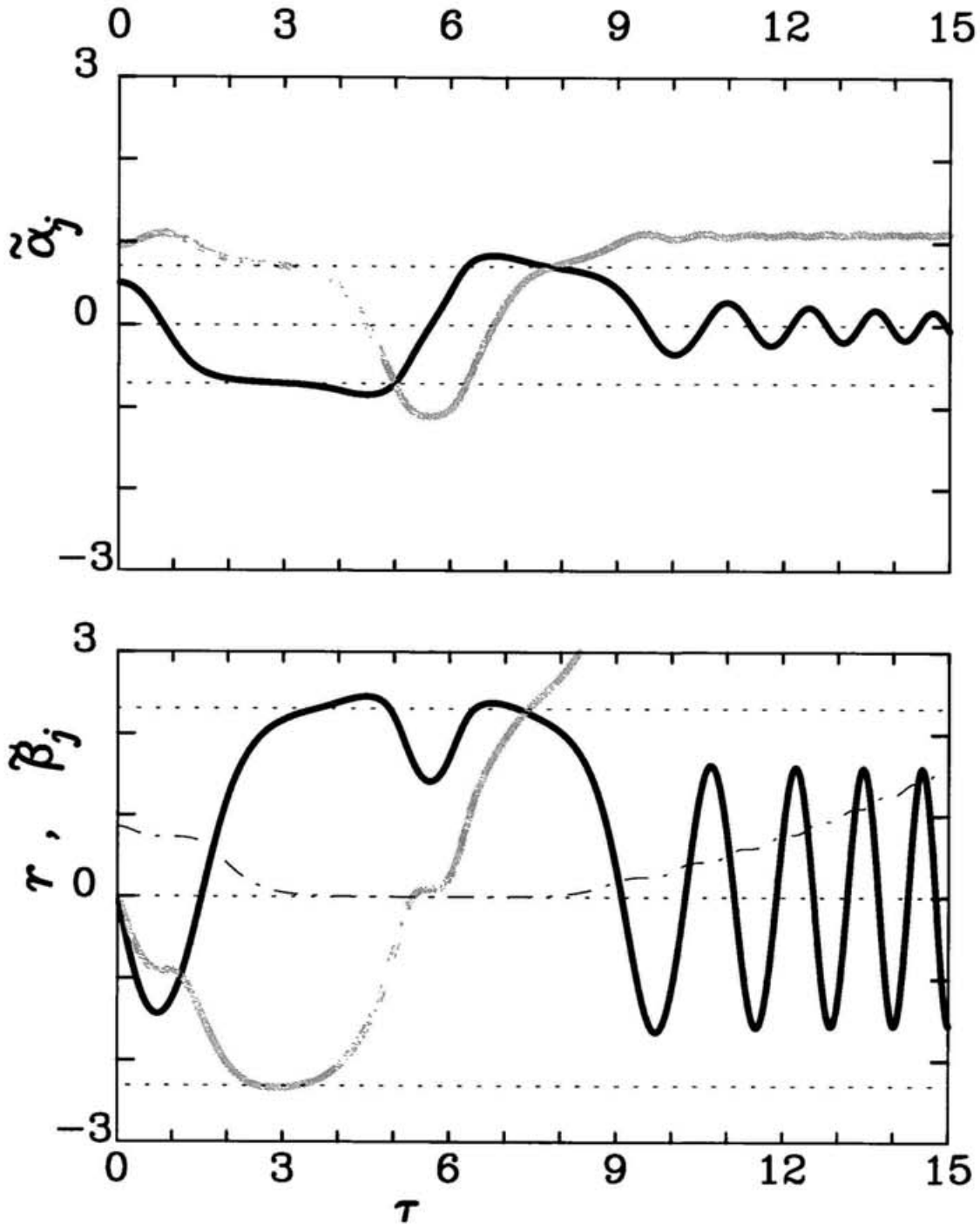

Figure A.4: In the blow-up coordinate system the time evolution of the solution on the isosceles line: the fatter triangle near T_2.

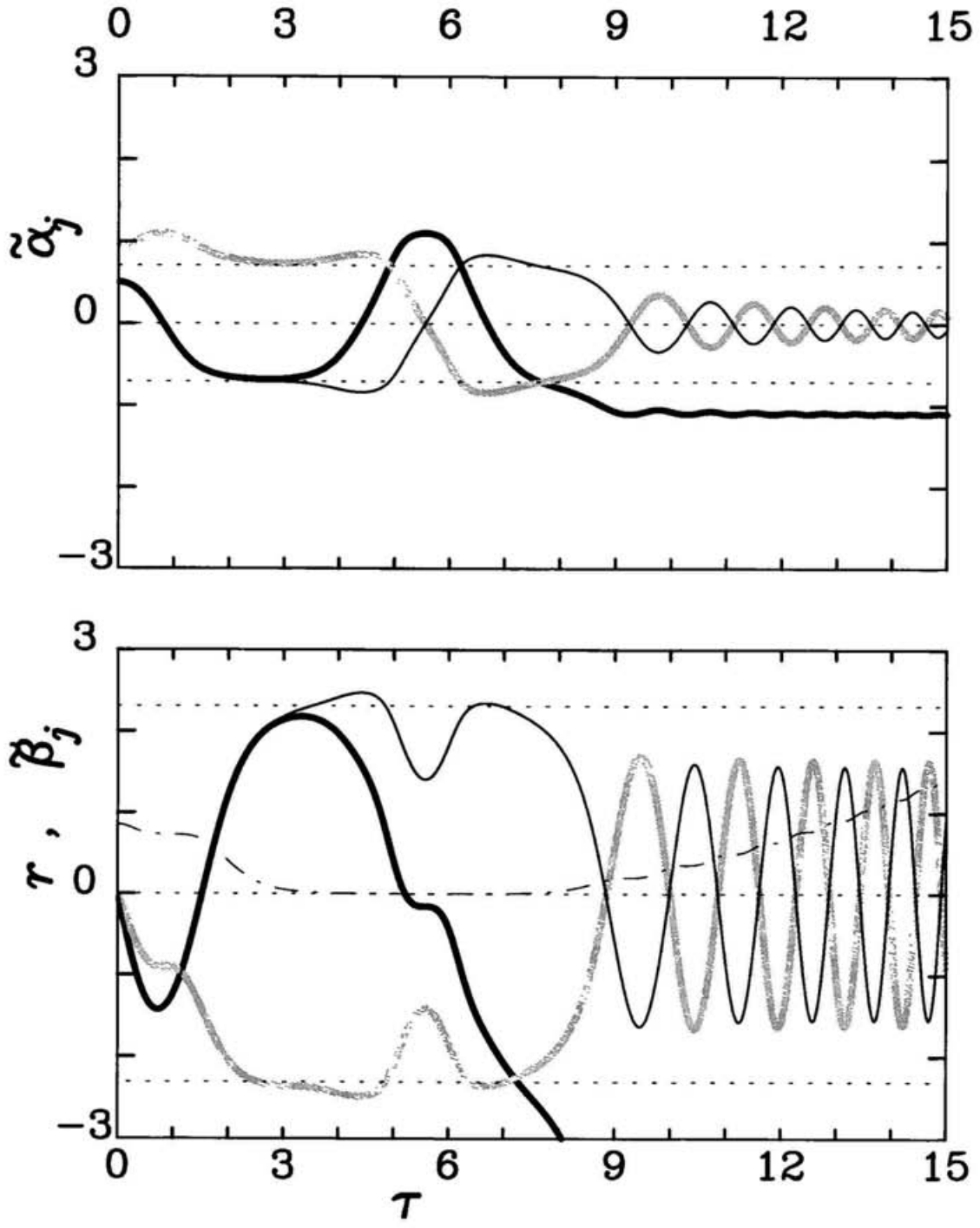

Figure A.5: In the blow-up coordinate system the time evolution of the solution which starts on the binary collision curve of type1 in D_2.

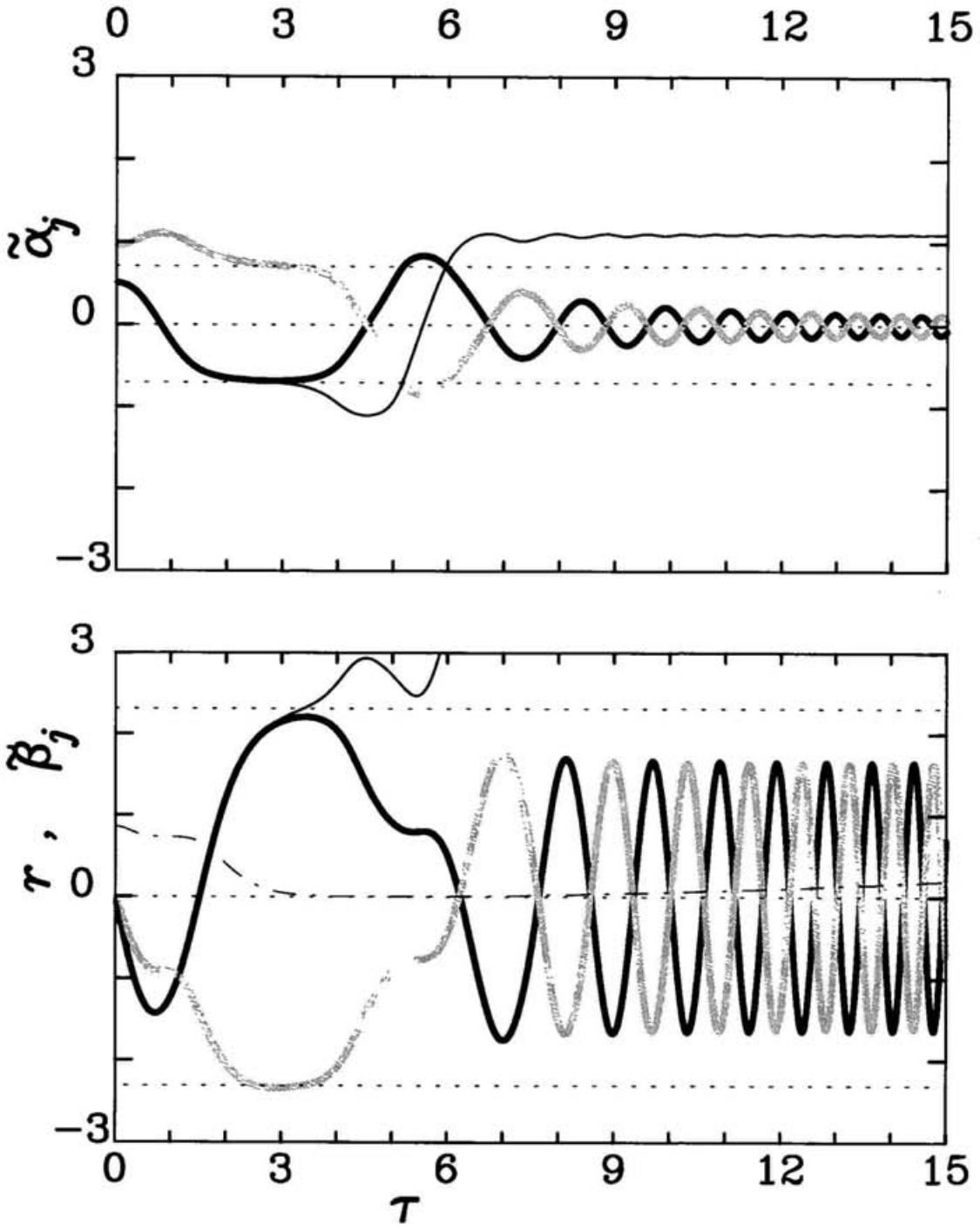

Figure A.6: In the blow-up coordinate system the time evolution of the solution which starts on the binary collision curve of type3 in D_2.

References

Aarseth,S.J., Anosova,J.P, Orlov,V.V. and Szebehely,V.G., 1994a, Global chaoticity in the Pythagorean three-body problem, *Celestial Mechanics and Dynamical Astronomy*, **58**, 1-16.

Aarseth,S.J., Anosova,J.P, Orlov,V.V. and Szebehely,V.G., 1994b, Close triple approaches and escape in the three-body problem, *Celestial Mechanics and Dynamical Astronomy*, **60**, 131-137.

Aarseth, S. J. and Zare, K., 1974; A regularization of the three-body problem, *Celestial Mechanics*, **10**, 185-205.

Agekian, T.A. and Anosova, J.P., 1967, A study of the dynamics of triple systems by means of statistical sampling, *Astron. Zh.*, **44**, 1261-1273; translated into English in *Soviet Astronomy*, **11**, 1006-1014 (1968).

Agekian, T.A. and Anosova, J.P., 1968, Investigation of the dynamics of triple systems by the method of statistical tests. II, *Astrofizika*, **4**, 31-40; translated into English in *Astrophysics*, **4**, 11-16 (1968).

Agekian, T.A., Anosova, J.P. and Bezgubova, V.N., 1969, Formation of binary systems during triple encounters, *Astrofizika*, **5**, 637-643; translated into English in *Astrophysics*, **5**, 329-331 (1969).

Agekian, T.A. and Anosova, J.P., 1971, Probability of binary-system formation through triple encounters, *Astron. Zh.*, **48**, 523-528; translated into English in *Soviet Astronomy*, **15**, 411-414 (1971).

Agekian, T.A. and Anosova, J.P., 1990, Distribution of minima of the current size of the triple systems and their disruption, *Celestial Mechanics and Dynamical Astronomy*, **49**, 145-149.

Agekian, T.A. and Anosova, J.P., 1991, Final motions in nonhierarchical triple systems, *Astron. Zh.*, **68**, 1099-1103; translated into English in *Soviet Astronomy*, **35**, 551-553 (1991).

Agekian, T.A. and Martynova, A.I., 1973, *Vestn. Leningrad Univ.*, 122.

Alekseev, V.M., 1981, Quasirandom oscillations and qualitative questions in celestial mechanics, *Amer. Math. Soc. Transl.* (2) Vol.116, 97-169. (Book title is *Three Papers in Dynamical Systems.*)

Anosova, J.P., 1969, Investigation of the dynamics of triple systems by the Monte Carlo method. III. the case of components with different masses, *Astrofizika*, **5**, 161-167; translated into English in *Astrophysics*, **5**, 81-84 (1969).

Anosova, J.P., 1986, Dynamical Evolution of triple systems, *Astrophys. Space Sci.*, **124**, 217-241.

Anosova, J.P., 1989, Binaries from Unstable Triples, *Comments Astrophys.*, **14**, 17-35.

Anosova, J.P., 1991, Strong triple interactions in the general three-body problem, *Celestial Mechanics and Dynamical Astronomy*, **51**, 1-15.

Anosova, J.P, 1996, Dynamical evolution of triple systems with big differences in the masses of bodies. A criterion for stability, *Astrophys. Space Sci.*, **238**, 223-238.

Anosova, J.P., 1997, Strong gravitational slingshot effect in central parts of stellar and galactic systems, in the *Proceedings of the Symposium No. 184 of the International Astronomical Union, Kyoto, Japan, August 18-22, 1997* (in press).

Anosova, J.P., Orlov, V.V., 1981, *Trudy Astron. Obs. Leningrad*, **36**, 109.

Anosova, J.P. and Orlov, V.V., 1992, The types of motion in hierarchical and non-hierarchical triple systems: numerical experiments, *Astron. Astrophys.* **260**, 473-484.

Anosova, J.P. and Orlov, V.V., 1994, Main features of dynamical escape from three-dimensional triple systems, *Celestial Mechanics and Dynamical Astronomy* **59**, 327-343.

Anosova, J.P. and Tanikawa, K., 1995, Binaries in the Universe. Possible Dynamical Mechanisms of formation, evolution and disruption of different kinds of constituents of the Universe., *Astrophys. Space. Sci.*, **234**, 191-205.

Anosova, J.P. and Zavalov, N.N., 1989, States of strong gravitational interaction in the general three-body problem, *Astron. Zh.*, **66**, 152-160; translated into English in *Soviet Astronomy*, **33**, 79-83 (1989).

Basu, D., Valtonen, M.J., Valtonen, H. and Mikkola, S., 1993, Jets from mergers of binary black holes, *Astron. Astrophys.*, **272**, 417-420.

Bhatnagar, K.B., 1990, Formation of a binary in the general three-body problem,

Bull. Astr. Soc. India, **18**, 363-369.

Birkhoff, G.D., 1927, Dynamical Systems, *Am. Math. Soc. Publ., Provedence RI.*

Black, D.C., 1982, A simple criterion for determining the dynamical stability of three-body systems, *Astron. J.*, **87**, 1333-1337.

Boyd, P.T., and McMillan, S.L.W., 1992, Initial-value space structure in irregular gravitational scattering, *Phys. Rev. A*, **46**, 6277-6287.

Boyd, P.T., and McMillan, S.L.W., 1993, Chaotic scattering in the gravitational three-body problem, *CHAOS*, **3**, 507-523.

Broucke, R. A., 1995; On the role of the moment of inertia in three-body scattering, *From Newton to Chaos* (eds. Roy, A. and Steves, B.), Plenum Press, New York, pp.327-341.

Bulirsch, R. and Stoer, J., 1966; Numerical treatment of ordinary differential equations by extrapolation methods, *Numer. Math.*, **8**, 1-13.

Chazy, J., 1922, Sur l'allure finale du mouvement dans le probléme des trois corps quand le temps croît indéfiniment, *Annales de l'Ecole Normale Sumérieure, 3éme Série*, **39**, p.29-130.

Chernin, A.D., Ivanov, A.V., Trofimov, A.V. and Mikkola, S., 1994, Configurations and morphology of triple galaxies: evidence for dark matter?, *Astron. Astrophys.*, **281**, 685-690.

Delgado-Fernández, J., 1988, Transversal ejection-collision orbits in Hill's problem for $C \gg 1$, *Celestial Mechanics*, **44**, 299-307.

Delibaltas, P., 1983, Families of periodic collision orbits in the general three-body problem, *Celestial Mechanics*, **29**, 191-204.

Devaney, R. L., 1979; Structural stability of homothetic solutions of the collinear n-body problem, *Celestial Mechanics*, **19**, 391-404.

Devaney, R.L., 1980, Triple collision in the planar isosceles three-body problem, *Inven. Math.*, **60**, 249-267.

Devaney, R.L., 1982, Blowing up singularities in classical mechanical systems, *Amer. Math. Monthly*, **89**, 535-552.

Ding, M., Grebogi, C., Ott, E. and Yorke, J.A., 1990, Transition to chaotic scattering, *Phys. Rev. A*, **42**, 7025-7040.

Dolgachev, V.P. and Chernin, A.D., 1997, Dynamics of wide galaxy triplets: numerical models and hidden mass estimates, *Astronomy Reports*, **41**, 284-290.

Elson, Hut and Inagaki, 1987, *Ann. Rev. Astro. Astrophys.*, **25**, 565.

Graziani, F. and Black, D.C., 1981, Orbital stability constraints on the nature of planetary systems, *Astrophys. J.*, **251**, 337-341.

Hadjidemetriou, J.D., 1984, Periodic orbits, *Celestial Mechanics*, **34**, 379-393.

Harrington, R.S., 1975, Production of triple stars by the dynamical decay of small stellar system, *Astron. J.*, **80**, 1081-1086.

Heggie, D.C., 1975, Binary evolution in stellar dynamics, *Mon. Not. R. Astron. Soc.*, **173**, 729-787.

Heggie, D.C. and Hut. P, 1993, Binary-single star scattering. IV. Analytic approximations and fitting formulae for cross sections and reaction rates, *Astrophys. J. Suppl.*, **85**, 347-409.

Heggie, D.C., Hut, P. and McMillan, S.L.W., 1996, Binary-single-star scattering. VII. hard binary exchange cross sections for arbitrary mass ratios: numerical results and semianalytic fits, *Astrophys. J.*, **467**, 359-369.

Heggie, D.C. and Seatman, W.L., 1991, Three-body scattering near triple collision or expansion, *Mon. Not. R. Astron. Soc.*, **250**, 555-575.

Hut, P. and Bahcall, J.N., 1983, Binary-single star scattering. I. Numerical experiments for equal masses, *Astrophys. J.*, **268**, 319-341.

Hut, P., 1983, Binary-single star scattering. II. Analytic approximations for high velocity, *Astrophys. J.*, **268**, 342-355.

Hut, P., 1993, Binary-single star scattering. III. numerical experiments for equal-mass hard binaries, *Astrophys. J.*, **403**, 256-270.

Hut, P. and Rees, M.J., 1992, Constraints on massive black holes as dark matter candidates, *Mon. Not. R. Astron. Soc.*, **259**, 27-30.

Johnstone, D and Rucinski, S. M., 1991, Statistical properties of planar zero-angular-momentum equal-mass triple systems, *Publications of the Astronomical Society of the Pacific*, **103**, 359-367.

Keck, J.C., 1960, Variational theory of chemical reaction rates applied to three-body recombinations, *Journal of Chemical Physics*, **32**, 1035-1050.

Khil'mi, G.F., 1951, *Dokl. Akad. Nauk SSSR*, **78**, 653.

Kiseleva, L.G., Eggleton, P.P. and Anosova, J.P., 1994, A note on the stability of hierarchical triple stars with initially circular orbits, *Mon. Not. R. Astron. Soc.*, **267**, 161-166.

Kiseleva, L.G., Eggleton, P.P. and Orlov, V.V., 1994, Instability of close triple systems with coplanar initial doubly circular motion, *Mon. Not. R. Astron.*

Soc., **270**, 936-946.

Lacomba, E.A. and Llibre, J., 1988, Transversal ejection-collision orbits for the restricted problem and the Hill's problem with applications, *Journal of Differential Equations*, **74**, 69-85.

Laskar, J. and Marchal, C., 1984, Triple close approach in the three-body problem: a limit for the bounded orbits, *Celestial Mechanics*, **32**, 15-28.

Laskar, J. and Robutel, P., 1995, Stability of the planetary three-body problem. I. Expansion of the planetary Hamiltonian, *Celestial Mechanics and Dynamical Astronomy*, **62**, 193-217.

Lin, D.N.C. and Saslaw, W.C., 1977, *Astrophys. J.*, **217**, 958-963.

Llibre, J., 1982, On the restricted three-body problem when the mass parameter is small, *Celestial Mechanics*, **28**, 83-105.

Llibre, J. and Piñol, C., 1990, On the elliptic restricted three-body problem, *Celestial Mechanics and Dynamical Astronomy*, **48**, 319-345.

Mansbach, P., 1970, Binary formation by three-body collisions, *Astrophys. J.*, **160**, 135-145.

Mansbach, P. and Keck, J.C., 1969, Monte carlo trajectory calculations of atomic excitation and ionization by thermal electrons, *Physical Review*, **181**, 275-289.

Marchal, C., 1990, The Three-Body Problem, *Elsevier, Amsterdam.*

Marchal, C., Yoshida, J. and Sun, Yi-Sui, 1984a, A test of escape valid even for very small mutual distances. I. the acceleration and the escape velocities of the third body, *Celestial Mechanics*, **34**, 65-93.

Marchal, C., Yoshida, J. and Sun, Yi-Sui, 1984b, Three-body problem, *Celestial Mechanics*, **34**, 65-93.

McGehee, R., 1974; Triple collision in the collinear three-body problem, *Inven. Math.*, **27**, 191-227.

McMillan, S.L.W., 1996, Binary-single-star scattering. VI. automatic determination of interaction cross sections, *Astrophys. J.*, **467**, 348-358.

Merman, G.A., 1952, On a criterion of hyperbolic-elliptic motion in the three-body problem (Russian), *Dokl. Akad. Nauk SSSR*, **85**, 727-730.

Merman, G.A., 1953, New criteria of hyperbolic and hyperbolic-elliptic motion in the three-body problem (Russian), *Astron. Zh.*, **30**, 332-329.

Merman, G.A., 1954, On Chazy's investigations in the three-body problem (Russian), *Byull. Inst. Teor. Astron.*, **5**, 594-605.

Merman, G.A., 1955, On a theorem of Birkhoff (Russian), *Byull. Inst. Teor. Astron.*, **6**, 232-239.

Merman, G.A., 1958, Qualitative investigations in the three-body problem (Russian), *Byull. Inst. Teor. Astron.*, **6**, 687-712.

Meyer, N., Benet, L., Lipp, C., Trautmann, D., Jung, C. and Seligman, T.H., 1995, Chaotic scattering off a rotation target, *J. Phys. A: Math. Gen.*, **28**, 2529-2544.

Mikkola, S., 1983, Encounters of binaries. I - equal energies, *Mon. Not. R. Astron. Soc.*, **203**, 1107-1121.

Mikkola, S., 1984a, Encounters of binaries. II - unequal energies, *Mon. Not. R. Astron. Soc.*, **207**, 115-126.

Mikkola, S., 1984b, Encounters of binaries. III - fly-bys, *Mon. Not. R. Astron. Soc.*, **208**, 75-82.

Mikkola, S. and Valtonen, M.J., 1990, The slingshot ejections in merging galaxies, *Astrophys. J.*, **348**, 412-420.

Mikkola, S. and Hietarinta, J., 1989, A numerical investigation of the one-dimensional newtonian three-body problem, *Celestial Mechanics*, **46**, 1.

Mikkola, S. and Hietarinta, J., 1990, A numerical investigation of the one-dimensional newtonian three-body problem – part two — positive energies, *Celestial Mechanics*, **47**, 4.

Mikkola, S. and Hietarinta, J., 1991, A numerical investigation of the one-dimensional newtonian three-body problem. III – mass dependence in the stability of motion, *Celestial Mechanics and Dynamical Astronomy*, **51**, 379-394.

Mikkola, S. and Tanikawa, K., 1998, Kozai resonance drives CH Cygni?, *Astron. J.* (in press).

Moeckel, R., 1983; Orbits near triple collision in the three-body problem, *Indiana Univ. Math. Journ.*, **32**, 221-240.

Nacozy, P.E., 1976, On the stability of the solar system, *Astron. J.*, **81**, 787-791.

Robinson, C., 1984; Homoclinic orbits and oscillation for the planar three-body problem, *J. Differential Equations*, **52**(3), 356-377.

Robutel, P., 1995, Stability of the planetary three-body problem. II. KAM theory and existence of quasiperiodic motions, *Celestial Mechanics and Dynamical Astronomy*, **62**, 193-217.

Saslaw, W.C., Valtonen, M.J. and Aarseth, S.J., 1974, The gravitational slingshot

and the structure of extragalactic radio sources, *Astrophys. J.*, **190**, 253-270.

Shebalin, J.V. and Tippens, A.L., 1996, Interplay and escape in three-body scattering, *Astron. Astrophys.*, **309**, 459-464.

Sibahara, R. and Yoshida, J., 1963, Erweiterungen der Birkhoff-Mermanschen Methoden im Dreikörperperproblem, *Publ. Astron. Soc. Japan*, **15**, 86-99.

Siegel, C.L., 1941, *Ann. Math.*, **42**, 127-168.

Siegel, C.L. and Moser, J.K., 1971 (reprinted in 1991), Lectures on Celestial Mechanics, *Springer-Verlag Berlin Heidelberg.*

Simó, C., 1980; Masses for which triple collision is regularizable, *Celestial Mechanics*, *21*, 25-36.

Simó, C. and Martínez, R., 1988; Qualitative study of the planar isosceles three-body problem, *Celestial Mechanics and Dynamical Astronomy*, **41**, 179-251.

Simó, C. and Susín, A. : 1989, Connections between critical points in the collision manifold of the planar 3-body problem, *The Geometry of Hamiltonian Sytems* (Ed., Ratiu, T.), Springer-Verlag, pp.497-518.

Sitnikov, K. A. : 1960, Existence of oscillatory motions for the three-body problem, *Dokl. Akad. Nauk. USSR*, **133**, 303-306.

Standish, E. M., 1971; Sufficient conditions for escape in the three-body problem, *Celestial Mechanics*, **4**, 44-48.

Susín, A. and Simó, C. : 1991, Equiliblium connections on the triple collision manifold, *Predictability, Stability, and Chaos in N-Body Dynamical Systems* (Ed., Roy, A. E.), Plenum Press, New York, pp.481-512.

Sundman, K.F., 1912, Mémoire sur le probléme des trois corps, *Acta Mathematica*, **36**, 105-179.

Szebehely, V., 1973a, Recent advances in the problem of three bodies, *Recent Advances in Dynamical Astronomy* (eds., Tapley, B.D. and Szebehely, V.), D.Reidel Publishing Company: Dordrecht-Holland, pp.75-106.

Szebehely, V., 1973b, Triple close approaches in the problem of three bodies, *Celestial Mechanics*, **8**, 163-167.

Szebehely, V., 1974a, Analysis of a one-parameter family of triple close approaches occurring in stellar systems, *Astron. J.*, **79**, 981-983.

Szebehely, V., 1974b, Numerical investigation of a one-parameter family of triple close approaches occurring in stellar systems. *Astron. J.*, **79**, 1449-1454.

Szebehely, V. and Zare, K., 1977, Stability of classical triplets and of their hierar-

chy, *Astron. Astrophys.*, **58**, 145-152.

Tanikawa, K., Umehara, H. and Abe, H., 1995, A search for collision orbits in the free-fall three-body problem. I. numerical procedure, *Celestial Mechanics and Dynamical Astronomy*, **62**, 335-362.

Tanikawa, K., Umehara, H., 1995, Collision orbits and chaos in the free-fall three-body problem, to be appeared in *Proceedings of the conference in "Structure and Evolution of Stellar Systems", Petrozavodsk, Russia in Aug.13-17,1995.*

Tanikawa, K. and Umehara, H., 1998, Oscillatory orbits in the planar three-body problem with equal masses, *Celestial Mechanics and Dynamical Astronomy* (in press).

Umehara, H., Tanikawa, K. and Aizawa, Y., 1995, Triple collision and escape in the three-body problem, *Dynamical Systems and Chaos* (Eds. Aizawa, Y., Saito, S. and Shiraiwa, K.), World Scientific, Singapore, Vol.2, pp.404-407.

Umehara, H. and Tanikawa, K., 1996, Dominant roles of binary and triple collisions in the free-fall three-body problem, *Chaos in Gravitational N-Body Systems* (Eds. Muzzio, J. C., Ferraz-Mello, S. and Henrard, J.), Kluwer Academic Publishers, Netherlands, pp.285-290.

Umehara, H. and Tanikawa, K., 1997, Orbital distribution arbitrarily close to the homothetic equilateral triple collision in the free-fall three-body problem with equal masses, submitted to *Celestial Mechanics and Dynamical Astronomy.*

Valtonen, M.J., 1988, The general three-body problem in astrophysics, *Vistas in Astronomy*, **32**, pp.23-48.

Valtonen, M.J., 1996, Triple black hole systems formed in mergers of galaxies, *Mon. Not. R. Astron. Soc.*, **278**, 186-190.

Valtonen, M. and Mikkola, S., 1991, The few-body problem in astrophysics, *Annu. Rev. Astron. Astrophys.*, **29**, 9-29.

Valtonen, M.J., Mikkola, S., Heinämäki, P. and Valtonen, H., 1994, Slingshot ejections from clusters of three and four black holes, *Astrophys. J. Suppl.*, **95**, 69-86.

van Kampen, E.R. and Wintner, A., 1937; On a symmetrical canonical reduction of the problem of three bodies, *Am. J. Math.*, **59**, 153-166.

Waldvogel, J., 1973, Collision singularities in gravitational problems, *Recent Advances in Dynamical Astronomy* (eds., Tapley, B.D. and Szebehely, V.), D.Reidel Publishing Company: Dordrecht-Holland, pp.21-33.

Waldvogel, J., 1979, Stable and unstable manifolds in planar triple collision, *Instabilities in Dynamical Systems* (ed., Szebehely, V.), D.Reidel Publishing Company, pp.263-271.

Waldvogel, J., 1982, Symmetric and regularized coordinates on the plane triple collision manifold, *Celestial Mechanics*, **28**, 69-82.

Xia, Z., 1992, The existence of noncollision singularities in newtonian systems, *Annals. of Mathematics*, **135**, 411-468.

Xia, Z., 1994, Arnold diffusion and oscillatory solutions in the planar three-body problem, *Journal of Differential Equations*, **110**, 289-321.

Yoshida, J., 1972; Improved criteria for hyperbolic-elliptic motion in the general three-body problem, *Publ. Astron. Soc. Japan*, **24**, 391-408.

Yoshida, J., 1974; Improved criteria for hyperbolic-elliptic motion in the general three-body problem. II, *Publ. Astron. Soc. Japan*, **26**, 367-377.

Junzo Yoshida, 1997; private communications.

Zare, K., 1981, Properties of the moment of inertia in the problem of three bodies, *Celestial Mechanics*, **24**, 345-354.

Zare,K. and Szebehely,V., 1995, Order out of chaos in the three-body problem: regions of escape, in *From Newton to Chaos* (eds., Roy and Steves), Plenum Press, New York, pp.299-313.